ELUCIDATING THE RED LUMINESCENT MECHANISM OF PROTEIN-GOLD COMPLEXES

by

Jacob Michael Dixon

A dissertation submitted to the faculty of
The University of North Carolina at Charlotte
in partial fulfillment of the requirements
for the degree of Doctor of Philosophy in
Nanoscale Science

Charlotte

2024

Approved by:

_____
Dr. Shunji Egusa

_____
Dr. Juan Vivero-Escoto

_____
Dr. Thomas Schmedake

_____
Dr. Christopher Bejger

_____
Dr. Didier Dreau

ABSTRACT

JACOB M DIXON. Elucidating the Red Luminescent Mechanism of Protein-Gold Complexes. (Under the direction of DR. SHUNJI EGUSA)

Protein-gold complexes, including serum albumin-gold (Au) complexes, exhibit strong, distinct red luminescence (λ_{em} = 660 nm) with an extremely large Stokes shift when excited using ultraviolet light (λ_{ex} = 365 nm). Initial reports on red luminescent serum albumin (BSA)-Au suggested a wide array of potential applications in nanomedicine, imaging, and sensing. However, current knowledge about this complex is limited, including its structure and formation mechanism, and the commonly assumed single-site nucleation model doesn't align with experimental results. Our investigation into BSA-Au and four other protein-Au complexes revealed a similar and consistent formation mechanism, better explained by a multiple-site adsorption model rather than a single-site nucleation model. Molecular cloning of human serum albumin (HSA) indicated that the luminophore site requires Au to bind to only one intact cystine disulfide bond. Further experiments with the smaller red luminescent glutathione (GSSG)-Au complexes demonstrated that merely two neutral Au atoms are necessary for the formation of the red luminescent complex. Understanding the Au binding site in proteins, luminescence mechanism, and the structure could evolve this easily synthesizable red luminescent complex into a versatile, next generation, fluorescent protein.

ACKNOWLEDGEMENTS

I would like to express my deepest gratitude to my professor, Dr. Egusa, whose guidance and mentorship have been invaluable throughout my academic journey. I am indebted to my dedicated committee members for their insightful feedback and support. A special thanks to my collaborators, whose efforts pushed my research forward. To my lab mates for their camaraderie, enhancing the research experience over the years. The Chemistry and Physics faculty have been instrumental in teaching me so many techniques and sharing their thoughts, and I am thankful for their expertise. I extend my heartfelt appreciation to my family and friends for their constant encouragement and understanding. This achievement is a collective effort, and I am profoundly grateful to everyone who has played a role in my academic and personal growth. Your support has been the driving force behind my success, and I am honored to have such a remarkable network of individuals in my life.

DEDICATION

To my partner Erin (and my dog Olive), your endless love and support has always been my motivation.

TABLE OF CONTENTS

LIST OF FIGURES

LIST OF TABLES

LIST OF ABBREVIATIONS

Å	Angstrom
A-form	Aged form of bovine serum albumin
APS	Ammonium persulphate
Asp	Asparagine
Au	Gold
B-form	Basic form of bovine serum albumin
BSA	Bovine serum albumin
^{o}C	Celsius
cDNA	Complimentary DNA
Cl	Chlorine
CPS	Counts per second
Cu	Copper
Cys	Cystine
Cys34	Cysteine 34 residue
Cys-Cys	Cysteine-cysteine (disulfide bond)
Da	Dalton
DNA	Deoxyribonucleic acid
DTT	dithiothreitol
E. coli.	*Escherichia* coli
EDTA	Ethylenediaminetetraacetic acid
EDX	Energy-dispersive X-ray spectroscopy
E-form	Extended form of bovine serum albumin

EE-map	Excitation-emission map
ESI	Electrospray ionization
eV	Electron volt
F-form	Fast form of bovine serum albumin
FP	Fluorescent protein
fs	Femtosecond
FT-IR	Fourier-transform infrared spectroscopy
FW	Finke-Watzky
GSH	Glutathione (reduced)
GSSG	Glutathione (oxidized)
GST	Glutathione S-transferase
$HAuCl_4$	Chloroauric acid
HIS	Histidine
HPLC	High-performance liquid chromatography
HSA	Human serum albumin
IgG	Immunoglobulin G
IR	Infrared
k_B	Boltzmann constant
kDa	Kilo-Dalton
kJ	Kilo-Joules
LMCT	Ligand to metal charge transfer
M	Molar
MES	2-(*N*-morpholino)ethane sulfonic acid

mg	Milligram
mL	Milli-liter
MLCT	Metal to ligand charge transfer
mM	Milli-molar
MWCO	Molecular weight cutoff
N-form	Normal form of bovine serum albumin
NaOH	Sodium hydroxide
NEM	N-ethylmaleimide
Ni	Nickel
NMR	Nuclear magnetic resonance
ns	Nanosecond
Ova	Ovalbumin
PBS	Phosphate-buffered saline
PDB	Protein data bank
PHE	Phenylalanine
ps	Picosecond
Pt	Platinum
SDS	Sodium dodecyl sulfate
TAS	Transient absorption spectroscopy
TCEP	Tris(2-caroxyethyl)phosphine hydrochloride
TCSPC	Time-correlated single-photon counting
TEM	Transmission electron microscopy
TEMED	Tetramethyl ethylenediamine

TRP	Tryptophan
TYR	Tyrosine
μL	Micro-liter
μM	Micro-molar
UV	Ultra-violet
UV-Vis	Ultra-violet-visible
V	Volts
XPS	X-ray photoelectron spectroscopy

CHAPTER 1: INTRODUCTION

Proteins are inherently precise and organic structures at nanoscale size. They are biomolecules comprised of long chains of twenty unique amino acid residues. Made in the cells of all living organisms, proteins carry out a vast array of functions including metabolic reactions, DNA replication, stimuli response, and transportation of molecules.[2] Each unique protein differs only by how the primary sequences of these twenty amino acids are organized and. A protein's actual functions are dictated by the way they are folded into precise three-dimensional shapes. As protein function is directly related to the precise folding and correct amino acid sequence, proteins could be considered highly monodispersed compounds. Contrary to protein structure, a current problem in the chemical synthesis of inorganic-based nanomaterials is the lack of this monodispersed precision.[3] The difficulty to perfectly control the size distribution limits our ability to design complex nanomaterials and reliably assemble them into long-range, ordered, structures. As such, proteins could provide a more natural and reliable starting point for achieving this desired precision.[4-6]

Beyond what proteins have naturally been evolved to do over millennia, humankind has found new avenues for proteins. Newer and more advanced applications of proteins have allowed proteins to be used for a variety of applications from targeting or protection of nanoparticles in the form of protein coronas around nanoparticles.[2] To unique protein cages which can act as drug carriers themselves.[3,4] These proteins can even be used as fluorescent tags and fluorescent sensors, such as the infamous green fluorescent protein (GFP).[5,6]

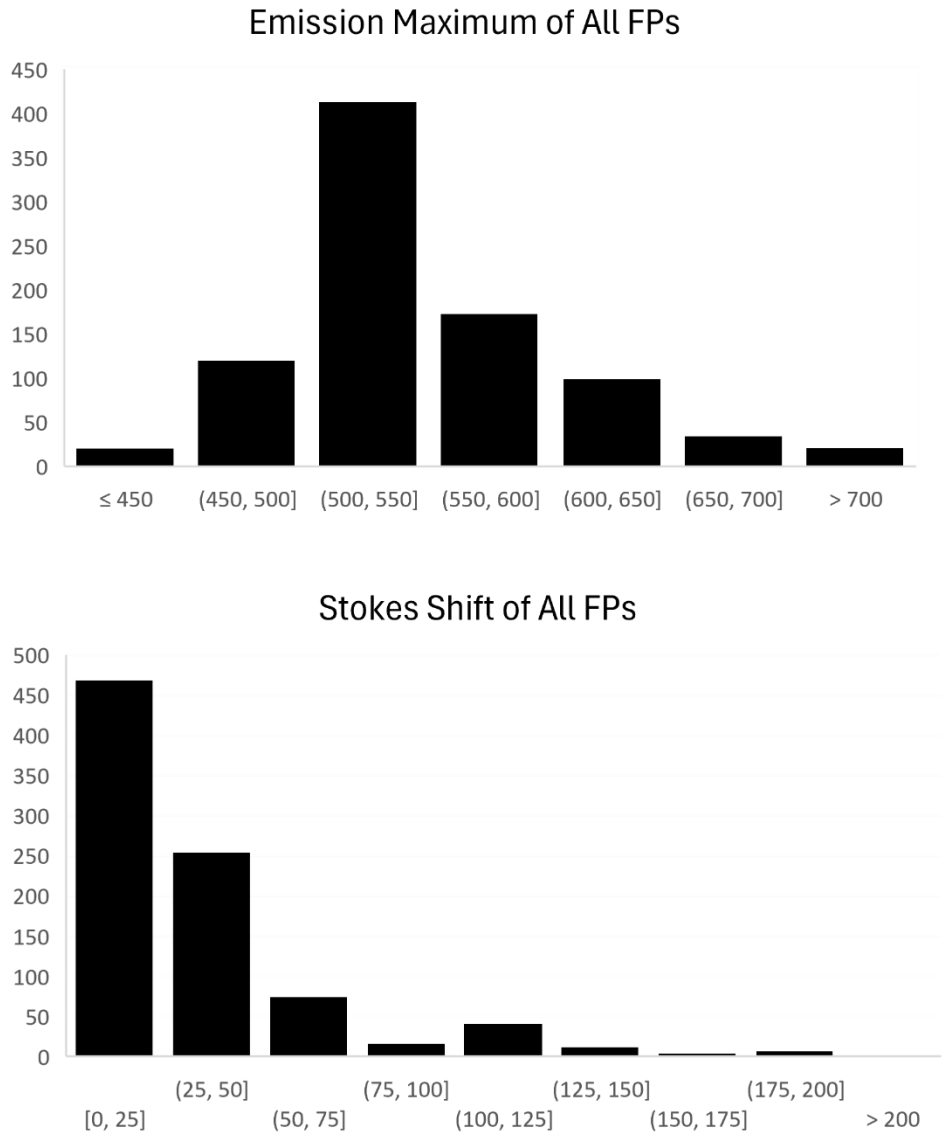

Figure 1. Histogram plot of all known fluorescent proteins organized by (top) emission maximum and (bottom) Stokes shift. For fluorescent proteins beyond 650 nm emission only 48 proteins exist and for large Stokes shift fluorescent proteins only 14 exist. For fluorescent proteins that have both an emission beyond 650 nm and a large Stokes shift, there are no monomeric-based fluorescent proteins in this category.

One of the major advances in synthetic protein function is their ability to act as fluorescent proteins. These proteins can be synthesized genetically like GFP or by synthesized through the addition of a cofactor like a small molecule or metal ion. Fluorescent proteins can be used in a large array of applications in both functional and structural studies.[7] This could range from measuring protein interactions or conformational

shifts, as fluorescent tags in confocal microscopy and flow cytometry, or in a myriad of other techniques. While there are nearly 1000 fluorescent proteins that exist across the visible spectrum, very few proteins are fluorescent beyond 650 nm. Even fewer fluorescent proteins have very large stokes shift (**Figure 1**).[8]

The benefits of a proteins that fluoresce beyond 650 nm is important to studies that are both *in vivo* and *in vitro* due to the greater penetrative depth of longer wavelengths and are less phototoxic.[9] Including the longer wavelength emission, large Stokes shift proteins have the benefit of being able to be excited at a wavelength significantly away from the emission wavelength. The added benefit of a large stokes shift includes diminishing self-absorption, minimizing inner filter effect, allowing for multi-color imaging experiments, and eliminating autofluorescence as a few examples.[10]

Currently, there are around 50 fluorescent proteins that emit beyond 650 nm and there are around 15 that have a large stokes shift over 150 nm, but combined there are no such monomeric fluorescent proteins that are both emissive beyond 650 nm and have a stokes over 150 nm. Thus, there is a major gap in the world of fluorescent proteins to fill which could have a great impact.[8]

As stated earlier, proteins are the workhorses of the cellular world and one of the primary roles of proteins is the transportation and removal of small molecules and ions. This transportation of ions is usually performed by a class of proteins called serum albumins, which are found in blood.[7] Due to their role as transporters, these proteins readily bind to many metals ions and have been shown to take up copper, nickel, iron, and other ions.[8-11] While the uptake of ions by albumin is its natural function, synthetic modifications of albumins with metal ions, specifically Au, produce unique protein-metal complexes with

interesting optical properties. Gold is not naturally found in blood and thus its removal via serum albumins has been scarcely studied. The addition of Au to serum albumin, under certain pH-driven reaction conditions, such as in human and cow (bovine) serum albumin, yields a brightly red luminescent compound which is excited in UV (Ex = 365 nm) but fluorescence in red (Em = 660 nm),[12,13] and has a vast potential for multiple areas of study. The Au-containing protein-complex can be used for sensing other toxic metals ions in solution, such as mercury,[14,15] for imaging, due to their bright luminescence,[16,17] or in nanomedicine.[18-20] The red luminescence of this complex is especially valuable as a fluorescent tag or attached to a drug carrier, as they are more easily detectable *in vivo*.[21] The lack of available fluorescent proteins (FP) in the red regime, which this complex fills, combined simultaneously with a\its large Stokes shift makes this red fluorescent complex highly attractive as a modern FP.

While this unique compound has been around for nearly a decade, the actual complex has not been characterized. Multiple theories on the organization of Au within the protein and the mechanism of the red luminescent complex exist. These theories differ and propose that the protein-Au could be made from a few to tens of Au atoms, and that many Au atoms are nucleated together into a single cluster.[12,22-24] Currently, no definitive evidence has been shown to fully support either theory.

Currently, these red luminescing protein-Au complexes have been cited numerous times as Au_{25} nanoclusters and studied for applications as sensors, imaging agents, and fluorescent tags. These studies have been completed under the assumption of an Au_{25} nanocluster without the proper understating of whether the system is a nanocluster or just a protein complex. Further applications, including such potential uses as drug carriers in

nanomedicine, could lead to difficulties in future trials if the red luminescing complex is not found to be a nanocluster at all. Red luminescence is valuable in *in vitro* and *in vivo* studies, as the penetrative depth of longer wavelengths is deeper than shorter wavelengths, making an easily synthesizable red-luminescent complex lucrative for biological applications.[25] It is of utmost importance to uncover the binding site of this complex within the protein along with the mechanism that produces red luminescence before further experiments by others are conducted on a potentially unknown compound.

It is of importance to fully uncover the origins of this complex, as this protein-Au complex has already been shown to have a variety of applicable uses and is currently used in different fields of nanotechnology. Understanding of the complexes red luminescence, its structure, and the mechanisms of formation could allow for these Au-albumin-complexes to be more useful. These results could also yield a complex that is more optically tunable, easier to synthesize, and prepared from more proteins than currently is known.

Thus, this work aims to uncover the structure and mechanism of this red luminescent complex. The goals of this work are separated into five primary parts: (1) To uncover the kinetics of the luminescent mechanism in the initially discovered, red luminescent bovine serum albumin-gold complex. Understanding of the kinetics of this complex will provide important evidence as to whether the complex is a single, large, nucleated cluster of Au or a smaller, few-atom-containing complex. Modification of all reaction parameters will reveal what type of mechanism of formation is most likely in the red luminescent complex – single-site nanocluster-nucleation or multiple-site adsorption. (2) To use other proteins, besides bovine serum albumin, which have also been found to be red luminescent and compare their luminescent characteristics to

determine if this luminescence is common in many other proteins.[26-30] This will allow for a common binding motif to be found within all of these red luminescent proteins. (3) Using human serum albumin and bovine serum albumin, molecularly clone and fragment the proteins to find the binding domain and ultimately the binding site of the red luminophore. (4) Further experimentation into smaller red luminescent small-molecule analogs to reveal the structure of the red luminescent complex, as well as the mechanism of formation and mechanism of luminescence. (5) Determine the role of nanoparticles in the formation of this red luminescent complex as well as reveal the formation mechanism. This will provide further evidence as to the source of red luminescence.

The elucidation of this red luminescent is primarily reliant on uncovering the reaction kinetics of BSA, molecular cloning procedures of HSA, and the resolution of the structural information via reduced and oxidized glutathione. Due to this, the exact same protein or small molecule will not be used for every experiment completed in this work. As this is the case, many experiments are required intermittently to show that red luminescence from one luminescent complex to another is equivalent before moving forward with more detailed experimentation. Furthermore, resolving the luminescent mechanism and structure within the small molecules will be used to assume the same structure is present in the protein-Au complexes without completing the same experiments for all protein-Au complexes. These are the primary limitations of this work and ultimately, without resolving the crystal structure of all protein-Au complexes and small-molecule-Au complexes, a few assumptions must be made when comparing each system. While a crystal structure of each complex is required, this falls outside the

scope of this dissertation but is ideally the next step for future experiments and is work that is currently in progress.

Overall, this work is organized into five primary chapters followed by a brief discussion and conclusion. Elucidation of both the binding site within HSA and the mechanism of red luminescence will allow for a transparent use of this protein-Au complex for its proposed applications. With the determination of both binding site and formation mechanism, this unique protein-Au complex could become a more versatile and widely used organic fluorophore, which is both easy to synthesize and optically tunable.

CHAPTER 2: BACKGROUND AND MOTIVATION

Bovine serum albumin (BSA),[31-33] along with other proteins display unique fluorescent properties when complexed with Au under certain reaction conditions. These protein-Au complexes show strong, stable, and consistent red luminescence (λ_{em} = 660 nm) when excited in the UV (λ_{ex} = 365 nm) and are thus lucrative as FPs due their extremely large Stokes shift (~300 nm). These luminescent protein-Au complexes were initially synthesized a decade prior using BSA and have since been a continuously explored compound.[12] Red luminescence was first presumed to be caused by the nucleation of multiple Au to a single site within the protein itself. Compounding reports by many others perpetuated that this luminescence was due to a small Au nanocluster, but this hypothesis was never fully supported. Due to their small size and interesting optical properties,[34] these small Au-based complexes have been shown to have vast potential for applications as sensors,[35-37] as metal-ion detectors,[38-40] in imaging due to their tunable fluorescence,[41-43] or in nanomedicine as a fluorescent tag or drug carrier.[18-20,44-46]

Initially,[12] the synthesis of BSA and Au produced a brightly red luminescent complex in water and was attributed to a gold cluster bound within the protein structure. The presumed nanocluster was assumed to be Au_{25}[47] - the most well-studied Au nanocluster. For Au clusters of this small size, they are predicted to be luminescent based on the theoretical Jellium model.[48] In this theoretical model the fluorescent emission energy of the nanocluster can be potentially predicted based on the number of Au atoms contained within a small cluster, as long as the cluster is around 1 to 50 Au atoms. Currently, these protein-bound nanoclusters have been studied in detail without a full understanding of the

mechanism of luminescence or definitive evidence that a nanocluster is even formed within the protein, or even where Au binds within the protein.[12,24,49,50]

While the binding sites of other metals within BSA have been studied extensively in the past and other metal binding sites have been determined, the Au binding site responsible for luminescence has remained elusive. Metals play a critical role in life processes and are involved in biological systems for cellular and subcellular functions.[51] The importance of metal ion-protein complexes is also very prominent in the blood, as serum albumin acts as a metal ion scavenger.[11] BSA has been shown by others to uptake copper,[11,52,53] nickel,[54-56] cobalt,[57-59] zinc,[60,61] and iron,[62-64] but no work has shown how or where gold binds within serum albumins. Within BSA, four common binding sites have been found for various metal ions, including Cys34, the Asp-fragment (Asp1-Thr2-His3), His67 binding site, and a fourth undetermined location. This fourth undetermined location could also be the binding site of Au within BSA. Metals also seem to non-specifically bind to albumin, as is the case for iron and nickel. In all these cases of metal ion binding to serum albumins, no evidence of nanocluster formation has been presented.

Since the initial study of BSA with Au, multiple other proteins such as insulin, lysozyme, pepsin, trypsin, and more have been found to show the same red-luminescing properties when complexed with Au at alkaline pH.[1,13,27,28,65] Despite vast differences in the molecular weight of each protein, their crystal shape, and overall function, each protein appears to exhibit the same luminescing characteristics, but this has also not been confirmed in great detail. Importantly, the spectral properties observed in these protein-Au complexes do not appear to be consistent with what is traditionally observed in Au-based

nanoclusters.[1,13] . In this way, it is important to step back and re-examine this unique red-luminescing complex to determine the underlying cause of red luminescence.

The currently prevailing hypothesis of the BSA-Au complex as well as the other protein-Au complexes is that red luminescence is the result of a neutral Au nanocluster contained somewhere inside the protein space. Gold is reduced to neutral Au^0 through amino acid residues, mainly tyrosine, controlled by the adjustment of pH. After reduction, Au^0 aggregates around cysteine residues(s) to form a nanocluster, yet the exact steps of this process have never been outlined.

It was found that a pH of only 9.8 was required for red luminescence and was not nearly high enough for tyrosine reduction to occur, which usually happens above a pH 11.[13] Furthermore, it has been determined that a conformational change in the protein's shape, sterically determining the availability of binding site or sites, allowed for the formation of the red-luminescent complex. Synthesizing the protein-Au complex in acidic conditions also does not result in red luminescence, potentially indicating the importance of the conformational shift occurring in alkaline conditions, or the overall charge of the protein. Additionally, it was also found that binding to a cystine residue was required for red luminescence, without the exact binding site being revealed. Thus, the mechanism of red luminescence has continued to remain elusive.

Currently, the same fluorescence patterns have been found in insulin, trypsin, and ovalbumin, compared to the more extensively studied BSA.[66] Lending to the idea that this luminescence can be found in multiple protein species and could occur in a larger subset of all proteins. Uncovering the mechanism of luminescence could result in a compound

with far greater usability than what is currently being applied and could be optically tunable in the future.

This red luminescent protein-Au complex utilizes a similar reaction pathway as that of an organic fluorophore, in which a cystine group is required for the luminescent mechanism to be activated. Thus, similar advantages such as the low frequency of cystine disulfides could allow for a greater flexibility in choosing the binding location, while the disadvantages remain; such as binding to multiple target residues or the lack of cystine disulfides in general, making the luminescent complex nonviable.[67] In addition to these attributes, the protein-Au complex also maintains its luminescent properties at nearly all pH values after initial synthesis, and luminescence emission can be achieved through excitation at multiple wavelengths in the visible regime, with a large stokes shift between excitation and emission.[13] This could allow the complex to be viable in a greater number of environments where multiple fluorophores are needed at once. Due to the current synthetic protocol, and unknown structure and mechanism of the luminescent complex, some limitations remain for the Au-protein to be viable as a fluorescent tag. The synthesis of the Au-protein complex requires highly alkaline conditions (pH > 10) to activate red luminescence. Furthermore, red luminescence does not occur in every protein, even if a protein contains an accessible cystine disulfide site.[68] Thus, further studies and modifications may be required to make this system viable as a fluorescent-based assay. Before any modifications can potentially be made to improve this fluorophore, the mechanism of luminescence and ultimately, the structure of the complex must be revealed.

While the red luminescing protein-Au complex is not intrinsically novel to this work, no definitive evidence confirming the existence of a nanocluster has been performed.

Additionally, the structure and mechanism of formation of this complex are completely unknown. Thus, a comprehensive study of the protein-Au complex is necessary to reveal the mechanism and common binding motif of the protein-Au complex within BSA and of other proteins that appear to show similar properties. Through an iterative process of molecular cloning of HSA with different amino acid mutations, changes in luminescence can be attributed to changes in amino acid sequences. In tandem with this procedure, structural analysis of all known luminescing proteins will be performed to identify common structural motifs, which can be later applied to find new luminescing proteins.

Along with uncovering the binding site or sites of Au within the protein that causes luminescence, it is also important to determine the mechanism of luminescence. With both the binding motif within proteins and the uncovered mechanism, it may be possible to find new proteins that can also be luminescent in the presence of Au. Revealing the structure of the red luminescent complex will require the use of a smaller system that has the same fluorescent properties and reaction kinetics. A combination of nuclear magnetic resonance (NMR), electrospray ionization (ESI), X-ray photoelectron spectroscopy (XPS), as well as other techniques not viable in large proteins can resolve how Au is bound near cysteine and the number of Au that are required for luminescence.

The determination of a binding site and thus, a common binding motif, could expand the currently small list of known red luminescing protein-Au complexes. The value of a red luminescent compound, which is easy to synthesize, is biologically safe, and uses pre-existing protein structure as a scaffold for complex formation is extremely valuable. The elucidation of the luminescent mechanism could expand the use of this compound to more proteins that share these optical properties. Understanding of the mechanism may

also lead to the tunability of the luminophore, further expanding the potential of this unique complex.

CHAPTER 3: REACTION KINETICS OF THE RED LUMINESCENT BOVINE SERUM ALBUMIN-GOLD COMPLEX

The BSA-Au complex is a considerably attractive compound due to its unique luminescence and potential applications as an organic sensor.[37,69,70] The compound of BSA-Au is obtained by combining a solution of BSA with chloroauric acid and adjusting the pH above 10.[13] This adjustment leads to a conformational shift within the protein, allowing for the ultraviolet excitable red fluorescence to occur. It has been suggested that fluorescence is due to a single-site nucleation of Au(0) within the protein.[12,71] In BSA there possibly presents space for up to 25 Au atoms to fit, however such space considerations have all been done for the neutral pH 7 structure of BSA (**Figure 2**).[24] Studies have not considered the conformation of the protein at pH 10 and above, and may consider that theses spaces are likely not solvent-accessible at these pH values. Furthermore, the overall mechanism and the kinetics of fluorophore formation have not been studied in detail.

Understanding the mechanism of the fluorescence is important for realizing the proposed applications of this compound and further, may be valuable for realizing new, novel properties of BSA and this complex, as well as other proteins complexed with Au. BSA is a well-studied, 66.4 kDa protein which is comprised of 583 amino acid residues. Within the protein is contained 35 individual cysteine residues where one cysteine (CYS34) is exposed at the protein surface and the other 34 residues are bound into 17 cysteine-cysteine (Cys-Cys) disulfide bounds. These 17 disulfide bonds form the internal backbone of the protein and significantly contribute to its tertiary structure. These disulfide

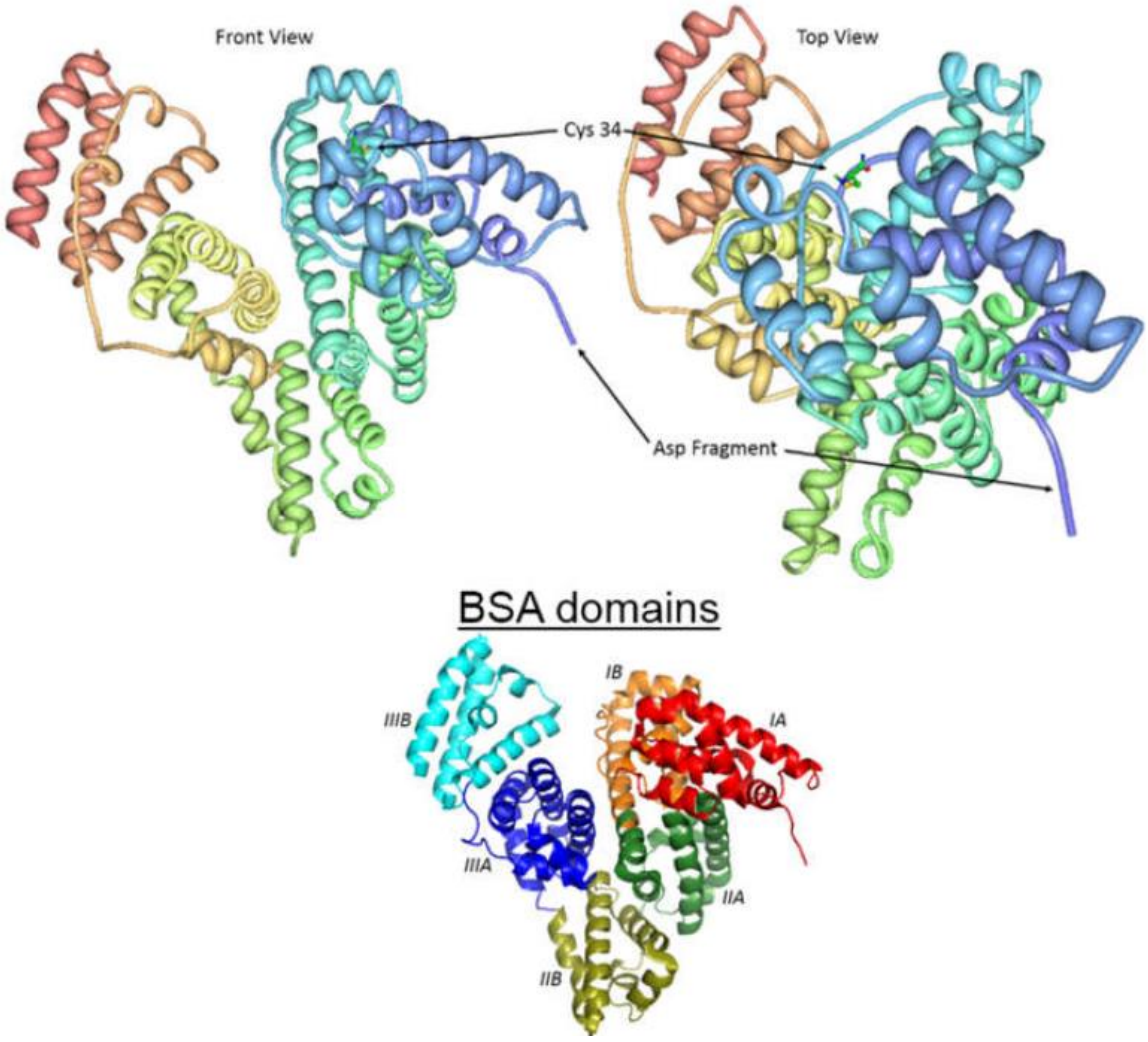

Figure 2. Structure of bovine serum albumin (BSA) in its native, pH 7, conformation. The locations of the Asparagine 'Asp fragment' (the first 4 amino acids at the N-terminus of the protein) and the cystine34 (the only free thiol within BSA) are indicated. The commonly used domain names are also shown which are comprised of domain I,II, and III and can be further subdivided into two A and B subdomains. Crystal structures are taken from PDB ID: 4F5S.

bonds can further be grouped into 8 Cys-Cys / Cys-Cys disulfide clusters disturbed throughout the protein.[31-33]

BSA itself is a dynamic molecule that contains five reversible conformational shapes at various pH values. The molecular details and dynamic nature of these structures have been explored in many other metal cations binding to BSA but overall have not studied the kinetics of BSA-Au. Some studies have found that the fluorescence of the BSA-

Au complex is associated with a particular reversible conformation of BSA, formed above a pH of 10.[13,72] The BSA-Au complexes were further reducible after formation, indicating the presence of some cationic Au. The binding site(s) of Au within the protein are likely to a Cys-Cys disulfide region, the accessible cystine34, and the known metal binding site at the N-terminal of the protein known as the Asparagine 'Asp'-fragment.[52,53,73,74] Cys-Cys disulfide bonds are required in some capacity for the formation of the red luminescent complex, and that a cascaded energy transfer process within the BSA-Au complex by excitation-emission spectroscopy could account for the large Stokes shift observed for the UV-excited complex.

Elucidation of the mechanism of Au binding to BSA shows strong characteristics of a multiple-site adsorption, along with the chemisorption of Au to a fluorophore-forming site or sites. This mechanism is also dominated by many nonspecific surface physisorption and adsorptions to known metal binding sites that do not contribute to red luminescent formation. In order to understand this complex, a multiple-site binding model could be used, and this model is compared to a LaMer-type single-site nanocluster nucleation model.[75-78] In both cases, the dependence of the kinetics on pH, temperature, and relative BSA to Au stochiometric concentration is considered. By comparing both a multiple-site adsorption model to a single-site nanocluster nucleation model it can be determined what type of kinetic processes are more likely responsible in creating the red luminescent complex. The kinetic studies of this conformational-change-induced fluorescence within the BSA-Au complex reveals a highly dynamic nature of BSA as a substrate.

3.1 Experimental Methodology and Instrumentation

The BSA-Au complexes were prepared via the following protocol at various pH above 10 (from pH 10.5 to 12.5) to achieve the A-form of BSA and was performed at various constant temperatures (from 20°C to 50°C). In this standard protocol 1 mL of HAuCl4 aqueous solution was added to 1 mL of aqueous BSA (0.375 mM, or 25 mg/mL, like the typical serum albumin concentration in blood). BSA-to-Au molar ratio was adjusted depending on the experiment (for example: for a BSA : Au ratio equal to 1:13, 1 mL of 5 mM HAuCl4 solution was added). The two solutions were combined under vigorous stirring at 750 rpm. Upon addition of the HAuCl4 solution to the BSA solution, the color changed from clear to light yellow, and the pH of the solution was 3.0. After 2 min, 1 M NaOH was added to achieve the desired pH. For the standard synthesis, the reaction proceeded for approximately 2 h, and then the solution was stored at room temperature. For all the kinetics studies, the temperature was maintained constant for the duration of the measurements.

Gel electrophoresis of the BSA-Au complexes was performed to study the surface-mediated aggregation due to the increasing concentration of Au that was added. As such, precast 3−8% gradient Tris-acetate gels and MES running buffer were used for the gel electrophoresis. The sample buffer contained 5 μg of protein per lane. No denaturing agents, such as urea, sodium dodecyl sulfate (SDS), dithiothreitol (DTT) or heat, were applied to the sample buffer before running the gel. The importance of omitting denaturing agents is to maintain, as best as possible, the disulfide bonds within the protein. Electrophoresis was performed at room temperature for approximately 1 hr, at a constant voltage of 150 V. The gels were subsequently stained with Coomassie Blue R-250 for the

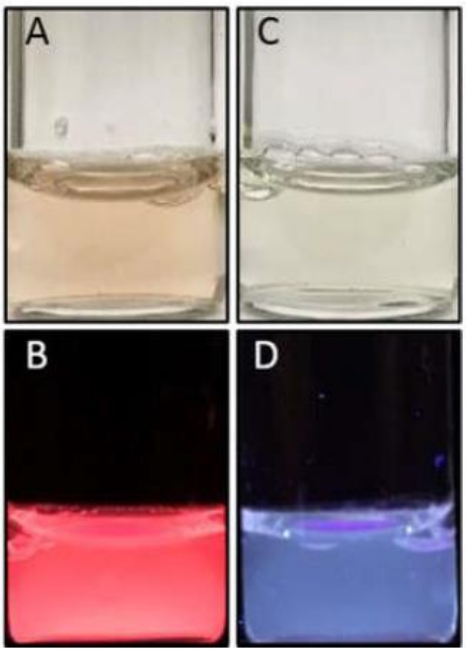

Figure 3. Dithiothreitol (DTT), a Cys-Cys disulfide bond-cleaving agent, readily quenched the red fluorescence of BSA-Au complex. (A) BSA-Au complex was prepared using the standard protocol (BSA : Au = 1 : 13). (B) The UV (λ = 365 nm)-excited red fluorescence of the BSA-Au complex. (C) BSA-Au complex was treated with 10 mM DTT and 1% SDS and was incubated for 30 minutes at 37oC, following the commonly used protocol for protein gel electrophoresis sample preparation. (D) The red fluorescence of the DTT-treated BSA-Au complex was readily quenched. The blue fluorescence is from the aromatic residues of BSA at pH = 12. This blue fluorescence is identical to that of BSA at pH = 12, without the addition of Au.[1]

molecular weight analyses of the in-gel bands. Any Au nanoparticles that were formed due to surface-mediated aggregation were imaged with transmission electron microscopy.

Analysis of all kinetic studies of the BSA-Au complex are performed using fluorescence and absorption spectroscopies. For fluorescence spectroscopy, single line scans and excitation-scanned spectroscopy (three-dimensional excitation-emission mapping) was performed. For the excitation-emission mapping, the samples were excited at 5 nm wavelength intervals and their emissions recorded in 1 nm wavelength intervals. Different slit widths were used for line scans (slit width: 5 nm resolution; integration time: 0.1 s) and for excitation-emission mapping (slit width: 1 nm; integration time: 0.1 s),

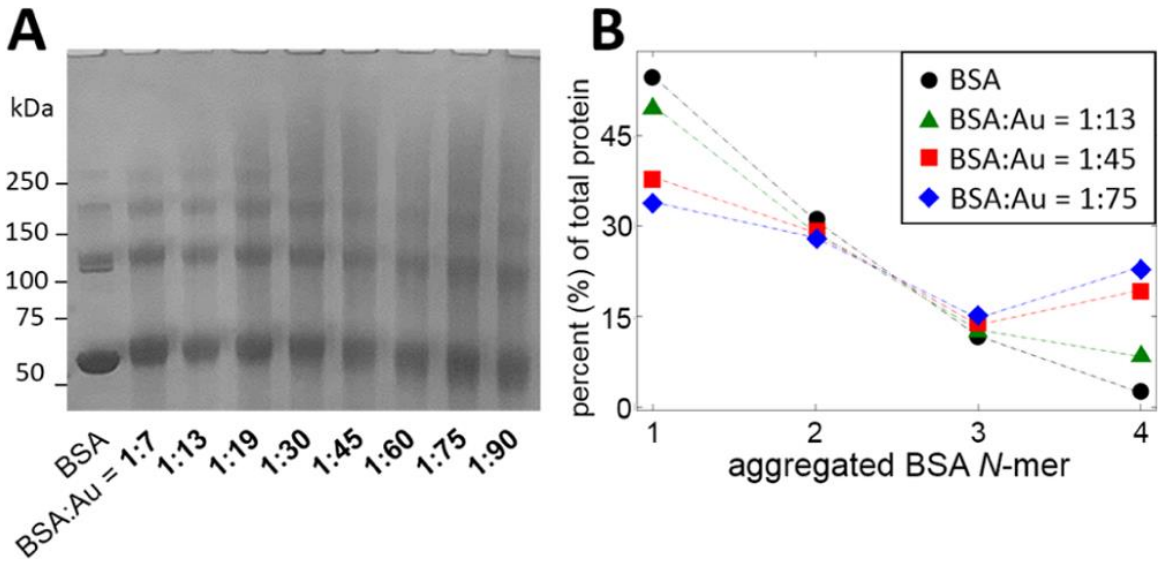

Figure 4. Au binding to BSA surface can cause aggregation of BSA. (A) From left to right: BSA-alone, BSA-Au complex with the BSA-to-Au ratio = 1:7, 1:13, 1:19, 1:30, 1:45, 1:60, 1:75, and 1:90, at 2 h. (B) Fraction of aggregated multimer (N-mer) BSA increases for higher Au concentrations.

respectively, and results in different measured intensities (counts per second, CPS) when measuring the same sample. Ultraviolet-visible (UV-Vis) absorbance spectra were collected the same for all samples using a 0.5 nm increment in wavelength.

3.2 Nonspecific Binding of Au to the BSA Surface.

The identification of the mechanism responsible for the formation of the red luminescent fluorophore in the BSA-Au complex is a crucial step toward the understanding of the mechanism for the large Stokes shift observed. Along with this, elucidating the mechanism of fluorophore formation will reveal the energy transfer process and potentially the local charge transfer that may be responsible for luminescence.[79,80]

Initial studies on the BSA-Au complex revealed that the red fluorophore appeared to be associated with Au binding at or near one of the nine Cys-Cys disulfide bond sites within the protein.[13] Thus, the first step was to additionally verify the role of cystine(s) or cysteine(s) utilizing common disulfide bond-cleaving agents. The use of dithiothreitol

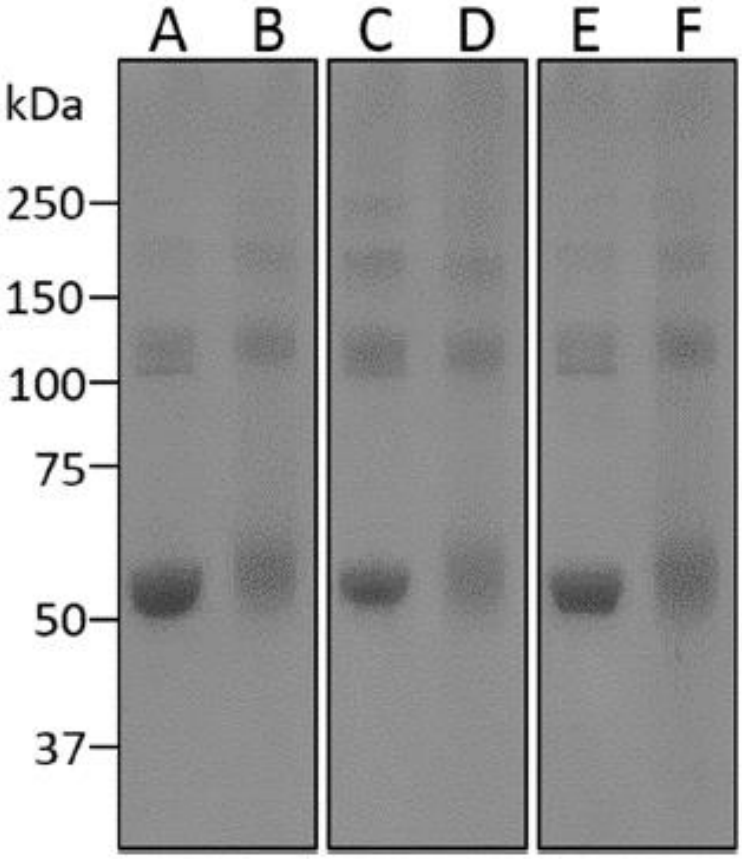

Figure 5. Comparison of the commercially available BSA's with different purities (all proteins are fraction V) and the synthesized BSA-Au complexes. (A) BSA (used in the present experiments and investigation), heat-shock-fractionated, lyophilized powder, essentially IgG free, ≥96%. (B) BSA-Au complex (BSA : Au = 1 : 10) synthesized with lane A. (C) BSA, ethanol- and heat-shock-fractionated, lyophilized powder, essentially fatty acid free and essentially globulin free, ≥99%. (D) BSA-Au complex (BSA : Au = 1 : 10) synthesized with lane C. (E) BSA, heat-shock-fractionated, 30% in saline IgG free, aseptically filled. (F) BSA-Au complex (BSA : Au = 1 : 10) synthesized with lane E. All BSA's were used as received and showed aggregation with the gel protocol used (without DTT or TCEP). Dimer (66.4 × 2 = 132.8 kDa) and trimer (66.4 × 3 = 199.2 kDa) bands were consistently observed with all the commercial BSA samples tested.

(DTT) as a disulfide cleaving agent readily quenched the red luminescence of the already-formed BSA-Au complex (**Figure 3**). The quenching of red luminescence was also observed by using tris(2-carboxy-ethyl) phosphine (TCEP) at 20^{o}C.

TCEP is another disulfide-cleaving agent, stronger than DTT and can readily cleave all disulfides within a protein. Disulfide bond cleaving with DTT requires an addition of

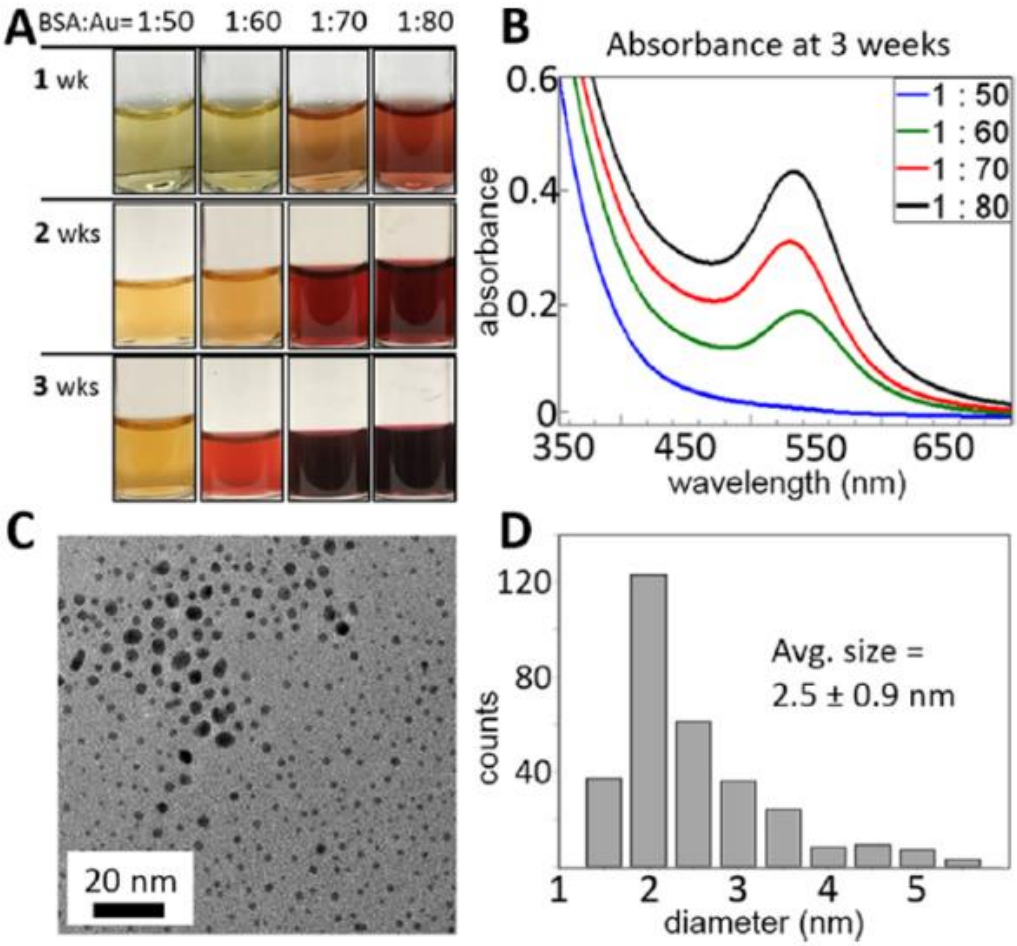

Figure 6. Surface-bound Au-mediated aggregations of BSA result in Au nanoparticle formation at BSA-to-Au molar ratios higher than ~1:60. (A) Ruby-red color indicates formation of Au nanoparticles at high Au concentrations. (B) Surface plasmon peak at λ = 520 nm confirms the presence of Au nanoparticles. (C,D) TEM image and size analysis of the Au nanoparticles (BSA:Au = 1:80 at ~2 weeks).

1% SDS and incubation at 37°C for the quenching of red luminescence. In each case, the use of TCEP or DTT resulted in the loss of luminescence and illustrates the necessity of Au binding at or near an intact disulfide bond(s) within BSA.

In addition to the three specific binding sites of Au in BSA that have already been identified (1) Cys-Cys disulfide bond, (2) Cys34, and (3) Asp-fragment at the N-terminus there is also the consideration of non-specific Au adsorption on the BSA surface by van

der Waals forces. The surface-bound Au on BSA may lead to the aggregation of BSA with itself by the Au bridging two or more BSA molecules together. Such a process of Au-mediated aggregation was further exacerbated by an increase in the Au concentration in solution. Thus, gel electrophoresis of BSA-Au complexes that were prepared with a broad range of Au concentrations indeed shows aggregation of BSA at only 2 hours post-synthesis (**Figure 4**). The addition of higher Au concentrations relates to the formation of higher ratios of dimers, trimers, and higher ordered N-mers of BSA. There were significant amounts of dimers and trimers in the BSA-alone lane of the gel as well. This natural aggregation of BSA without the addition of Au is likely due to the protocol for preparing the gel which omits DTT. The omission of DTT as is normally performed results in natural dimerization of BSA with its free cystine34 residue with another cystine34. Conducting the same gel electrophoresis experiments on other commercially available BSA samples of different purities shows the same result (**Figure 5**).

Thus, it appears the presence of multiple nonspecific Au binding sites to the BSA surface must be considered, in addition to the binding of Au at the specific sites when resolving the binding process of Au to the luminophore site. Regardless, this binding is an extremely slow process. The nonspecific surface binding of Au on BSA induced further surface-mediated aggregation and eventually lead to the formation of nanoparticles. The formation of nanoparticles when synthesizing BSA-Au at high Au concentration was confirmed by both the TEM and by surface plasmon peaks in absorption spectra (**Figure 6**). The formation of nanoparticles was particularly prevalent when synthesizing BSA-Au complexes at a BSA-to-Au ratios of 1:60 and greater.

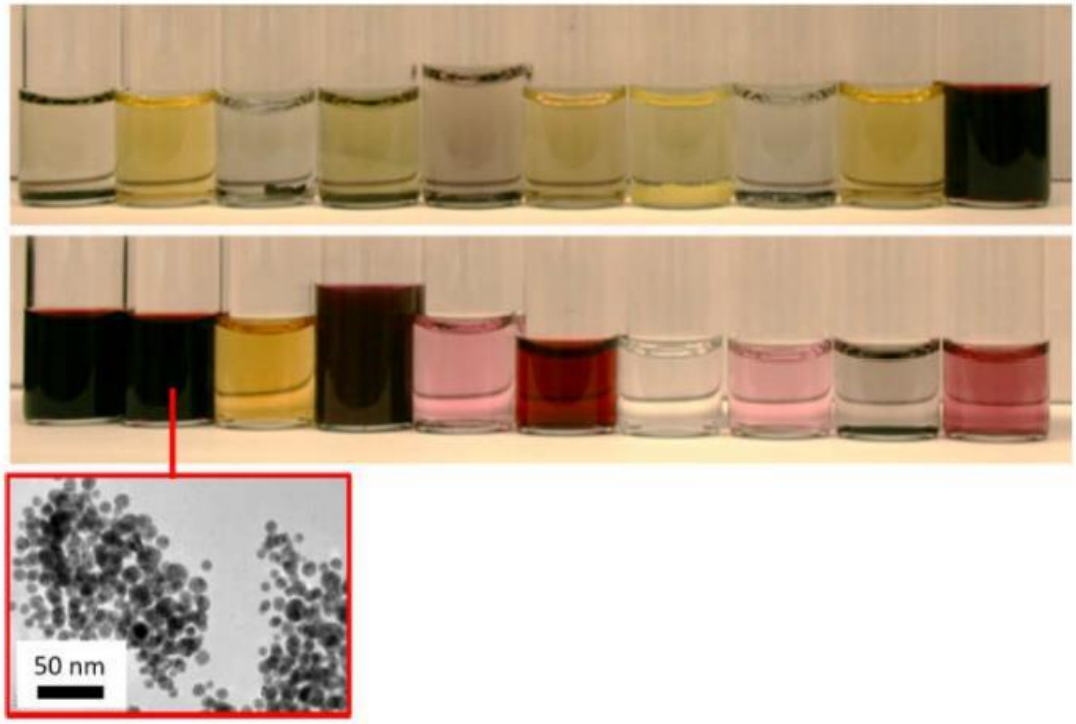

Figure 7. Reactivity of individual amino acid residues in the synthesis of BSA-Au complex. HAuCl4 was mixed with the twenty common amino acids individually, followed by the pH adjustment to 12, mimicking the synthesis of BSA-Au complex with BSA-to-Au molar ratio = 1 : 13. The total number of amino acid residues in BSA is 583. An individual amino acid (with *X* residues in BSA) was mixed with HAuCl4, with the amino acid-to-Au molar ratio = $\frac{X}{583}$: 13. For example, there are 35 Cysteine residues in BSA: therefore, Cysteine was mixed with HAuCl4 with the Cys-to-Au molar ratio = $\frac{35}{583}$: 13.
The ruby-red color of the solution indicates the formation of Au nanoparticles. TEM image of tyrosine-Au nanoparticles shown as a representative.
Top, left to right: Isoleucine, Leucine, Proline, Valine, Aspartic Acid, Glutamic Acid, Arginine, Methionine, Alanine, Glycine.
Bottom, left to right: Tryptophan, Tyrosine, Histidine, Lysine, Serine, Phenylalanine, Cysteine, Threonine, Asparagine, Glutamine.

While the current experiments do not go into detail on the reduction process of Au(III) into Au(0), it is possible that the side chains of surface-exposed amino acid residues within BSA could act as weak reducing agents, especially in highly basic pH conditions. This reduction is, in principle, possible by mixing 20 amino acids individually with $HAuCl_4$ at a pH of 12 (**Figure 7**). From this mixing of amino acids, eight amino acids (glycine, tryptophan, tyrosine, lysine, serine, phenylalanine, threonine, and glutamic acid) reduced

Au(III) and formed stable nanoparticles, while six amino acids (isoleucine, proline, asparagine, methionine, cysteine, and asparagine) resulted in large and precipitated Au(0) aggregates. The remaining six amino acids did not reduce Au(III) to Au(0).

The formation of Au nanoparticles at the higher BSA-to-Au molar ratios at and above 1 : 60 were observed to occur within 1 to 3 weeks when left at room temperature. The Au nanoparticle formation was observed to be accelerated at higher temperatures for example when keeping the BSA-Au 1 : 80 reactions at 37^{o}C constantly, nanoparticles formed within just 4 days. Furthermore, samples synthesized at ratios greater than 1 : 30 but less than 1 : 60 appeared to have their red luminescence suppressed while no nanoparticle formation was observed even after several months. This suppression of protein luminescence may be due to the excess of surface-bound metal cations and has been observed in other work for systems containing Cu and Ni, and since there are not a great enough excess of metal cations, nanoparticle formation may not take place.[81] Additionally, once the metal Au nanoparticles are formed due to aggregation, fluorescence of the remaining BSA-Au complexes and their luminescence could be effectively quenched due to nonradiative decay.[82]

3.3 Kinetic Model for BSA-Au Complex Formation.

Incorporating the nonspecific surface binding with the known metal binding sites, a model can be generated to help explain the process and mechanism of the BSA-Au complex formation and the generation of the luminophore. When the BSA-to-Au molar ratio was varied between 1 : 1 to 1 : 60, the intensity of the red luminescence, measured after 48 hours, was higher as the concentration of Au was increased This increase relative to Au concentration was only for a ratio between 1 : 1 and ~ 1 : 25 (**Figure 8**). The intensity

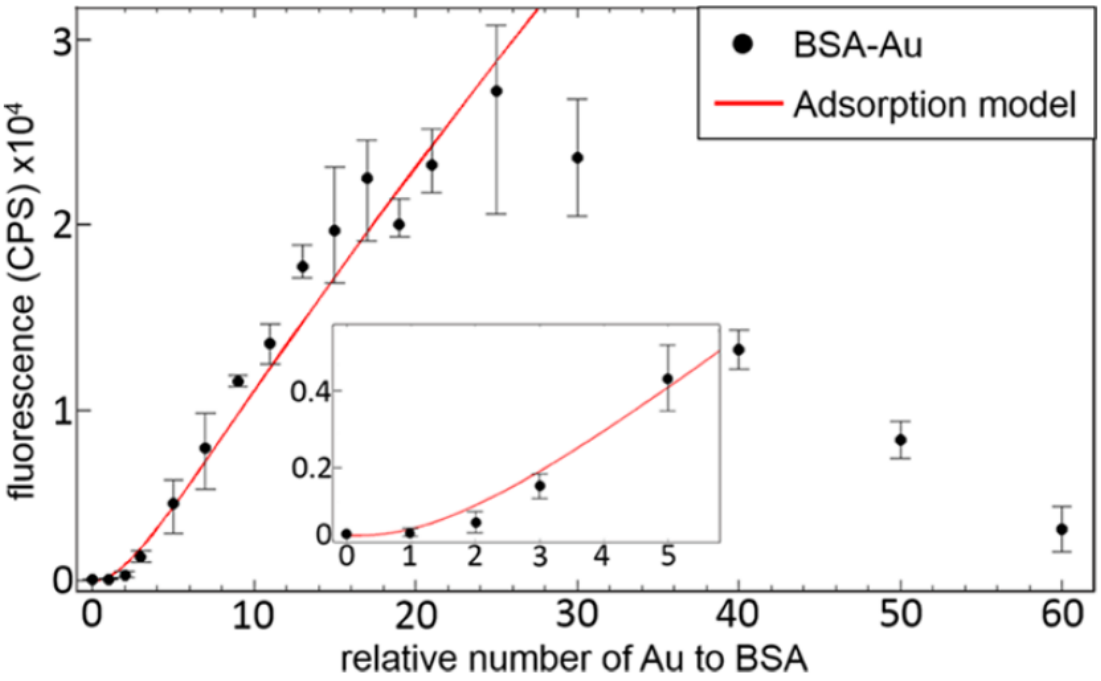

Figure 8. The red fluorescence ($\lambda_{ex}/\lambda_{em}$ = 470/640 nm) intensity of BSA−Au complexes measured at 2 days, with the BSA-to-Au molar ratio in the range of 1:1 and 1:60. The fitted curve is based on the Langmuir-type adsorption model, assuming a number of surface binding sites on BSA as N = 125. The inset is zoomed into the BSA-to-Au molar ratio < 1 : 6.

of red luminescence was suppressed as the Au ratio was increased further beyond 1 : 25. Due to the large abundance of surface-bound Au causing quenching via non-radiative decay and through nanoparticle formation at even higher Au concentrations.[13,81] The fluorescence intensity was also non-zero, even at a BSA-to-Au molar ratio of 1 : 1, indicating that a very small amount of Au, stoichiometrically is required for the formation of the red luminescent complex.

To describe the observed dependence of the fluorescence intensity, a new kinetic model based on the adsorption of Au to multiple sites on BSA can be postulated. This new adsorption model can then be compared to one assuming the single-site nucleation model for neutral Au nanoclusters – a model that has been first suggested by others and is discussed in further detail later below.[12] When comparing how well each model predicts

the luminescent intensity relative to Au atoms, will reveal which method of red luminescence generation is more likely.

To start a Langmuir-type multiple-site adsorption model can be constructed,[83-85] considering that Au will act as the adsorbate. The Au binding sites that have been identified in prior studies and current experiments can be considered into the model. In this model it will be considered that each site will accept a single Au independently (which is a Langmuir-type adsorption). This assumption is considered reasonable as no multilayer adsorption characteristics were present in **Figure 8**.[86] These specific Au binding sites namely are the Asp-fragment, located at the N-terminus of BSA, the Cys34 site, the Cys-Cys disulfide bond that may be responsible for red luminescence, and the N number of surface-bound non-specific binding sites for Au. It is also considered that only the Cys-Cys disulfide bond site is responsible for any red luminescence formation. For non-specific surface binding to BSA, it is also assumed that these sites are independent adsorption sites and do not influence each other. Based on the globular size of BSA[87] (~5.5 nm) and the size of an Au atom (~0.2 nm), it can be assumed that there are $N = 125$ surface adsorption sites to consider. Thus, it is considered that there are a total of 128 binding sites within the protein.

While the exact affinities of all these Au sites are not exactly known, approximate values for their affinities can be estimated, including the Au-to-disulfide, Au-to-thiol, and the van der Waals force for surface binding.[88,89] For both the Au-to-disulfide and Au-to-thiol the binding energy can be estimated at $E_0 \sim 400$ kJ/mol and the van der Waals force can be estimated at $E_s \sim 0.01\ E_0$. Using the experimental results of competitive binding of Au to BSA at the Asp-fragment (Cu > Au > Ni), the estimated binding energy of Au-to-

Asp-fragment can be considered as $E_A \sim 0.5\ E_0$. Thus, assuming these Au-to-binding site affinities the expected red fluorescence intensity of the sample *I* can be assumed to be proportional to:

$$I \sim \frac{x^{1+1+0.5+0.01N}}{Z} \quad (1)$$

where the grand canonical partition function, is represented by *Z*,

$$Z = (1+x)^{1+1}(1+x^{0.5})(1+x^{0.01})^N \quad (2)$$

Since μ is the chemical potential of an adsorbed molecule the grand canonical partition function can be simplified and take the form of a binomial series. The simplified form of the partition function is shown in equation (2) above. Where $x = \lambda \exp[E_0/k_BT]$ and is representative of the canonical ensemble of all adsorbents adsorbed. Furthermore, $\lambda = \exp[\mu/k_BT]$ and is representative of the partition function of a single adsorbed molecule. Because of this, once simplified, *x* will only be dependent on the change in temperature of the reaction as the adsorption energy, E_0, and chemical potential, μ, will be considered a constant. For the sake of some rigor, μ will also be considered the same value for both free Au and adsorbed Au.

This Langmuir-type multiple-site adsorption model reproduced the general trend of the increased fluorescence intensity according to the Au adsorbate concentration before the fluorescence suppression took effect at higher BSA-to-Au concentrations above 1 : 30. The loss in luminescence again, is likely due to the formation of Au nanoparticles and multilayered adsorption of Au, which does not fit in the scope of the single-site Langmuir-model. Nevertheless, this Langmuir-type model ideally fits the increase in luminescent intensity and is also shown in **Figure 8** as the red curve.

3.4 Kinetics of Au Binding: pH Dependence.

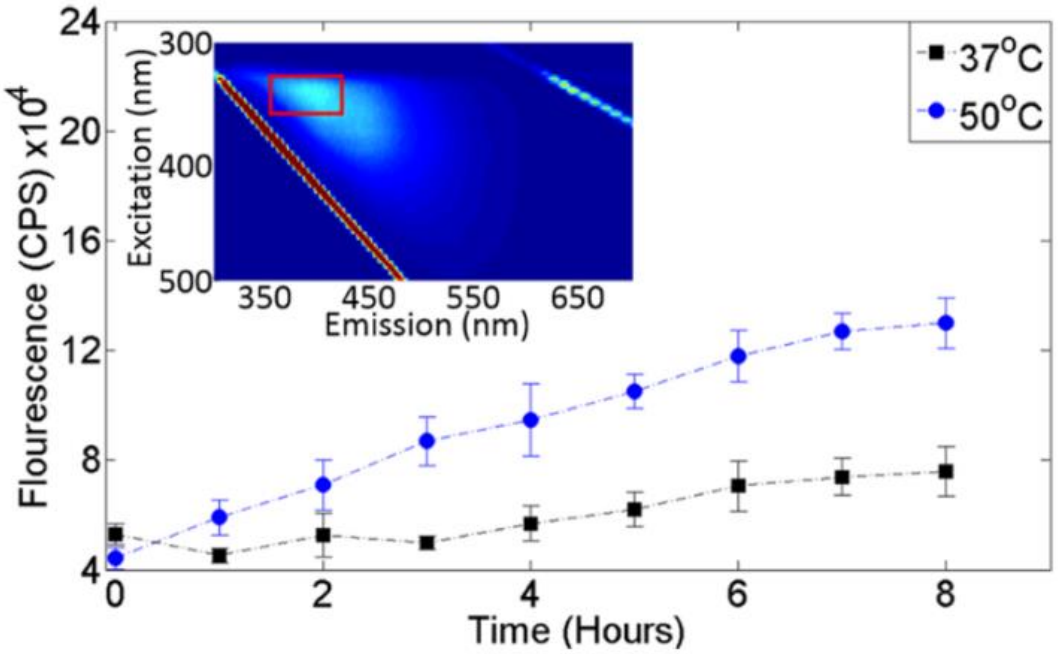

Figure 9. Temperature-dependent kinetics of the conformation change of BSA from neutral (pH = 7, N-form) to A-form at pH = 12.5. The blue fluorescence peak, a characteristic of the A-form BSA, is plotted over the course of the conformation change from N-form toward A-form. The peak intensity was determined by excitation−emission scanning in the range of $\lambda_{ex}/\lambda_{em}$ = 325−365/350−420 nm (marked with a red box in the inset). The data points are connected with dotted lines for visual aid.

In the above adsorption model, BSA is treated as a static substrate, in which its shape and conformation remain unchanged, and the above Langmuir-type model does agree well with the experimental results. However, BSA undergoes a slow and dynamic conformational transition due to the alteration of pH during the reaction process. This conformational change could also possibly change the local environment for the individual adsorption sites. When adjusting pH in the outlined standard protocol, the pH changes from ~ 3.5 immediately after Au has been added and then to a highly basic pH above 12 after NaOH is added.

The intrinsic blue luminescence ($\lambda_{ex}/\lambda_{em}$ = 365 / 420 nm) of BSA at and above the pH of 10 is due to the conformational change of the protein from its N-form (which occurs between a pH of 4.3 – 8.0) to its A-form (above pH 10) by the changing of its local

environment of the UV-fluorescent aromatic amino acid residues which include tryptophan, tyrosine, histidine, phenylalanine, and proline.[90] This blue luminescence was monitored during the pH-induced BSA conformational change, and could be observed to increase steadily over the course of more than 8 hours (**Figure 9**).

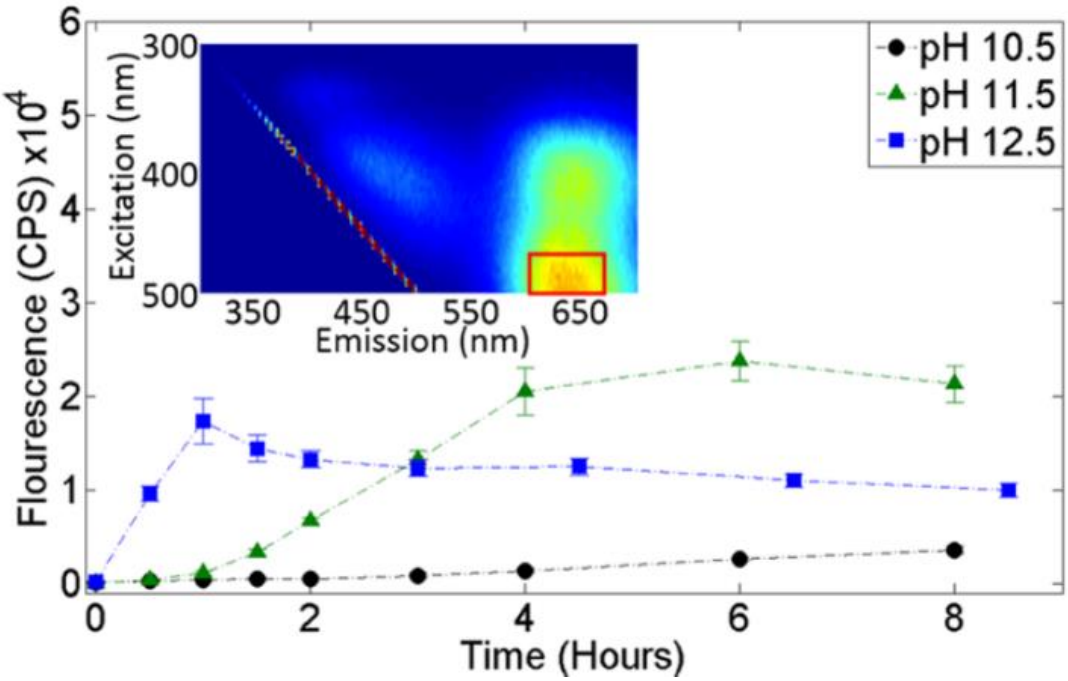

Figure 10. pH-dependent kinetics of the red fluorophore formation in BSA−Au complex, at the BSA-to-Au molar ratio of 1:13 and at a constant temperature of 37 °C. The red fluorescence peak intensity of the BSA−Au complex, determined by excitation-emission scanning in the range of $\lambda_{ex}/\lambda_{em}$ = 460−510/620−680 nm (marked with a red box in the inset) is plotted over the time course. The data points are connected with dotted lines for visual aid.

The $\lambda_{ex}/\lambda_{em}$ peak position of the blue-fluorescence, in the excitation-emission measurements seen in the insert in **Figure 9** also continue to shift slightly to longer wavelengths, both in excitation and emission. This shifting is consistent with the slow conformational change of BSA, which takes around 2 days in total to occur when leaving BSA at room temperature, altering the local environment of the fluorophore.[90] The conformational change-induced increase of the blue-peak intensity of BSA also occurred faster as the reaction was kept at higher temperatures.

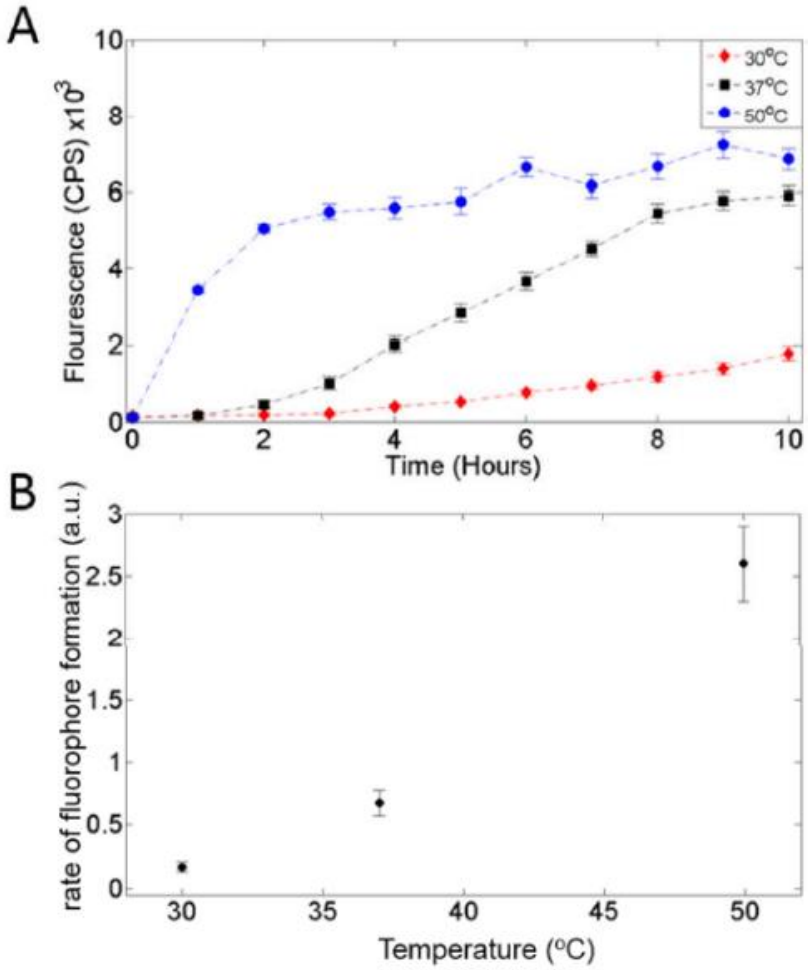

Figure 11. The temperature-dependent kinetics of the red fluorophore formation in BSA-Au complex, at the BSA-to-Au molar ratio of 1 : 7, and at a pH of 11.5. The red fluorescence peak of the BSA-Au complex is plotted over the time course.

The binding of Au is also expected to affect the conformational change kinetics of BSA, both sterically and electrostatically.[91] The general trend overall was that the rate of the red fluorophore formation in the BSA-Au complex was very sensitive to the change in pH and the rate of red fluorophore formation was highly dependent on an increase in pH. As the final pH of the reaction was increased red luminescence onset time was decreased (**Figure 10**). Because the pH-induced conformational change of BSA is an equilibrium transition, the rate of conformational change of BSA is also pH dependent, and the rate of exposing the fluorophore-forming Cys-Cys disulfide bond for solvent accessibility would

also be accelerated at a higher pH. Thus, the adsorption model is further consistent with the observed dependence of pH. Based on this analysis, it is still possible to consider that the nanocluster-nucleation model, assuming a specific Au nucleating space within BSA, could also be consistent. For this nucleation model to be true, the diffusive accessibility of Au to such a nucleation space would also have to be dependent on the BSA conformation.[92]

3.5 Kinetics of Au Binding: Temperature Dependence.

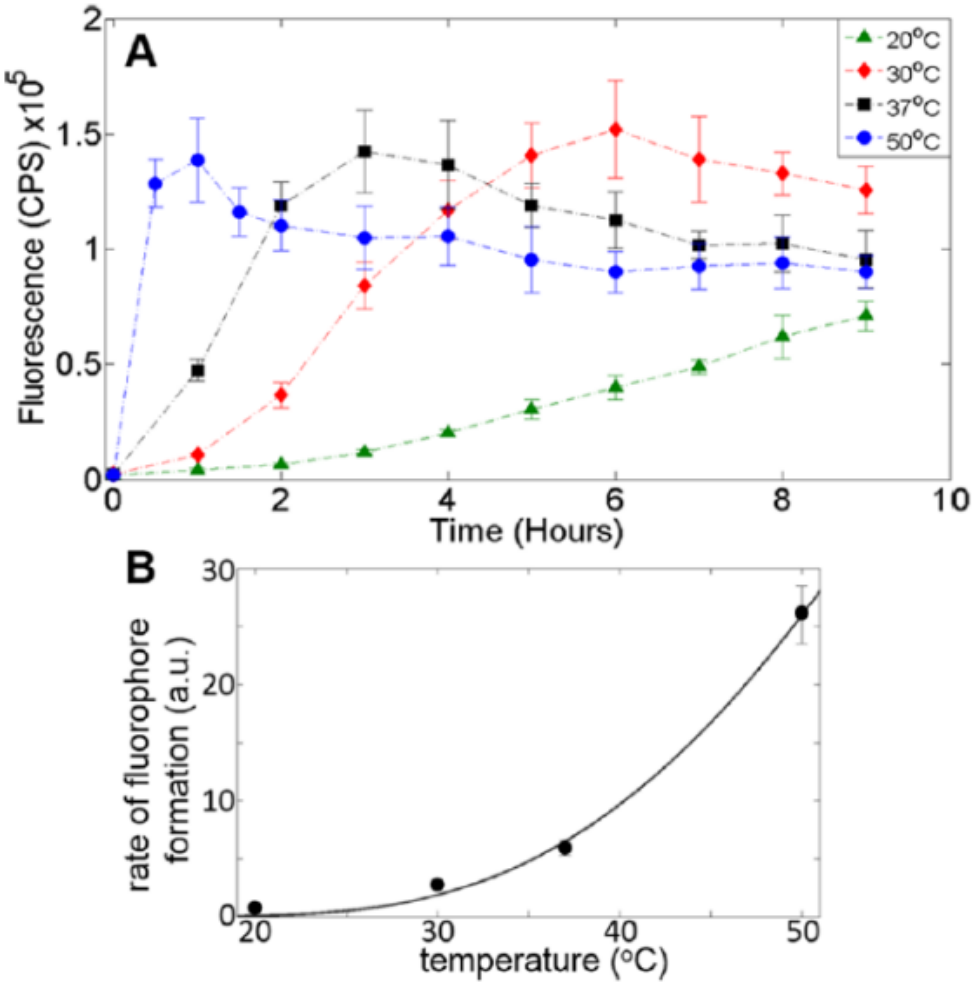

Figure 12. Temperature-dependent kinetics of the red fluorophore formation in BSA−Au complex, at the BSA-to-Au molar ratio of 1:13 and at a pH of 12.5. (**A**) Red fluorescence peak intensity of the BSA−Au complex is plotted over the time course. The data points are connected with dotted lines for visual aid. (**B**) Rate of fluorophore formation depending on the temperature. The fitted curve is based on the Arrhenius equation, $k = A \exp[-E_A/k_BT]$, where k, EA, and T are the rate coefficient, activation energy, and temperature, respectively.

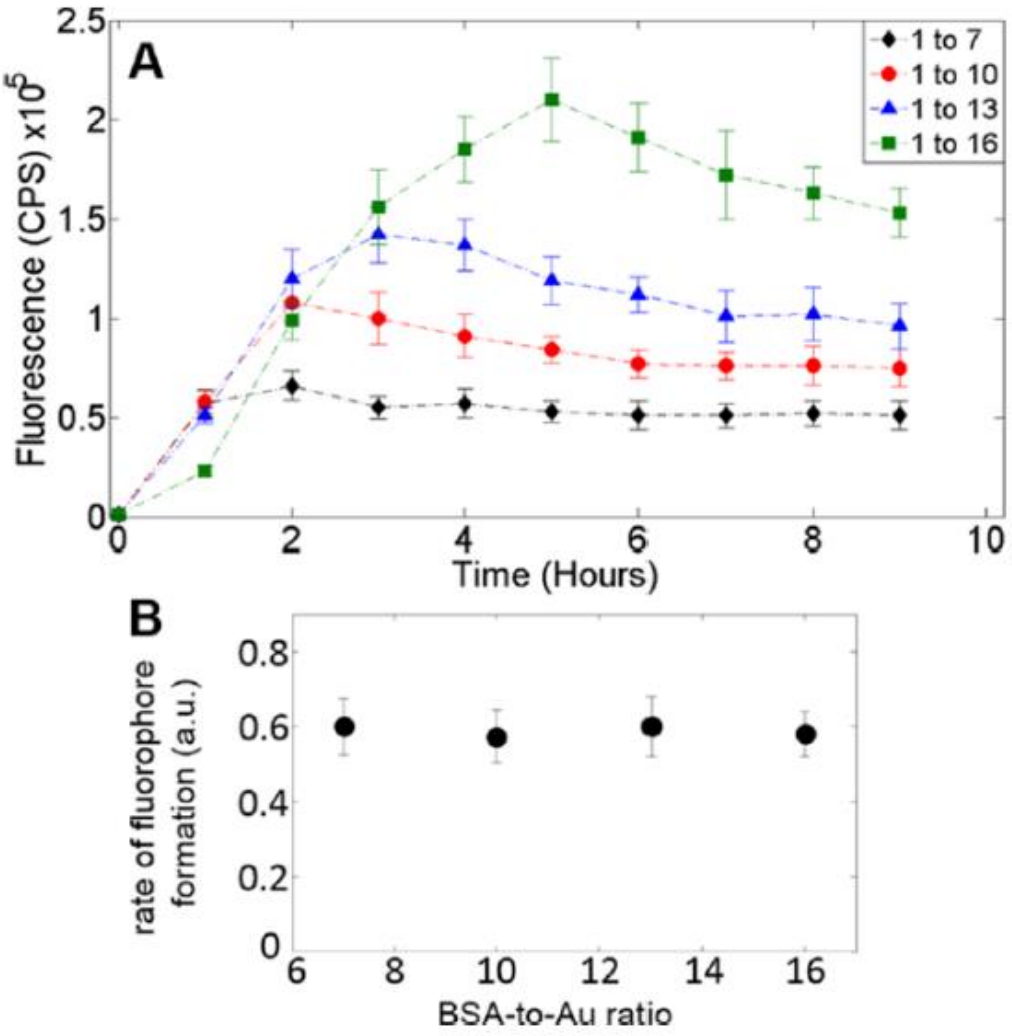

Figure 13. Kinetics of the red fluorophore formation in BSA−Au complex at a constant temperature of 37 °C and at a pH of 12.5, and the dependence on the Au concentration. (**A**) The red fluorescence peak intensity of the BSA−Au complex is plotted over the time course. The data points are connected with dotted lines for visual aid. (**B**)The rate of fluorophore formation depending on the Au concentration (BSA-to-Au molar ratio).

For the temperature-dependent kinetics of the red fluorophore within BSA-Au complexes, the BSA-to-Au ratio was kept static at 1 : 13 at a pH of 12.5 (**Figure 12**) as well as for the BSA-to-Au ratio of 1 : 7 at a pH of 11.5 (**Figure 11**). The temperature varied in the range well below 60°C to avoid the known irreversible denaturation of BSA, which occurs at these elevated temperatures. While the reaction can proceed at temperatures greater than 60°C and will result in the red luminescent complex, the conformation of BSA

may be further altered beyond the scope of these experiments. The kinetic rate of the fluorophore formation was also calculated from the slope of the emergence of the ensemble fluorescence intensity, which increased for higher temperatures (**Figure 12**).

This temperature dependence, measured with the fixed Au concentrations appears to favor the Langmuir-type adsorption model instead of the nanocluster-nucleation model. Thus, for a moment, consider a simple nanocluster-nucleation which contains *n* binders (Au) for *M* independent binding sites. Of these *M* binding sites each one contains *L* identical pockets, which represent the substrate (BSA). Based on this it can be considered whether these binders would tend to entropically favor being clustered at a single site (i.e., forming a nanocluster) or be more uniformly distributed.

Assume the energy of the binder binding to the substrate and the adhesion energy among the *n* binder is $-\omega$ and $-\varepsilon_n$, respectively. Then the canonical partition functions for the clustered and the distributed configurations are $(LM!/[n!(M-n)!]\cdot\exp[(n\omega + \varepsilon_n)/k_BT]$ and $(M^nL!/[n!(L-n)!]\cdot\exp[n\omega/k_BT]$, respectively. Thus, the clustered configuration favors forming in the temperature range below.

$$k_BT < \varepsilon_n \left(ln \frac{M^n L!(M-n)!}{L(L-n)!M!} \right)^{-1} \quad (3)$$

Using the expected number of binders and binding sites the temperature for a clustered formation is expected to be more likely for the lower temperatures (< 200 K), far below the lowest reaction temperature completed in the above experiments at ~293 K.

3.6 Kinetics of Au Binding: Concentration Dependence.

The time-course of the red fluorophore formation was measured at a range of Au concentrations at a constant pH of 12.5 and at a constant temperature of 37°C, within the Au concentration range that yields red luminescence. The rate of fluorophore formation

did not show any strong dependence on the Au concentration but did change the time at which peak fluorescence was reached (**Figure 13**). This lack of dependence on the Au concentration can also be consistently explained via the Langmuir-type multiple-site adsorption model. As the rate is strongly dominated by a physisorption to multiple, individual sites,[93] but overall the rate of fluorophore formation is limited by the chemical process between Au and the amino acid residue(s) at one of the sites. Thus, regardless of

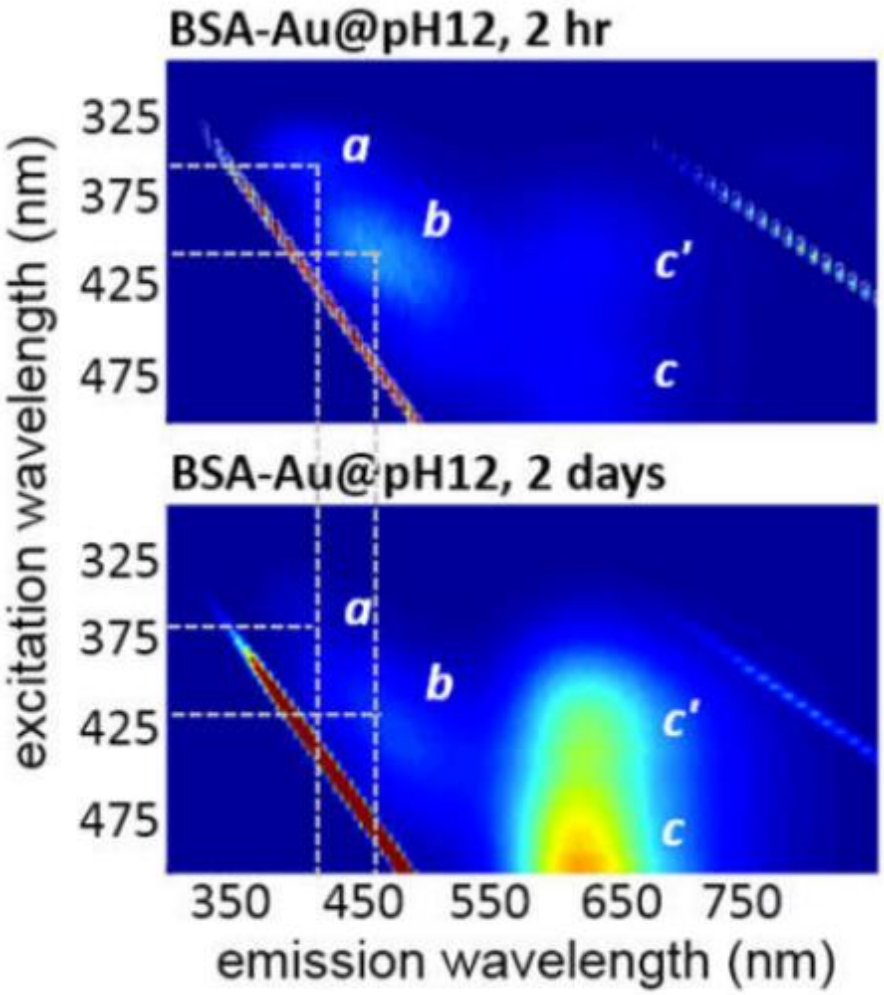

Figure 14. The cascaded energy transfer within BSA-Au complex. The peaks at λ_{ex} /λ_{em} = 370/400 nm (peak *a*); 400/460 nm (peak *b*); 400/640 nm (peak *c'*); 470/640 nm (peak *c*) suggest the possible energy transfer pathways, $a \rightarrow b$, $a \rightarrow c'$, and $b \rightarrow c$.

the amount of Au, the chemical interaction to form the Au-to-amino acid bond still requires the same energy.

In contrast to the Langmuir-type model, the single-site nanocluster-nucleation model does not explain the observed weak dependence on Au concentrations. Since an increase in Au concentration should relate to complex formation by increasing the rate of complex formation when Au concentration is increased. The well-known LaMer's diagram provides a conceptual description of the process of nucleation and growth, and this strong dependence of this process on concentration has been outlined by others.[94]

More recently, the general theory of nanocluster nucleation can be modeled and related to the BSA-Au system.[95-98] Firstly, one can consider an open system with some small volume, *v* (which is situated around the nucleation site), within a larger but isolated system with at a constant temperature, *T*, and a chemical potential, μ. The reversible work, *W*, which is required to create a critical nucleus inside this open volume, *v*, is determined by the rate of nucleation, *J*, where $J = J_0 \exp[-W/k_B T]$. This rate, *J*, can be related to the global concentration or equivalently to the number of Au, N_{Au} in the open system at a constant temperature. This is the nucleation theorem and can be estimated and represented by the following equation:

$$\left(\frac{\partial \ln J}{\partial \mu}\right)_{T,v} = \left(\frac{\partial ln J_0}{\partial \mu}\right)_{T,v} - \frac{1}{k_B T}\left(\frac{\partial W}{\partial \mu}\right)_{T,v} \approx \frac{1}{k_B T} N_{Au} \qquad (4)$$

Thus, the rate of nanocluster nucleation appears to be strongly dependent on the concentration of Au in this closed system. The same should then be true in the case of a nanoparticle nucleating within a free space of BSA, which is acting as the substrate. Yet in the case of BSA, the free energy of the system would be lowered by some factor *f*, which is determined by the contact angle of nucleating cluster on the substrate.[99] This arbitrary

term still does not change the fact that for the fluorophore to be an Au-based nucleating nanocluster, the rate of fluorescence formation must increase as the concentration of Au increases. This of course cannot be seen in **Figure 13B**, as the rate of fluorophore formation overall remains constant. With this, it is thus more realistic to assume nanocluster nucleation is not the mechanism of fluorophore formation and assuming a single Au adsorbing to the fluorophore site and multiple other dispersed sites appears more likely.

The kinetics of the red fluorophore forming BSA-Au complex were investigated by measuring the time-course of the fluorescence intensity of the $\lambda_{ex}/\lambda_{em}$ = 470 / 640 nm peak in the excitation-emission spectra. Over the time-course of the experiment it was found that the position of this peak shifted slightly (around 10 nm) toward longer wavelengths both in excitation and emission. Completing the excitation-emission mapping was found to be more accurate in determining the overall peak luminescent intensity, compared to taking single excitation fluorescence measurements due to this peak shifting. It was previously determined that a cascaded energy transfer mechanism involving multiple fluorophores lead to the generation of red fluorescence from the BSA-Au complex (**Figure 14**).[13]

The fluorophores for this cascaded energy transfer are λ_{ex} /λ_{em} = 370/400 nm (peak *a*); 400/460 nm (peak *b*); 400/640 nm (peak *c'*); 470/640 nm (peak *c*). In general, a detailed study of all these fluorophores and their dynamics under different reaction conditions would need to be studied to fully understand the kinetic processes of the red luminescent BSA-Au complex formation. Using the above results which analyze, in detail, peak *a* and peak *c*, the generation of the red fluorophore can be speculated. This involves the reduction of the starting Au(III) to either Au(0) or Au(I) through the interaction of the Au with the thiol(s) at or near the Cys-Cys disulfide bond binding site as well as some type of ligand-

to-metal or metal-to-ligand charge transfer.[100,101] Overall, a more detailed study is required to confirm this.

These experiments have also shown that a significant degree of nonspecific Au binding on the BSA occurred based on results using native gel electrophoresis techniques. The 'smearing' of the gel bands when adding in more Au to BSA, making each individual band less well-defined shows this nonspecific binding effect. Nearly the same degree of smearing was observed when adding the other metal cations of Cu and Ni to BSA to create non-red-luminescent BSA-Cu and BSA-Ni. Furthermore, the addition of SDS in the loading buffer, used to equilibrate charge in standard gel electrophoresis protocols or dialyzing the sample beforehand did not change the results of the gel samples. Other combinations of the gel including Bis-tris or Tris-glycine and the running buffer using Tris-acetate, Tris-glycine, or Tris-glycine-SDS also did not change the results of the gel. Overall, the higher concentration of metal cations caused nonspecific surface binding to BSA and resulted in the formation of more N-meres with greater degrees of gel smearing.

Proteins and protein-metal complexes, such as BSA and others may provide a more natural starting point as nanoscale-sized building blocks for functionalizing larger materials, as the current issue in traditional nanomaterial synthesis is the lack of monodispersed size distribution.[3] Assembling proteins and peptides into two-dimensional and three-dimensional-ordered structures is possible and BSA-Au may be a new starting point for these materials.[4-6,102,103] The conformational change of BSA plays a critical role the kinetics of Au binding, and is in fact, highly important in regulating many biological processes and are the targets of drugs in some treatments of disease.[104,105]

These experiments thus have detailed the kinetic and mechanistic studies of protein conformational change and ligand binding in the context of fluorophore-forming protein-metal complexes. It is proposed that a new Langmuir-type multiple-site adsorption model for the BSA-Au complex is more likely compared to the well-known LaMer-type model of a single-site nanocluster-nucleating Au complex. The results were consistent with the adsorption model, in which Au binds specifically to (1) the fluorophore-forming cysteine−cysteine disulfide bond site, (2) Cys34, and (3) Asp-fragment of BSA, and nonspecifically to many surface sites via van der Waals interaction. This has been determined by exploring the fluorophore formation of BSA-Au at a range of pH, temperatures, and BSA-to-Au ratios. Further exploration into the kinetics and mechanism of this complex could lead to highly precise tunable or adaptive functional nanomaterials. As other proteins complexed with Au have shown luminescent properties, exploration into a common binding motif may lead to this tunable or adaptive material and is the next step in uncovering the overall structure and mechanism of this red fluorophore complex.

CHAPTER 4: COMMON MOTIFS IN RED LUMINESCENT PROTIEN-GOLD COMPLEXES

BSA reacted at a highly basic pH above 10.0 with gold exhibits a strong UV-excitable red luminescence. Along with this red luminescence there appears to be a large Stokes shift from the innate blue luminescence of the protein. This large shift in fluorescence with the addition of gold may be attributable to the presence of fluorescent aromatic amino acid residues within the protein. Currently, two prevailing possible mechanisms of the formation of the red luminescence protein-Au complex have been suggested. In the first case it has been assumed that BSA acts as a cage to encapsulate and provide a scaffolding for the formation of a neutral Au_{25} nanocluster.[12] In this scenario the Au(III) are reduced by the surrounding tyrosine residues as they enter the protein and nucleate. The ability of tyrosine to function as a reducing agent is possible above pH 10.5 when tyrosine begins to deprotonate its side group. In the second scenario BSA is examined in a more dynamic way, allowing for the conformational shifts that happen within in the protein at higher pH to facilitate the formation of the red luminescent complex.[1,13]

In this second suggested mechanism, it was shown that a Langmuir-type chemisorption of single Au at a Cys-Cys disulfide bond sites was responsible for red luminescence and could reproduce the kinetic of the complex while attempts to fit kinetic results assuming the formation of a neutral Au(0) nanocluster did not work. Suggesting that conformational changes, brought on by pH adjustments were a key factor in the formation of the red luminescent complex.

The emergence of red luminescence upon the addition of Au, is not exclusive to just BSA and HSA. Other than for bovine serum albumin and human serum albumin, this

Table 1. The general traits of proteins that yield red luminescence, along with the general traits that do not yield red luminescence upon the addition of Au at alkaline pH. Proteins that are red luminescent upon the addition of Au are: BSA (bovine serum albumin), HSA (human serum albumin), ovalbumin, trypsin, and insulin (measured in the present work); lactotransferrin, pepsin, horseradish peroxidase, papain, and lysozyme (found in literature).
Proteins that do not yield red luminescence are: α-2-macroglobulin and trypsin inhibitor (measured in the present work).

Protein (PDB-ID)	Molecular Weight (kDa)	Primary Function	α-helix %	β-sheet %	random coil %	# of Cys residues	# of His residues	# of Tyr residues	# of Trp residues	# of Phe residues
BSA (4F5S)	66.4	transport	84.1	0	15.9	35	17	20	2	27
HSA (1AO6)	66.5	transport	77.0	0	23.0	35	15	18	1	31
Ovalbumin (1OVA)	42.7	storage	33.7	30.3	36	6	7	10	3	20
Trypsin (1S0Q)	23.3	enzyme	11.2	32.3	56.5	12	3	10	4	3
Insulin (4M4L)	5.7	hormone	60.4	5.7	33.9	6	2	4	0	3
Lactotransferrin (1LFG)	80	transport	40.8	22.1	37.1	32	9	21	10	30
Pepsin (4PEP)	37	enzyme	12.6	48.2	39.2	6	1	16	5	14
Horseradish Peroxidase (1HCH)	35	enzyme	53.1	2.2	44.7	9	3	5	1	20
Papain (1PPN)	24	enzyme	34.0	17.9	48.1	7	2	19	5	4
Lysozyme (1DPX)	15	enzyme	50.4	6.2	43.4	8	1	3	6	3
α-2-macroglobulin (4ACQ)	126	Protease inhibitor	18.7	31.6	49.7	23	31	45	11	52
Trypsin Inhibitor (1BA7)	16.3	Protease inhibitor	1.8	35.2	63.0	4	2	4	2	8

red luminescence has been reported for ovalbumin,[65] trypsin,[28] insulin,[29] lactotransferrin,[106] pepsin,[27] horseradish peroxidase,[30] papain,[107] and lysozyme.[26]

Thus, it is possible that red luminescence in protein-Au complexes could be more common than in these select few cases, and that a much larger set of proteins that share a similar feature may have the ability to be transformed into red luminescing complexes. Identifying the common red luminescent properties would aid in furthering the understanding of this red luminescent complex bound in some proteins and could further assist in determining other proteins that may be red luminescent but have yet to be discovered. While details into the kinetics of red luminescence have been studied

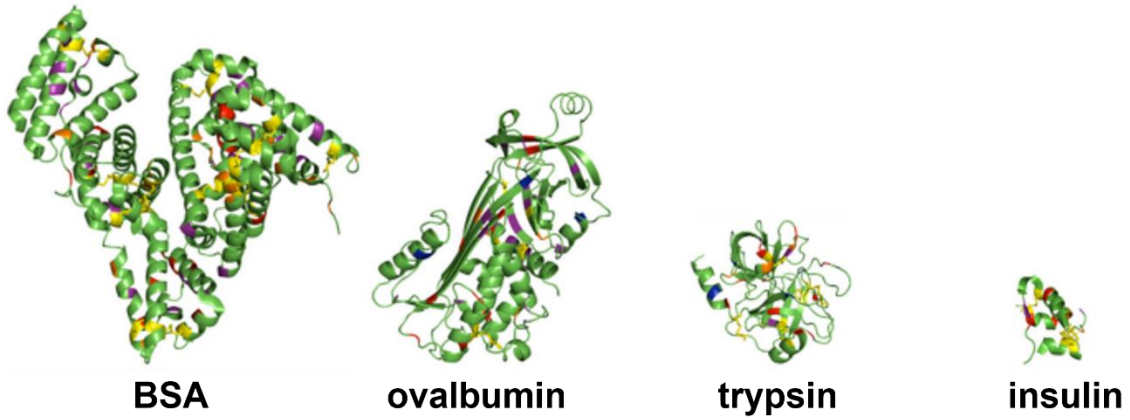

Figure 15. The crystal structures of BSA, ovalbumin, trypsin, and insulin monomer at a pH of 7. BSA (PDB ID: 4F5S), ovalbumin (1OVA), trypsin (1S0Q), insulin (4M4L) are depicted according to their relative sizes. BSA is a 66.4 kDa transport protein comprising 583 amino acid residues; ovalbumin is a 42.7 kDa protein (386 amino acids) that makes up most of egg white; trypsin is a 23.3 kDa (223 amino acids) protease; insulin (51 amino acids) is a 5.7 kDa hormone.
Cys residues are highlighted in yellow, with disulfide bonds indicated by yellow sticks. Aromatic residues are also highlighted in color: histidine = orange; tyrosine = red; tryptophan = blue; phenylalanine = purple.
BSA has 35 cysteine residues with one surface-exposed Cys34, in addition to one disulfide bond and eight Cys-Cys/Cys-Cys disulfide bond clusters that constitute the internal structural backbone: and 66 aromatic residues (17 histidine, 20 tyrosine, 2 tryptophan, and 27 phenylalanine).
Ovalbumin has six cysteine residues with one disulfide bond and four free cysteines, and 40 aromatic residues (7 histidine, 10 tyrosine, 3 tryptophan, and 20 phenylalanine).
Trypsin has 12 cysteine residues forming six disulfide bonds, and 20 aromatic residues (3 histidine, 10 tyrosine, 4 tryptophan, and 3 phenylalanine).
Insulin is comprised of two chains: A-chain and B-chain. It has 6 cysteine residues with one disulfide bond in A-chain and two disulfide bonds bridging the two chains: and 9 aromatic residues with no tryptophan (2 histidine, 4 tyrosine, and 3 phenylalanine).

intensively in BSA, it has not been done in other luminescent protein-Au complexes. This leads to a question of how these multiple proteins are related, and what do they have in common to yield the characteristic red luminescence.

4.1 Comparison of Luminescence Spectra in Protein-Au Complexes.

The initial findings of multiple red luminescent proteins are interesting, as each of these proteins are vastly different from one another, in both molecular weight, tertiary structures, and function (**Table 1**). For example, BSA and HSA are both approximately

Table 2. An analysis of the common primary amino acid sequences of the four red luminescent proteins. The analysis was performed between 2 proteins (BSA/ovalbumin; BSA/trypsin; BSA/insulin; trypsin/ovalbumin; trypsin/insulin; ovalbumin/insulin), and among 3 proteins (BSA/Trypsin/ovalbumin; BSA/trypsin/insulin; BSA/ovalbumin/insulin; trypsin/ovalbumin/insulin), and finally among all 4 proteins.
The analysis is summarized in the table: for example, BSA and trypsin have 16 common sequences of the length 3 (ASI; ASL; CAS; IKQ; KLK; KQT; LGE; LIK; LKA; NTL; QVS; SLI; TKV; VAS; VEG; VVS). No common sequence of length more than 2 exists in the four proteins, BSA, ovalbumin, trypsin, and insulin.

Comparing Common Sequences Between BSA, OVA, Trypsin, and Insulin

Sequence Length	BSA/ OVA	BSA/ Trypsin	BSA/ Insulin	Trypsin/ OVA	Trypsin/ Insulin	OVA/ Insulin	BSA/ Trypsin/ OVA	BSA/ Trypsin/ Insulin	BSA/ OVA/ Insulin	Trypsin/ OVA/ Insulin	BSA/ Trypsin/ OVA/ Insulin	Common Sequences
1	20	20	17	20	17	17	20	17	17	17	17	A; C; E; F; G; H; I; K; L; N; P; Q; R; S; T; V; Y
2	158	98	36	86	20	29	63	16	24	13	11	AS; EQ; GS; IV; KA; LE; QC; SL; VE; YL; YQ
3	41	16	7	13	3	2	1	1	0	0	0	--
	(AAD; AKD; ALA; DKL; EKL; EQL; ESL; EVS; FDK; FEK; FGD; FKD; FKG; ILN; ISS; KAF; KGL; KVH; KYN; LLP; LPD; LTE; LTS; LVL; LVN; PDE; PEY; QTA; RAD; SAL; SEK; SLR; SSA; SVL; TKP; TSS; VAS; VLL; VME; VSE; YLQ)	(ASI; ASL; CAS; IKQ; KLK; KQT; LGE; LIK; LKA; NTL; QVS; SLI; TKV; VAS; VEG; VVS)	(CAS; CCA; GER; HLV; LVE; NFV; PKA)	(AAH; AAS; GDS; GTS; INS; KDS; LIN; PIL; QIT; RVA; SGI; SGT; VAS)	(CAS; GIV; VCS)	(ASV; QLE)	(VAS)	(CAS)				
4	3	0	0	2	0	0	0	0	0	0	0	--
	(FDKL; FEKL; FKGL)			(LINS; RVAS)								
5	0	0	0	0	0	0	0	0	0	0	0	--

66.4 kDa with their role primary being to act as transport proteins, while ovalbumin (OVA) is a 42.7 kDa protein and is the primary protein in egg whites. Further comparisons of proteins that produce the red luminesced complex show even greater differences, such as trypsin, which is a 23.3 kDa protease and insulin which is only a 5.7 kDa sized protein and acts as a hormone (**Figure 15**). It is apparent that red luminescent protein-Au complexes are not bound to their size or function, and the reason why the red luminescence occurs in these proteins, with vastly different sizes, structures, and functions, has not been addressed.

It is important to resolve why proteins with vastly different defining characteristics still share a similar ability to produce a luminescent complex upon addition of Au. The

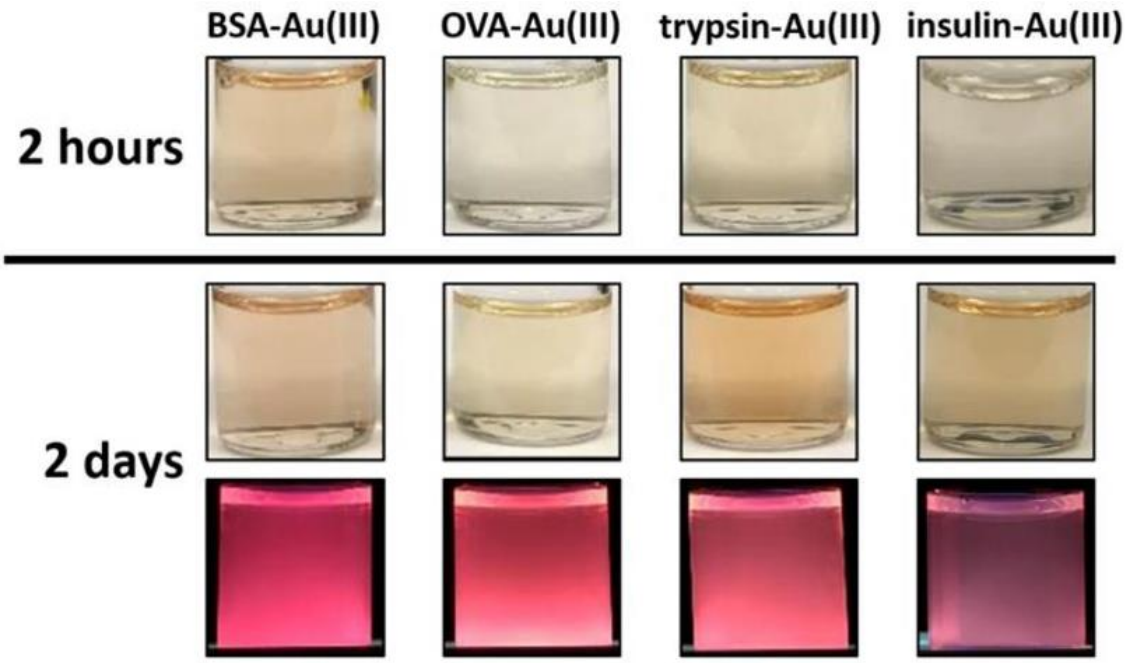

Figure 16. The visible appearance of BSA, ovalbumin, trypsin, and insulin all reacted with Au following the same standard protocol after 2 hours and 48 hours. The red luminescence of each sample is also shown after 48 hours (excitation 365 nm) and shows how each sample generates a similar luminescent color and intensity.

important comparisons to be made would be to look at primary, secondary, and tertiary structures of these proteins to reveal any commonalities between them. Determining what makes all these proteins similar could reveal a common motif that could be found in other, undiscovered proteins that share these luminescent abilities. Thus, an initial starting point to search for these commonalties would be by comparing the primary amino acid sequences.

If red luminescence in protein-Au complexes is the result of a particular amino acid sequence, aligning the sequence of all the proteins would reveal the binding site and common motif. When performing this primary amino acid sequence analysis on only BSA, OVA, trypsin, and insulin no common amino acid sequences with the length greater than two were found (**Table 2**). Indicating that the primary protein structure, or the organization of the amino acid sequence, does not play any significant role in the formation of the red

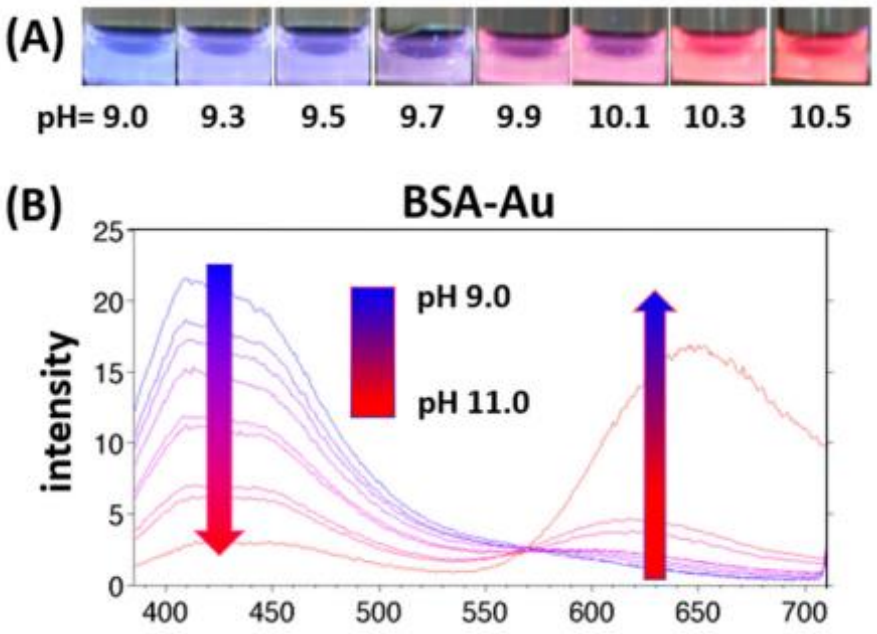

Figure 17. The pH dependence of red luminescence in BSA-Au complexes. The pH of BSA was finely adjusted above and below ~10 and the emergence of red luminescence was found to take place at and above a pH of 9.7 ± 0.2. This transformation coincides with the well-known conformational change in BSA to its 'aged' form (A-form) above a pH of ~9.6. As the pH increased, the innate blue fluorescence of BSA diminished as the red luminescence increased in intensity. The violet color under UV illumination around the transition pH, as well as the presence of the isosbestic point, suggested the coexistence of two species, consistent with the equilibrium transition of a BSA conformation.

luminescent complex, and higher ordered structures must be integral to the formation of the complex.

Conducting further detailed analysis of a set of proteins, including luminescent and non-luminescent proteins would aid in revealing a common binding motif. Before performing a comparative analysis of the protein secondary and tertiary structures, the luminescent spectra of some red luminescent protein-Au complexes must be examined in greater detail. While red luminescence after the addition of Au occurs in other proteins besides BSA and HSA, it has not been shown that the fluorescent spectral patterns or the kinetics of luminescent formation are the same. Thus, the first step in uncovering the common structure of all these proteins is to first confirm that the red luminescence that is

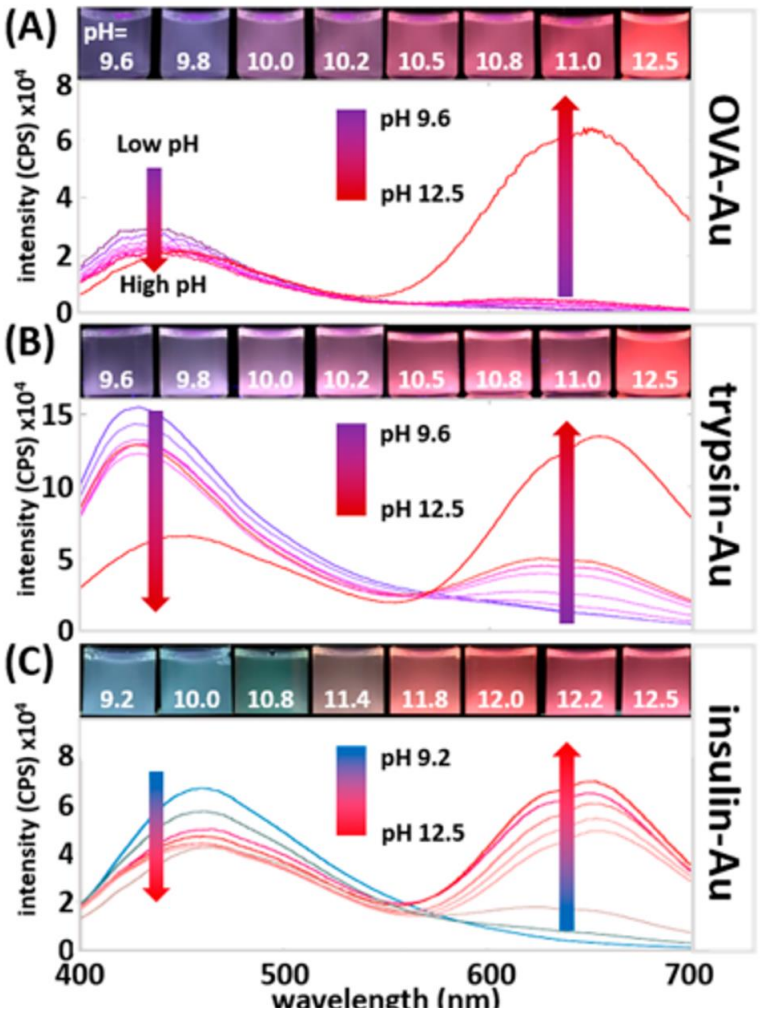

Figure 18. Luminescence (λ_{ex} = 365 nm) of protein−Au complexes synthesized at a range of pH around 10 and scanned at 48 hours. The emergence of red luminescence occurred (A) around pH = 9.9 ± 0.2 for ovalbumin, (B) pH = 9.8 ± 0.2 for trypsin, and (C) pH = 10.6 ± 0.4 for insulin. These values all closely correspond to values described in BSA-Au where red luminescence occurs at a pH of 9.7 ± 0.2.

formed occurs from the same mechanism. Without ensuring that the red luminescence of the other proteins is indeed from the same Au-based complex, a quantitative analysis cannot be employed.

We initially examined the luminescent spectra of ovalbumin, trypsin, and insulin and compared those results to the reports on red luminescent BSA-Au complexes. The initial experiment was first to recreate the complex using these different proteins to ensure

that the red luminescent complex did indeed form, following a similar protocol used to make BSA-Au. To form ovalbumin-Au, trypsin-Au, and insulin-Au a standard protocol was used for each protein.

Since the formation of BSA-Au starts with a solution of BSA at 376 μM (25 mg/ml) dissolved into HPLC-grade water each protein was dissolved in HPLC-grade water at the same molarity (ovalbumin = 16.1 mg/ml; trypsin = 8.8 mg/ml; insulin = 2.2 mg/ml). Into 1 ml of each protein solution, 1 mL of Au was also added at a concentration equal to 10 times the concentration of the protein or 3.76 mM (1.5 mg/ml). After 2 minutes of stirring each solution at room temperature 100 uL of 1 M NaOH was added to each solution to bring the pH to ~12-13. After adding in NaOH each solution, now containing both protein and Au were allowed to mix in a water bath heated to 37^{o}C for 2 hours, after which the now red luminescent protein-Au complexes were allowed to sit overnight at room temperature before analysis. All measurements were done after 48 hours of the complexes sitting at room temperature, and after this time no changes in the observable intensity of the luminescence were seen. The standard reaction resulted in the same visible red luminescence for each protein-Au complex (**Figure 16**).

After two days the emergence of red luminescence was analyzed within the three protein-Au complexes (ovalbumin-Au; trypsin-Au; insulin-Au) through three-dimensional excitation-emission fluorescent spectral scans. This included taking single, fluorescent spectral scans across a varied range of pH between neutral and basic to reveal any changes in luminescence due to changes in pH. In BSA-Au samples red luminescence does not emerge until around a pH of 9.6 and seems to coincide with a pH-induced conformational shift that occurs in the protein in highly alkaline conditions (**Figure 17**). For the ovalbumin-

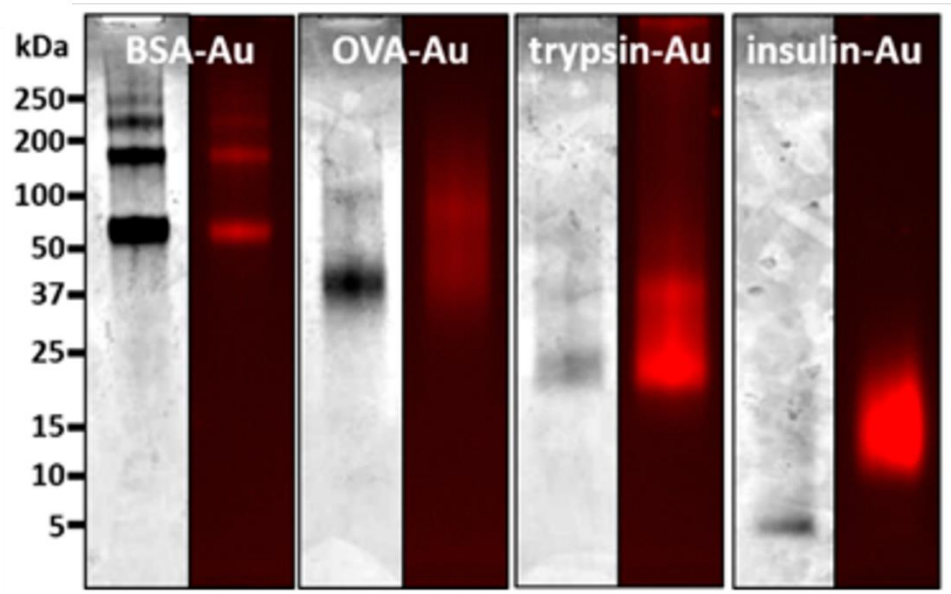

Figure 19. Native gel electrophoresis of the protein− Au complexes synthesized at a pH of 12 show that BSA, ovalbumin, and trypsin monomers yielded the red luminescence. For insulin, only the multimers (dimer ~ tetramer; 11.4 ~ 22.8 kDa) exhibited red luminescence while the insulin monomer at around 5.7 kDa was not red luminescent.

Au complex, red luminescence appears to have occurred at and above a pH of approximately 9.9 ± 0.2. The occurrence of red luminescence in trypsin-Au complexes appears to occur at and above a pH of 9.8 ± 0.2, and for insulin-Au complexes the pH at which red luminescence beings to emerge is around pH 10.6 ± 0.2. These results are displayed in **Figure 18**.

Further examination of the luminescence of each protein-Au complex across a broad range of pH values shows that a violet luminescence can be seen under UV illumination around the transition pH for each protein. This violet color suggests the coexistence of both blue luminescent and red luminescent species as red luminescence is formed for the blue luminescent proteins. Further analysis of the fluorescent spectral patterns of each protein-Au complex reveals an isosbestic point, which indicates a conversion of one state to the next and supports the idea that blue luminescence is indeed

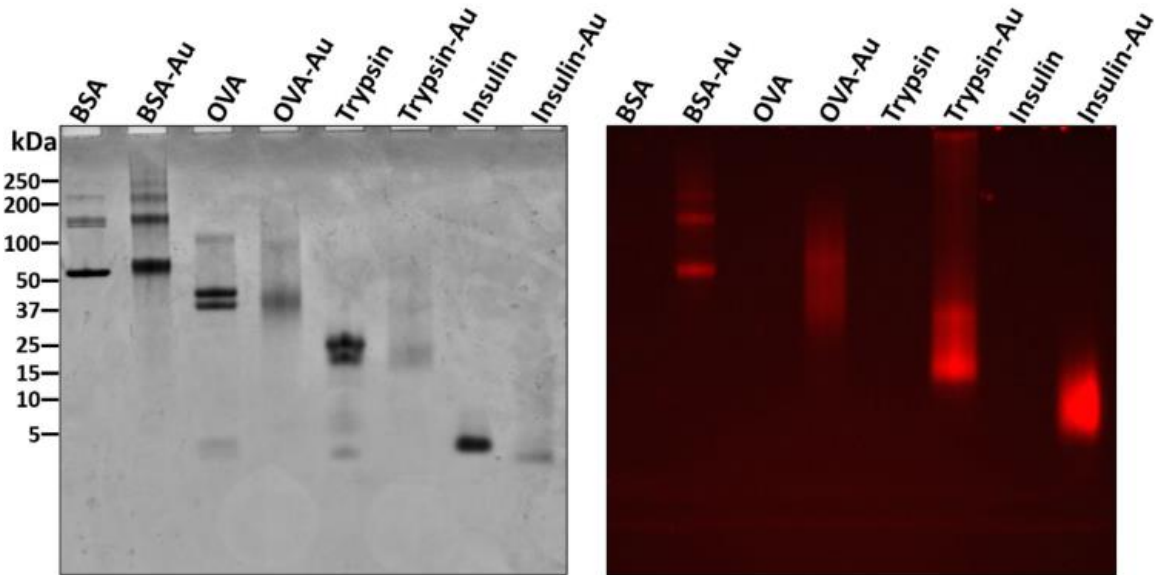

Figure 20. Full gels showing the in-gel luminescence of BSA-Au, ovalbumin-Au, trypsin-Au, and insulin-Au, including their controls. The native gel electrophoresis was performed without the addition of denaturants to avoid the cleaving of cystine disulfide bonds and preserve the red luminescent intensity. Thus, protein multimers are readily observed in the native gels.
For insulin alone, no significant degree of multimerization was observed. However, it is evident that the addition of Au causes multimerizations in the dimer to trimer weight regime.
For trypsin, several fragments are seen below the monomer weight due to sself-digestion of trypsin which can occur at high trypsin concentration in water.

transforming into the red luminescent complex. This isosbestic point can be seen in all the protein-Au complexes and is present in BSA-Au as well. Thus, these initial observations of red luminescence within these proteins could infer that the red luminescence in ovalbumin, trypsin, and insulin complexes is due to the same mechanism.

In the case of each synthesized protein-Au complex, the common pH was approximately ~10.0 for BSA, HSA, ovalbumin, trypsin, and insulin. Furthermore, each sample did yield a red luminescent complex with emission around 640 nm when excited in the UV at 365 nm, and the presence of an isosbestic point around 570 nm indicates that for all proteins an internal conversion occurs. This internal conversion of luminescence may be the result of the transition of the protein conformational state as changes in pH alter the three-dimensional structure of proteins.

In general, conformational changes in proteins occurs around pH values of ~10.[108] BSA has five well known conformational states which are primarily directed by the surrounding pH. In BSA a pH between 8 and 10 places the protein in its B-form while pH values above 10.0 change the conformational state of the protein to A-form. Similarly, it has been shown that ovalbumin undergoes a non-reversible conformational shift to an S-ovalbumin form when the pH is raised above 9.9[109] and trypsin undergoes a reversible conformational shift when the pH is brought above 10.[110] In the case of insulin however, a large conformation change also takes place in the protein, but in has not been determined in literature what the alkaline pH is for a conformational shift to occur.[111,112]

While each protein-Au complex shows similar visible luminescence and fluorescence emission spectra, there was one notable difference observed in insulin-Au. While the red luminescence of BSA-Au, ovalbumin-Au, and trypsin-Au all were found within the monomers of each of these proteins, insulin-Au was not red luminescent within its monomer. In the case of insulin-Au a dimer and/or trimer of the protein were required for the generation of red luminescence (**Figure 19** and **Figure 20**). It is likely that the multimerization of insulin was triggered by the addition Au. In Chapter 3 it was shown that the addition of more Au into BSA-Au complexes will result in greater distributions of dimers and higher ordered N-meres. A similar effect may be present in the formation of the red luminescent insulin-Au complex and thus the overall structure needed to create the luminescent complex in insulin-Au may look structurally different than other known multimers already found in insulin.

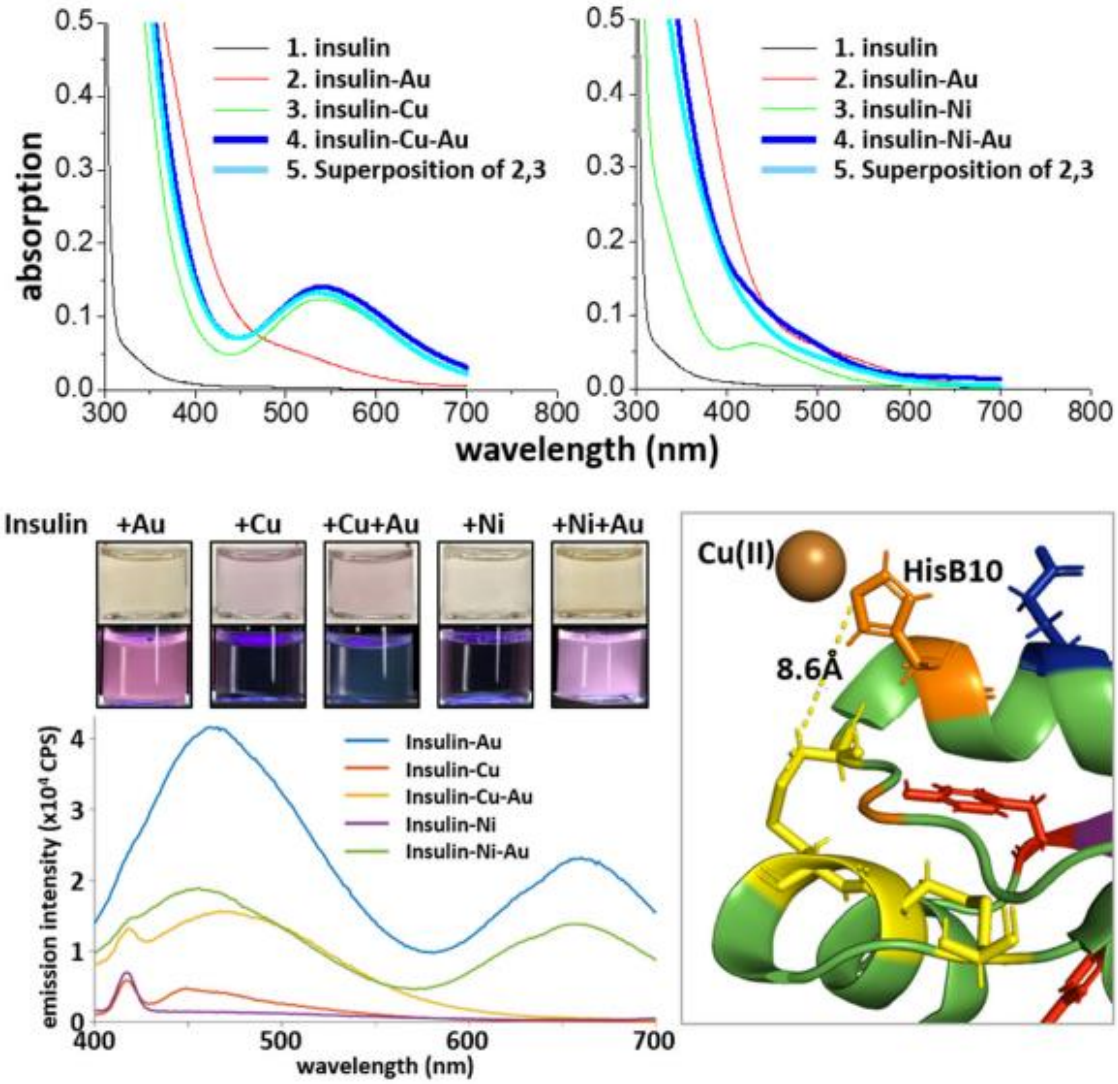

Figure 21. Insulin monomer has one known Cu(II) binding site coordinating histidineB10-glutamic acidB13 in B-chain, determined by X-ray crystallography. Competitive binding of Cu(II), Ni(II), and Au(III) via square planar coordination to this site was performed. Fluorescence spectra shows that both Cu(II) and Ni(II) binding to this site and the addition of Cu(II) appears to disrupt the binding of Au at the luminophore site. Absorption spectra of insulin-Cu(II)-Au(III) and the superposition of insulin-Cu(II) with insulin-Au(III) were identical, indicating Cu(II) is not displaced by Au(III) at this site. While spectra comparing insulin-Ni(II)-Au(III) to the superposition of insulin-Ni(II) and insulin-Au(III) are different, suggesting the displacement of Ni(II) by Au(III). These observations overall show that histidineB10-glutamic acidB13 in B-chain is near the red luminophore-forming site.

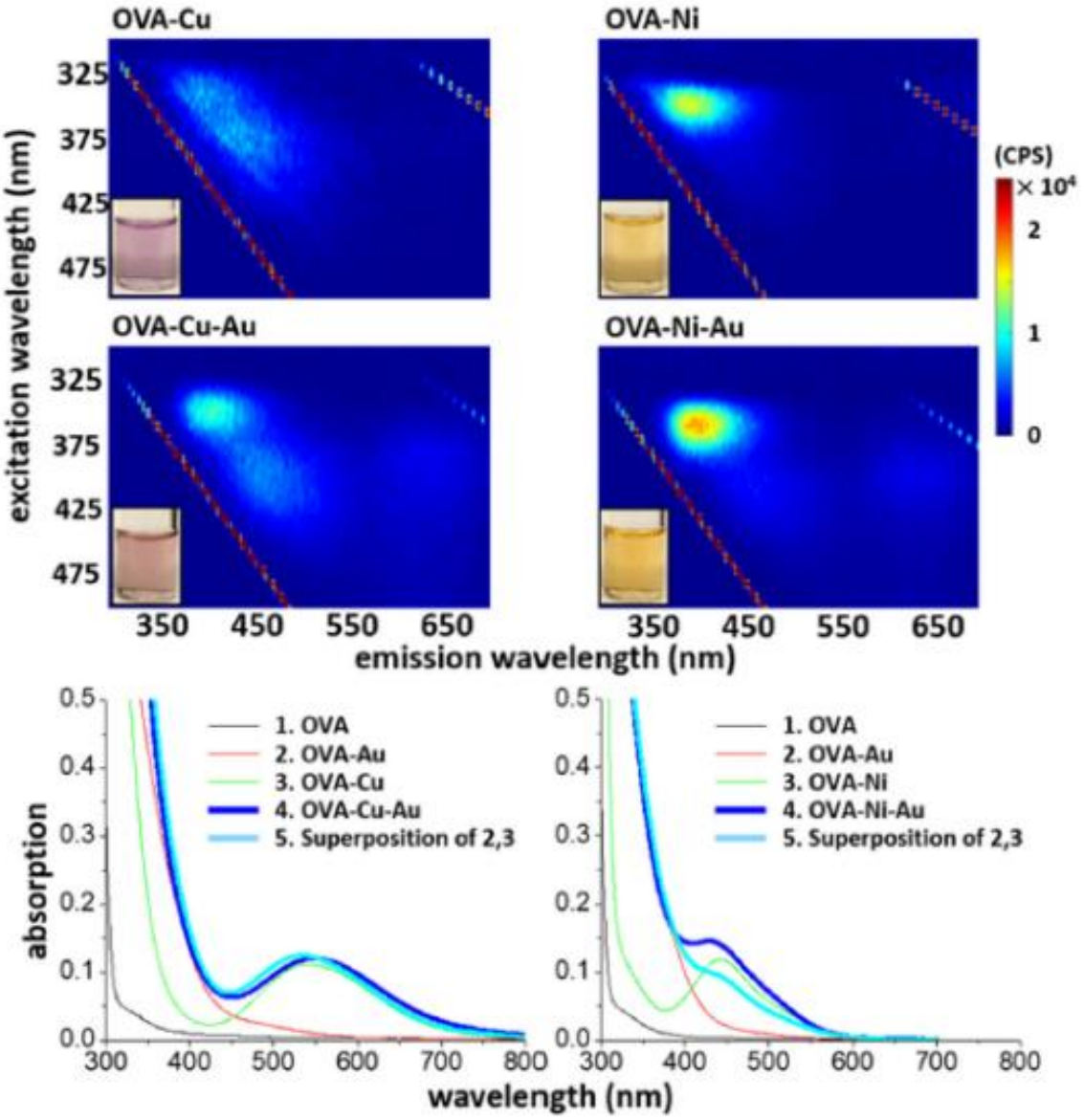

Figure 22. Ovalbumin has one known binding site at serine68-serine344 and competitive binding of Cu(II), Ni(II), and Au(III) via square planar coordination to this site was performed. Three-dimensional excitation-emission spectra shows that both Cu(II) and Ni(II) binding to this site do not disrupt the formation of red luminescence. Absorption spectra of ovalbumin-Cu(II)-Au(III) and the superposition of ovalbumin-Cu(II) with ovalbumin-Au(III) were identical, indicating Cu(II) is not displaced by Au(III) at this site. While spectra comparing ovalbumin-Ni(II)-Au(III) to the superposition of ovalbumin-Ni(II) and ovalbumin-Au(III) are different, suggesting the displacement of Ni(II) by Au(III). These observations overall show that serine68-serine344 is a binding site of Au(III) but is not a site of red luminophore formation.

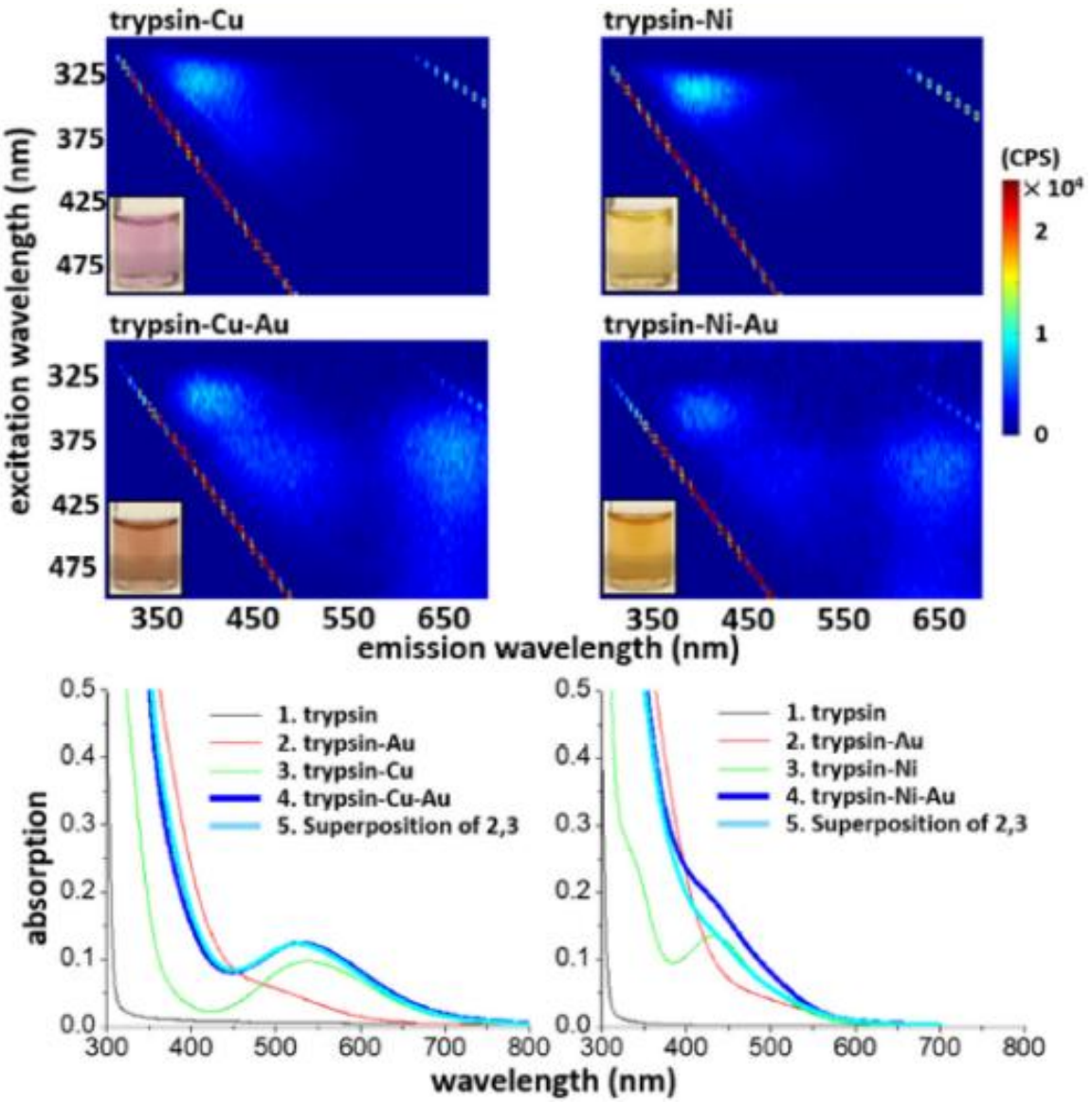

Figure 23. Trypsin has one known Cu(II) binding site coordinating histidine57-asparagine102-serine195 – a catalytic triad. Competitive binding of Cu(II), Ni(II), and Au(III) via square planar coordination to this site was performed. Excitation-emission spectra shows that both Cu(II) and Ni(II) binding to this site do not disrupt the formation of red luminescence. Absorption spectra of trypsin-Cu(II)-Au(III) and the superposition of trypsin-Cu(II) with trypsin-Au(III) were identical, indicating Cu(II) is not displaced by Au(III) at this site. While spectra comparing trypsin-Ni(II)-Au(III) to the superposition of trypsin-Ni(II) and trypsin-Au(III) are different, suggesting the displacement of Ni(II) by Au(III). These observations overall show that the catalytic triad is a binding site of Au(III) but is not a site of red luminophore formation.

4.2 Comparisons of Reaction Kinetics in Protein-Au Complexes.

To confirm the mechanism of Au binding Au in the red luminescent complex is the same in all protein-Au systems, further assessment of the kinetics of Au binding is performed, using the same protocols and experiments applied to BSA-Au, and outlined previously in Chapter 3 of this work. Furthermore, it must be determined what binding site or sites may play a role in the formation of the red luminescent complex. The BSA-Au complex, the protein contained two non-luminophore-forming Au binding sites.[13] These binding sites are the first three amino acids of BSA at the N-terminal site, known as the Asparagine fragment, which chelate Au around the first three amino acids, and the second site is the free thiol, cystine34, which binds Au and is generally responsible for the formation of a BSA dimer under normal conditions.

Ovalbumin, trypsin, and insulin each contain at least one known metal binding site. Ovalbumin metal is known to bind at a serine68-serine344 site,[113] trypsin metal is known to bind at a histidine57-asparagine102-serine195 catalytic triad,[114] and insulin monomers histine10B-glutamic acid13B in the B-chain is known to bind metal.[115] From here, each of these metal binding sites can be denoted as a general site ‘S’. Thus, to determine if these known metal binding sites may be important to the formation of the red luminescent complex, a competitive metal binding experiment was conducted to each of these ‘S’ sites using Cu, Ni, and Au.

Competitive binding works by taking advantage of the different binding affinities of each metal ion with their binding site. In general, nickel is a weak binder and copper is a strong binder, while gold has a binding affinity in between these two metal ions. The binding affinities of the three metals is Ni(II) < Au(III) < Cu(II). Thus, by reacting

ovalbumin, trypsin, or insulin first with Ni(II) the subsequent addition of Au(III) will displace Ni(II) away from any binding sites and preferentially bind Au(III). By adding Ni(II) before Au(III) the final resultant compound should still only bind Au(III) and be like that of a control sample that only started with Au(III). In a reaction that starts with Cu(II) , the affinity of Cu(II) is much higher than Au(III) and thus after the addition of Au(III), Cu(II) will have already preferentially bound to any free metal binding sites, blocking Au(III) from binding. The result of this experiment will prevent Au(III) from binding to any known binding sites and will elucidate if any of these sites are responsible for red luminescence and these results can be seen in **Figures 21-23**.

The competitive binding experiment is performed by reacting ovalbumin, trypsin, and insulin with either Cu(ii) or Ni(ii) and then allowing these protein-Cu or protein-Ni complexes to be reacted with Au(iii). Synthesis of the copper and nickel bound proteins followed a standard protocol. Ovalbumin, trypsin, and insulin were prepared in an aqueous solution of HPLC-grade water to a concentration of 0.376 mM. Into 1 mL of each protein was added 0.5 mL of either 3.0 mM copper II chloride dihydrate ($CuCl_2 \cdot 2H_2O$; Cu(II)) or 3.0 mM nickel II chloride hexahydrate ($NiCl_2 \cdot 6H_2O$; Ni(II)). The solution was allowed to mix for 2 minutes at 37°C under vigorous stirring at 750 rpm. After 2 minutes, approximately 100 μL of 1 M NaOH was added to each solution to bring the pH above 12. The reaction of either protein-Cu(II) or protein-Ni(II) proceeded for 2 hours at 37°C.

To determine the competitive binding of Au(III), two hours after the formation of either protein-Cu(II) or protein-Ni(II) 0.5 mL of 3.0 mM Au(III) was added to each solution. After 2 minutes of stirring, 1 M NaOH was added again to bring the pH back above 12 as a solution of Au(III) is acidic in water. The reaction of protein-Cu(II)-Au(III)

and protein-Ni(II)-Au(III) proceeded for 2 more hours at 37^{o}C and the final solution was stored at room temperature for 2 days for further analysis.

Upon the addition of Ni(II) and NaOH into each solution of ovalbumin, trypsin, and insulin all samples turned a dark yellow color. In the presence of Cu(II) and NaOH every solution appeared light purple, indicating the adsorption of the metal ions onto each protein. After the addition of Au(III) into either the protein-Cu(II) or protein-Ni(II) compounds, the dark yellow or light purple color was lost and the resultant solution became a brownish color, indicating the uptake of Au(III) in every protein. The addition of Au(III) also resulted in red luminescence for every sample. The only exception for red luminescence after the addition of Au(III) was in the insulin-Cu(II)-Au(III) compound wherein no red luminescence was observed, even after 2 days.

Comparisons of control samples of ovalbumin-Au, trypsin-Au, and insulin-Au complexes to their protein-Ni(II)-Au(III) show that there was no difference in either complex. This indicates that Au(III) did indeed displace Ni(II) at each ‘S’ site. Comparing the control samples to those of protein-Cu(II)-Au(III) it can be concluded that Au(III) did not displace Cu(II) as expected but that the proposed ‘S’ binding sites did not play a role in the formation of red luminescence for ovalbumin or trypsin. Thus, these ‘S’ sites are binding sites of Au(III) but do not play a role in the formation of ed luminescence. In the case of insulin-Cu(II)-Au(III) it appears that the ‘S’ site of histine10B-glutamic acid13B in the B-chain may influence red luminescence formation. It is possible that the binding of Cu(III) to the insulin ‘S’ site leads to an obstruction of the binding for Au(III). Thus, it’s possible that there is a steric relevance of the local environment of ‘S’ in insulin for the formation of luminescence. The lack of red luminescence generation could be due to Cu(II)

inhibiting the proper dimerization of insulin, which appears to be necessary for luminescence in just this protein.

The summarized results of this experiment indicate that the known ‘S’ metal binding sites in each of these proteins do not play a direct role in the formation of red luminescence with the potential exception of site ‘S’ in insulin. These results agree with what has been found in BSA-Au complexes and indicate that a Cys-Cys disulfide bond is also required for luminescent generation. To further compare the binding kinetics of Au(III) to each of these proteins a multi-site absorption model is applied as done with BSA-Au in Chapter 3 in this work.

The binding kinetics of these three protein-Au complexes was performed to further show their similarities to that of BSA-Au. Included in showing that these protein-Au complexes are comparable to BSA-Au, resolving their reaction kinetics can provide further evidence of weather the reaction is best explained by the nucleation and formation of a nanoparticle or by the formation of a small complex. A Langmuir-type multi-site absorption model was devised to fit the gold-based binding of each protein-Au complex. In this multi-site absorption model, Cys-Cys disulfide bond sites were incorporated into the model. This model includes the Cys-Cys disulfide bond location as the luminophore-forming Au(III) chemisorption site in addition to the non-luminophore-forming site(s) and nonspecific surface sites. It is additionally noted that the luminophore-forming site is included without specifying the structure of coordination.

The binding of Au at all different possible sites can be evaluated using the multi-site absorption model. This model predicts the increase in red luminescence intensity as the stochiometric amount of Au is increased, which is observed for ovalbumin-Au, trypsin-

Au, and insulin-Au. These sites include the actual binding site of Au responsible for luminescence, all 'S' sites which are known to bind metal but are not responsible for luminescence, and finally non-specific surface binding of Au to protein, which is known to occur across the surface when Au is in high concentration. Using this model, the affinity of Au to the sulfur (or possibly the disulfide bond itself) can be estimated and that value is approximately E_0 ~ 400 kJ/mol. This value does depend on the local environment of the site and may be slightly different due to the conditions of the reaction, or where the binding site is located within each protein, respectively. To all 'S' sites indicated earlier, the binding constant is estimated as $E_x \sim 0.5*E_0$, which was determined from the affinity strength of different metals [Cu(II) > Au(III) > Ni(II)]. Finally, the affinity of Au to the surface of the protein is due to van der-Waals forces and thus the binding energy is $E_s \sim 0.01*E_0$. The multi-site absorption model of ovalbumin-Au, trypsin-Au, and insulin-Au is this proportional to:

$$I \propto \frac{x^{1+0.5+0.01*N}}{(1+x)(1+x^{0.5})(1+x^{0.01})^N}$$

where $x = \lambda\exp[E_0/k_BT]$, $\lambda = \exp[\mu/k_BT]$, and N is the number of surface-bound Au atoms, which is uniquely determined for each protein based on the surface area from their native crystal structures.

Since μ is the chemical potential of an adsorbed molecule the grand canonical partition function can be simplified and take the form of a binomial series. The simplified form of the partition function is shown in the equation above. Where *x* is representative of the canonical ensemble of all absorbents absorbed. Furthermore, λ is representative of the partition function of a single adsorbed molecule. Because of this, once simplified, *x* will

only be dependent on the change in temperature of the reaction as the adsorption energy, E_0, and chemical potential, μ, will be considered a constant. For the sake of some rigor, μ will also be considered the same value for both free Au and adsorbed Au.

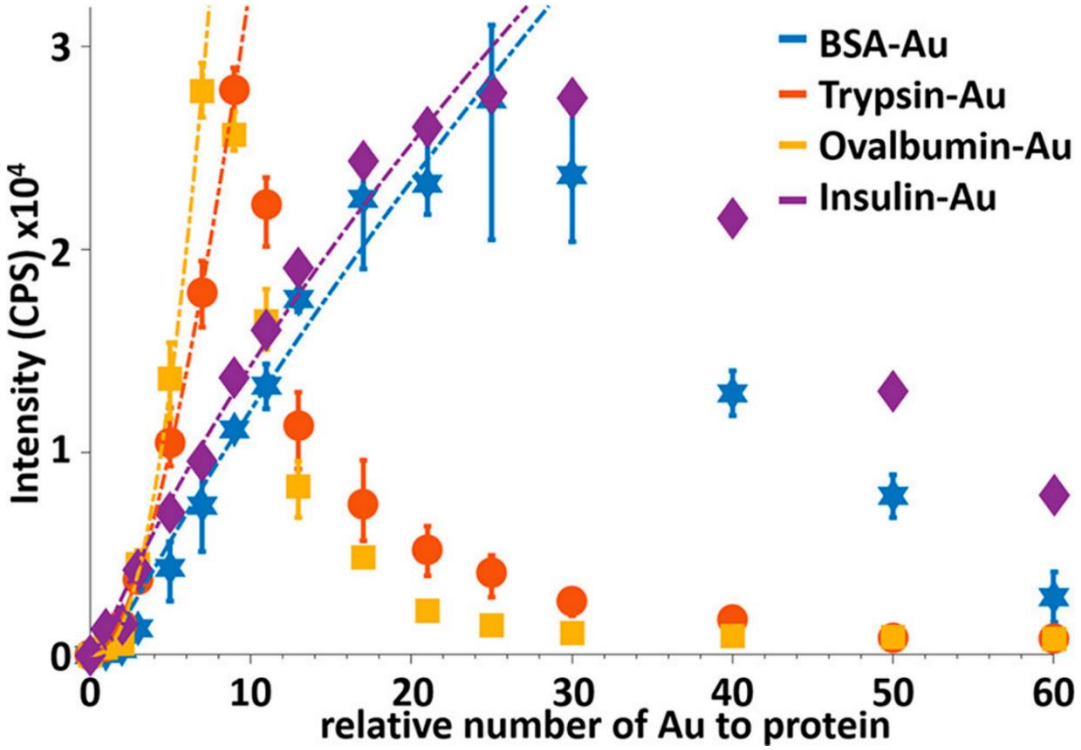

Figure 24. The red luminescence intensity (λ_{ex} / λ_{em} = 495 / 640 nm) intensity of ovalbumin-Au, trypsin-Au, and insulin-Au compared to BSA-Au at pH 12. Data was collected at 48 hours between the ratios of protein : Au = 1 : 1 to 1 : 60. The dotted lines represent the fitted Langmuir-type multi-site adsorption model of Au for each protein.

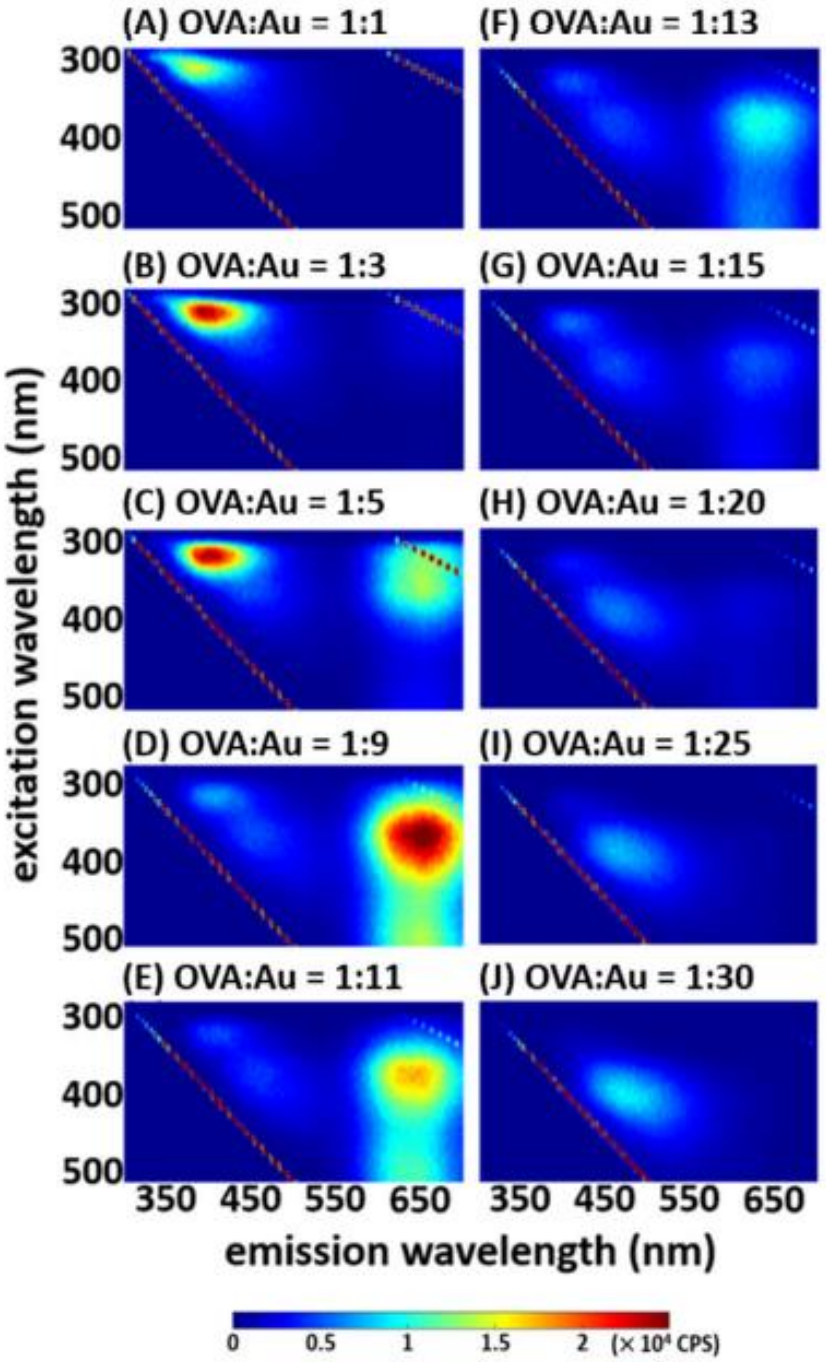

Figure 25. Ratio-metric studies of ovalbumin-Au complexes. Excitation-emission maps of ovalbumin-Au complexes at pH = 12 at 48 h after synthesis, for the ovalbumin-to-Au molar ratios of (A) 1:1, (B) 1:3, (C) 1:5, (D) 1:9, (E) 1:11, (F) 1:13, (G) 1:15, (H) 1:20, (I) 1:25, (J) 1:30. The excitation-emission spectra show a general increase in red luminescence intensity followed by a decay in red luminescence as the protein to Au ratio slowly increased.

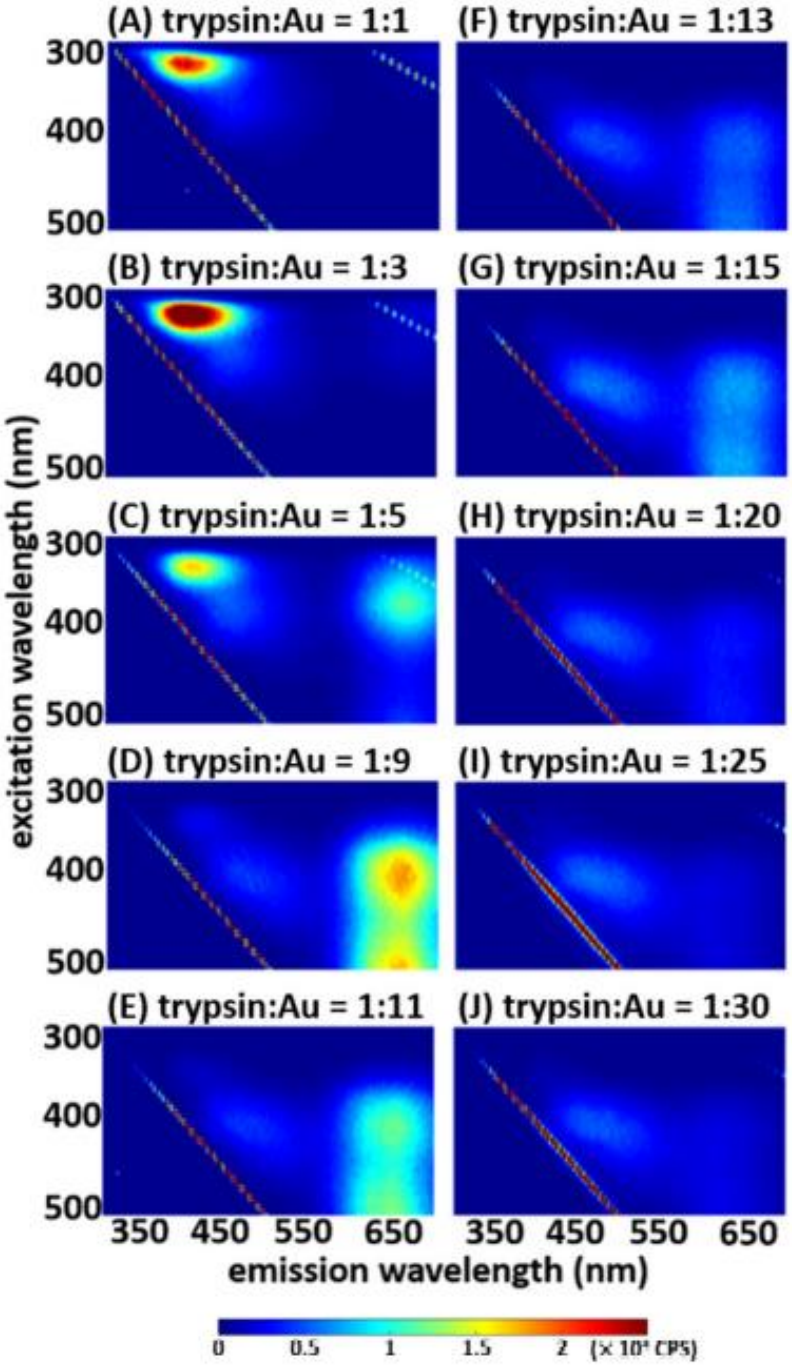

Figure 26. Ratio-metric studies of trypsin-Au complexes. Excitation-emission maps of trypsin-Au complexes at pH = 12 at 48 h after synthesis, for the trypsin-to-Au molar ratios of (A) 1:1, (B) 1:3, (C) 1:5, (D) 1:9, (E) 1:11, (F) 1:13, (G) 1:15, (H) 1:20, (I) 1:25, (J) 1:30. The excitation-emission spectra show a general increase in red luminescence intensity followed by a decay in red luminescence as the protein to Au ratio slowly increased.

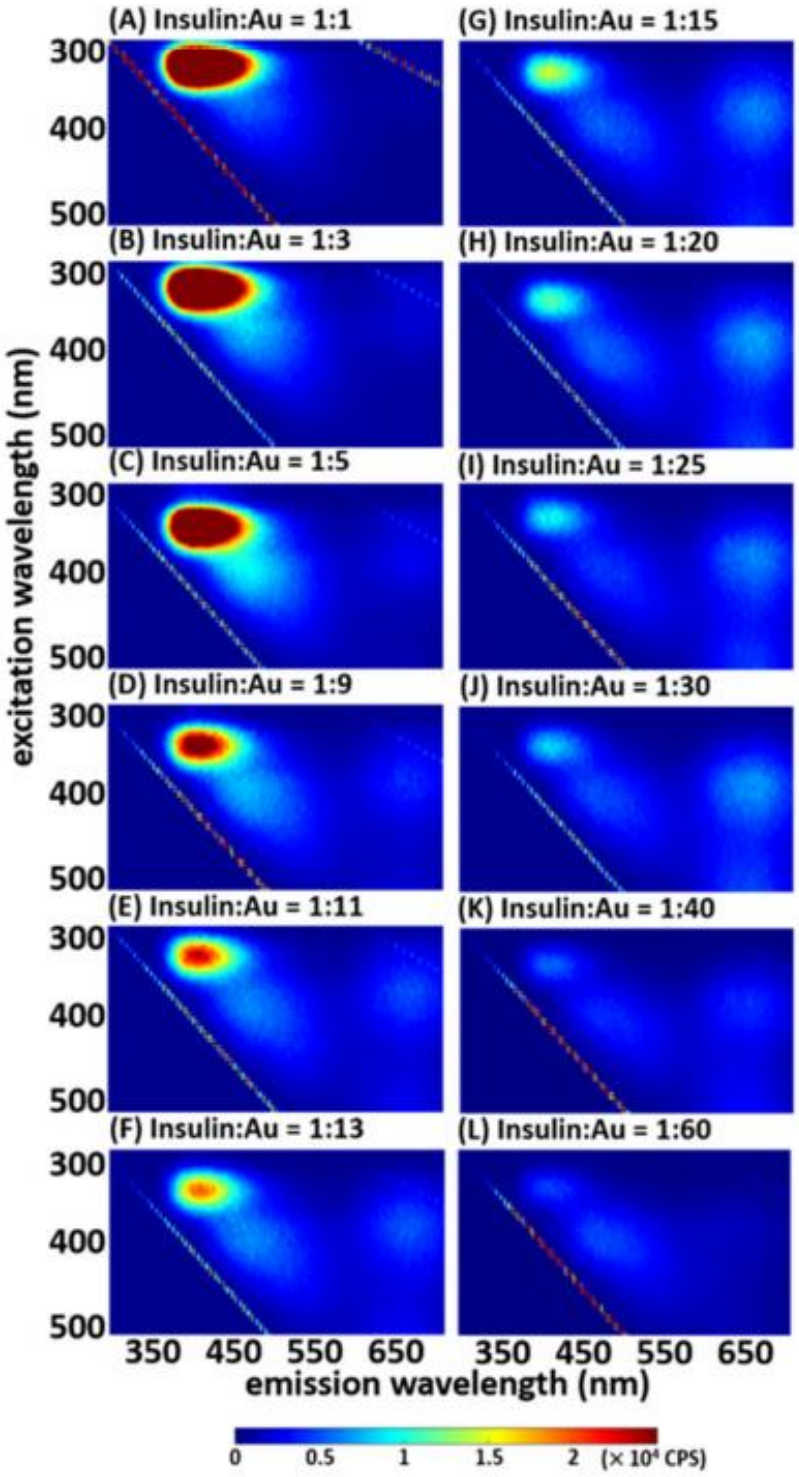

Figure 27. Ratio-metric studies of insulin-Au complexes. Excitation-emission maps of insulin-Au complexes at pH = 12 at 48 h after synthesis, for the insulin-to-Au molar ratios of (A) 1:1, (B) 1:3, (C) 1:5, (D) 1:9, (E) 1:11, (F) 1:13, (G) 1:15, (H) 1:20, (I) 1:25, (J) 1:30, (K) 1:40, (L) 1:60. The excitation-emission spectra show a general increase in red luminescence intensity followed by a decay in red luminescence as the protein to Au ratio is slowly increased

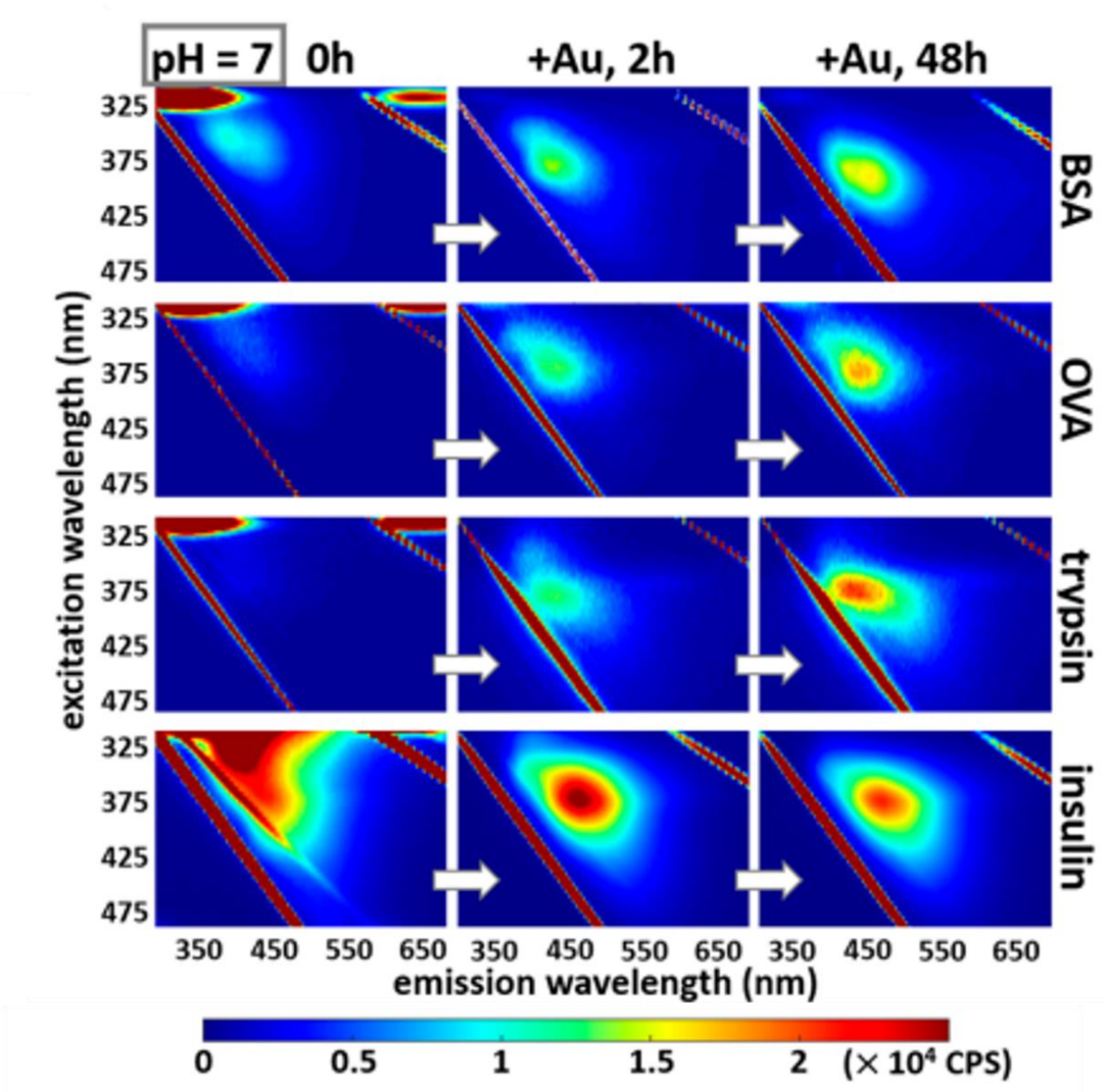

Figure 28. Time-course excitation-emission spectra a (λ_{ex} = 300− 500 nm; λ_{em} = 300−700 nm) of BSA, ovalbumin (OVA), trypsin, and insulin at 0, 2, and 48 hours after the addition of Au at pH 7. At neutral no red luminescence is formed and no relative change in the spectra pattern for any protein is observed.

The statistical model reproduced the red luminescence intensities that were measured according to the protein to Au molar ratios used (**Figure 24**). Beyond the maximal luminescence intensities that were observed in each sample there was followed a suppression of luminescence intensity as the protein to Au molar ratio increased further. This intensity suppression is likely due to the non-specifically surface-bound Au that

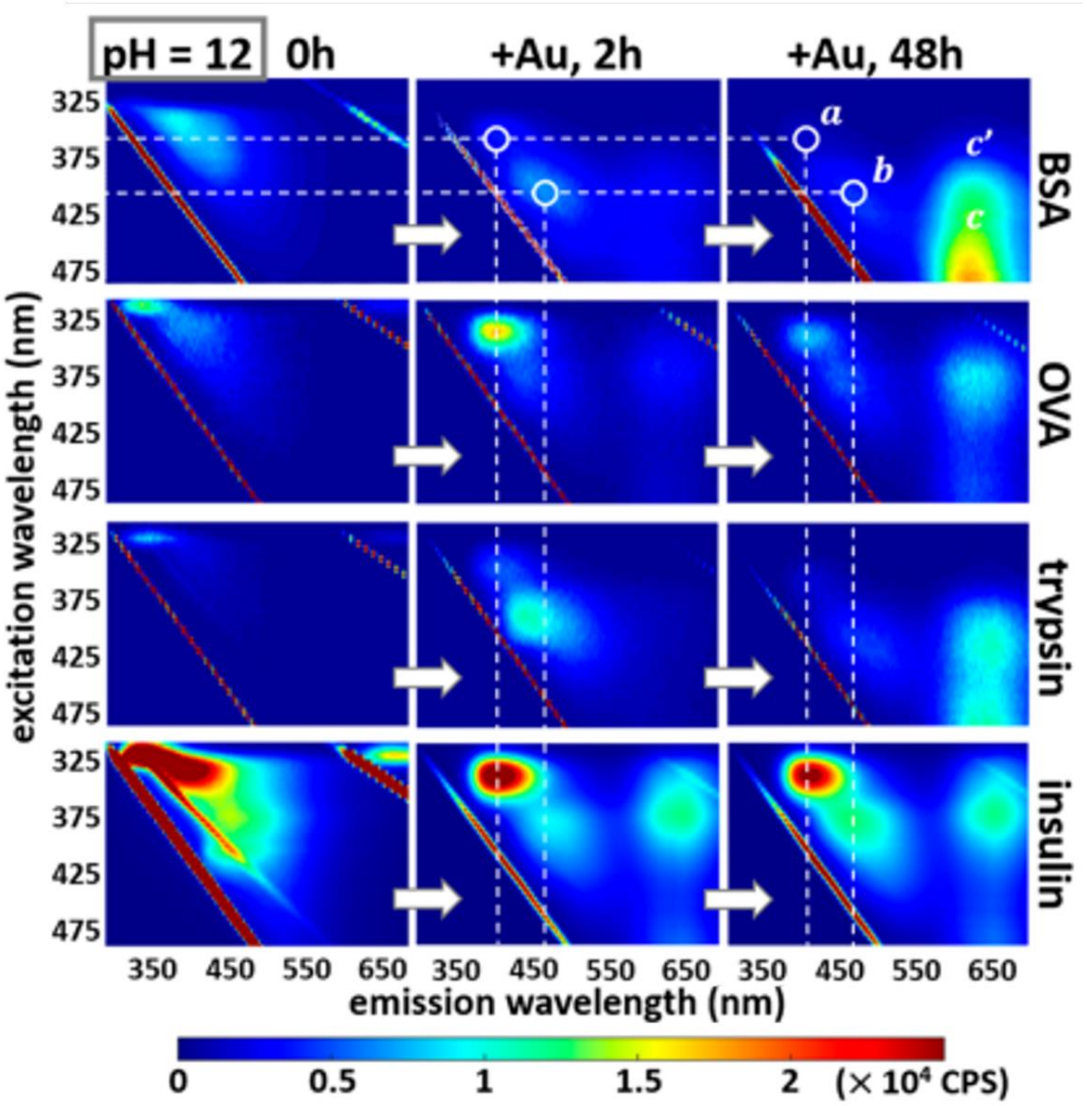

Figure 29. Time-course excitation-emission spectra a (λ_{ex} = 300− 500 nm; λ_{em} = 300−700 nm) of BSA, ovalbumin (OVA), trypsin, and insulin at 0, 2, and 48 hours after the addition of Au at pH 12. The letter insets in the top right panel indicate (a) $\lambda_{ex}/\lambda_{em}$ = 370/400 nm, (b) $\lambda_{ex}/\lambda_{em}$ = 400/460 nm, (c′) $\lambda_{ex}/\lambda_{em}$ = 400/640 nm, (c) $\lambda_{ex}/\lambda_{em}$ = 470/640 nm, with possible energy transfer pathways a → b, a → c′, and b → c.

begins to occur at higher molar ratios (**Figures 25-27**). This mechanism of luminescence suppression has been observed by others, but is not described by the above multi-site absorption model.[81]

This suppression of intensity may also be due to further nucleation of the proteins as the large number surface bound Au cause aggregation, suppressing the luminescence of

the complex. While the multi-site absorption model does not fully encompass the observed luminescence intensity values at all protein to Au molar ratios, it does describe the increase in luminescence caused by the binding of Au to the luminescent site. If luminescence was the result of the nucleation of a nanocluster to a single absorbable site, then the above model would not fit the data. The results of this luminescent study thus further aid in showing that the luminescence is not due to nanoparticles nucleating within the protein space but rather support our alternative model of a single small thiol-bound-Au complex.

The similarities of the luminescent properties between all the protein-Au complexes can further be seen when comparing their three-dimensional excitation-emission spectra. To determine the similarities between all proteins it is important to determine whether only the red luminescence is what is common in all complexes or if the same fluorescence shifts happen across all wavelengths. When comparing all the proteins at a pH of 7, the intrinsic UV and blue fluorescence peaks can all be seen and is generally caused by the large presence of aromatic amino acids residues (tryptophan, phenylalanine, tyrosine, and histidine) (**Figure 28**) . In each protein the large UV peaks with an excitation wavelength of 300 nm and an emission wavelength of 340 nm can be seen and is due almost entirely from the presence of tryptophan residues. The large, sweeping peak in the blue regime around an excitation wavelength of 340 nm and an emission wavelength of 420 nm is due to the aromatic amino acid residues in general. The large variability in the observed blue-peak intensities is likely due to the local environments around these residues.[116] The lack of tryptophan residues within insulin also resulted in the natural absence of the UV peak (λ_{ex} / λ_{em} = 300 / 340 nm).

At a pH of 7 and upon the addition of Au, the observed UV peak in each protein was suppressed significantly. Furthermore, the blue peak in each protein red-shifted to a longer wavelength, approximately ~ 30 nm for all pH = 7 protein-Au complexes. The shift in the blue peak luminescence suggests that the addition of Au may be due to an interaction of Au with the aromatic residues. The addition of Au may be leading to both the suppression and shifting in luminescence, yet how Au alters the luminescence either directly or indirectly cannot be determined from these results. Finally, for all protein-Au complexes at a pH of 7 no red luminescence was observed. This is expected as red luminescence does not emerge until a pH ~ 10 for all protein-Au complexes.

When all protein-Au complexes were synthesized at a pH of ~ 12, the pH-induced conformational changes within the proteins caused a gradual shift in the peak locations within the excitation-emission spectra (**Figure 29**). Interestingly, the excitation-emission spectra of all the protein-Au complexes after 48 hours are remarkably similar, indicating the same complex may be forming between all proteins.

For ovalbumin-Au, trypsin-Au, and insulin-Au along with the BSA-Au control, the expected UV peak (when excited at 300 nm) was absent at the sub-2-hour time point. The cause of this peak loss is most likely attributable to the local changes around aromatic amino acid residues in the presence of a highly basic solution. The blue peak of each protein-Au complex (λ_{ex} / λ_{em} = 300 / 340 nm), denoted as peak '*a*' in the figure also diminished while subsequently another peak in the blue-green emission regime appeared. This peak with an excitation wavelength of ~ 400 nm and an emission wavelength of ~ 460 nm, noted as peak '*b*' in **Figure 29** increased during the 2-hour incubation at 37^{o}C. During the 48-hour incubation at 20^{o}C this '*b*' peak further increased in intensity. Simultaneously,

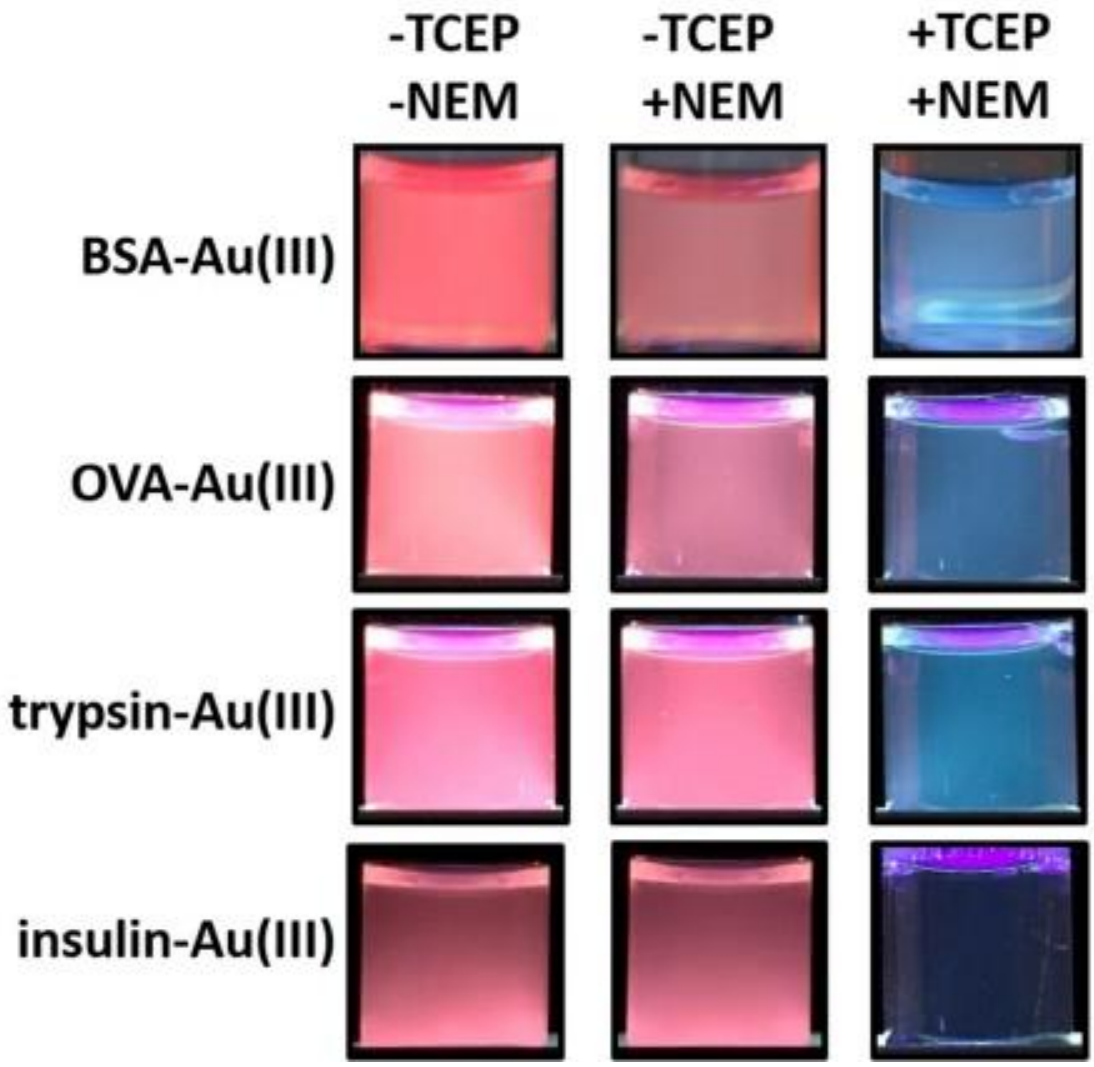

Figure 30. Cysteine is necessary to produce the red luminescence in all the protein-Au complexes. The Cys-Cys disulfide bonds were cleaved by TCEP (tris(2-carboxyethyl)phosphine hydrochloride) and the resulting free cysteine residues were capped with NEM (N-ethylmaleimide), preventing Au from binding to any thiol. For the four proteins, BSA, OVA, trypsin, and insulin, +TCEP+NEM samples did not yield the red luminescence. The controls (-TCEP-NEM and -TCEP+NEM) are also shown.

as peak '*b*' increased the characteristic red luminescence or 'red peak' noted as peak '*c*' emerged slowly from the 2-hour time point to the 48-hour time point and was stable with no further increases beyond 48 hours.

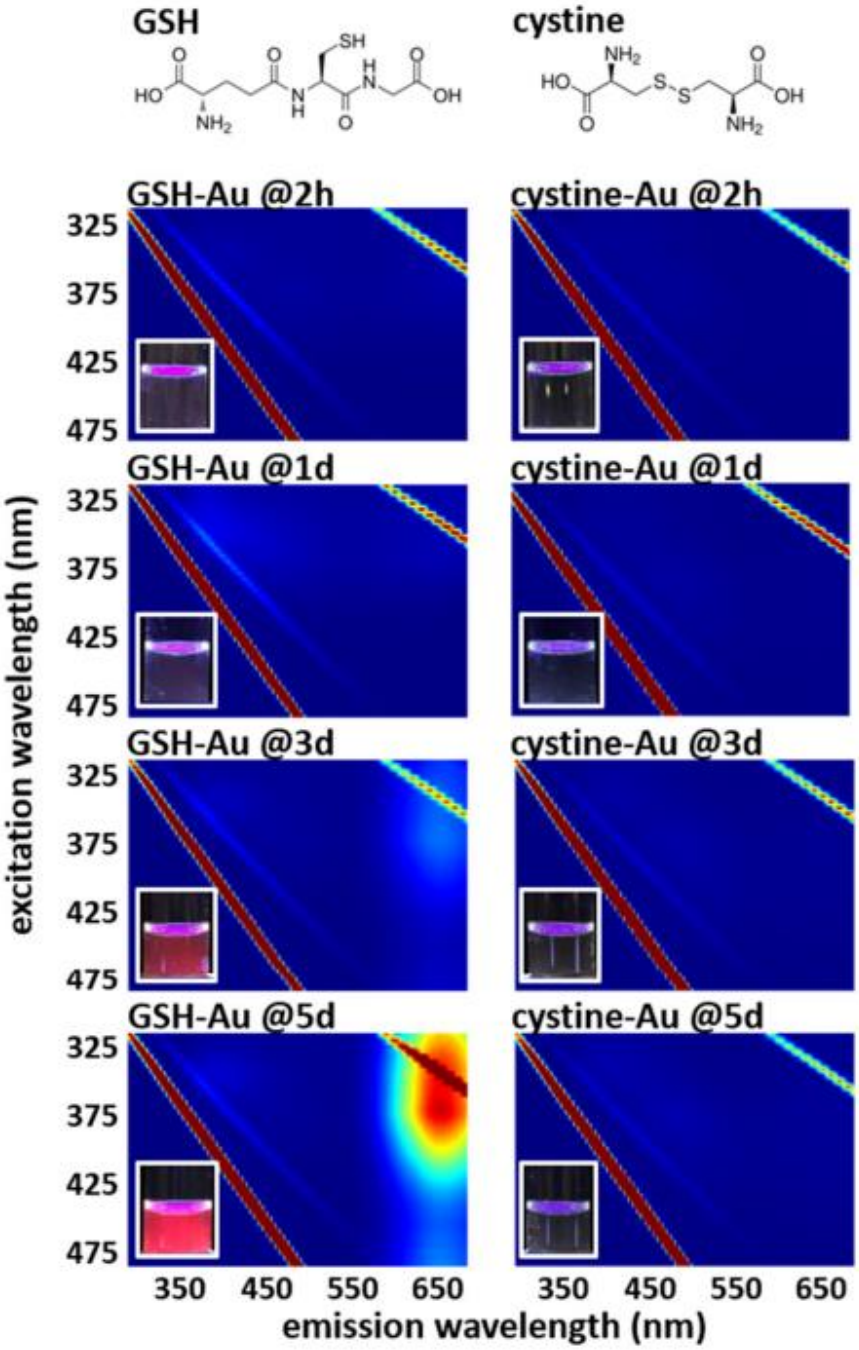

Figure 31. Excitation-emission spectra of red luminescence of GSH-Au and cystine-Au complexes scanned over the course of 5 days. GSH and cystine (1.6 mM) were reacted with Au at a ratio of 1 : 1 following the standard protein-Au protocol. After 5 days only GSH-Au appears to be red luminescent and is equivalent to protein-Au complexes.

This '*c*' peak has multiple excitation wavelengths which correspond to an excitation of ~ 475 nm and an emission wavelength of 640 nm, while a secondary red peak, noted as

c′ is observed to form with an excitation of ~ 400 nm and an emission wavelength of 640 nm. Based on these results two distinct excitation wavelengths are possible for the emission of the red peak. Thus, it is possible that red luminescence corresponding to both peak *c* and *c′* is indicative of a cascaded energy transfer mechanism wherein energy is transferred among the peaks. This energy transfer may look something like a → b and then b → c, or a → c′ directly, and appears to be a common mechanism between all four of the observed protein-Au complexes synthesized at pH 12. Beyond the 48-hour time point no further changes were observed in any of the excitation-emission spectra peaks either in peak location or intensity when stored at 20°C.

4.3 Comparing Protein-Au Complexes to Thiol-Containing Complexes.

When comparing OVA-Au, trypsin-Au, insulin-Au, and BSA-Au it is evident from pH-dependent reactions, stoichiometric protein-to-Au reactions, and time-course fluorescence excitation-emission spectra that all four complexes share the same characteristics. These strikingly similar characteristics, especially the similarities in their excitation-emission patterns, warrants consideration that there is a common binding motif at the red luminophore-forming Au-binding site.

In particular, the apparent interactions that occur in the UV and blue peaks seem to correlate to the interactions of aromatic amino acid residues with Au. While the interactions of aromatics with Au seem to be a primary factor in luminescent formation, interactions with local amino acids in some capacity near the luminescing binding site play the critical role in complex formation. Among the aromatic's amino acids, histidine and tyrosine are also known to coordinate metal cations.[117] In addition to these amino acids, cysteine thiols appear to be most important in Au coordination and complex formation (**Figure 30**). By

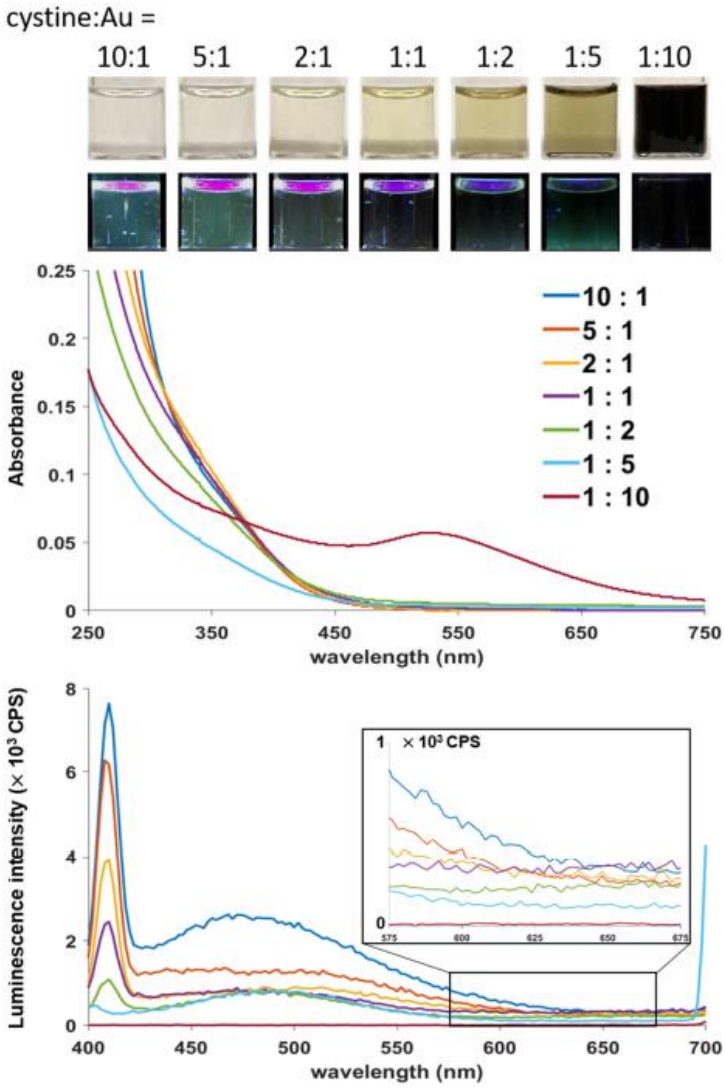

Figure 32. Red luminescence of cystine-Au compounds where cystine (1.6 mM) was reacted with HAuCl4 at a range of molar ratios between 10 : 1 and 1 : 10. Measurements were performed at 1 day. The intensities of red luminescence (λ_{ex} = 365 nm) for these samples were extremely weak (<500 CPS). The 1 : 10 sample resulted in formation of Au nanoparticles, as indicated by the surface plasmon peak at ~ 520 nm. The luminescence was completely quenched in this sample, likely due to metal-mediated non-radiative decay.

removing cystine disulfides as binding sites for Au via NEM to break the disulfide bond and TCEP to take away the sulfur for binding all red luminescence was inhibited from forming. Samples where only TCEP was added and no NEM was added still resulted in red luminescence, suggesting there may be an important role for disulfides in the formation of the luminescent complex. Thus, it is important to assess the involvement of local

aromatic amino acids and other amino acids that are near the luminophore-forming site, as they may be responsible for the coordination of Au.

Cysteine appears to be important in red luminescent complex formation and as a way to gain further insights into the local interactions of Au at the Cys-Cys disulfide bond site, multiple small cysteine-containing compounds were complexed with Au. Cystine (dicystiene, representing Cys-Cys), and reduced glutathione (GSH, γ-Glutamic Acid−Cysteine− Glycine tripeptide, representing cysteine) was reacted with Au following the same standard protocol for protein-Au complexes. The GSH-Au complex formed at pH 12 yielded the red luminescent complex, which had a luminescent intensity and spectral pattern that was equivalent to that of the protein-Au complexes (**Figure 31**). On the other hand, the complex formed of cystine-Au at a pH of 12 only yielded weak red luminescence which was an order of 50-fold weaker than what was observed in protein-Au complexes (**Figure 32**). In each case, both samples appeared red luminescent following the standard protocol, indicating cystine is a required component in complex formation. Based on these small, cystine-containing compounds cystine was taken as the Au binding center of the red luminescent complex.

As mentioned, there appears to be a dependence on higher ordered structures within proteins that are luminescent beyond simple amino acids sequences. Secondary and tertiary structures most likely play a role in complex formation. Using cystine as the binding center, the local arrangements of histidine, tyrosine and other aromatics including tryptophan and phenylalanine residues can be assessed relative to Au. For each amino acid, the residues were examined within ∼15 Å of cystine thiols using the native protein crystal structures found in the Protein Data Bank (PDB).

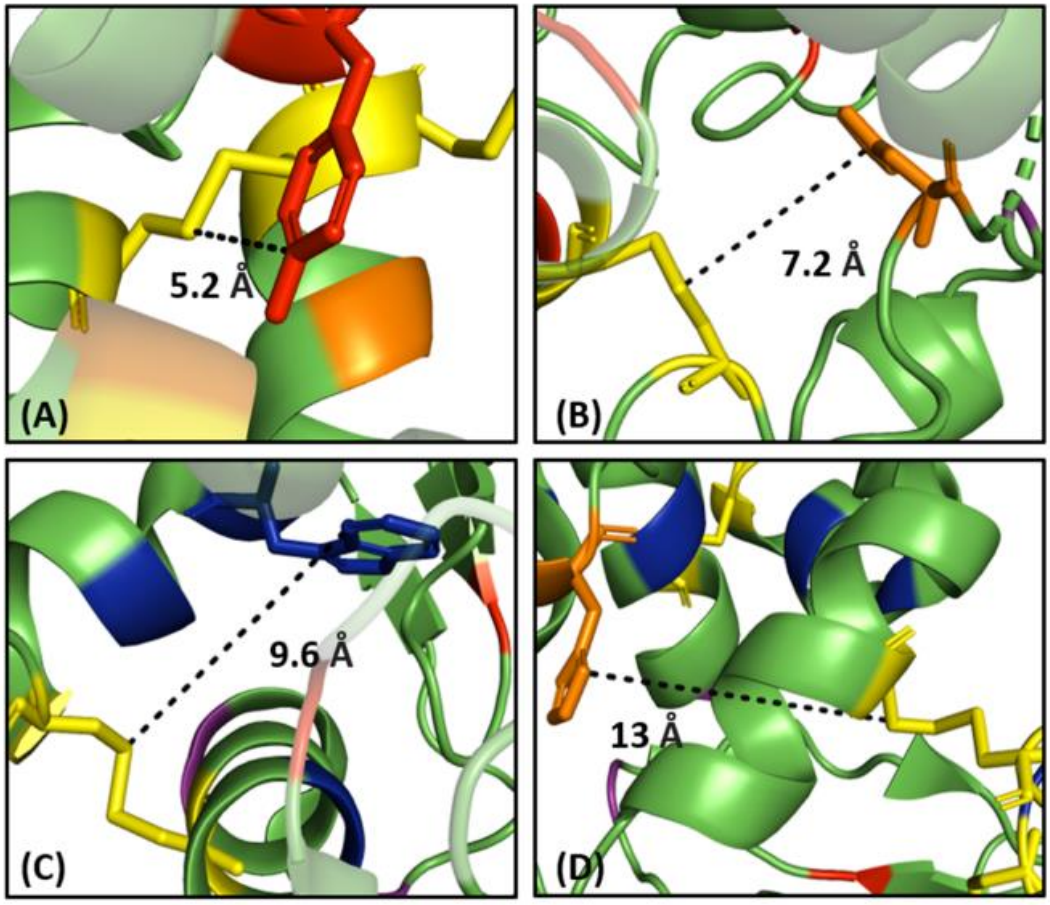

Figure 33. Analysis of local aromatic residue motif at disulfide bond locations. From a given cystine center (shown in yellow in the panels), the distance, orientation, and the obstruction were determined, as the following examples: (A) In BSA, measured from the sulfur atom in cystine, the closest carbon atom in a tyrosine residue (shown in red) is at 5.2 Å distance, and attain "σ"-orientation (a side of aromatic ring is facing Cys center). There are no residues between cystine and tyrosine (unobstructed). (B) Similarly, in ovalbumin, a histidine is at 7.2 Å distance and attain "π"-orientation (the plane of aromatic ring is facing Cys center), unobstructed. (C) In Lysozyme, a tryptophan is at 9.6 Å distance and attains an orientation neither "σ" nor "π", which can be called "mid"-orientation, unobstructed. (D) In Lysozyme, a histidine is at 13 Å distance and attain "mid"-orientation, and this histidine doesn't have direct line of sight to Cys, obstructed by a α-helix.

4.4 Using Crystal Structures to Find a Common Binding Motif.

Including analysis of the distance from the cystine centers to amino acids, the spatial orientation of the aromatic rings with respect to the cystine centers, and the local obstructions due to other amino acids were considered in the tertiary structural analysis of the crystal structures. It is important to note that these detailed configurations provide only

an initial analysis of the amino acids relative to cysteine centers. Further, the necessity of protein structural information at pH values greater than 10 is truly needed for an exact determination of the common motif responsible for red luminescence that is shared between these proteins.

Analysis of protein tertiary structures was expanded beyond the four proteins just shown to share the same red luminescence patterns. Including ovalbumin, trypsin, insulin, and BSA, all proteins found in the literature which form a red luminescent complex upon the addition of Au were also analyzed to provide further support of a common binding motif. This analysis was expanded to include lactotransferrin, pepsin, horseradish peroxidase, papain, and lysozyme. Included in the analysis were a few proteins that are not red luminescent upon addition of Au following the described standard protocol, which are α-2-macroglobulin, trypsin inhibitor, and the monomer form of insulin.

Analysis of the local amino acid residue motif at Cys-Cys disulfide bond centers is performed by looking at three primary parameters of protein crystal structures local tertiary motifs. These parameters are the distance from center, orientation of amino acid, and obstruction of other residues.

Distance of an amino acid is conducted by taking the distance of the disulfide center to the nearest carbon atom in the R-group of either tryptophan, phenylalanine, histidine, or tyrosine. If the distance of the nearest carbon atom in the R-group is greater than ~15 Å, then that amino acid will not be considered for further orientation analysis. Orientation is performed by determining the orientation of the aromatic ring of each amino acid relative to the disulfide center. The orientation of the aromatic ring can either be parallel, noted as a “σ”-orientation (a side of the aromatic ring is facing the disulfide center), orthogonal,

noted as “π”-orientation (the plane of the aromatic ring directly faces the disulfide center), or is mixed, noted as 'mid'-orientation (the plane of the aromatic ring is somewhere between “σ” or “π”). Finally, the analyzed amino acid can be obstructed or unobstructed from the disulfide center. In an unobstructed aromatic the theoretical line that can be drawn from the disulfide center to the nearest carbon atom in the R-group does not cross through another amino acid. In an obstructed aromatic, the theoretical line that can be drawn passes through a part of another amino acid. In obstructed amino acids, the amino acid itself could be considered obstructing if the R-group of the aromatic in question faces 'away' from the disulfide center (explained further in **Figure 33**).

As mentioned, alkaline pH is required for the generation of red luminescence within protein-Au complexes. Thus, the PDB analysis performed on tertiary structures at natural pH may not provide the accurate luminophores structure after pH is altered. Considering this, the distance of analysis conducted (≤15 Å) covers >30% of the size of every protein (≤5 nm), and thus the residue(s) that may be involved in red luminescence are expected to be captured in this overall analysis.

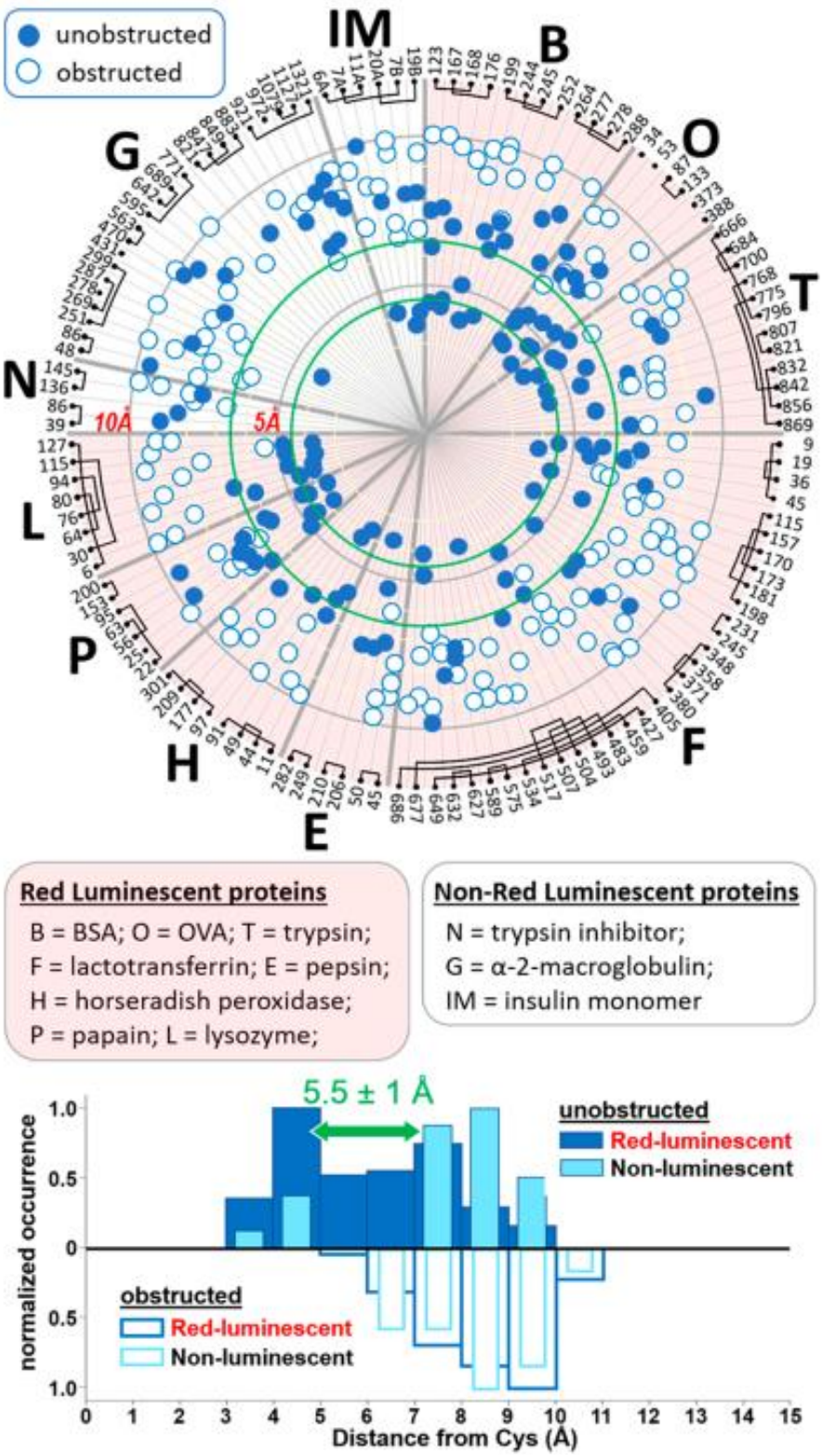

Figure 34. Analysis of the distances (<15 Å) of the fluorescent residues (His, Tyr, Trp, Phe) with respect to Cys as the Au(III) binding site, based on the protein database (PDB). Cys site identifiers, as well as Cys−Cys disulfide bond structures, are indicated on the perimeter. Green circles indicate distances of 5.5 ± 1 Å, which are also shown in the histogram.

In the tertiary structural analysis at least one unobstructed aromatic amino acid residues were found for each of the red luminescent proteins, while this was not the case for the non-red luminescent proteins within the range of 5.5 ± 1 Å from the disulfide center (**Figure 34** and **Table 3**). In general, the coordination distance of Au to thiols is ~2.6 Å and the typical metal-to-residue distance found in PDB structures is ~3.0 Å.[118] Thus, the distance observed of ~5.5 Å seems a plausible size of a cystine-to-Au-to-residue, or ligand-metal-ligand coordination complex. Furthermore, the lack of this available space that occurs in non-red luminescent protein-Au complexes (**Figure 35)** may indicate that the local tertiary structure is responsible for coordination of Au to occur, and that the local aromatic amino acid residues may play a role in this coordination.

Analysis of the excitation and relaxation dynamics of the four studied protein-Au complexes of BSA, ovalbumin, trypsin, and insulin provide further insight into the potential involvement of aromatic residues in Au-to-cystine coordination. This was carried out by probing near the '*c*' peak (λ_{ex} / λ_{em} = 389 / 650 nm), using time-correlated single photon counting (TCSPC). All four protein-Au complexes exhibited a slow lifetime decay of $\tau_1 \sim 300$ ns as the dominant component (>90% when applying triple exponential fit). These results can be seen in **Figure 36**, along with the lifetime dynamics of the small thiolate-Au compound – GSH-Au. This long lifetime is at least an order of magnitude longer that the fluorescence decay of the protein-Au complexes in the blue regime and of aromatic amino acid residues, which are on the order of $\tau \sim 10$ ns (**Figure 37** and **Table 4**). The other lifetime decay values were $\tau_2 \sim 40$ ns (~5% when applying triple exponential fit), and $\tau_3 \sim 1.5$ ns (~4% when applying triple exponential fit), these values likely correlate to this innate lifetime of the aromatic residues.

Table 3. Local aromatic residue motif at Cys residue (continued next page). The Cys-Cys disulfide bond sites for the proteins were analyzed for their local tertiary motifs, based on protein data base (PDB). His, Tyr, Trp, and Phe residues were analyzed, with respect to the distance from the sulfur (S) of Cys residue to the closest carbon (C) of the aromatic ring, and the ring orientation. For the orientation, "π" was used for the aromatic ring plane facing the Cys-center, "σ" for the side of the ring facing the center, and "mid" for an in-between angle. "π (x)", "σ (x)", and "mid (x)" indicate the line between Cys-center and the residue in consideration is obstructed by other residue(s) or secondary structures.

Protein (PDB-ID)	#	Location	His	Tyr	Trp	Phe
BSA (4F5S)	1	Cys123		10.0 Å, π (x)		**4.4 Å, σ** **6.4 Å, mid** **7.5 Å, π**
	2	Cys167				**7.7 Å, π** 10.0 Å, π (x)
	3	Cys168		9.7 Å, π (x)		**4.2 Å, σ** **4.4 Å, mid** **7.0 Å, π**
	4	Cys176				9.3 Å, π (x)
	5	Cys199	8.9 Å, mid (x) 9.8 Å, σ (x)	**5.1 Å, σ**		
	6	Cys244	**7.1 Å, σ**	**4.0 Å, σ** 10.0 Å, mid (x)		9.6 Å, σ (x)
	7	Cys245	**7.5 Å, mid** 9.1 Å, σ (x)	**6.6 Å, σ** 7.6 Å, π (x)		
	8	Cys252	**7.0 Å, mid**	**4.2 Å, σ**		
	9	Cys264		10.0 Å, mid (x)		9.4 Å, mid (x)
	10	Cys277	8.2 Å, mid (x)			**8.2 Å, σ**
	11	Cys278				**8.7 Å, mid**
	12	Cys288	**6.9 Å, σ**			10.0 Å, σ (x)
Ovalbumin (1OVA)	1	Cys34		**4.1 Å, σ**		**4.9 Å, π** **5.0 Å, π** 6.4 Å, mid (x) **7.8 Å, mid** 9.3 Å, mid (x)
	2	Cys53	**5.2 Å, σ**	7.2 Å, σ (x)		**4.0 Å, π** **7.1 Å, σ** 9.5 Å, mid (x)
	3	Cys87	**7.3 Å, π**	6.9 Å, mid (x) 8.3 Å, σ (x)		
	4	Cys133	**7.1 Å, π**	**5.4 Å, mid** **8.1 Å, σ**		
	5	Cys373		9.5 Å, π (x)		**4.6 Å, σ** 7.4 Å, mid (x)
	6	Cys388				**3.8 Å, π** **4.6 Å, π** **5.5 Å, mid**

Table 3 (cont'd). Local aromatic residue motif at Cys residue (continued on next page).

Protein (PDB-ID)	#	Location	His	Tyr	Trp	Phe
Trypsin (1S0Q)	1	Cys666		**5.8 Å, π**	8.4 Å, π (x)	
	2	Cys684	**5.0 Å, π** 6.6 Å, π (x)	9.0 Å, σ (x)	10.0 Å, σ (x)	**3.8 Å, σ**
	3	Cys700	**4.3 Å, π** 8.3 Å, π (x)	9.5 Å, mid (x)		**5.1 Å, σ**
	4	Cys768		9.2 Å, mid (x)		**8.5 Å, mid**
	5	Cys775		**8.6 Å, π**		**5.8 Å, mid**
	6	Cys796		**4.4 Å, π**		
	7	Cys807		**5.5 Å, σ** 8.3 Å, mid (x)	**7.2 Å, π**	8.2 Å, mid (x)
	8	Cys821		**4.3 Å, σ** 7.0 Å, mid (x)	7.1 Å, π (x)	8.0 Å, mid (x)
	9	Cys832		7.0 Å, mid (x)		
	10	Cys842		**9.5 Å, π**		**5.8 Å, mid**
	11	Cys856		8.8 Å, mid (x)		
	12	Cys869		7.6 Å, mid (x)		**7.0 Å, mid**
Pepsin (4PEP)	1	Cys45	8.9 Å, mid (x)	8.4 Å, σ (x)	7.8 Å, mid (x)	
	2	Cys50	**7.2 Å, mid**	9.1 Å, σ (x)	6.9 Å, mid (x)	9.7 Å, mid (x)
	3	Cys206			**5.3 Å, π**	**7.3 Å, mid**
	4	Cys210			**3.8 Å, π**	**7.3 Å, σ**
	5	Cys249				
	6	Cys282				
Horseradish Peroxidase (1HCH)	1	Cys11		**6.0 Å, π**		9.7 Å, mid (x)
	2	Cys44	**3.7 Å, π** 9.5 Å, mid (x)			**6.4 Å, σ** **7.0 Å, σ**
	3	Cys49	**4.1 Å, mid**			7.6 Å, σ (x) 8.8 Å, σ (x)
	4	Cys91		**6.7 Å, π**		9.8 Å, mid (x)
	5	Cys97				
	6	Cys177		8.2 Å, σ (x)		9.0 Å, mid (x)
	7	Cys209		**7.1 Å, σ**		9.5 Å, mid (x)
	8	Cys301				9.0 Å, mid (x)

Table 3 (cont'd). Local aromatic residue motif at Cys residue (continued on next page).

Protein (PDB-ID)	#	*Location*	*His*	*Tyr*	*Trp*	*Phe*
Papain (1PPN)	*1*	Cys22		**5.0 Å, mid**	**6.7 Å, mid**	
	2	Cys25	**3.8 Å, σ**	10.0 Å, mid (x)	**4.5 Å, σ** **7.1 Å, σ**	7.3 Å, mid (x)
	3	Cys56	7.5 Å, σ (x)	**4.7 Å, σ** **7.2 Å, σ** 7.9 Å, mid (x) **9.6 Å, π**		
	4	Cys63		6.6 Å, mid (x)	**7.4 Å, mid**	
	5	Cys95	8.1 Å, σ (x)	**5.9 Å, σ** 6.9 Å, σ (x) **7.1 Å, σ** **9.5 Å, π**		
	6	Cys153				**4.4 Å, σ** **6.1 Å, σ**
	7	Cys200				**3.7 Å, σ** **4.6 Å, σ**
Lysozyme (1DPX)	*1*	Cys6			9.8 Å, mid (x)	9.0 Å, mid (x)
	2	Cys30			**4.4 Å, π** **6.0 Å, mid**	**3.9 Å, σ** 8.3 Å, mid (x)
	3	Cys64		**3.9 Å, π**	**6.6 Å, σ** 9.6 Å, mid (x)	
	4	Cys76			**4.7 Å, mid** 9.0 Å, mid (x)	
	5	Cys80		**3.8 Å, π**	8.3 Å, σ (x)	
	6	Cys94		9.5 Å, mid (x)	**4.7 Å, mid** 7.6 Å, mid (x)	
	7	Cys115			5.3 Å, mid (x) **4.8 Å, π**	**3.8 Å, σ** 9.2 Å, mid (x)
	8	Cys127			8.6 Å, mid (x)	9.0 Å, mid (x)

Table 3 (cont'd). Local aromatic residue motif at Cys residue (continued on next page).

Protein (PDB-ID)	#	Location	His	Tyr	Trp	Phe
Lacto-transferrin (1LFG)	1	Cys9			8.5 Å, mid (x)	
	2	Cys19			**4.5 Å, σ** **5.2 Å, mid**	**6.0 Å, π** **8.3 Å, mid**
	3	Cys36			**5.7 Å, mid** **6.9 Å, mid**	**3.9 Å, mid** 6.9 Å, mid (x)
	4	Cys45			8.5 Å, mid (x)	
	5	Cys115	6.4 Å, mid (x)	6.1 Å, π (x)		**7.7 Å, mid**
	6	Cys157	7.2 Å, mid (x)	**4.4 Å, σ**		8.1 Å, mid (x)
	7	Cys170				7.5 Å, σ (x) 9.9 Å, mid (x)
	8	Cys173	8.5 Å, mid (x)	**5.8 Å, σ**		8.7 Å, mid (x)
	9	Cys181	9.7 Å, mid (x)			8.4 Å, σ (x) 9.1 Å, mid (x)
	10	Cys198	7.2 Å, σ (x)	**4.1 Å, π**		9.9 Å, mid (x)
	11	Cys231	8.6 Å, mid (x)			
	12	Cys245	7.1 Å, mid (x)	10.0 Å, mid (x)		8.1 Å, mid (x)
	13	Cys348			7.0 Å, mid (x)	
	14	Cys358			**4.8 Å, mid** **6.7 Å, mid**	8.3 Å, σ (x) **9.0 Å, mid**
	15	Cys371			**6.7 Å, mid** **8.0 Å, mid**	9.2 Å, mid (x)
	16	Cys380		10.0 Å, mid (x)	7.6 Å, mid (x)	
	17	Cys405		9.8 Å, π (x) 9.9 Å, π (x)		
	18	Cys427		8.8 Å, mid (x)		7.7 Å, mid (x)
	19	Cys459	6.9 Å, mid (x)	5.8 Å, π (x)		7.4 Å, mid (x)
	20	Cys483		8.1 Å, mid (x)		**4.7 Å, σ** **6.4 Å, π**
	21	Cys493	7.4 Å, σ (x)	**5.6 Å, σ**		
	22	Cys504				
	23	Cys507	8.3 Å, σ (x)	**6.8 Å, mid**		
	24	Cys517		9.3 Å, mid (x)		
	25	Cys534	7.6 Å, mid (x)	**4.0 Å, π**		9.1 Å, mid (x)
	26	Cys575	8.6 Å, mid (x)		9.2 Å, mid (x)	
	27	Cys589	7.3 Å, mid (x)		9.2 Å, mid (x)	
	28	Cys627				**7.2 Å, σ** **7.3 Å, mid** 8.2 Å, mid (x)
	29	Cys632				7.1 Å, mid (x) 7.4 Å, σ (x) **8.2 Å, mid**
	30	Cys649	**9.8 Å, σ**	9.3 Å, mid (x)		6.8 Å, mid (x)
	31	Cys677		7.5 Å, mid (x)	8.9 Å, σ (x)	**4.1 Å, mid** **4.7 Å, mid**
	32	Cys686				9.1 Å, mid (x)

Table 3 (cont'd). Local aromatic residue motif at Cys residue.

Protein (PDB-ID)	#	Location	His	Tyr	Trp	Phe
Trypsin Inhibitor (1BA7)	1	Cys39				**8.9 Å, mid**
	2	Cys86				**8.3 Å, mid**
	3	Cys136			**7.6 Å, mid**	6.7 Å, mid (x) 7.9 Å, mid (x)
	4	Cys145			9.0 Å, σ (x)	8.0 Å, mid (x) 9.7 Å, mid (x)
α-2-macro globulin (4ACQ)	1	Cys48	7.9 Å, mid (x)	**9.5 Å, mid**		
	2	Cys86	6.4 Å, mid (x)			
	3	Cys251	7.5 Å, mid (x)	6.1 Å, π (x)		8.9 Å, σ (x) 9.7 Å, σ (x)
	4	Cys269	8.1 Å, mid (x)			**8.3 Å, mid**
	5	Cys278	8.1 Å, mid (x)			
	6	Cys287	9.9 Å, σ (x)			6.8 Å, mid (x)
	7	Cys299	7.3 Å, mid (x)	**3.9 Å, π**		8.2 Å, σ (x)
	8	Cys431		**7.9 Å, σ**		
	9	Cys470		10.0 Å, π (x)		**9.6 Å, mid**
	10	Cys563		8.2 Å, π (x)		**9.4 Å, mid**
	11	Cys595				**8.6 Å, mid**
	12	Cys642	8.5 Å, mid (x)			
	13	Cys689	10.0 Å, mid (x)			
	14	Cys771				7.8 Å, mid (x)
	15	Cys821				
	16	Cys847	**7.4 Å, mid**			
	17	Cys849				
	18	Cys883	9.2 Å, mid (x)			
	19	Cys921		**8.1 Å, mid** 8.6 Å, σ (x)		
	20	Cys972		6.4 Å, mid (x) 8.7 Å, mid (x)		**7.0 Å, π**
	21	Cys1079				**7.1 Å, mid** **8.8 Å, σ**
	22	Cys1127				**7.6 Å, σ** **8.1 Å, mid**
	23	Cys1321		**7.9 Å, mid** 9.4 Å, σ (x)		8.4 Å, mid (x)
Insulin monomer (4M4L)	1	Cys6A	9.1 Å, mid (x)	7.3 Å, mid (x)		
	2	Cys7A	**4.2 Å, mid** 8.6 Å, σ (x)	**9.9 Å, σ**		
	3	Cys11A	**7.8 Å, σ**	8.5 Å, mid (x)		
	4	Cys20A		7.2 Å, σ (x) 9.9 Å, π (x)		6.6 Å, mid (x) 9.5 Å, σ (x)
	5	Cys7B	**3.7 Å, mid** **7.2 Å, mid**			
	6	Cys19B		6.9 Å, σ (x) **8.2 Å, π**		**4.3 Å, mid** 9.4 Å, mid (x)

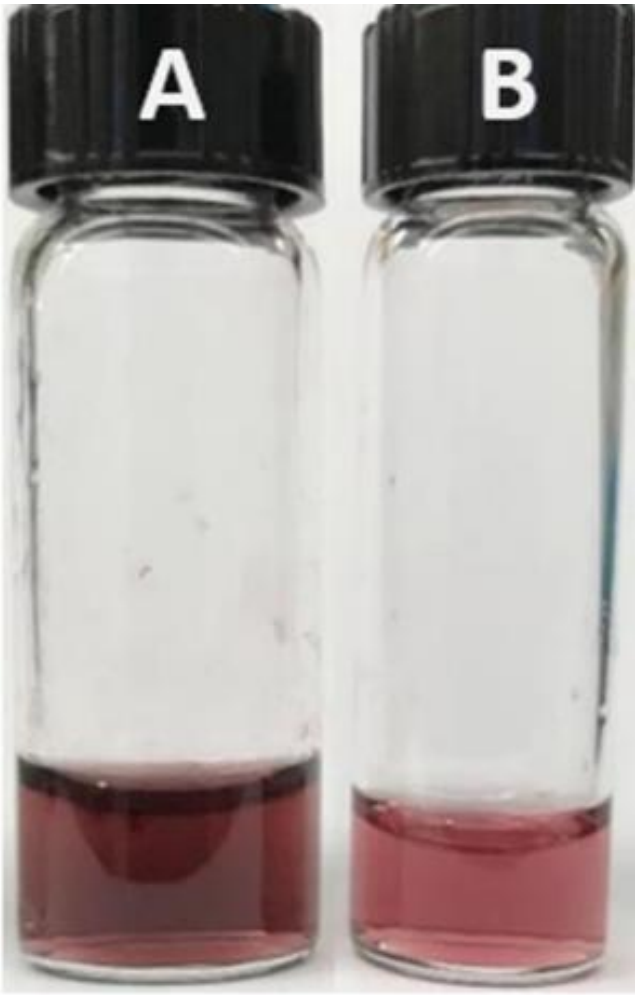

Figure 35. (A) α-2-macroglobulin and (B) trypsin inhibitor, reacted with Au(III) according to the Standard protocol. These samples did not exhibit the characteristic red luminescence and the colors of the solutions in ambient light were also different from the characteristic yellow-brown color exhibited in the red luminescent protein-Au complexes.

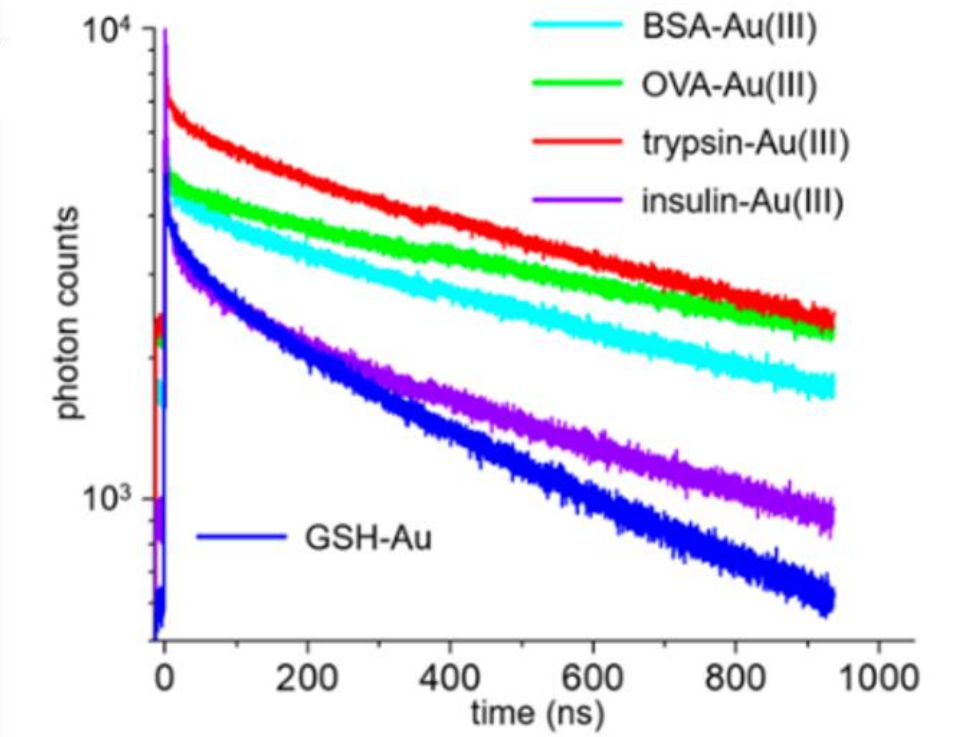

Lifetime	τ_1 (ns)	τ_2 (ns)	τ_3 (ns)
BSA-Au(III)	301.1 (93%)	38.3 (5%)	1.6 (2%)
OVA-Au(III)	372.8 (92%)	39.6 (5%)	1.6 (3%)
Trypsin-Au(III)	297.6 (91%)	36.1 (6%)	1.6 (3%)
Insulin-Au(III)	311.9 (90%)	50.6 (5%)	1.4 (5%)
GSH-Au	189.9 (95%)	16.4 (3%)	1.9 (1%)

Figure 36. Decay of the red luminescence at $\lambda_{ex}/\lambda_{em}$ = 389/665 nm, measured by TCSPC for the four proteins (BSA, OVA, trypsin, and insulin) and small thiol molecule GSH, ~48 h after reaction with Au(III). Triple-exponential fit, after deconvolution of instrument response, is shown in table.

The slow lifetime observed in the red luminescent protein-Au complexes is generally seen in other complexes which involve a ligand-to-metal or a metal-to-ligand charger transfer mechanism (LMCT or MLCT). This charge transfer is usually observed in Au ← S LMCT, and the mechanism assigned is the result of luminescence in Au(I)-thiolates.[119-122] Thus, to determine if the red luminescence observed is similar to Au-

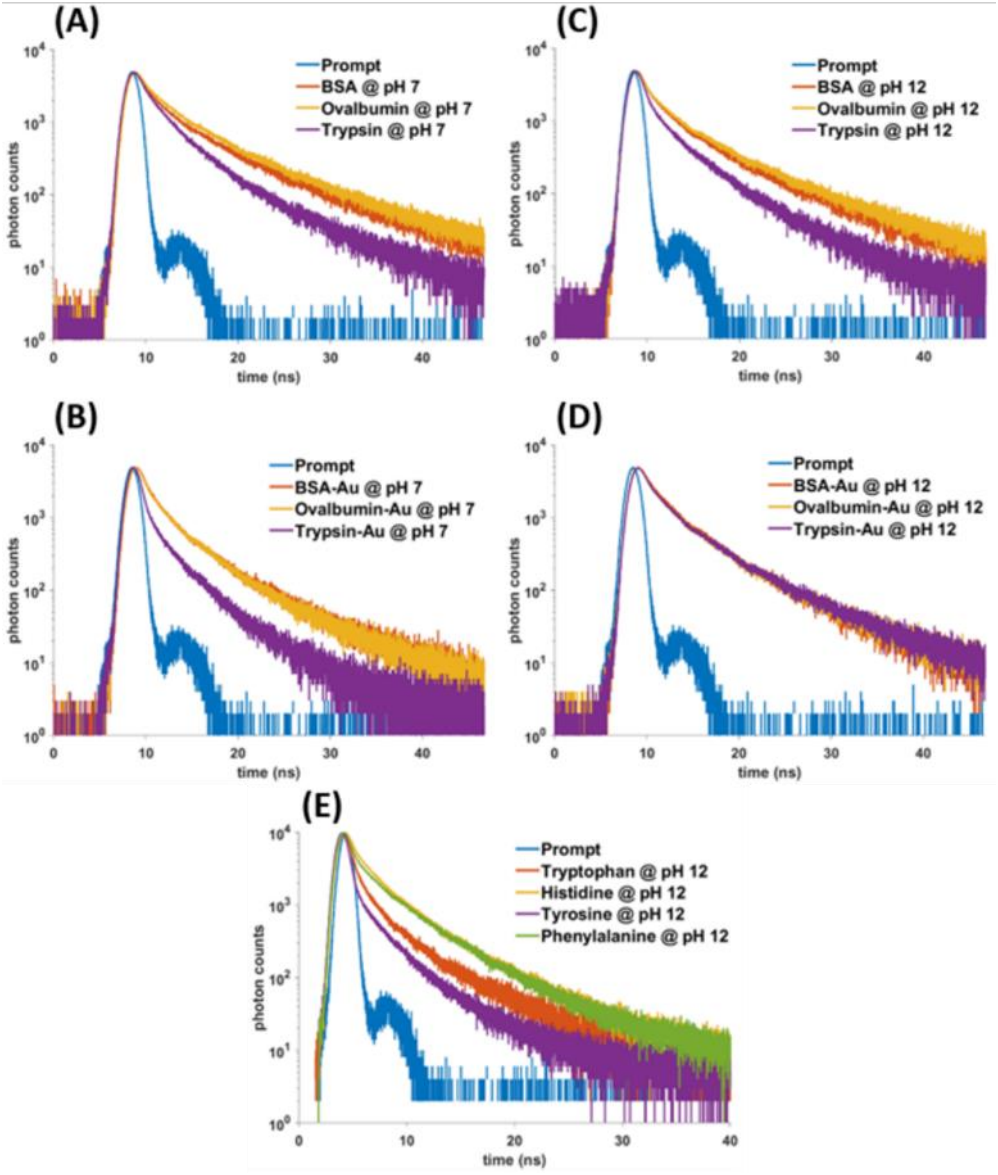

Figure 37. Luminescence (blue regime) lifetimes ($\lambda_{ex}/\lambda_{em}$ = 389/450 nm) by TCSPC for (A) proteins at pH = 7; (B) protein-Au compound at pH = 7; (C) proteins at pH = 12; (D) protein-Au compound at pH = 12. Excitation-emission spectra (λ_{ex}= 300-500 nm; λ_{em}= 300-700 nm) of proteins and protein-Au compounds showed the peak $\lambda_{ex}/\lambda_{em}$ = 400/460 nm ("peak b") in Figure 8. (E) Lifetimes of free aromatic residues were additionally measured at pH = 12, and no significant changes were observed from known literature values for pH = 7. Lifetime values are summarized in **Table 4**.

thiolate compounds reduced glutathione was reacted with Au(III), which is known to form these Au-thiolate complexes.[121,123,124]

Table 4. Analysis of luminescent 'blue-regime' TCSPC lifetime data of (A) proteins at pH = 7; (B) protein-Au compound at pH = 7; (C) proteins at pH = 12; (D) protein-Au compound at pH = 12; (E) Free aromatic amino acid residues. All lifetime compounds were <10 ns and like that of free aromatic amino acid residues.

	Lifetime (450 nm)	τ_1 (ns)	τ_2 (ns)	τ_3 (ns)
(A)	BSA, pH=7	8.25 (50%)	2.25 (35%)	0.310 (15%)
	OVA, pH=7	8.82 (52%)	2.60 (36%)	0.352 (12%)
	Trypsin, pH=7	7.26 (28%)	2.35 (55%)	0.417 (17%)
(B)	BSA-Au, pH=7	6.65 (36%)	1.88 (42%)	0.224 (22%)
	OVA-Au, pH=7	6.58 (34%)	2.09 (43%)	0.323 (23%)
	Trypsin-Au, pH=7	6.12 (15%)	1.80 (30%)	0.651 (55%)
(C)	BSA, pH=12	8.55 (41%)	2.41 (38%)	0.357 (21%)
	OVA, pH=12	8.80 (47%)	2.34 (35%)	0.305 (18%)
	Trypsin, pH=12	6.18 (15%)	1.92 (30%)	0.280 (55%)
(D)	BSA-Au, pH=12	6.75 (43%)	2.24 (43%)	0.238 (14%)
	OVA-Au, pH=12	7.21 (41%)	2.19 (42%)	0.233 (17%)
	Trypsin-Au, pH=12	7.29 (42%)	2.21 (41%)	0.240 (17%)
(E)	tryptophan, pH=12	7.45 (23%)	1.78 (36%)	0.363 (41%)
	histidine, pH=12	7.03 (43%)	2.40 (38%)	0.390 (19%)
	tyrosine, pH=12	5.37 (19%)	1.59 (20%)	0.227 (61%)
	phenylalanine, pH=12	6.74 (48%)	2.18 (26%)	0.331 (26%)

The red luminescence observed in the glutathione-Au complex (**Figure 38**) also exhibited a slow lifetime of $\tau_1 \sim 200$ ns (95%) on the order of magnitude of the protein-Au complexes, along with other comparable lifetimes when fit with a triple exponential): which are: $\tau_2 \sim 16$ ns (~3%), and $\tau_3 \sim 1.9$ ns (~1%). The primary lifetime of glutathione-Au is notably shorter than the primary lifetimes of protein-Au complexes. This observed difference in the lifetimes could be attributed to LMCT/MLCT with cystine and other residues in the luminophore site of protein-Au complexes. The addition of another amino acid may be possible as stable metal coordination in proteins involves multiple residues. It is further possible that the oxidation state of Au may change from its initial Au(III) due to

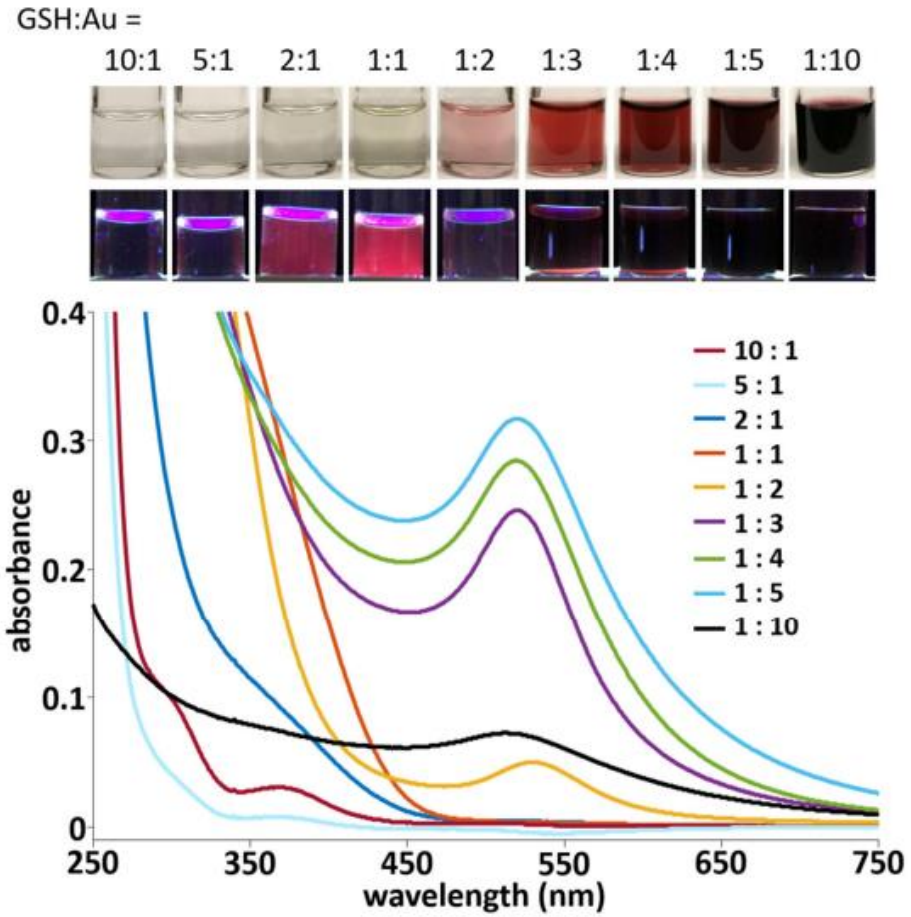

Figure 38. The luminescence of the GSH-Au complex reacted with GSH : Au molar ratio in the range 10 : 1 and 1 : 10, while keeping the moles of GSH constant. Samples in the range of 1 : 2 and 1 : 10 ratios exhibited surface plasmon peaks at ~520 nm, indicating Au nanoparticle formations, whereas in the range of 10 : 1 and 1 : 1 did not show surface plasmon peaks. Red luminescence resulted from the samples with 2 : 1 and 1 : 1 ratio.

the coordination of Au to cystine within the proteins; explaining how an Au(I)-thiolate or Au(0)-containing complex is formed similar to the glutathione-Au complex.

Overall, the static and dynamic characters of the red luminescence in the protein-Au complexes of BSA, ovalbumin, trypsin, and insulin were completed. Among these results it was determined that the red luminescence in ovalbumin-Au, trypsin-Au, and insulin-Au were due to the same mechanism of luminescence that was detailed for BSA-Au. Among these results it appears that an insulin of multimers is required for red luminescence while all other protein-Au complexes are derived from single monomers of

protein. Despite this difference, all four proteins showed that luminescence was similarly dependent on pH and stochiometric protein-to-Au ratio. Furthermore, these protein-Au complexes showed the same excitation-emission spectra at pH 12.

The synthesis of red luminescent protein-Au complexes appears to necessitate the presence of cystine, shown by smaller thiol-containing compounds. The kinetics of luminescence formation could consistently be described with a Langmuir-type multi-site absorption model of Au upon the change of protein conformation above the pH range of 10. This suggests that the complex formed is more likely a thiol-containing-Au compound than a small nucleating cluster of Au^0. Moreover, the lifetimes of the red luminescent complexes shared a common value of around 300 ns and were like that of a known glutathione-Au complex involving Au ← S LMCT, consistent with Au coordinating to a cystine residue. Finally, tertiary structural analysis indicates that the formation of the luminophore within proteins may be due to the additional coordination of local residues and that a large enough space of ~ 5.5 Å is required for Au to achieve this. The characterization of the static and dynamic properties of these red luminescent proteins along with structural analysis may lead to the discovery of other proteins that can produce similar fluorescent complexes. Determining the exact binding location and structure of this luminophore within proteins is the next critical step to fully elucidating this red luminescent complex.

CHAPTER 5: RESOLVING THE RED-LUMINOPHORE-FORMING DOMAIN WITHIN SERUM ALBUMIN-GOLD COMPLEXES

Proteins are inherently precise organic nanomaterials and the problem with the chemical synthesis of inorganic nanomaterials is the lack of precision, especially in the size distribution,[3] which limits the ability to construct long-range-ordered structures. Thus, proteins could act as a more ideal starting point for achieving this high order of precision.[4-6] On top of their predictably precise size, proteins contain inherent dynamic characteristics such as conformational changes,[125] which could be utilized to build new, tunable structures. This tunability could be in the form of a tunable fluorescence and some proteins appear to be luminescent under certain reaction conditions.

BSA-Au and HSA-Au complexes, along with 8 other protein-Au complexes have unique red luminescent properties.[23,126] Through the addition of gold(III) chloride to an aqueous solution of protein and a subsequent pH change from neutral to basic (> 10.0) a UV-excitable red luminescence is observed – described in further detail in the methods section. This luminescence has applications which could be utilized for sensing, imaging, or in nanomedicine, yet this mechanism is not fully understood and the complex responsible for red luminescence has not been isolated. Initial reports of this complex assign the luminophore as a nucleated nanocluster supported in a protein 'cage', but as shown by others,[13] a pH-controlled dynamic conformational change in BSA, HSA, and other proteins appears to be the primary pathway for red luminescence to occur. As well as pH-controlled luminescence, the luminophore in question appears to fit a Langmuir-type multiple-site adsorption model better than a classical LaMer model for single nucleating-

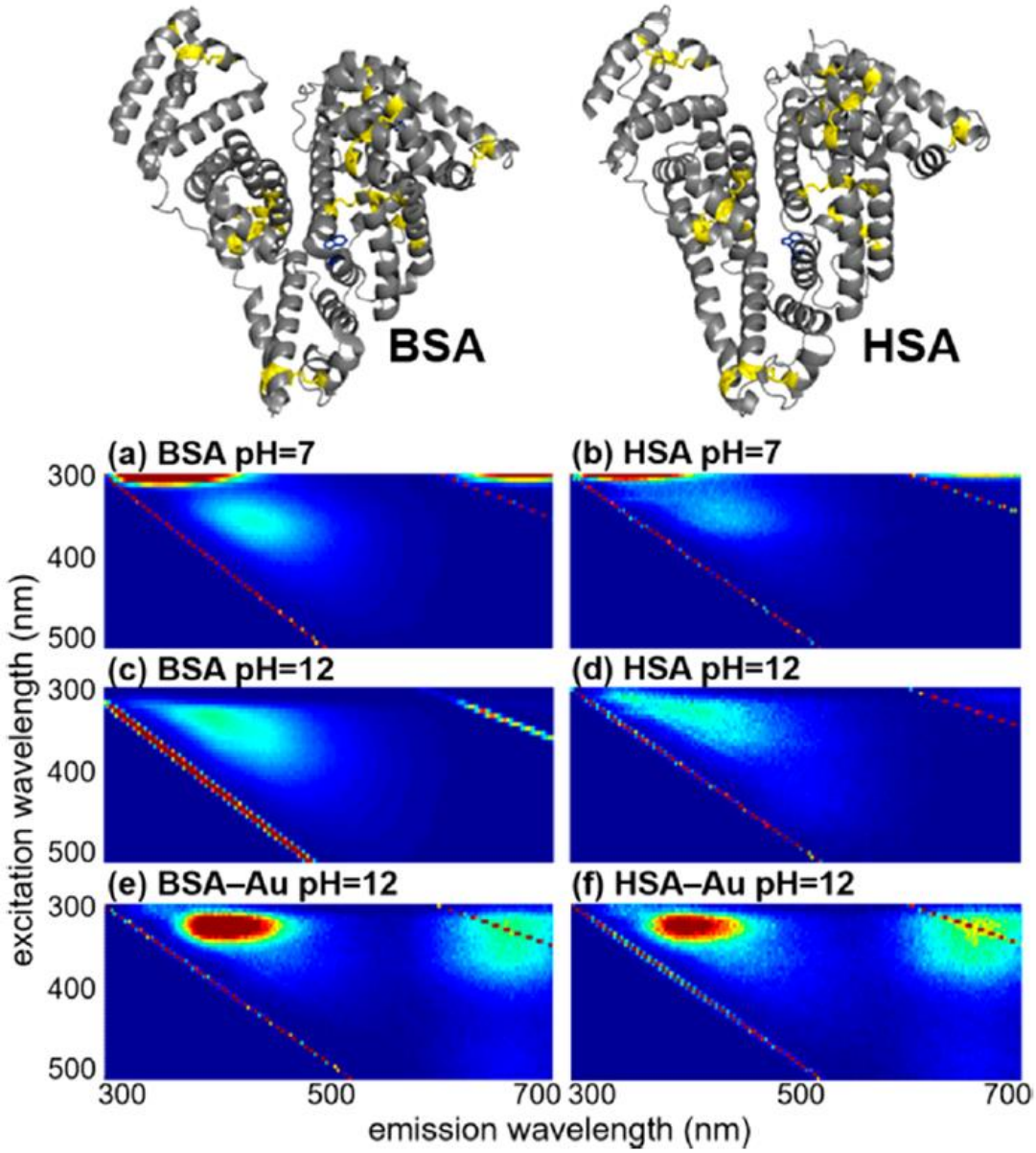

Figure 39. (top) Tertiary structures of BSA and HSA at pH 7. Cysteine−Cysteine disulfide bonds are indicated in yellow. PDB IDs 4F5S for BSA and 1AO6 for HSA. (a, b) Nearly identical innate luminescence properties of BSA and HSA at pH 7 and (c, d) 2 h after the pH was raised to 12. Excitation−emission maps show changes in the UV and blue luminescence of aromatic residues, indicating dynamic changes in their local environments. (e, f) Excitation−emission maps of BSA−Au and HSA−Au at 24 h.

nanoclusters. Thus, it would be of immense value to determine the adsorption site responsible for red luminescence.

BSA and HSA have very similar structures, amino acids sequences, and *in vivo* properties (**Figure 39**).[127] BSA and HSA are comprised of 583 and 585 amino acid residues

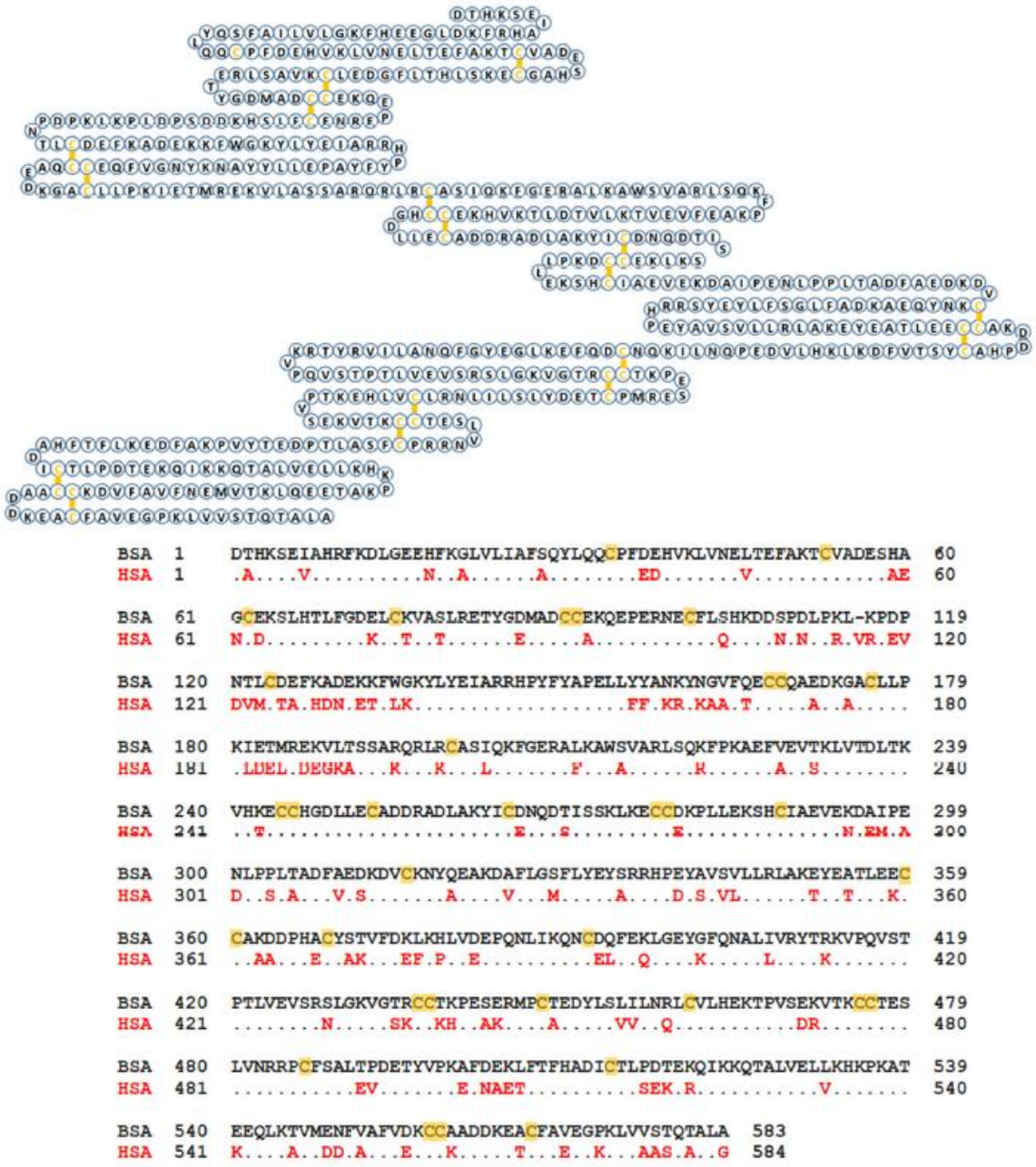

Figure 40. The amino acid sequences of BSA and HSA share identical Cysteine contents and locations, resulting in similar tertiary structures. Top panel: Amino acid sequence of BSA. Cys-Cys bonds are indicated as yellow. Bottom panel: Amino acid sequences are 76% identical between BSA and HSA. In terms of luminescence properties, the distributions of aromatic residues are also similar between BSA and HSA, while one major difference is the number of tryptophan residues (BSA: two tryptophan, Trp134 and Trp213; and HSA: single tryptophan, Trp214). PDB ID: 4F5S (BSA); 1BM0 (HSA).

(66.4 kDa and 66.5 kDa), respectfully. Both proteins have 35 cysteine residues, with one surface-exposed Cys34 residue and the others forming the internal backbone of the tertiary

structure via one Cys-Cys disulfide bond and eight localized Cys-Cys/ Cys-Cys disulfide bond clusters. The luminescent properties of BSA-Au and HSA-Au complexes are also identical in excitation-emission maps and appear to have the same cascaded energy transfer mechanism responsible for red luminescence just like ovalbumin-Au, trypsin-Au, and insulin-Au (**Figure 40**).[1,13,66]

The dynamics of luminophore formation in the BSA-Au complex and other protein-Au complexes was described wherein Au binds to one of the cystine disulfide bond locations that have become solvent accessible at higher pH. For BSA specifically, of the five reversible conformations at various pH values, only the A-form of BSA (and HSA, which has similar pH-induced conformational shapes), allowed for this solvent accessibility of a cystine disulfide bond. However, the exact location of the luminophore has yet to be determined in BSA, HSA, or any other protein with red luminescent properties. Therefore, it is an important first step to identify the domain in which the luminophore residues in BSA and HSA, and then further investigate the exact binding site(s) of the luminescent complex. Thus, two complementary methods of protein fragment preparation which preserve the cysteine disulfide bonds of the protein can be used to isolate the domain and ultimately the exact binding site. These techniques are limited enzymatic proteolysis and molecular cloning of protein fragments.

5.1 Experimental Methodology and Instrumentation.

The BSA-Au or HSA-Au complex was prepared by adding 1 mL of aqueous $HAuCl_4$ solution into 1 mL of aqueous BSA at 75 μM or 5 mg/mL. The BSA-to-Au molar ratio was BSA : Au = 1 : 10 for all standard reactions. The solutions were combined under vigorous stirring for 2 minutes at 700 rpm and upon the addition of Au to BSA, the color

of the solution turned from clear to a faint yellow and the pH was ~ 6.0. After 30 seconds 100 μL of fresh 1 M NaOH was added to bring the pH to 12.5. This reaction then proceeded at 37°C for 2 hours and was stored at 20°C.

The synthesis of enzyme-digested BSA-Au or HSA-Au to form complex-fragments was prepared as follows: An aqueous solution of Trypsin was prepared freshly in water containing 50 mM Tris-HCl and 50 mM NaCl with a pH of 8.0. The aqueous solution of trypsin was added to an aqueous solution of BSA (75 μM, or 5 mg/mL) also containing 50 mM Tris-HCl and 50 mM NaCl with a pH of 8.0. The weight ratio of trypsin to BSA was 1 : 50 (protease : protein) and was incubated at 37°C for 2 minutes. No sodium dodecyl sulfate (SDS), dithiothreitol (DTT), or urea was added to the solution. No temperature annealing was performed in order not to cause further denaturation of the protein. 1 mL of aqueous HAuCl4 was added to 1 mL of the digested BSA-trypsin with a molar ratio of BSA : Au = 1 : 10. After 2 minutes, 1 M NaOH was added until a pH of 12.5 was achieved. The basic pH quenches the enzymatic activity of trypsin. The sample was stirred at 750 rpm for 2 hours at 37°C. The final product was used immediately to ensure no more digestion took place and was used without further purification.

Proteins that were enzymatically digested were also run through a gel for fragment size analysis using the following protocol: A pre-cast 4-12% gradient Bis-Tris (NuPAGE) and MES running buffer (NuPAGE) were used for gel electrophoresis. The sample buffer contained the same amount of protein in a 20% glycerol solution for all lanes. No sodium dodecyl sulfate (SDS), dithiothreitol (DTT), or urea was added to the sample buffer. No temperature annealing was performed to maintain the relative structure of the protein fragments. The gel was run for 1 hour at a constant voltage of 150 V. After electrophoresis,

the in-gel luminescence was measured with a gel imaging system (Azure C400) using λ = 365 nm excitation and a bandpass filter of $\lambda = 685 \pm 25$ nm, to record the red luminescence. The gel was subsequently stained with Coomassie Brilliant Blue for the molecular weight analyses of the fragmented bands.

To study the red luminescence of molecularly cloned GST-HSA fragments a protocol must first be followed to create the domain-based fragments without digestion. HSA was used in place of BSA for this protocol as the cDNA sequence for HSA was more readily available and the structure of BSA and HSA is nearly identical as well as the red luminescence between BSA-Au and HSA-Au.

Human serum albumin (HSA) cDNA was obtained from Sino Biological. The HSA cDNA was cut into two separate fragments (residues 1-313 and 314-585(C-terminus)). The cDNA encoding HSA amino acids 1-313 was PCR amplified with 5′ HSA (XhoI) primer and 3′ HSA N-313 rev (NotI) primers (5′-CCGCTCGAGGATGCACACAAGAGTGAGGTTGC and 5'-TAAAAGCGGCCGCTTACTTACTTTCAACAAAATCAGCAGC), and then cloned into vector pETDuet-1.

The cDNA encoding HSA amino acids 314-C-terminus was PCR amplified with 5′ HSA 314-TAA (XhoI) primer and 3′ HSA with TAA (NotI) primer (5′-CCGCTCGAGGATGTTTGCAAAAACTATGCTGAGGC and 5'-TAAAAGCGGCCGCTTATAAGCCTAAGGCAGCTTGAC), and then cloned into vector pETDuet-1. The cDNA XhoI–NotI fragments from HSA 1-313/pETDuet-1 or HSA 314-C-terminus/pETDuet-1 were cloned into pGEX6P-1 (GE Healthcare). After construction, all expression vectors were confirmed by DNA sequencing. The *E. coli* strain

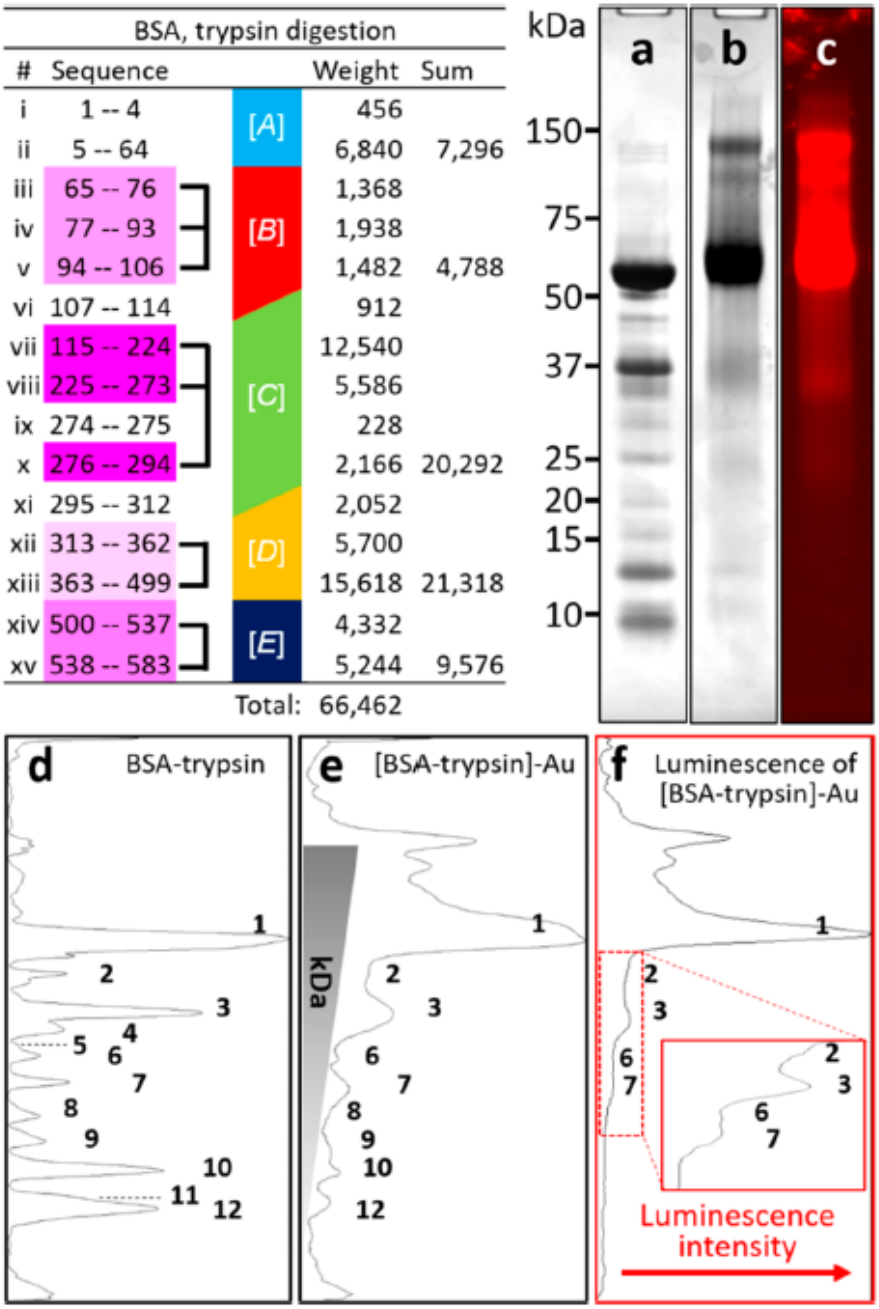

Figure 41. Cys−Cys bond-preserving limited proteolysis of BSA by trypsin. The table shows the results of tryptic cleavage in the random coil regions, which can result in 15 fragments (i–xv), with Cys−Cys bonds connecting the sequences as indicated. (a) Gel electrophoresis of the tryptic fragments of BSA obtained by the limited proteolysis. A total of 12 bands were observed. (b) Tryptic BSA fragments reacted with Au(III). (c) In-gel luminescence of (b). (d–f) Line sections of (a–c).

for the GST fusion protein purification was as described in the literature,[128] and the protein was purified from *E. coli* following an already published procedure.[129,130]

To describe the essential details, a single colony was incubated in 1,200 mL of Terrific Broth medium (TB) containing 0.5% glycerol, 0.05% glucose, 0.2% α-lactose, 100 μg/ml carbenicillin, and 50 μg/mL chloramphenicol at 18°C for 72 h. Cells were harvested by centrifugation (5000 x *g* for 20 min) and washed with ice-cold phosphate-buffered saline (PBS). After centrifugation (5000 x *g* for 15 min), 10 volumes of buffer C (50mM Tris–HCl (pH 8.0), 10% glycerol, 0.5 M NaCl, 1 mM EDTA, 0.1% Nonidet P-40 and 5 mM 2-mercaptoethanol) was added to the pellet. The resuspended mixture was sonicated on ice (50 cycles of 5 sec with a 10 sec pause). DNA and debris were removed by centrifugation (14,000 rpm for 40 min). The supernatant was filtrated by 0.45 μm filter and incubated with 500 μL of Glutathione Sepharose 4B (GE Healthcare) at 4°C for 2 h. The resin was washed three times with 5 mL (10 times resin volume) of buffer C and then washed three times with 4 mL (8 times resin volume) of buffer C containing 1 M NaCl.

The protein was eluted by buffer C containing 20 mM reduced glutathione. Protein was applied to Econo-Pac 10DG Column (Bio-Rad) and equilibrated with buffer A (100 mM NaCl and 100 mM Tris–HCl (pH 8.0)). Purified GST-[HSA1-313] and GST-[HSA314-585] were concentrated to 150 μg/mL and 50 μg/mL respectively and were stored at -80°C prior to the next steps. The protein was resuspended in HPLC-grade water by buffer exchange to remove Tris-HCl and NaCl, via repeated centrifugation using a 3 kDa-cutoff centrifuge filter tube (Amicon Ultra), by reducing the volume to half (3500 rpm for 20 min) and refilling with water subsequently each time. This centrifugation was repeated 5 times at 4°C. The solution was concentrated to 1 mg/mL by vacuum concentrator (Savant SpeedVac), while avoiding the samples to freeze. The final product was used immediately.

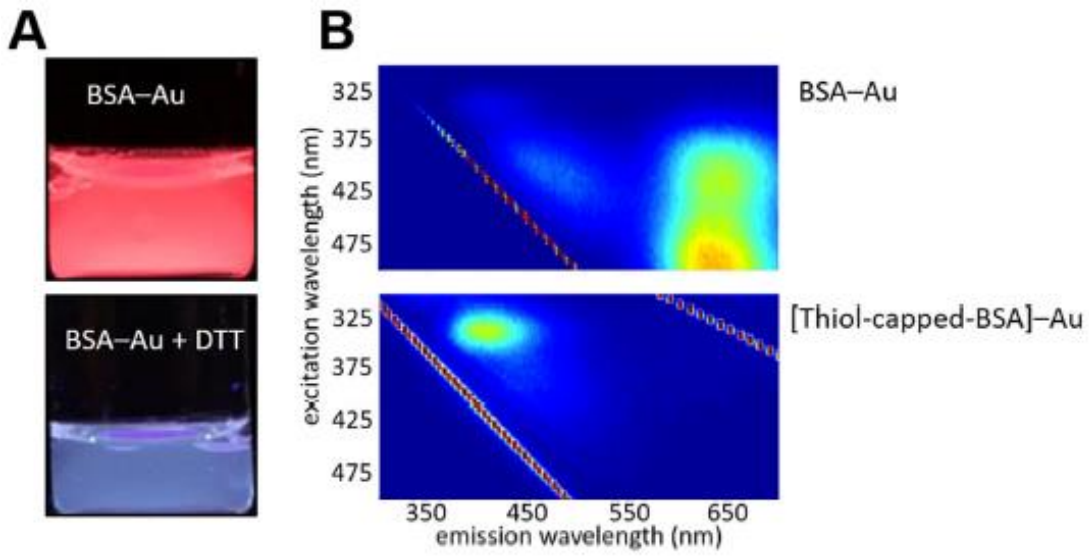

Figure 42. (**A**) Cleaving of the Cys-Cys disulfide bonds in the BSA–Au complex quenched the UV (λ = 365 nm)-excited red fluorescence of the BSA–Au complex. The red fluorescence of the dithiothreitol (DTT)-treated BSA–Au complex was readily quenched. The blue fluorescence is from the aromatic residues of BSA at pH = 12. It is noted that this blue fluorescence is identical to that of BSA at pH = 12, without the addition of Au (Dixon and Egusa, *J. Am. Chem. Soc.* **2018**, 140, 2265 – 2271). (**B**) Disulfide bonds in BSA were cleaved with tris(2-carboxyethyl)phosphine (TCEP) and capped with N-ethylmaleimide (NEM). This thiol capped BSA did not yield the red luminescence upon reaction with Au. The excitation-emission maps for BSA–Au and [Thiol-capped-BSA]-Au were measured at 48 h.

To synthesize GST-[HSA1-313]–Au and GST-[HSA314-585]–Au complexes as well as HSA–Au and GST–Au controls, the concentrations were modified to accommodate the small quantity of protein, from Protocol 1 as follows. 200 µL of HAuCl4 aqueous solution was added to 200 µL of aqueous solutions of the proteins (GST-[HSA1-313] and GST-[HSA314-585], as well as HSA and GST) (25 µM). The protein-to-Au molar ratio was 1 : 10. The two solutions were combined under stirring at 750 rpm for 2 minutes. Upon addition of HAuCl4, the pH of the solution was 7.0. 1 M NaOH was then added to the solution until a pH of 12.5 was achieved. The reaction proceeded for 2 hours at 37°C.

5.2 Limited Tryptic Proteolysis of BSA and HSA.

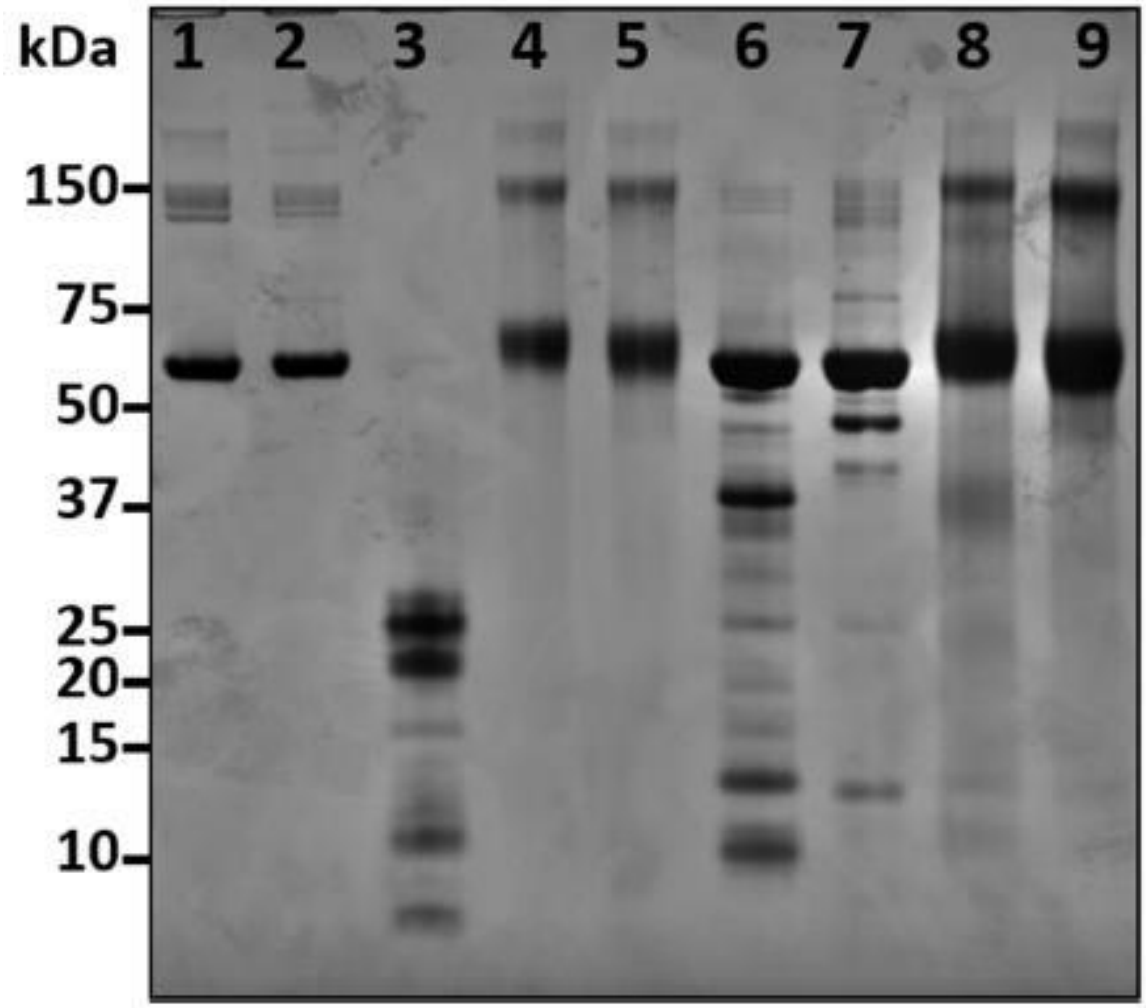

Figure 43. Lane (1) BSA; (2) HSA; (3) Trypsin; (4) BSA–Au; (5) HSA–Au; (6) BSA-trypsin; (7) HSA-trypsin; (8) [BSA-trypsin]–Au; (9) [HSA-trypsin]–Au. The protein loading was 5 μg/lane for all lanes. The image shows the black and white contrasted image of the gel after the addition of Coomassie blue staining solution was added.

Limited enzymatic proteolysis of BSA and HSA was performed using trypsin as the enzyme and the obtained fragments were evaluated for their luminescence (**Figure 41**). Cleavage of all the cystine disulfide bonds and complete linearization of the protein, via denaturing agents such as dithiothreitol, urea, and SDS is necessary for conventional proteolysis. However, the preservation of the Cys-Cys bond is critical for the formation of the red luminophore, and thus non-standard proteolysis techniques are required (**Figure 42**).

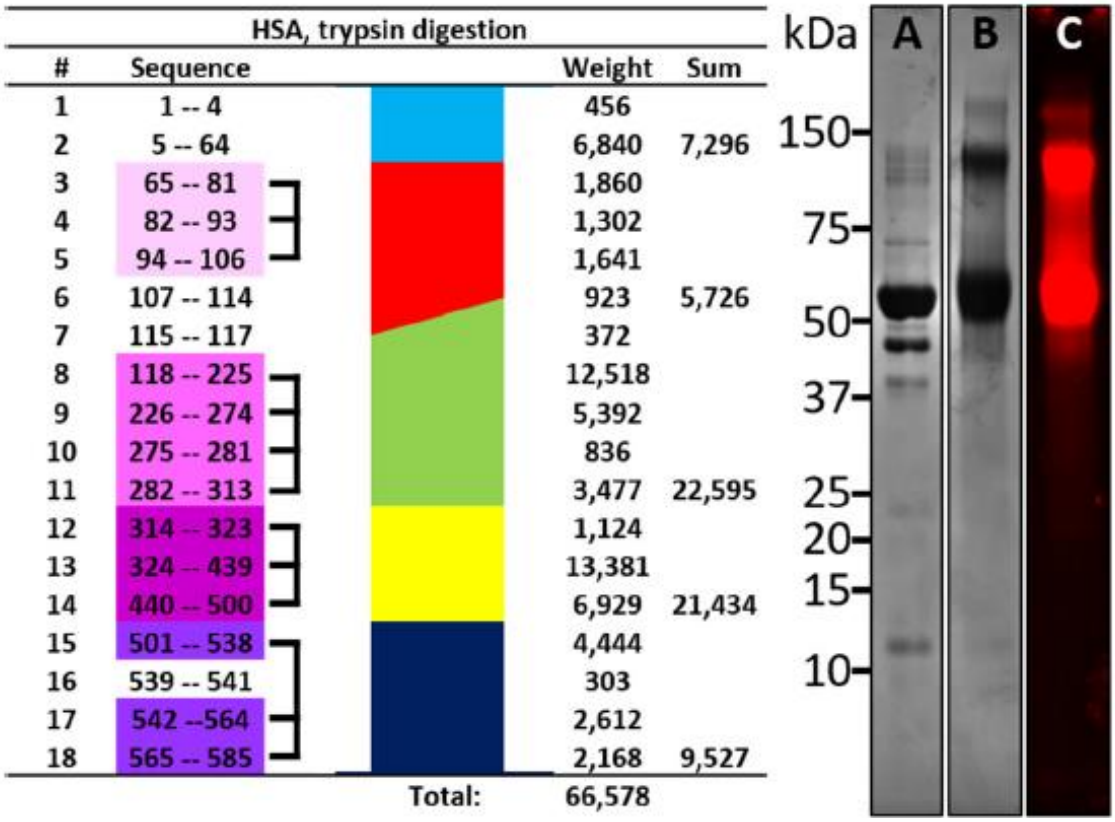

HSA, trypsin digestion

#	Sequence	Weight	Sum
1	1 -- 4	456	
2	5 -- 64	6,840	7,296
3	65 -- 81	1,860	
4	82 -- 93	1,302	
5	94 -- 106	1,641	
6	107 -- 114	923	5,726
7	115 -- 117	372	
8	118 -- 225	12,518	
9	226 -- 274	5,392	
10	275 -- 281	836	
11	282 -- 313	3,477	22,595
12	314 -- 323	1,124	
13	324 -- 439	13,381	
14	440 -- 500	6,929	21,434
15	501 -- 538	4,444	
16	539 -- 541	303	
17	542 --564	2,612	
18	565 -- 585	2,168	9,527
	Total:	66,578	

Figure 44. The limited tryptic proteolysis of HSA resulted in eight bands, Band(1) = undigested HSA, Band(2) ~48 kDa; Band(3) ~45 kDa; Band(4) ~43 kDa; Band(5) ~27 kDa; Band(6) ~23 kDa; Band(7) ~13 kDa; Band(8) ~12 kDa. The expected tryptic cuts at Lys and Arg locations in random coil regions produce five fragments connected by Cys-Cys bonds: [*A*] (7.3 kDa, residues 1 – 64); [*B*] (4.8 ~ 6.1 kDa, residues 65 – 106/117); [*C*] (22.2 ~ 23.5 kDa, residues 107/118 – 313); [*D*] (21.4 kDa, residues 314 – 500); and [*E*] (9.5 kDa, residues 500 – 585) (color coded in Table as blue, red, green, yellow, and dark blue).

The observed eight gel bands can be assigned using these fragments as: Band(1) = [*ABCDE*] (undigested); Band(2) = [*CDE*] (connected fragments); Band(3) = [*BCD*]; Band(4) = [*CD*]; Band(5) = [*BC*]; Band(6) = [*D*]; Band(7) = [*A*]+[*A*]; Band(8) = [*AB*]. There were four clearly visible bands in the [HSA-trypsin]–Au Lane. These were Band(1), (3), (6), and (8). The in-gel luminescence was observed in Band(1) = [*ABCDE*] (undigested) and Band(3) = [*BCD*], but not observed in Band(6) = [*D*]; Band(8) = [*AB*].

This in-gel luminescence band pattern can be explained by the presence of a red luminophore in the tryptic fragment [*C*].

While the crystal structures of BSA and HSA are known for neutral pH conformations, these structures are unknown for non-neutral pH conformations, including the A-form of BSA and HSA. Thus, the focus is placed on identifying the luminophore-forming domain without addressing the structural details of the Au coordination at these

non-neutral pH conditions. In Chapter 3, the kinetics of luminophore formation showed that Langmuir-type chemisorption better explains the mechanism of luminophore formation over a LaMer-type nucleating model. Furthermore, a change in the oxidation sate of Au from Au(III) to Au(0) or Au(I) may likely be involved in the luminophore formation, but further studies are needed to determine the exact oxidation state of Au after the protein-Au complex has been formed, which are addressed in a later chapter.

The limited tryptic fragments of BSA and HSA were reacted with Au and then analysis of the resulting in-gel luminescence was performed after electrophoresis. The details of the experimental procedure for BSA are outlined in **Figure 41** and the digested samples of BSA, HSA, BSA-Au, and HSA-Au are outlined in **Figure 43**. Similarly, the results of tryptic digestion of HSA are shown in **Figure 44**. The yield of digestion of HSA was lower than that of BSA. This is likely due to the residues 64, 106, 313, and 500, which are the expected tryptic cut locations, but are either preceded by, or followed by, an acidic residue. An acidic residue on either side of lysine or arginine can decrease trypsin activity at that site.[131]

In BSA it would be expected that five large fragments connected by unbroken Cys-Cys disulfide bonds would be produced as the result of the limited proteolysis of the protein. These major fragments are noted as [A] (7.3 kDa, corresponding to residues 1 - 64), [B] (5.9 kDa, corresponding to residues 65 – 114), [C] (20.1 – 22.4 kDa, corresponding to residues 115/177 – 294/312), [D] (21.3 – 23.4 kDa, corresponding to residues 295/313 – 499), and [E] (9.5 kDa, corresponding to residues 500 – 583). These results are further shown in **Figure 41**.

Table 5. An ideal total tryptic proteolysis of BSA is shown above, where the letters in sequence represent the expected fragments. The largest peptide observed from this theoretical proteolysis would be fragment 5, with a mass of 2,419 Da. The average and median peptide weights would be 857 Da and 736 Da, respectively. Significantly less than the ~8-50 kDa fragments observed for the standard proteolysis.

BSA, total proteolysis

#	Residues	Amino Acid Sequence	Weight (Da)	#	Residues	Amino Acid Sequence	Weight (Da)	#	Residues	Amino Acid Sequence	Weight (Da)
1	1 -- 4	DTHK	484	27	197 -- 198	LR	272	53	378 -- 388	HLVDEPQNLIK	1288
2	5 -- 10	SEIAHR	696	28	199 -- 204	CASIQK	634	54	389 -- 396	QNCDQFEK	994
3	11 -- 12	FK	278	29	205 -- 208	FGER	492	55	397 -- 409	LGEYGFQNALIVR	1464
4	13 -- 20	DLGEEHFK	956	30	209 -- 211	ALK	315	56	410 -- 412	YTR	423
5	21 -- 41	GLVLIAFSQYLQQCPFDEHVK	2419	31	212 -- 217	AWSVAR	674	57	413	K	131
6	42 -- 51	LVNELTEFAK	1146	32	218 -- 221	LSQK	460	58	414 -- 427	VPQVSTPTLVEVSR	1496
7	52 -- 64	TCVADESHAGCEK	1329	33	222 -- 224	FPK	375	59	428 -- 431	SLGK	388
8	65 -- 76	SLHTLFGDELCK	1389	34	225 -- 232	AEFVEVTK	905	60	432 -- 435	VGTR	416
9	77 -- 81	VASLR	642	35	233 -- 239	LVTDLTK	773	61	436 -- 444	CCTKPESER	1036
10	82 -- 93	ETYGDMADCCEK	1345	36	240 -- 242	VHK	367	62	445 -- 458	MPCTEDYLSLILNR	1651
11	94 -- 98	QEPER	641	37	243 -- 256	ECCHGDLLECADDR	1557	63	459 -- 465	LCVLHEK	825
12	99 -- 106	NECFLSHK	961	38	257 -- 261	ADLAK	501	64	466 -- 471	TPVSEK	644
13	107 -- 114	DDSPDLPK	868	39	262 -- 273	YICDNQDTISSK	1369	65	472 -- 474	VTK	331
14	115 -- 127	LKPDPNTLCDEFK	1503	40	274 -- 275	LK	244	66	475 -- 483	CCTESLVNR	1008
15	128 -- 131	ADEK	444	41	276 -- 285	ECCDKPLLEK	1160	67	484 -- 499	RPCFSALTPDETYVPK	1808
16	132	K	131	42	286 -- 294	SHCIAEVEK	998	68	500 -- 504	AFDEK	592
17	133 -- 136	FWGK	522	43	295 -- 312	DAIPENLPPLTADFAEDK	1936	69	505 -- 520	LFTFHADICTLPDTEK	1833
18	137 -- 143	YLYEIAR	911	44	313 -- 316	DVCK	448	70	521 -- 523	QIK	372
19	144	R	159	45	317 -- 322	NYQEAK	736	71	524	K	131
20	145 -- 159	HPYFYAPELLYYANK	1873	46	323 -- 335	DAFLGSFLYEYSR	1551	72	525 -- 533	QTALVELLK	998
21	160 -- 173	YNGVFQECCQAEDK	1616	47	336	R	159	73	534 -- 537	HKPK	495
22	174 -- 180	GACLLPK	686	48	337 -- 347	HPEYAVSVLLR	1267	74	538 -- 544	ATEEQLK	801
23	181 -- 185	IETMR	745	49	348 -- 350	LAK	315	75	545 -- 556	TVMENFVAFVDK	1383
24	186 -- 187	EK	259	50	351 -- 362	EYEATLEECCAK	1369	76	557 -- 563	CCAADDK	708
25	188 -- 194	VLTSSAR	718	51	363 -- 375	DDPHACYSTVFDK	1480	77	564 -- 573	EACFAVEGPK	1033
26	195 -- 196	QR	287	52	376 -- 377	LK	244	78	574 -- 583	LVVSTQTALA	1001
						Total = 66,462 Dalton					
						Average = 857 Dalton					

HSA similarly produces five large fragments connected by unbroken Cys-Cys disulfide bonds following the limited tryptic proteolysis: [A] (7.3 kDa, corresponding to residues 1 − 64), [B] (4.8 − 6.1 kDa, corresponding to residues 65 − 106/117), [C] (22.2 − 23.5 kDa, corresponding to residues 107/118 − 313), [D] (21.4 kDa, corresponding to residues 314 − 500), and [E] (9.5 kDa, corresponding to residues 500 − 585) and further details into the assignment of the HSA protein bands can be found in **Figure 44**.

In the limited proteolysis, the tryptic cuts produce large units of the whole protein which are connected by Cys-Cys disulfide bonds. In the case of BSA these would be residues 65 − 106, 115 − 294, 313 − 499, and 500 – 583 while there are some segments that are outside this range. These segments include sequence vi (residues 107 – 114, 0.9

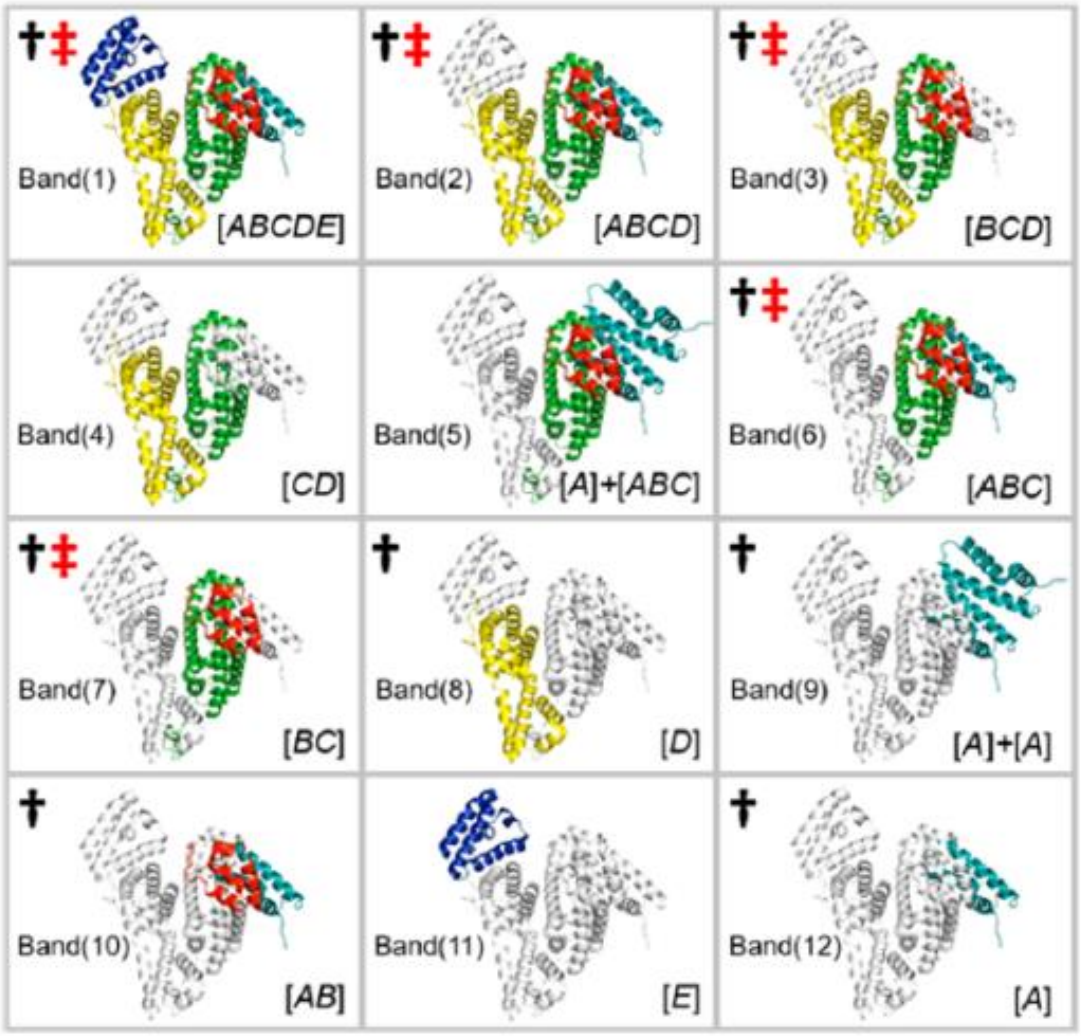

Figure 45. Drawing of the observed in-gel bands that resulted from limited tryptic proteolysis of BSA, reconstructed from the theoretical fragments [A], [B], [C], [D], and [E]. Out of the nine bands observed from [BSA-trypsin]−Au (indicated by †), the in-gel red luminescence (indicated by ‡) was observed with Band(1) = undigested BSA, Band(2) = [ABCD], Band(3) = [BCD], Band(6) = [ABC], and Band(7) = [BC].

kDa) and segment xi (residues 295 – 312, 2.1 kDa) (**Figure 41**) which were not seen in the gel. These sequence do appear as part of either fragment [B] or [C] (vi) and [C] or [D] (xi), which results in a slight ambiguity in the definitions of these residual sequences and why there are noted as diagonal slanted boarders in the color-coded column in **Figure 41**. This ambiguity is likely due to the limited proteolysis done by trypsin as both BSA and HSA

are digested in as close to their native conformations as possible, likely causing trypsin to be unable to access these cut sites easily.

The limited proteolysis of HSA yielded fragment gel bands with molecular weights ranging between ~8 kDa to ~ 50 kDa. These large fragments are to be expected as the disulfide bonds are not cleaved, and thus larger fragments are expected, overall. As a reference, an ideal total proteolysis of BSA via trypsin cleaving (with all cleaving occurring at the C-terminal sides of lysine and arginine resides, except when followed by a proline) should produce 78 total fragments all with a mean mass of less than 1 kDa (**Table 5**).

On the other hand, the limited proteolysis of BSA via trypsin resulted in only 12 large, observable bands (**Figure 41a,d**) including the undigested BSA (Band(1)) and Cys-Cys bond-preserving fragment bands: Band(2), ~50 kDa; Band(3), ~44 kDa; Band(4), ~42 kDa; Band(5), ~36 kDa; Band(6), ~32 kDa; Band(7), ~26 kDa; Band(8), ~21 kDa; Band(9), ~15 kDa; Band(10), ~12 kDa; Band(11), ~10 kDa; and Band(12), ~8 kDa. No fragmented bands were observed below a molecular weight of 8 kDa. Along with the undigested BSA (Band(1)), dimers, above ~66 kDa were also observed. This inclusion of dimers in the gel is the result of a lack of a denaturing process in the limited proteolysis, which keeps all disulfides intact, and thus dimers which form due to surface exposed CYS34 residues.

Previous work has also shown a similar number of observed bands when performing a limited proteolysis on BSA.[132-135] These reports also concluded that these cut locations are mostly all located in the random coil sequences, which tend to be easier to access for enzymatic cleaving. Furthermore, the major substructures, or secondary structures of the protein including the alpha-helices and beta-strands are preserved after

proteolysis. This also appears to be trend across multiple proteins when limited proteolysis is performed, and agrees with our protocol.[136]

While 12 total bands could be observed in gel, only a combination of five expected fragments were determined to be needed to produce all the gel bands consistently. Thus the 12 observed bands can be renamed using only the five primary fragments A,B,C,D,E and are as follows: Band(1) = [ABCDE] (undigested); Band(2) = [ABCD] (connected fragments); Band(3) = [BCD]; Band(4) = [CD]; Band(5) = [A] + [ABC]; Band(6) = [ABC]; Band(7) = [BC]; Band(8) = [D]; Band(9) = [A] + [A]; Band(10) = [AB]; Band(11) = [E]; and Band(12) = [A]. These 12 fragments are shown in **Figure 45**. The single black cross in each frame indicates bands that were further observed after the addition of Au, and the double red cross indicates bands that were also red luminescent. Of the 12 bands, Band(5) and Band(9) contain two [A] fragments (residues 1-64), which can be justified by the dimerization of cystine34 via the formation of a disulfide bond.

The [tryptic BSA fragment]-Au bands in the gel were not as well-defined as the tryptic BSA fragments due to the smearing that occurred after the addition of Au. This smearing of the bands after the addition of Au may be due to the interaction of the surface-bound Au cations on BSA with the gel matrix, and may be a common occurrence when metal ions interact with the gel.[137,138] Overall, the clarity of the [tryptic BSA fragment]-Au bands was sufficient to deduce their molecular weights and differentiate them from other bands. Out of the 12 total bands that were observed that could be produced from 5 primary fragments as shown in **Figure 41b,e**, only 9 bands were visible after the reaction with Au. These observed bands were (1), (2), (3), (6), (7), (8), (9), (10), and (12). Thus, further analysis of the gel is limited to these nine bands because Band(4), Band(5), and Band(11)

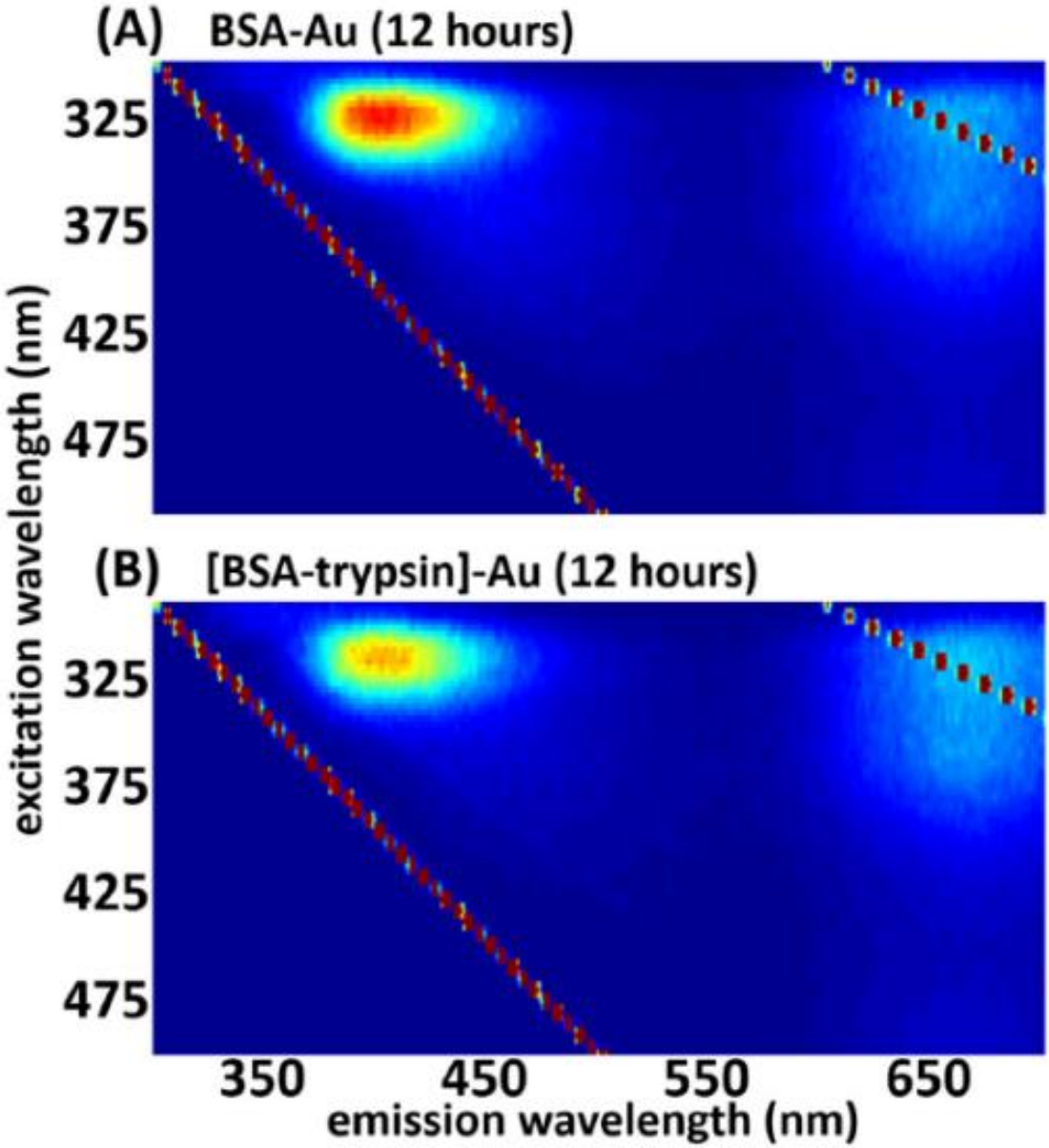

Figure 46. The excitation-emission maps of BSA-Au and [BSA-trypsin]–Au are shown above. BSA was digested using limited tryptic proteolysis, then was reacted with Au. This [BSA-trypsin]–Au, containing the mixture of the BSA fragments reacted with Au, showed the luminescence pattern identical to that of BSA–Au in excitation-emission measurements which was measured at 12 hours.

were not detectable after the reaction of the fragments with Au (**Figure 41a,d**). Multimer bands located above 66 kDa due to the aggregation caused by surface-bound Au were also more pronounced. This increase in multimerization is expected, as described in Chapter 3, and that the addition of substantial amounts of metal ions causes a greater portion of

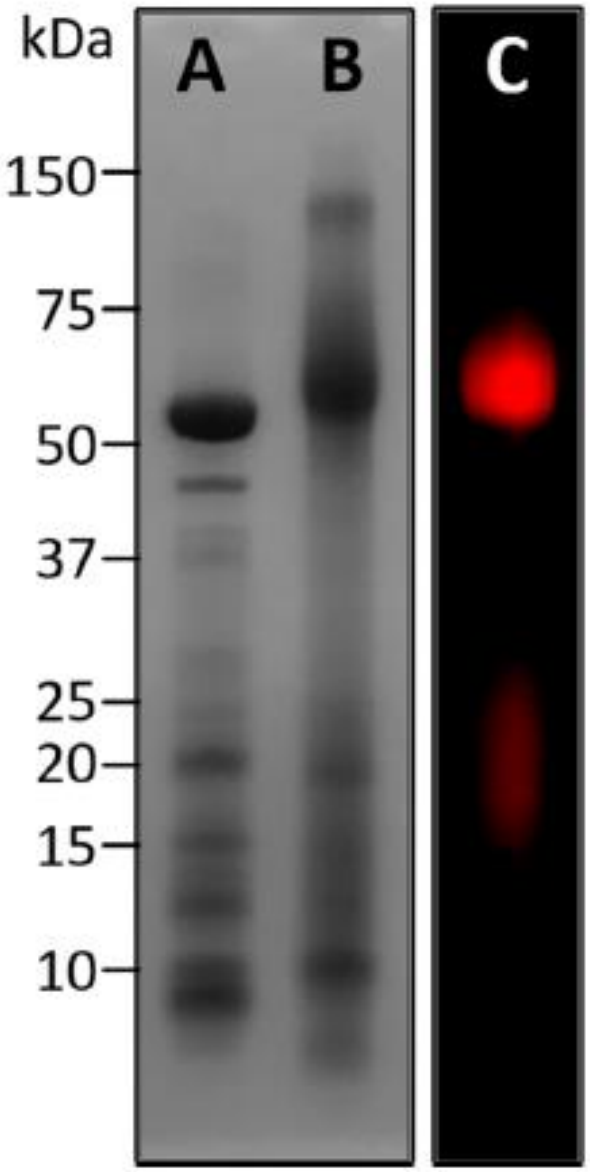

Figure 47. The limited tryptic proteolysis performed overnight as opposed to in 1 hour is shown above. The extended duration of enzymatic digestion enables more cuts. (A) Limited tryptic proteolysis of BSA after 12 h show significantly increased fragment bands at <20 kDa. (B) These fragments were reacted with HAuCl4, and (C) in-gel luminescence was measured. The fragment bands were well-separated and visible around 20 kDa and at smaller molecular weights. The luminescence was absent in the bands below ~15 kDa.

monomeric BSA to form multimers through van der Waals forces and is discussed further in Chapter 3.

Measurements of the in-gel red luminescence of the [tryptic BSA fragment]-Au bands under UV excitation at λ_{ex} = 365 nm were taken using a red bandpass filter at λ_{em} =

685 ± 25 nm. The red luminescence of the bands was centered around λ_{em} = 660 ± 30 nm and there was no significant luminescence within the spectral region of 500 nm < λ < 600 nm. This result is confirmed from the excitation-emission map measured in solution of both BSA-Au and BSA-trypsin-Au (**Figure 46**). Of the nine bands that could be observed in the [tryptic BSA fragment]-Au sample, only a further five bands were found that exhibited any notable red luminescence (**Figure 41c,f**). These red luminescing bands were Band(1) = [ABCDE] (undigested BSA), Band(2) = [ABCD], Band(3) = [BCD], Band(6) = [ABC], and Band(7) = [BC]. Luminescent bands were absent at other molecular weights, including Band(8) = [D], Band(10) = [AB], and Band(12) = [A] (**Figure 41**).

This in-gel luminescence band pattern can be explained by the presence of a red luminophore in the tryptic BSA fragment of [C] residing in residues 115/117 – 294/312, which corresponds to a region of BSA which is only 30% of the whole protein. It should be noted that trypsin alone (23.3 kDa) was also found to react with Au and produced the same red luminescence and is described in more detail in Chapter 4. However, the presence of a small amount of trypsin equal to less than 0.1 μg did not affect the evaluation of the in-gel luminescence as each lane contains more than 10 μg of BSA, at least a 100-fold difference in protein by weight.

The results of this fragmented study are also consistent with the non-luminophore-forming specific Au binding sites in BSA that have been identified.[13] These sites include the 'Asp fragment' at the N-terminus (aspargine1 – theronine2 – histidine3) and cystine34, both of which are contained in the non-luminescent fragment [A]. Additionally, it was verified that the in-gel red luminescence was absent below 20 kDa even after an extended amount of digestion time following the same limited proteolysis protocol (**Figure 47**). This

further excludes the likelihood that fragments [A] (7.3 kDa), [B] (5.9 kDa), and [E] (9.5 kDa) could be possible locations of the red luminophore.

To validate that fragment [C] is indeed the luminophore-containing fragment, two segments of serum albumin were prepared separating the segments between residue 313 and residue 314 by molecular cloning. A detailed procedure for the molecular cloning process is described above in this chapter. For the molecular cloning of these segments the cDNA of HSA was used because of its commercial availability, and as discussed earlier is identical to BSA, including its red luminescence spectra and reaction kinetics.

5.3 Molecular Cloning of HSA Fragments to Locate the Au Binding Domain.

Glutathione S-transferase (GST) (26.9 kDa) was linked to the N-terminus of each cloned segment of HSA and is a required addition to molecularly cloned segments as it allows for the segments to be eluted after required filtration and purification steps. Including the bound GST, the first segment can then be termed GST-[HSA_{1-313}] (64 kDa) corresponding to the fragments of [ABC] of HSA which contain amino acid residues 1-313 and has GST bound at residue 1. The second segment is termed GST-[$HSA_{314-585}$] (59 kDa), corresponding to the fragments [DE] of HSA which contain amino acid residues 314-585 and has GST bound at residue 314. These segments were prepared following the outlined protocol and then reacted with Au to produce two different molecularly cloned segmented-HSA-Au complexes (GST-[HSA_{1-313}]-Au or GST-[$HSA_{314-585}$]-Au). By producing two molecularly cloned segments, the results of the limited proteolysis experiment can be confirmed. The intensities of red luminescence from the control group

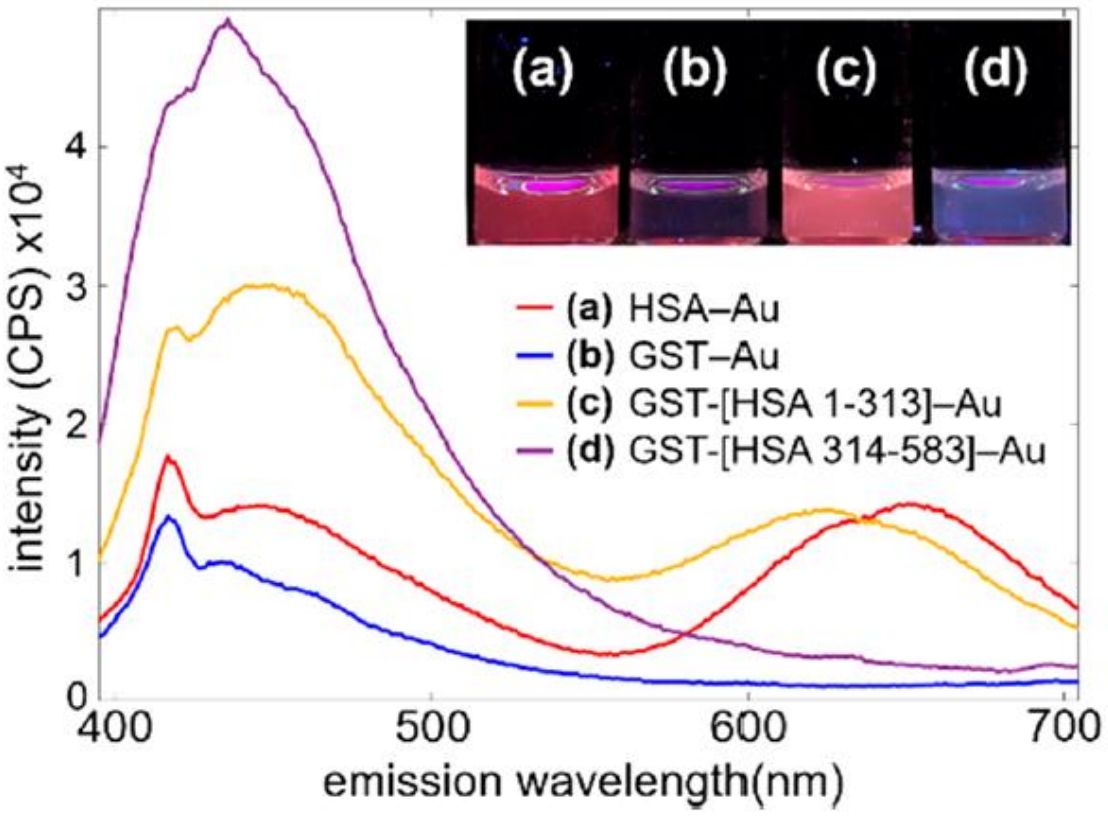

Figure 48. Luminescence spectra of the molecularly cloned HSA fragments, measured at 24 h, indicate that the red luminophore is in the N-terminus half (segment 1−313) of HSA, but not in the C-terminus half (segment 314−585). The inset shows a photograph under UV illumination (λ_{ex} = 365 nm). (a) HSA−Au control; (b) GST−Au control; (c) GST-[$HSA_{1–313}$]−Au; (d) GST-[$HSA_{314–585}$]−Au.

of HSA-Au and the GST-[HSA_{1-313}]-Au were comparable both in solution (**Figure 48**) and in-gel (**Figure 49**).

The luminescence peak of GST-[$HSA_{1–313}$]−Au was at λ_{em} = 625 nm, which is slightly shifted from that of HSA−Au. This may be attributed to the difference in the local environments of the luminophore.[90] In contrast, GST-[$HSA_{314–585}$]−Au showed negligible red luminescence similar to that of control containing just GST (GST−Au), indicating the absence of the luminophore in [$HSA_{314–585}$], i.e., segment [DE] of HSA.

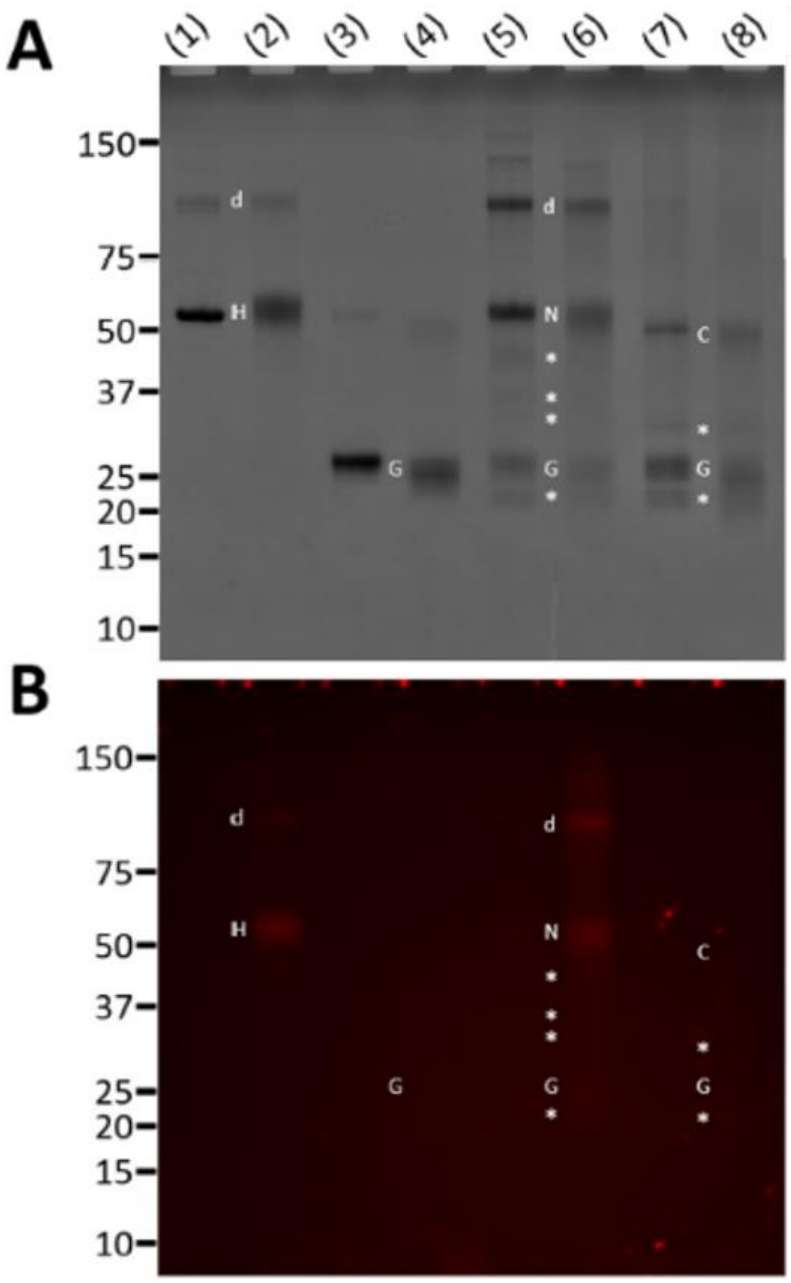

Figure 49. The in-gel fluorescence of molecularly cloned HSA fragments. (A) Coomassie-stained gel; (B) Red luminescence of the same gel. Lane (1) HSA; (2) HSA–Au; (3) GST; (4) GST–Au; (5) GST-[HSA_{1-313}]; (6) GST-[HSA_{1-313}]–Au; (7) GST-[$HSA_{314-585}$]; (8) GST-[$HSA_{314-585}$]–Au. Label details are given in the text below.

The in-gel luminescence of both GST-[HSA_{1-313}]-Au and GST-[$HSA_{314-585}$]-Au and their controls are shown in **Figure 49**. Molecularly cloned GST-[HSA_{1-313}] (64 kDa) and GST-[$HSA_{314-585}$] (59 kDa) samples indicate the presence of unlinked GST (26.9 kDa), as

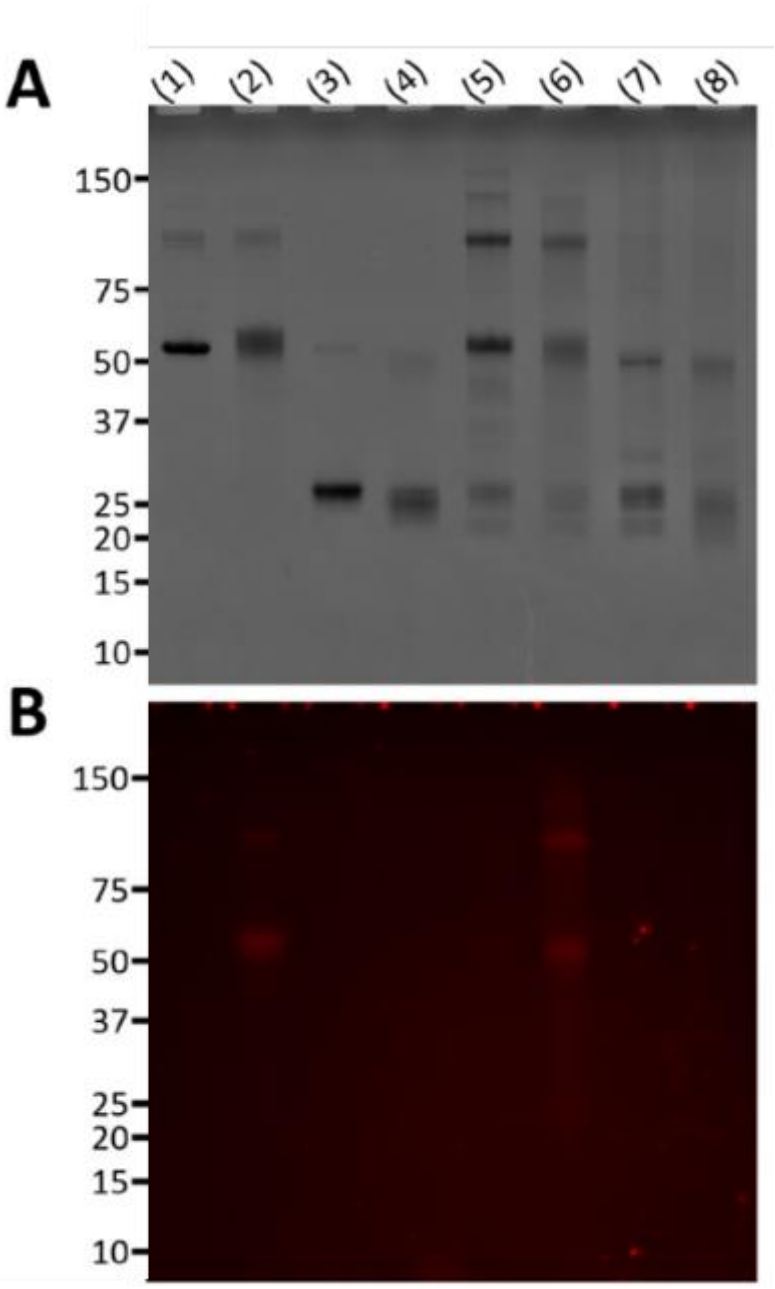

Figure 50. The unmarked, original gel described in Figure 48 of the main text. Lane (1) HSA; (2) HSA–Au; (3) GST; (4) GST–Au; (5) GST-[HSA_{1-313}]; (6) GST-[HSA_{1-313}]–Au; (7) GST-[$HSA_{314-585}$]; (8) GST-[$HSA_{314-585}$]–Au.

well as small amounts of unknown fragments as impurities. These impurities were from the process of molecular cloning and purification and were not removed from the samples to maximize the yield of the target proteins. Red luminescence was observed only in HSA–Au (labeled in gel as “H”) and GST-[HSA_{1-313}]–Au (labeled as “N”) and their dimers

(likely through Cys34, labeled as “d”) and was absent in GST-[$HSA_{314-585}$]–Au (labeled as “C”) as well as in GST–Au (labeled as “G”) and impurity bands (labeled as “*”). The unlabeled original gel is also shown in **Figure 50**.

As elucidated and described in Chapter 3, a significant degree of non-specific Au binding on the protein surface occurs, which is up to ~125 surface sites, based on the surface area. These surface bound sites do not appear to contribute to the formation of the red luminophore, in addition to the specific Au binding sites such as the Asp-fragment or Cys34. Through the separation of HSA into nearly equal halves via molecular cloning, additional nonspecific binding sites become available and thus change the overall Au binding kinetics, relative to the whole, unmodified HSA protein. It should be noted that, the structures of HSA and their halves are not known at basic pH the degree of change due to surface area differences is likely small as the two halves compared to HSA all have a relatively similar molecular weight (HSA at ~67 kDa, GST-[HSA_{1-313}] at ~64 kDa, and GST-[$HSA_{314-585}$] at ~59 kDa). Also, additional specific binding sites could become solvent accessible due to the molecular cloning procedure, but the emergence of new luminophore formation was not presently observed.

Thus, combining the present molecular cloning experiment with the limited proteolysis results suggest that the red luminophore is located within fragment [C], which is bound between amino acid residues 118 – 313, constituting only 30% of the original protein. This result is further validated by the limited tryptic proteolysis of GST-[HSA_{1-}

Band	Weight [kDa]	Fragment
1	~63	GST-[*ABC*]
2	~45	(impurity)*
3	~40	GST-[*AB*] (& *)
4	~35	[*ABC*]
5	~27	GST & [*BC*]
6	~23	[*C*] (& *)
7	~14	[*AB*]
8	~8	[*A*]
9	~7	[$^{+}$*B*]
10	~6	[*B*]

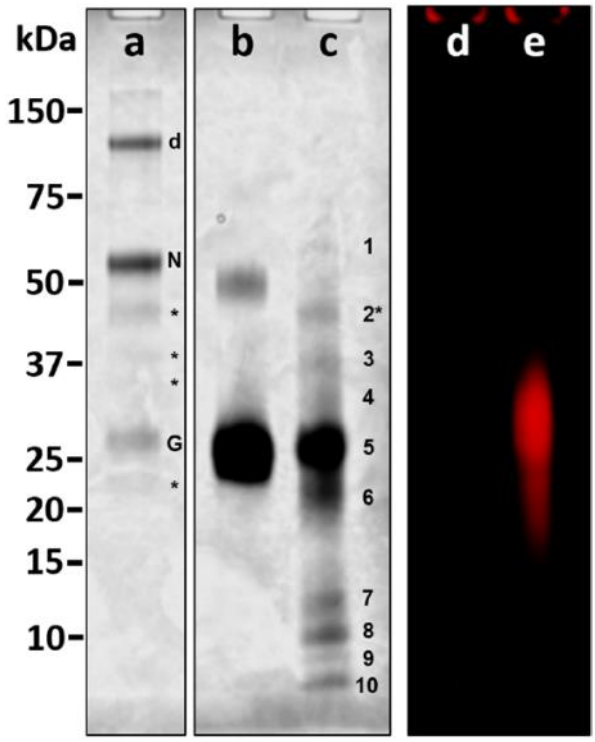

Figure 51. The limited proteolysis and in-gel luminescence of GST-[HSA_{1-313}] reacted with Au is shown above. (a) GST-[HSA_{1-313}], (b) [GST-trypsin]–Au; (c) [GST-[HSA_{1-313}]-trypsin]–Au; (d, e) are in-gel luminescence of (b, c). As shown in (a), the molecularly cloned GST-[HSA_{1-313}] (indicated as "N") contained small amounts of unknown impurities (indicated as "*"), as well as a dimer (indicated as "d") and an unlinked GST (indicated as "G"). The labeled bands in (c) are shown in the left table and described in more detail in the text below.

$_{313}$], where the in-gel luminescence was present in the bands corresponding to [BC] and [C] but absent in [AB], [A], and [B] (**Figure 51**).

Limited tryptic proteolysis of GST-[HSA_{1-313}] (or GST-[*ABC*]) produced 10 bands, as shown in **Figure 51c**. These bands are: Band(1) ~63 kDa; Band(2) ~45 kDa; Band(3) ~40 kDa; Band(4) ~35 kDa; Band(5) ~27 kDa; Band(6) ~23 kDa; Band(7) ~14 kDa; Band(8) ~8 kDa; Band(9) ~7 kDa; and Band(10) ~6 kDa. These bands can be uniquely assigned to combinations of GST and the three fragments of HSA_{1-313} ([*A*], [*B*], and [*C*]) as shown in the table of **Figure 51**. The molecular weights of the individual expected fragments are GST (26.9 kDa); [*A*] = HSA_{1-64} (7.3 kDa); [*B*] = $HSA_{65-106/117}$ (5.7-7.0 kDa);

[*C*] = $HSA_{107/118-313}$ (22.6-23.9 kDa). The tryptic cuts produce a small fragment which is not connected by Cys-Cys bonds ($HSA_{107-117}$ ~1.3 kDa, see **Figure 51**), resulting in a small ambiguity observed in Band(9) and Band(10). This small ambiguity is noted as a (+) in the table of **Figure 51**. Band(2) is an impurity of the molecularly cloned GST-[HSA_{1-313}], marked as * in **Figure 51a** (also in **Figure 49**). The in-gel red luminescence of [GST-trypsin]–Au was negligible (**Figure 51d**). The in-gel red luminescence of the [GST-[HSA_{1-313}]-trypsin]–Au overlapped with three bands (**Figure 51e**). These bands are Band(4) = [*ABC*]; Band(5) = [*BC*] (luminescence from GST was negligible); and Band(6) = [*C*]. Band(1) = GST-[*ABC*] was not enough in quantity (**Figure 51b**) to yield detectable luminescence. The in-gel luminescence was absent in the bands corresponding to [*A*] and [*B*], including Band(7) = [*AB*], Band(8) = [*A*], and Band(9,10) = [*B*].

This further analysis again shows that only fragment [C] is constantly found in all the red luminescent bands while fragment [A], [B], and [AB] are not always within the luminescent bands. These results support the evidence from Chapter 4 that the red luminophore must be contained within a subdomain of the total HSA protein between amino acid residues 118 – 313. Interestingly, this subdomain of the protein also seems to overlap with the suggested binding site for some drug molecules ('Sudlow's site I' in domain IIA). These experiments do not presently confirm if this site is the site of the red luminophore.[139-141]

As outlined earlier in this chapter, a Cys-Cys disulfide bond does appear to be necessary for the formation of the red luminophore. These disulfide bond sites within fragment [C] are (I) Cys124−Cys169 / Cys168−Cys177, (II) Cys200−Cys246 / Cys245−Cys253, and (III) Cys265−Cys279 / Cys278−Cys289 in the present HSA

fragment. In a similar fashion for BSA, these Cys-Cys binding sites are (I) Cys123−Cys168 / Cys167−Cys176, (II) Cys199−Cys245 / Cys244−Cys252, and (III) Cys264−Cys278 / Cys277−Cys288. Thus, the red luminophore may be contained at a single site, and not more than six total disulfide bonds spread across only three unique disulfide cluster sites.

To summarize these results, the domain in serum albumin (BSA and HSA) where Au binds and produces red luminescence has been found. The uncovering of this binding domain is a critical step for a full understanding of the mechanism and structure of luminescence. The molecular cloning of protein fragments can be technically difficult in some cases due to low solubility of the segment or a low expression in *E.coli*. The combination of limited tryptic proteolysis and molecular cloning that has been presented above may be a way to subvert those problems. In these molecular cloning experiments GST was used as the tag, but other methods for expression may further help elucidate the Au binding site.[142] Thus, to this end, further molecular cloning of the identified fragment [C] with specific amino acid residue mutations may lead to uncovering the exact binding site of Au. Fully discovering the binding site of this luminophore may lead to a complete understanding of the mechanism and could lead to new engineered luminescent proteins or peptides.

CHAPTER 6: IDENTIFYING THE BINDING SITE OF GOLD AND DETERMINING THE STRUCTURE OF THE RED LUMINESCENT PROTEIN-GOLD COMPLEX

The identification of the binding site in the HSA-Au complex, as well as other protein-Au complexes, is an essential step toward understanding the mechanism for red luminophore formation. In Chapter 5, molecular cloning of HSA segments and the limited tryptic proteolysis of BSA showed that the binding domain of Au is localized within a small subdomain of the first half (GST-[HSA_{1-313}]) of the HSA protein. More precisely, the location of the luminophore site is contained within amino acid residues 118-313 (noted as fragment [C] in Chapter 5) of the 584 amino acid residues of HSA. Additionally, a Cys-Cys disulfide is required for red luminescence to occur. Thus, the number of available binding sites within this subdomain of HSA is significantly reduced to only a handful of possible locations.

6.1 Locating the Exact Au Binding Site in HSA Using Molecular Cloning.

Due to the necessity of the cys-cys disulfide bond for the formation of luminescence, it can be suggested that the binding site of Au within the protein would likely be localized to one of three major cystine disulfide clusters. These cystine disulfide clusters are: (I) Cys124−Cys169 / Cys168−Cys177, (II) Cys200−Cys246 / Cys245−Cys253, or (III) Cys265− Cys279 / Cys278−Cys289 and the luminophore could potentially be localized within just one of these unique cluster regions or even localized to a single cysteine disulfide site. Finely targeted molecular cloning of HSA at each cystine disulfide can be performed to determine the site or sites that are responsible for luminescence .

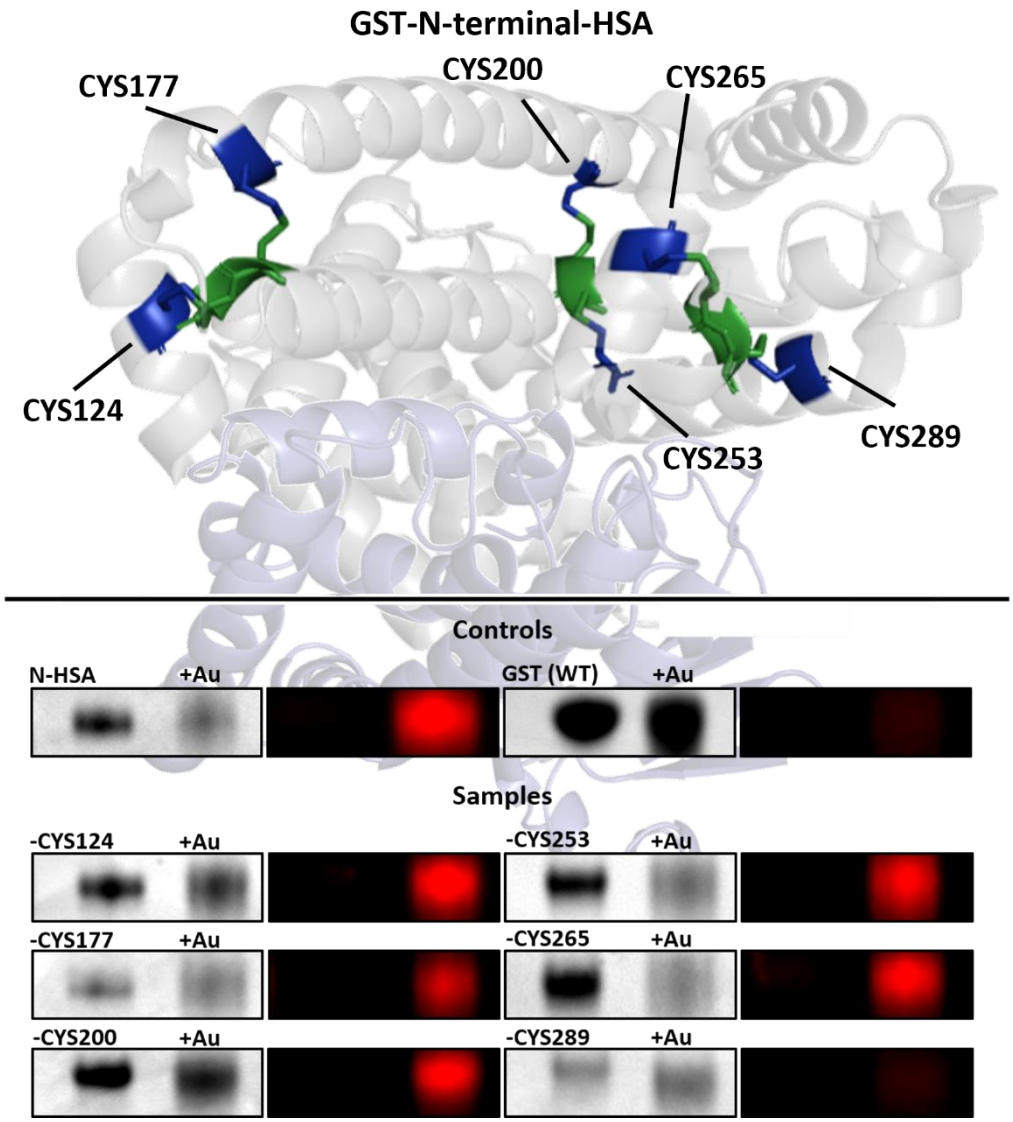

Figure 52. Schematic illustration of N-terminal human serum albumin. The three primary cystine disulfide cluster sites are highlighted in green, and the 6 modified sites are labeled. Molecular cloning of each site is done by replacing the cysteine residues with an alanine. From the above image only the synthesis of GST-N-HSA$_{\text{-CYS289}}$ resulted in a lack of red luminescence. Indicating the site of red luminescence to this CYS278-CYS289 disulfide site.

Initial molecular cloning of the segment containing the first 313 amino acid residues of HSA (GST-[HSA$_{1\text{-}313}$]) revealed red luminescence was preserved within this domain of HSA after complexing it with Au. On the other hand, molecularly cloned HSA containing amino acids 314-584 (GST-[HSA$_{314\text{-}584}$]) lacked the characteristic red luminescence after the addition of Au. The modification of HSA fragments required a

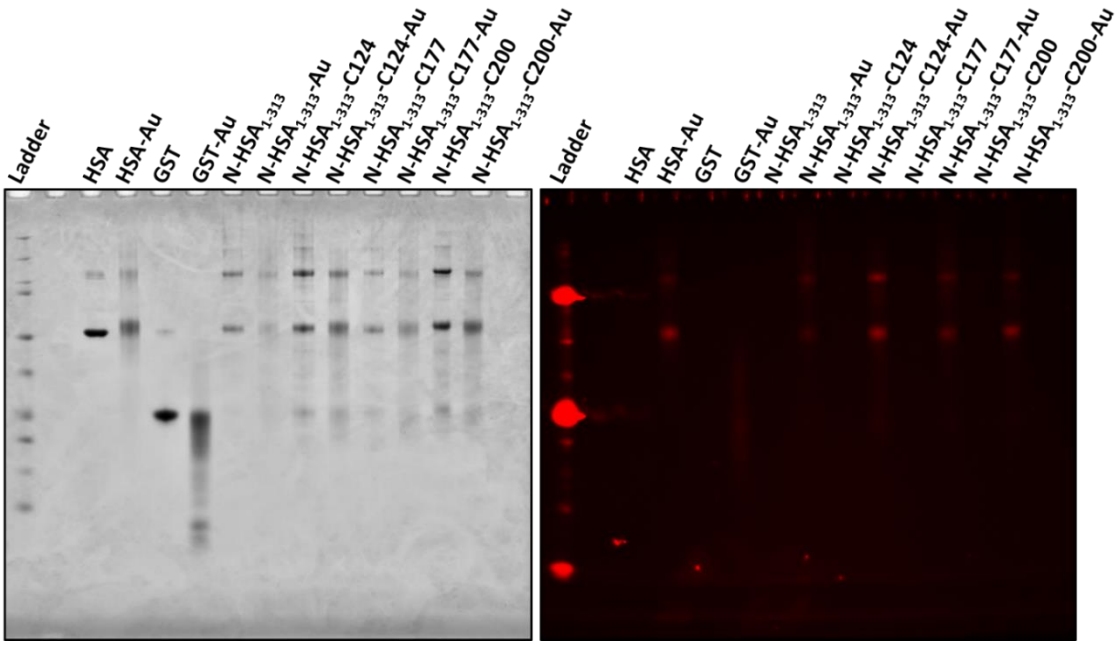

Figure 53. Gel image of C124, C177, and C200 modifications. Raw visible and UV image of gel containing three cysteine modifications, each lane was loaded with ~ 2ul of sample. The ten lanes from left to right are as follows: (1) ladder; (2) [blank]; (3) HSA; (4) HSA-Au; (5) GST; (6) GST-Au; (7) GST-[HSA_{1-313}]; (8) GST-[HSA_{1-313}]-Au; (9) GST-[HSA_{1-313}]-C124; (10) GST-[HSA_{1-313}]-C124-Au; (11) GST-[HSA_{1-313}]-C177; (12) GST-[HSA_{1-313}]-C177-Au; (13) GST-[HSA_{1-313}]-C200; (14) GST-[HSA_{1-313}]-C200-Au; (15) [blank]. Lanes 8, 10, 12, and 14 show comparable luminescence to that of control lane 4, while lane 6 shows minimal luminescence.

glutathione-S-transferase tag (GST, ~26 kDa) bound to the N-terminal site of each segment. Therefore, each segment has the GST-[HSA_n] nomenclature. Without the addition of this GST tag the molecularly cloned protein would not be able to be eluted after purification. GST itself shows signs of being red luminescent when interacted with Au. This red luminescence may be a result of excess glutathione molecules in solution, which could be left behind from protein elution and may not be due to a binding site specific to the protein itself. Most importantly, the addition of the GST tag was found to not influence the resulting luminescence of the HSA-Au interaction and displayed minimal luminescence, more than an order of magnitude below that of a control HSA-Au complex.

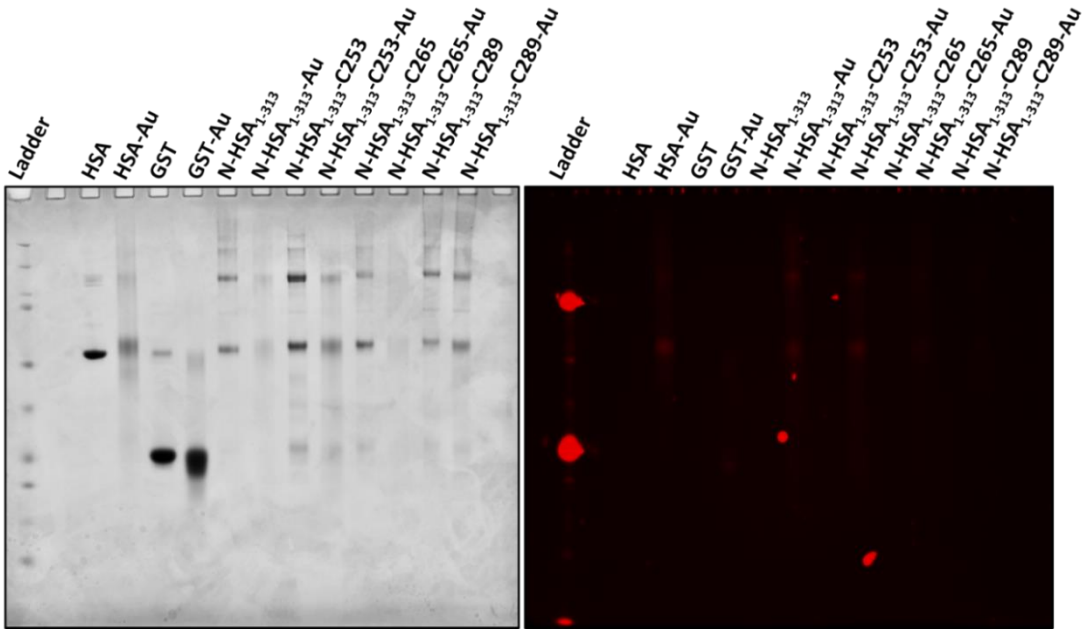

Figure 54. Gel image of C253, C265, and C289 modifications. Raw visible and UV image of gel containing three cysteine modifications, each lane was loaded with ~ 2ul of sample. The ten lanes from left to right are as follows: (1) ladder; (2) [blank]; (3) HSA; (4) HSA-Au; (5) GST; (6) GST-Au; (7 GST-[HSA_{1-313}]; (8) GST-[HSA_{1-313}]-Au; (9) GST-[HSA_{1-313}]-C253; (10) GST-[HSA_{1-313}]-C253-Au; (11) GST-[HSA_{1-313}]-C265; (12) GST-[HSA_{1-313}]-C265-Au; (13) GST-[HSA_{1-313}]-C289; (14) GST-[HSA_{1-313}]-C289-Au; (15) [blank]. Lanes 8, 10, and 12 show comparable luminescence to that of control lane 4, while lane 6 and 14 shows minimal luminescence.

Synthesis of further molecular cloned GST-[HSA_{1-313}] fragments was performed to identify the exact binding site of Au which contributes to luminescence. Thus, modification of single cystine thiols was carried out at each disulfide site, one at a time, in order to optimally maintain the overall structure and elucidate the thiol or thiols responsible for luminescence. Further modifications of aromatic amino acids including tryptophan, histidine, and tyrosine was also performed to observe the effects of local aromatic amino acid residues on the generation of red luminescence. In total, ten GST-[HSA_{1-313}] samples were synthesized, the following modified residues within GST-[HSA_{1-313}] were all replaced by alanine amino acids: (i) Cys124; (ii) Cys177; (iii) Cys200; (iv) Cys253; (v) Cys265; (vi) Cys289; (vii) all tryptophan; (viii) all histidine; (ix) all tyrosine; (x) N-HSA_{1-}

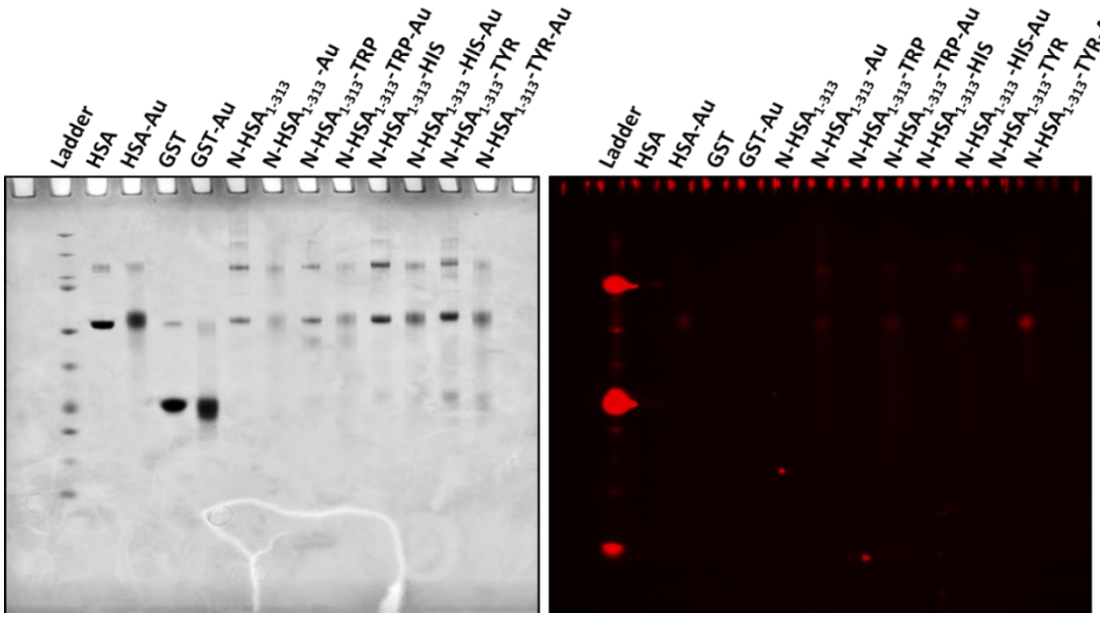

Figure 55. Gel image of tryptophan, histidine, and tyrosine modifications. Raw visible and UV image of gel containing three aromatic amino acid residue modifications, each lane was loaded with ~ 2ul of sample. The fifteen lanes from left to right are as follows: (1) [blank]; (2) ladder; (3) HSA; (4) HSA-Au; (5) GST; (6) GST-Au; (7 GST-[HSA_{1-313}]; (8) GST-[HSA_{1-313}]-Au; (9) GST-[HSA_{1-313}]-TRP; (10 GST-[HSA_{1-313}]-TRP-Au; (11) GST-[HSA_{1-313}] -HIS; (12) GST-[HSA_{1-313}]-HIS-Au; (13) GST-[HSA_{1-313}] -TYR; (14) GST-[HSA_{1-313}] -TYR-Au; (15) [blank]. Lanes 8, 10, 12, and 14 show comparable luminescence to that of control lane 4, while lane 6 shows minimal luminescence.

$_{313}$ (**Figure 52** and **Figures 53-55)**. A more detailed explanation of the procedure is given in the methods section below and in the methods section of Chapter 5.

6.2 Experimental Methodology and Instrumentation.

HSA-Au is synthesized following a standard procedure, similar to the protocol outlined by Xie et al. Briefly, 1 mL of $HAuCl_4$ aqueous solution (0.75 mM) is added to 1 mL of aqueous HSA (0.075 mM or 5 mg/mL) and the solutions are combined at 750 rpm. Addition of $HAuCl_4$ to HSA changes the solution color from clear to light yellow. After 1 minute, 1 M NaOH is added to the solution to bring the sample to the targeted alkaline pH. The reaction proceeds for 2 hours at 40^{o}C and then is stored at room temperature.

The procedure for synthesizing the molecularly cloned fragments of GST-bound-HSA is described in detail in the methods section of chapter 5. The further steps to produce the single-point mutations is detailed below.

To synthesize GST-[HSA_{1-313}]–Au and GST-[HSA_{1-313}]-Au mutated complexes as well as HSA–Au and GST–Au controls, the concentrations were modified to accommodate the small quantity of protein, from the protocol to synthesize a standard HSA-Au complex. 200 μL of HAuCl4 aqueous solution was added to 200 μL of aqueous solutions of the proteins (GST-[HSA_{1-313}] and GST-[HSA_{1-313}]-mutations, as well as HSA and GST) (25 μM). The protein-to-Au molar ratio was 1 : 10. The two solutions were combined under stirring at 750 rpm for 2 minutes. Upon addition of HAuCl4, the pH of the solution was 7.0. Next, 1 M NaOH was then added to the solution until a pH of 12.5 was achieved. The reaction proceeded for 2 hours at 37°C.

A pre-cast 4-12% gradient Bis-Tris (NuPage) and MES running buffer (NuPage) were used for gel electrophoresis. The sample buffer contained the same amount of protein in a 20% glycerol solution for all lanes. No sodium dodecyl sulfate (SDS), dithiothreitol (DTT), or urea was added to the sample buffer. No temperature annealing was performed. The gel was run for 1 h at a constant voltage of 150 V. After electrophoresis, the in-gel luminescence was measured with a gel imaging system (Azure C400) using $\lambda = 365$ nm excitation and a bandpass filter of $\lambda = 685 \pm 25$ nm, to record the red luminescence. The gel was subsequently stained with Coomassie Brilliant Blue for the molecular weight analyses of the bands.

To separate extremely small molecular weight GSSG-Au and maintain red luminescence, a large gel is hand cast without SDS. A 30% acrylamide resolving gel is

made by adding 30 mL of 40% acrylamide (containing 5% crosslinker), with 10 mL of 1.5 M Tris-HCL (pH 8.8). Next, 400 μL of 10% APS and 16 μL of TEMED are added to polymerize the resolving gel. The stacking gel is made in the same way, but the concentration of acrylamide is reduced to produce a 5% acrylamide stacking gel and 1.0 M Tris-HCL (pH 6.8) is used. The running buffer is made fresh wherein 28.2 grams of glyceride powder is mixed with 33.4 mL of 1.5 M Tris-HCL (pH 8.8). A final volume of 2 L is then achieved by adding deionized water.

Using the standard protocol, 1 mL of glutathione (GSH) aqueous solution (1 mM) was mixed with 1 mL of $HAuCl_4$ aqueous solution, with a GSH-to-Au ratio of 1 : 1 under vigorous stirring at 750 rpm at 750 rpm at a range of temperatures between 20^{o}C. After 30 seconds, 75 μL of 1 M NaOH was added to bring the final pH of the solution to ~12. The reaction proceeded for 2 hours and was then stored at room temperature. For reactions involving GSSG, the same synthesis procedure was used except that the ratio of GSSG-to-Au was 1 : 2. For time-course experiments all reactions conditions remained constant except for the variation in reaction temperature, which ranged between 20^{o}C and 70^{o}C, in 10^{o}C increments.

Fluorescence spectroscopy (line scan) and excitation-scanned spectroscopy (excitation-emission mapping) were performed with a HORIBA FluoroMax-4 fluorescence spectrophotometer. For excitation-emission mapping, samples were excited with 5 nm intervals in wavelength between 300-500 nm and their emissions were recorded in 2 nm increments in wavelength between 300-700 nm. Different slit widths were used for line scans (slit width: 5 nm resolution; integration time: 0.1 s) and for excitation- S3 emission mapping (slit width: 1 nm resolution; integration time 0.1 s). This resulted in

different measured intensities (photon counts per second, or CPS). Either line scans or excitation-emission mapping was performed to obtain any set of measurements. Ultraviolet-visible (UV-Vis) spectra were collected using a Shimadzu UV1800 spectrophotometer with 0.5 nm increments in wavelength.

After synthesis of the GSSG-Au complex as described above, GSSG-Au is purified using a 1 kDa molecular weight cutoff (MWCO) filter. 20 mL of GSSG-Au at 1 mM are washed at 4000 rpm at 20^{o}C until the final concentration is ~15 mM. The purified and concentrated GSSG-Au is mixed with 100% glycerol solution at a volume ratio of GSSG-Au : glycerol = 1 : 1, to be used for gel electrophoresis. 100 ug of the glycerol-containing GSSG-Au is loaded into a hand-cast gel, as described above. The gel is then run at 200 V on ice for 18 hours. After the gel run has completed the luminescent bands are cut from the gel and crushed in a 45 mL conical tube with 10 mL of water and rocked on a nutating mixer overnight to extract the luminescent complex from the gel. The crushed gel and water mixture are pressed through a 0.22 um PTFE filter to separate the crushed gel pieces from the GSSG-Au complex. This 10 mL of GSSG-Au is then washed again using a 1 kDa MWCO filter until it has been concentrated to 1 mL. This gel-run and concentrated GSSG-Au sample is then used as-is for NMR and ESI or is dried and crushed into a powder for FT-IR.

Nuclear magnetic resonance was performed on a JEOL 400 MHz NMR. GSH-Au and GSSG-Au samples that were prepared for NMR were made following the above protocol but the initial concentration of GSH and GSSG used was 16.2 mM, resulting in a final concentration of GSH and GSSG of 5 mg/mL. Samples for NMR were also prepared in D_2O and pH-adjusted using NaOD. Electrospray Ionization of GSH and GSSG samples

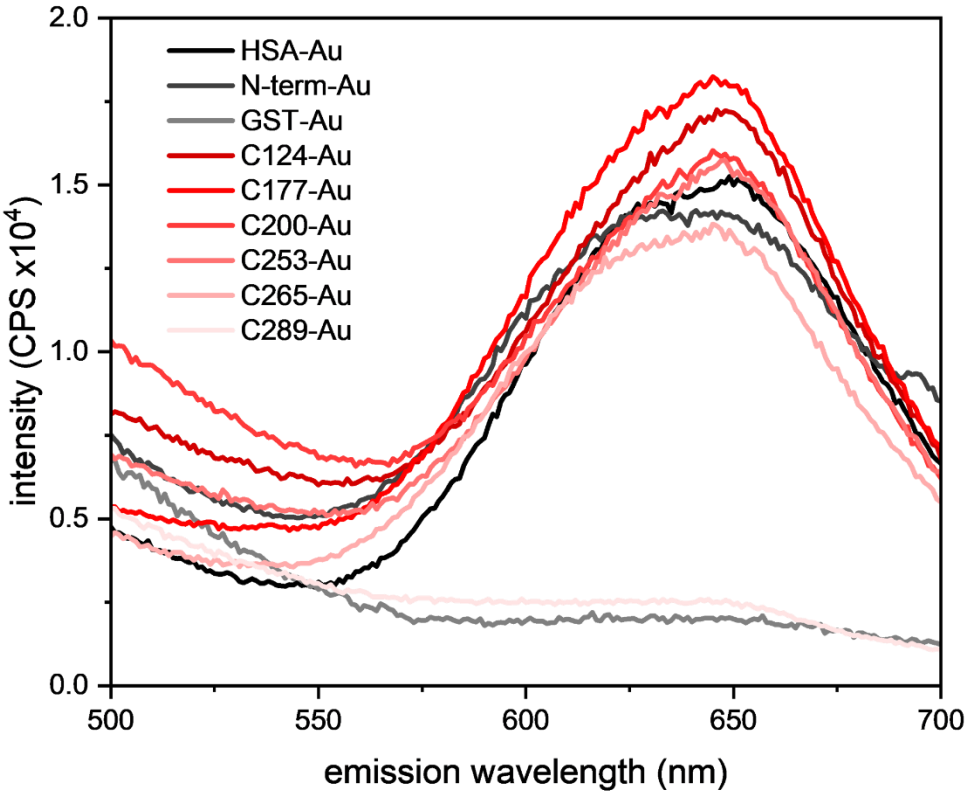

Figure 56. Fluorescence line scans (Ex = 365 nm) of all modified GST-N-$HSA_{1\text{-}313}$ proteins reacted with Au to produce red luminescence. All CYS-modified proteins show a similar red luminescence to that of the wild-type HSA-Au complex except for the GST-Au control and the CYS289-modified protein which show a similar lack of red luminescence.

were synthesized according to the standard protocol outline above. A further purification step of the as-synthesized GSH-Au and GSSG-Au samples was performed to remove any nanoparticles that may have formed. The purification of the GSH-Au and GSSG-Au complexes was done by first adding 25 µL of aqueous NaCl to 1 mL of the freshly synthesized complexes so that the final concentration of NaCl in solution was 12 mg/mL. MeOH was then added to the salted complexes in a volume ratio of complex to MeOH of 1 : 2. Finally, the samples were centrifuged at 10,000 rpm for 10 minutes at room temperature. After centrifugation, a small pellet was formed, leaving a clear supernatant which retained its luminescent properties. After purification, samples were taken immediately for ESI analysis.

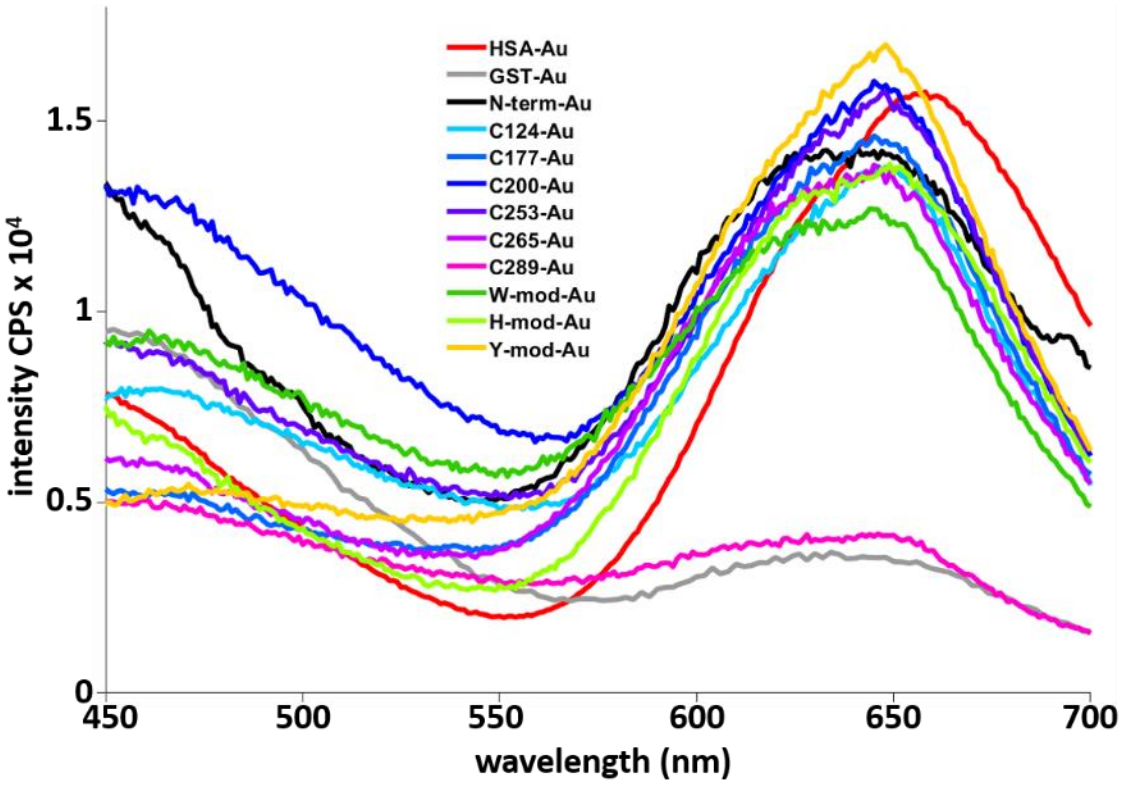

Figure 57. The luminescence of all modified GST-HSA_{1-313}-Au samples. Line scans of all modified proteins show that the red luminescent intensity of all samples complexed with Au are the except for the non-luminescent control sample containing GST and the GST-[HSA_{1-313}]-C289, indicating that modification of C289 results in a loss of luminescence and is the binding site of Au.

6.3 Location of the Red Luminescent Binding Site Using Molecular Cloning.

After molecular cloning of each sample was conducted, the amino acid modified GST-[HSA_{1-313}] samples were complexed with Au following a standard protocol. Briefly, using 200 µL of the modified protein (15 µM), 200 µL of $HAuCl_4$ (150 µM) was added followed by 11 µL of 1 M NaOH 1 minute later. The samples were mixed for 2 hours at 37°C and data collected 24 hours post-synthesis. The luminescent intensity of all the amino acid modified GST-[HSA_{1-313}] appeared equal except for the GST-Au control sample, containing no HSA, and the C289-Au modified sample, where Cys289 was replaced by alanine (**Figure 56**).

Additionally, the luminescent intensity of the aromatic amino acid modified GST-[HSA_{1-313}] samples were unchanged upon the addition of Au, indicating that aromatic residues may not directly contribute to red luminescence (**Figure 57**). Crucially, the coordination of Au must be to the disulfide bond of Cys278-Cys289 as breaking the disulfide bond at Cys289 in HSA results in the loss of the red luminescence. Thus, for the first time, the exact binding site of Au within a red luminescent protein-Au complex has been found. To fully understand this complex, the number of Au bound, and the mechanism of this luminescence must be elucidated. To achieve this, a similar, and less complex disulfide-containing system is used. This is exceedingly important, as conventional characterization techniques are too difficult to be applied to HSA, including the fragmented GST-HSA_{1-313}, due to their size.

6.4 Comparing Red Luminescence in HSA-Au and GSSG-Au Complexes.

While this red luminescent complex appears in other protein-Au systems, these proteins are all too large and complex (>10 kDa in the smallest known system), which prove to be difficult to study under conventional characterization techniques. Furthermore, while native crystal structures of these proteins exist, no such structures have been determined in highly alkaline conditions – a requirement for red luminescence. To determine the number and location of Au bound near cystine and to further understand the mechanism of red luminescence in our HSA-Au system, a small commonly studied thiolate molecule can be used. This molecule is oxidized glutathione (GSSG) which is only 0.6 kDa and contains a single disulfide bond. As this molecule is less than 1 kDa in size and contains

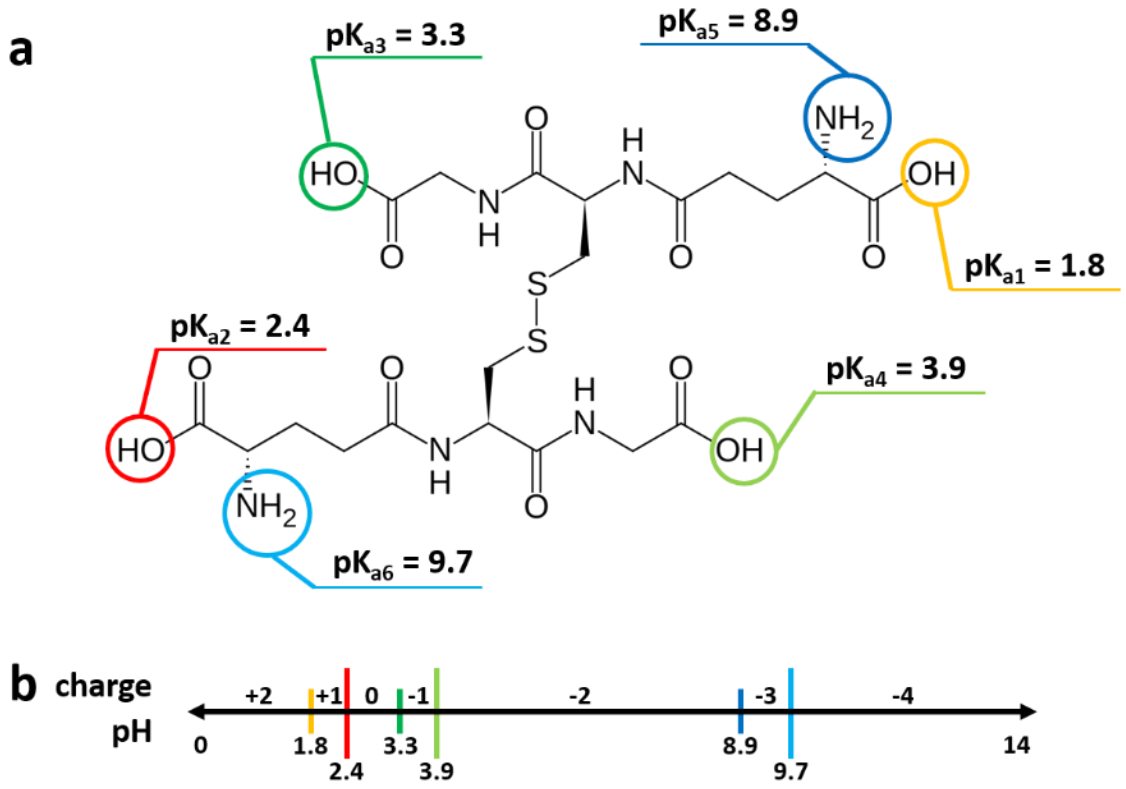

Figure 58. Schematic of oxidized glutathione (GSSG). (**a**) Schematic image of oxidized glutathione (GSSG). GSSG is a 612 Dalton molecule made of two glutathione molecules bound by a disulfide. The colored indicators show the pK_a of each side group which are (orange) pK_{a1} = 1.8, (red) pK_{a2} = 2.4, (dark green) pK_{a3} = 3.3, (light green) pK_{a4} = 3.9, (dark blue) pK_{a5} = 8.9, and (light blue) pK_{a6} = 9.7. (**b**) The overall charge of GSSG based on the overall pH GSSG is dissolved in. GSSG can be in up to 7 different charged states depending on the overall pH. When the pH of solution is close to a pK_a, GSSG will form an equilibrium in solution and can take different charged states in the same solution.

a cysteine, it is an ideal small molecule which can aid in simplifying the red luminescent system through isolation of a cysteine disulfide.

GSSG (**Figure 58**) is composed of two GSH molecules which have a tripeptide structure containing only three amino acids, glutamic acid, cysteine, and glycine (**Figure 59**).[143] GSH contains a single free thiol and upon oxidation, two GSH molecules are converted into GSSG, which form a single cystine disulfide bond.[144] GSSG was chosen as a model molecule due to its cystine disulfide, but most notably, upon following the same

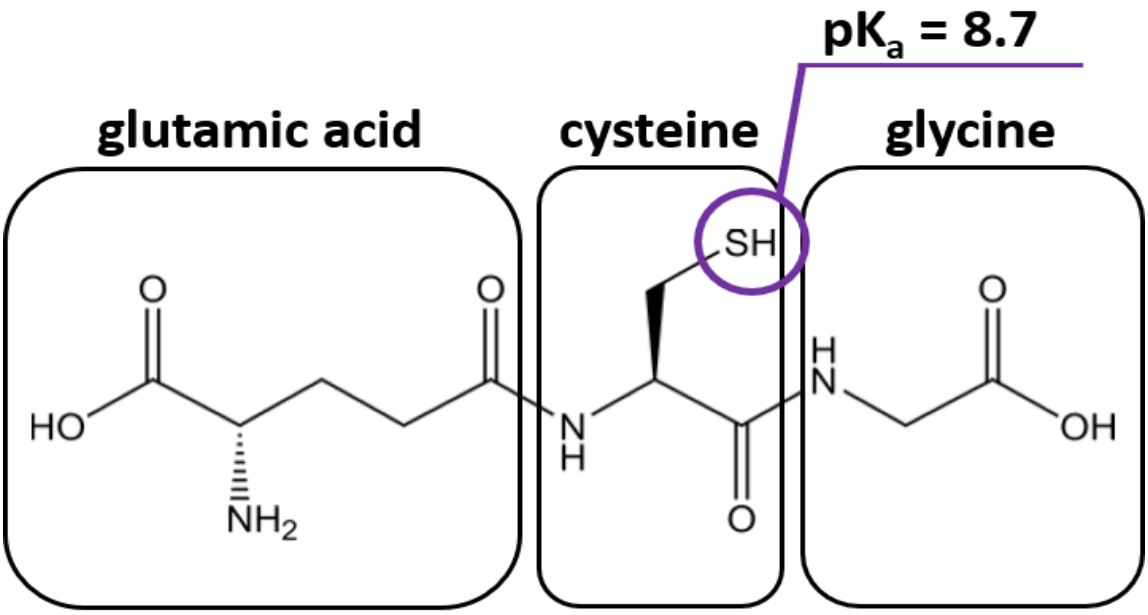

Figure 59. Schematic image of reduced glutathione (GSH). GSH is a 307 Dalton tripeptide made of glutamic acid, cysteine, and glycine. The three amino acids that make up GSH are outlined in black, while the pK_a of the thiol side group is outlined in purple. Above a pH of 8.7 the thiol side group will deprotonate and form GSSG.

protocol for synthesizing luminescent HSA-Au, GSSG-Au also formed the red luminescent complex. When reacting GSSG with Au at the stochiometric ratio of GSSG to Au = 1 to 2, red luminescence intensity was found to be like that of HSA-Au (**Figure 60**).

Along with the familiar red luminescence, the overall fluorescence excitation-emission spectra were all the same, suggesting the exact same mechanism of luminescence (**Figure 61**). Along with the excitation-emission spectra of HSA-Au and GSSG-Au, the overall reaction kinetics between the two complexes is also almost entirely equivalent including fluorescence decay rate, pH-dependence, temperature-time dependence, and stochiometric sulfur-to-Au ratio (**Figure 62** and **Figure 63**). As GSSG-Au and HSA-Au appear to form the same luminescent complex, GSSG-Au can be used in place of HSA-Au for further elucidation of the complex, including resolving the state of the cysteine disulfide within the complex.

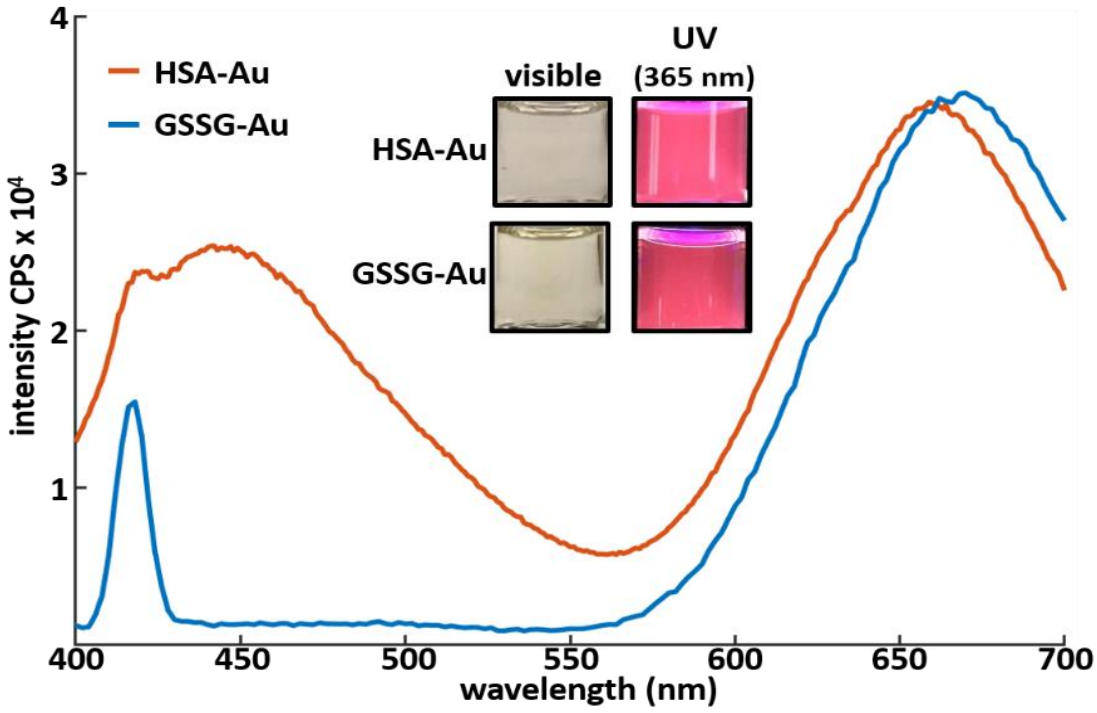

Figure 60. Initial fluorescence line scan of HSA-Au and GSSG-Au. They show nearly identical red luminescence (600 nm to 700 nm) . The major difference in luminescence in the blue regime (400 nm to 500 nm) is likely due to the large amount of aromatic amino acid residues in HSA, creating a large broad luminescence peak. The inset picture shows the visible and UV (365 nm) images of HSA-Au and GSSG-Au, which appear to have formed similar light-yellow compounds under ambient light which are simultaneously red luminescent under ultraviolet excitation.

Results from Chapter 4 showed that cystine is involved in the red luminescent complex in proteins, it remains to be determined if the complex requires a free cysteine thiol or an intact cystine disulfide within GSSG-Au. It also needs to be further confirmed if red luminescence requires a single cysteine thiol or a cystine disulfide bond. Thus, to determine whether the binding site for Au is a single thiol or a disulfide, GSH is also used for comparison. Upon following the same synthetic protocol for GSSG-Au and HSA-Au, GSH-Au also appears red luminescent (**Figure 64**). These results initially indicate that the red luminescent complex could be formed in the presence of either a free thiol or a cysteine

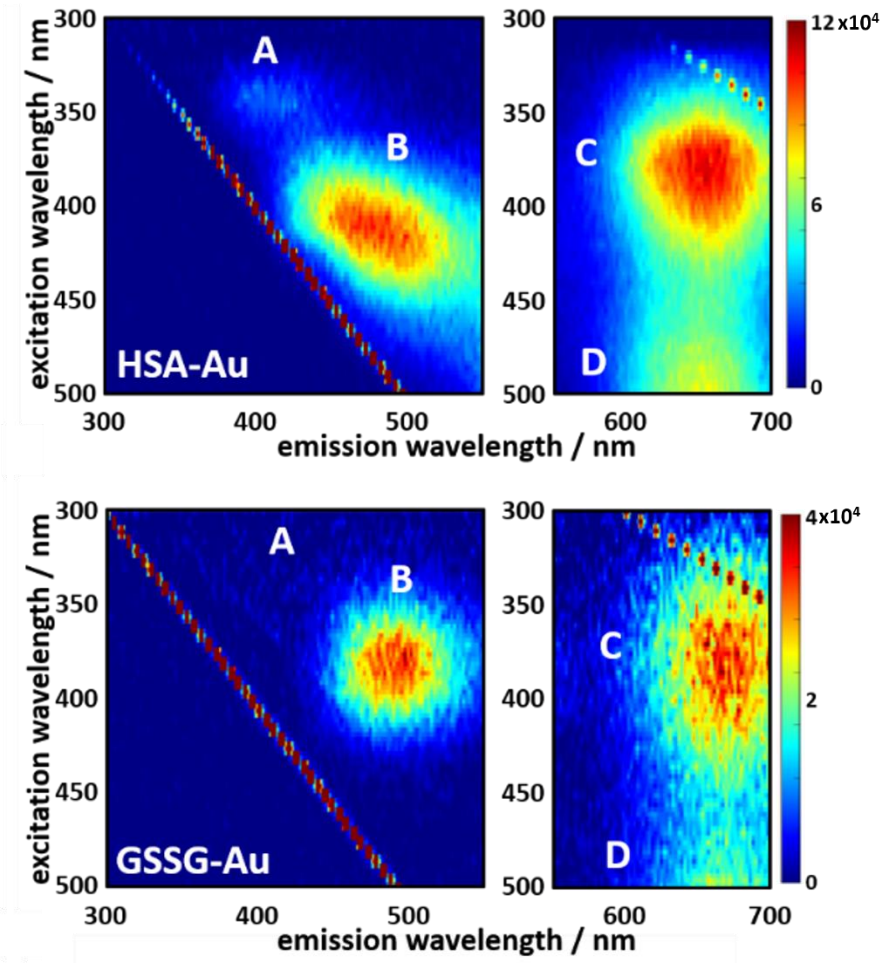

Figure 61. Comparisons of the red luminescent GSSG-Au complex to the HSA-Au complex. Fluorescence excitation-emission maps of HSA-Au at a ratio of HSA : Au = 1 : 13.3 and GSSG-Au at a ratio of GSSG : Au = 1 : 2, peak luminescence in the red regime can be observed around 650 nm when excited at 365 nm while peak luminescence in the blue regime can be observed around 340 nm when excited at 325 nm. Four primary regions of detectable luminescence can be observed across the entire excitation emission spectra at (A) ex/em = 340/400 nm; (B) ex/em = 400/500 nm; (C) ex/em = 365/650 nm; and (D) ex/em = 495/650 nm.

disulfide. Before further elucidation of the number of Au bound and the mechanism, the state of cystine within the complex must be determined and can be achieved by comparing both GSSG and GSH and their Au-containing complexes.

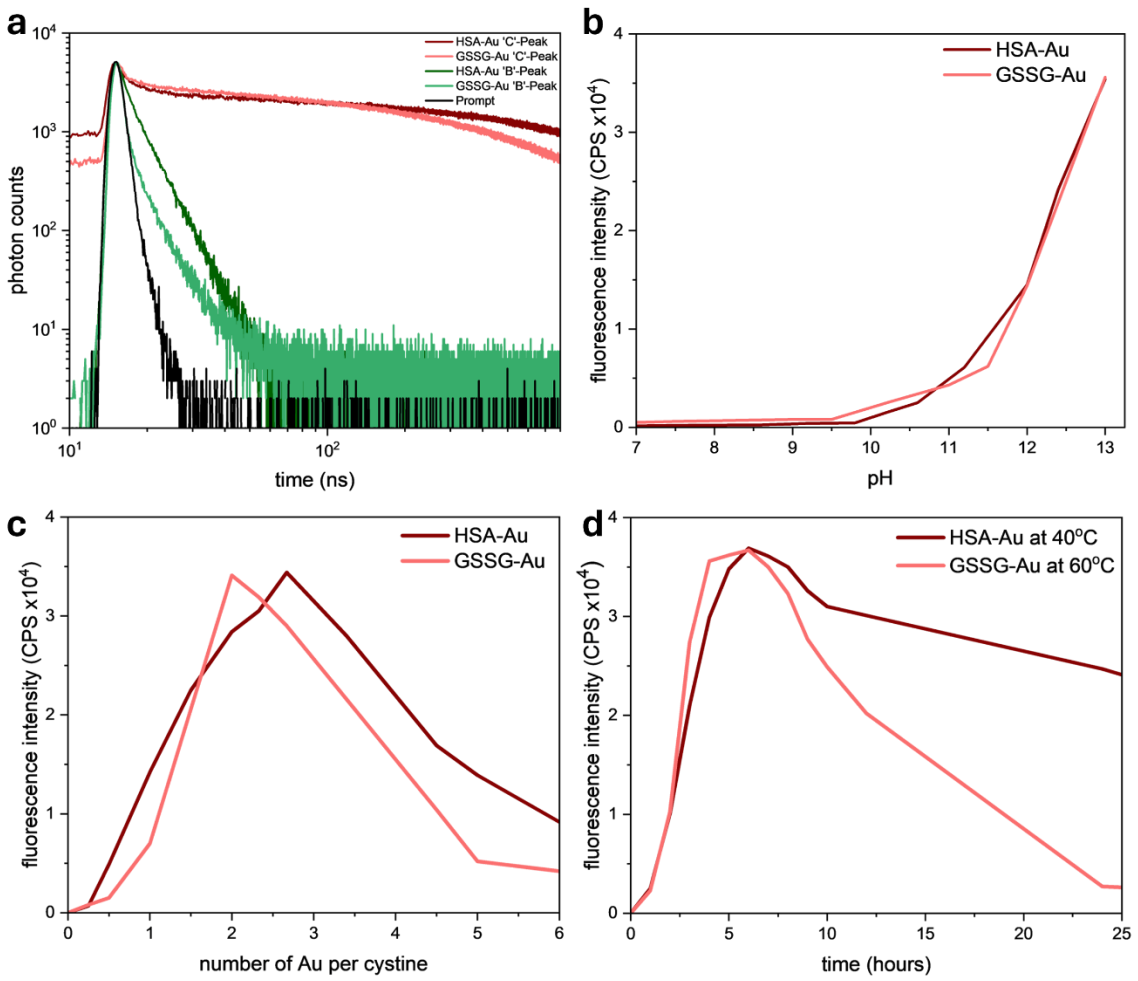

Figure 62. (**a**)TCSPC data of HSA-Au and GSSG-Au complexes show the 'red luminescent' regime has an equivalently long decay, while the 'green luminescent' regime is also equivalent but extremely short. (**b**) Dependence of luminescence on pH shows that red luminescence emerges as pH is raised beyond 10.0-10.5 for both HSA-Au and GSSG-Au. (**c**) Peak luminescence intensity based on the number of Au to disulfide bonds shows that the ideal ratio is between 2 to 3 Au per disulfide bond. (**d**) Time-course luminescence (λ_{ex}/ λ_{em} = 365/650) of HSA-Au at 30^{0}C and GSSG-Au at 60^{o}C, in each sample, peak luminescence occurs around 6 hours followed by a gradual loss of luminescence as time progress.

Lifetime	τ_1 (ns)	τ_2 (ns)	τ_3 (ns)
HSA-Au 'C' Peak	**315 (97%)**	**31.1 (2%)**	**1.2 (1%)**
HSA-Au 'B' Peak	**4.9 (1%)**	**1.5 (2%)**	**0.2 (97%)**
GSSG-Au 'C' Peak	**182 (96%)**	**13.1 (3%)**	**0.8 (1%)**
GSSG-Au 'B' Peak	**3.9 (1%)**	**0.8 (1%)**	**0.2 (98%)**

Figure 63. TCSPC data of HSA-Au and GSSG-Au measured using ex=389 nm and measured at 400 nm and 650 nm. In both samples the number of decay terms required to fit the data was three. Both samples also showed similar lifetime decay rates when fit with a triple-exponential decay function.

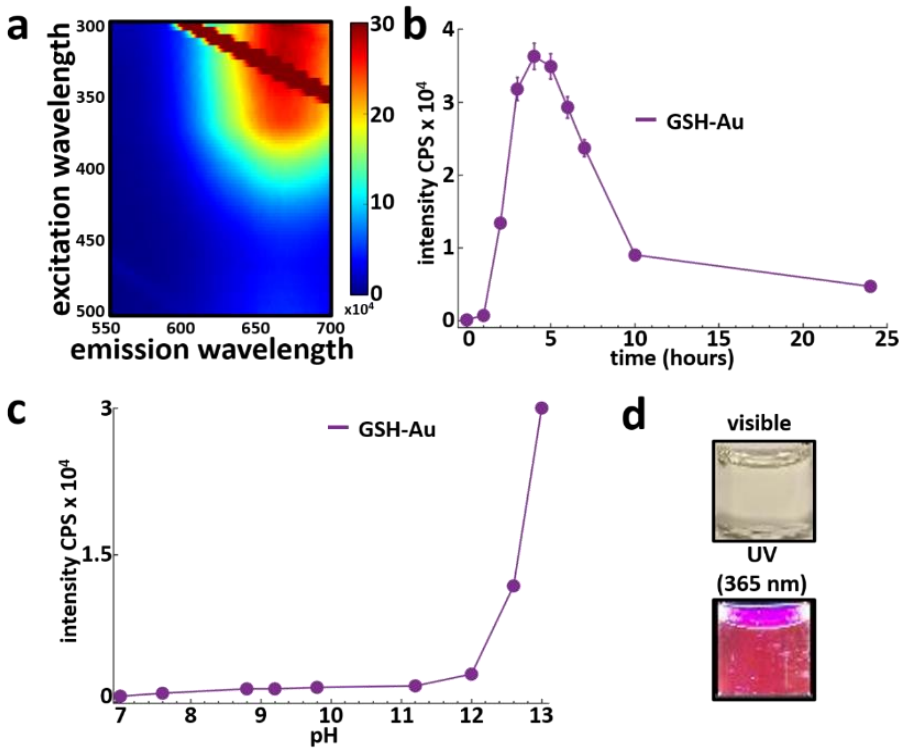

Figure 64. Fluorescence spectra and reaction kinetics of GSH-Au. GSH-Au synthesized at pH 12, shows similar luminescence patterns as that of HSA-Au and GSSG-Au, indicating red luminescence originates from the same mechanism. (a) Fluorescence excitation-emission map of GSH-Au at a ratio of GSH : Au = 1 : 1, peak luminescence can be observed around 650 nm when excited at 365 nm. (b) Time-course luminescence ($\lambda_{ex}/\lambda_{em}$ = 365/650) of GSH-Au at 60°C, peak luminescence occurs around 6 hours followed by a gradual loss of luminescence as time progress. (c) Dependence of luminescence on pH shows that red luminescence emerges as pH is raised beyond ~10.0. (d) Visible and UV (λ_{ex} = 365) images of GSH-Au 1 day after synthesis.

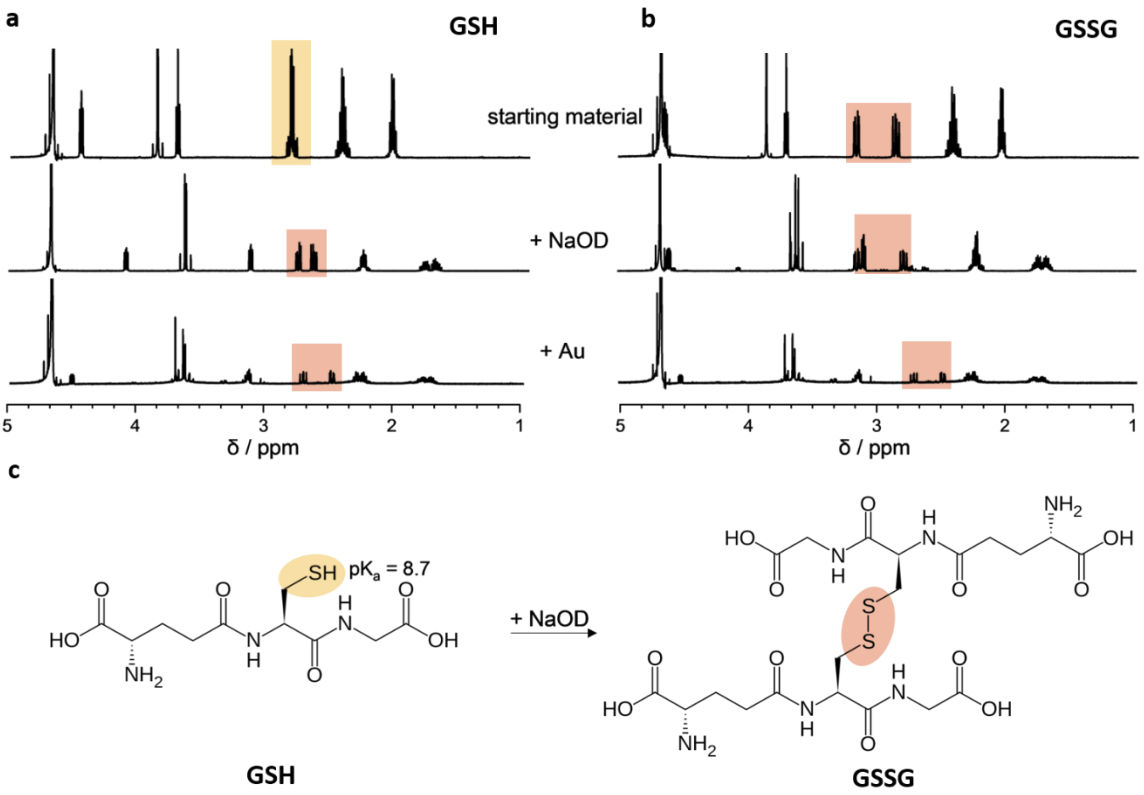

Figure 65. Comparison of NMR spectra between GSH and GSSG. (**a**) NMR spectra of GSH as is, after the addition of NaOD, and finally after the addition of Au. (**b**) NMR spectra of GSSG as is, after the addition of NaOD, and finally after the addition of Au. (**c**) Schematic drawing of the conversion that occurs at a pH greater than 8.7 where GSH is converted into GSSG. From the image above it can be seen that after the addition of NaOD both GSH and GSSG are nearly identical and after the addition of Au both GSH-Au and GSSG-Au are identical, indicating the formation of the exact same complex.

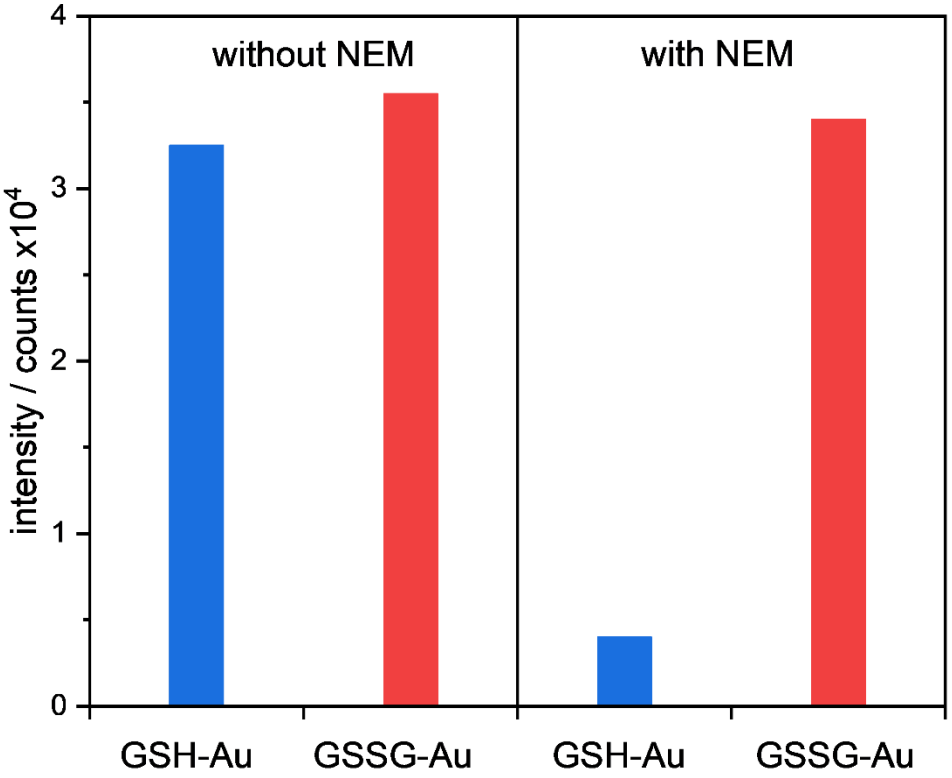

Figure 66. NEM effect on the formation of luminescence in GSH-Au and GSSG-Au. Both GSH-Au and GSSG-Au are luminescent (λ_{ex}/ λ_{em} = 365/650) under the same standard protocol. The addition of NEM before adding Au, to block the free thiol results in no luminescence in NEM-capped-GSH-Au and has no effect on NEM-capped-GSSG-Au. These results indicate that an intact disulfide bond is required for the red luminescent complex to form.

6.5 Determining the Role of Disulfides Using GSH and GSSG

In GSH, deprotonation of the free thiol is expected to occur around a pH of 8.7.[145,146] Upon deprotonation, the thiol of GSH will react with another GSH, resulting in the formation of GSSG, even without the need for reactive oxygen species to be present.[147] These results could also just be inferred from the pK_a values of the thiol side groups of GSH.[148,149] Using nuclear magnetic resonance (NMR) spectroscopy of GSH and GSSG, the NMR spectra of both GSH and GSSG at a pH of 12 were identical (**Figure 65**).[150] Most notably, is the presence of a doublet centered at 2.7 ppm, indicating the existence of a cysteine disulfide, meaning that GSH has converted into GSSG. Additional NMR

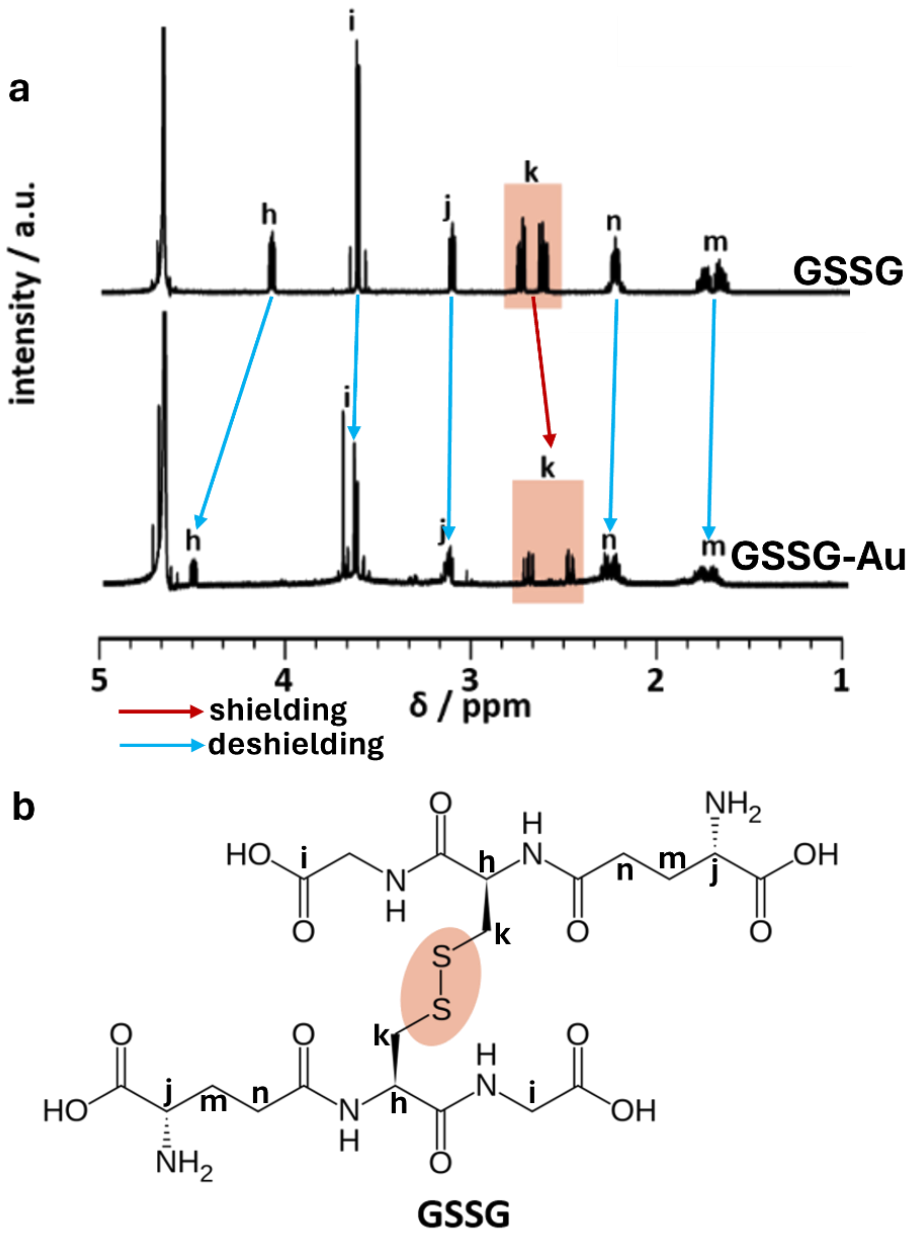

Figure 67. Effects of the addition of Au on the structure of GSSG as seen through NMR. (**a**) Disulfide formation can be observed in NMR as the characteristic doublet resulting from thiol at 2.7 ppm can be observed. NMR of GSH-Au and GSSG-Au at pH 12 also shows the exact same complex has formed and contains a disulfide. The addition of Au causes a shielding effect near the disulfide bond, and a variable degree of deshielding to all other peaks. (**b**) Schematic illustration of the conversion of GSH into GSSG at highly alkaline pH – the free thiol will form a disulfide bond.

comparisons of GSSG-Au and GSH-Au also showed no difference in spectral pattern, indicating that the same red luminescent complex had formed after the addition of Au.

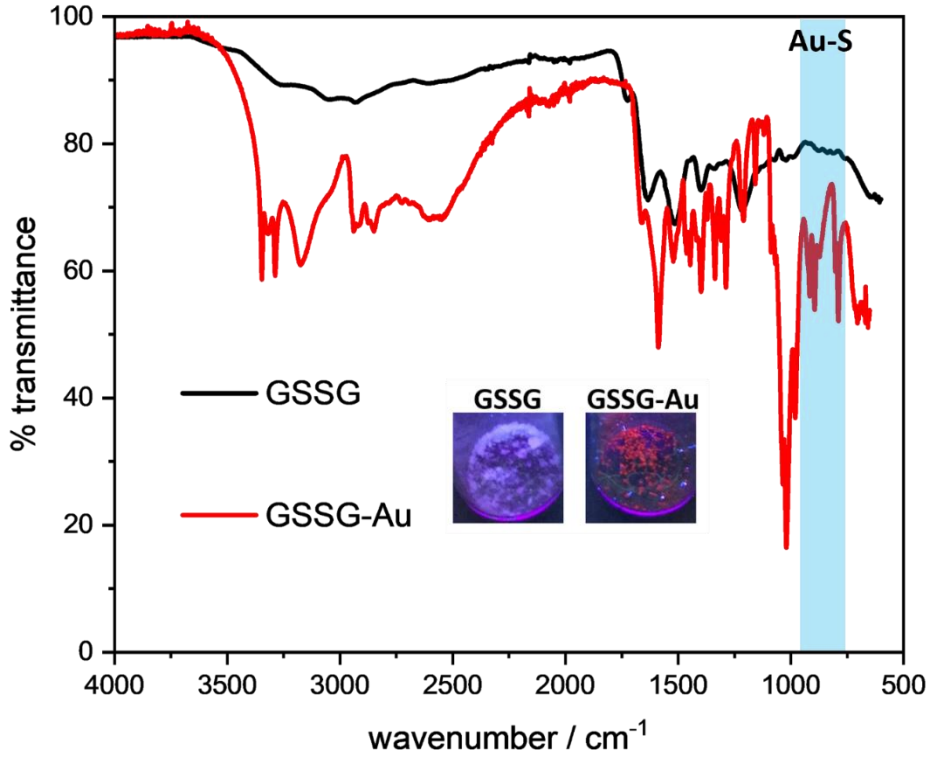

Figure 68. FT-IR of gel-purified GSSG-Au shows the presence of Au-S stretching modes around 650 cm^{-1} to 900 cm^{-1}.

Further probing into the state of thiols within the luminescent complex also supported the theory that disulfides are present in the final complex. Additionally, the highly alkaline conditions of the synthesis result in the transformation of GSH into GSSG. Thus, a thiol-blocking experiment was performed, in which the free thiol of GSH was permanently capped before the addition of Au.

Preferential blocking of the free thiol in GSH was carried out by N-ethylmaleimide (NEM) capping.[151] After thiol capping the standard protocol to form the Au-containing complex was performed. After 24 hours the NEM-capped-GSH-Au samples showed no red luminescence relative to the control GSH-Au and GSSG-Au sample. In the control samples using GSSG-Au the addition of NEM had no effect on red luminescence generation, indicating that disulfide formation is critical in the emergence of the red luminescent complex (**Figure 68**). Thus, for both GSH and GSSG to form the red

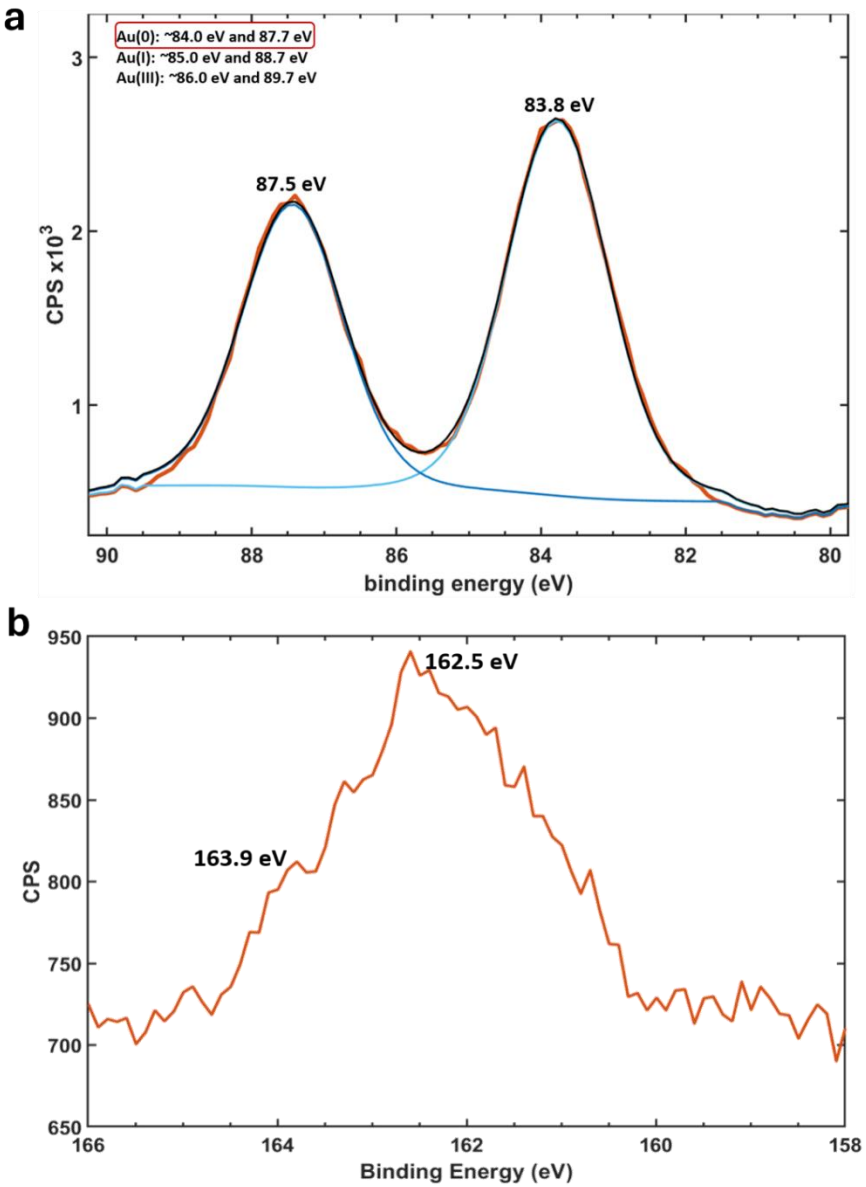

Figure 69. (a) XPS of gel-purified GSSG-Au at the Au 4f binding energy shows that Au is entirely in a single state of Au(0). The light-blue and dark blue-lines in the figure represent the fit-function for Au(0). (**b**) XPS analysis of the S 2p binding energy regime. XPS analysis of sulfur reveals that an ideal fitting involves two distinct states of sulfur. The first major state is that of Au-S, indicated by the presence of a large peak around 162.5 eV. The secondary state of sulfur is that of the disulfide S-S, indicated by the presence of a peak around 163.9 eV. Both states being observed simultaneously indicate that Au is bound to sulfur and the disulfide remains intact.

luminescent complex, GSH must first be oxidized into GSSG to form the cysteine disulfide necessary for red luminescence generation. These results also agree with why red luminescence is lost when GST-[$HSA_{1\text{-}313}$]-CYS289 is complexed with Au: the disulfide

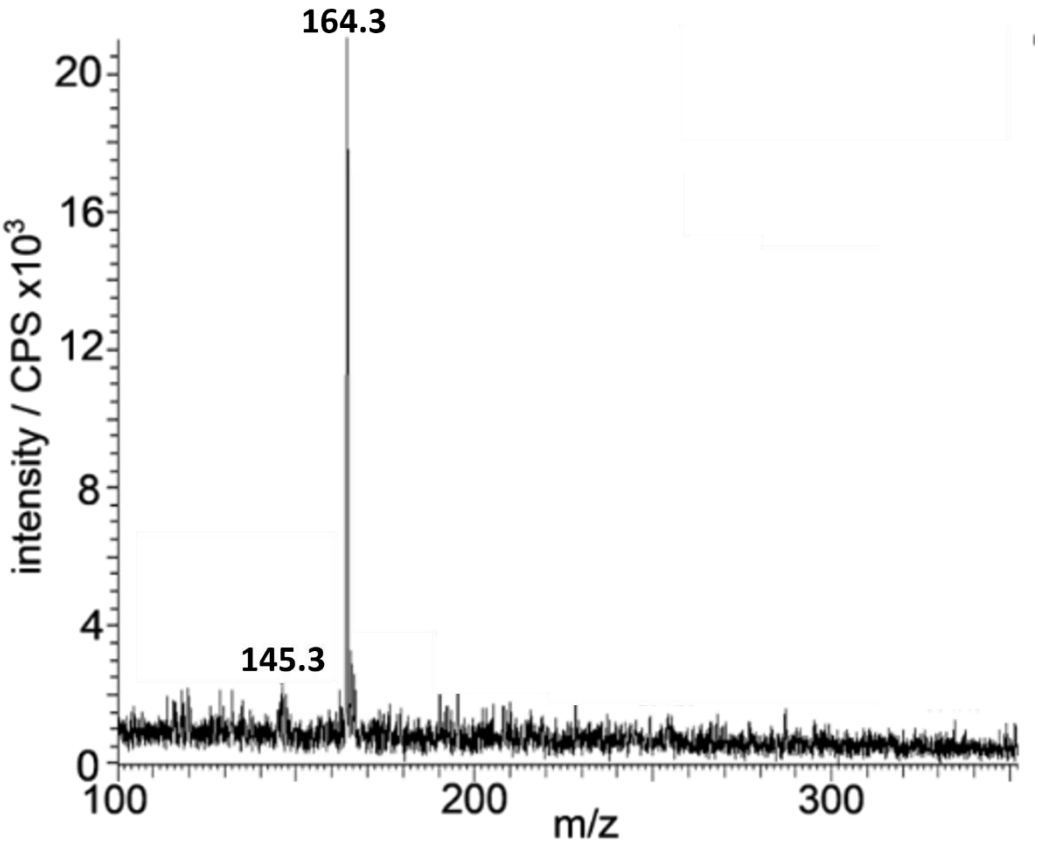

Figure 70. ESI of gel-purified GSSG-Au shows a single, prominent peak at 164.3 m/z, indicative of GSSG-Au_2Cl_4 with a -7 charge and a true mass of 1150.1 kDa

bond no longer exists. These results also support why modification of the other complimentary cysteine residues in GST-[$HSA_{1\text{-}313}$] would not yield different results, such as GST-[$HSA_{1\text{-}313}$] where CYS278 is modified.

The elucidation of an intact disulfide bond in the red luminescent complex is the first step in resolving the number of Au bound and their location within the complex. The luminescence in the complex has been attributed to alternative Au nucleation models, yet none have confirmed these results or shown the overall mechanism of formation.[12,22] With the current results it is apparent that the red luminescent complex must contain an intact disulfide bond and is likely smaller than a nanoparticle or even a very small Au_{25}

nanocluster. Thus, further experimentation can be done to reveal the structure of the luminescent complex.

6.6 Resolving the Structure and Number of Au in GSSG-Au Complexes.

First, the general location of Au within the GSSG-Au complex can be determined from NMR and FT-IR analysis. NMR spectra comparing GSSG before and after the addition of Au shows that three primary peaks are affected by the presence of Au which are *h*, *k*, and *k'* (**Figure 67**). The addition of Au causes an upfield shift in the doublet of *k* and *k'*, while a downfield shift of *h* is observed. It is known that the addition of large, transition-metal atoms can have a shielding or deshielding effect on the local electron density around the metal atom.[152] In the case of Au, simultaneous shielding and deshielding is possible.[153] Thus, an upfield shift in the doublet of *k* and *k'*, and a simultaneous downfield shift of *h*, would indicate that Au is bound directly adjacently to the disulfide bond in GSSG, pulling electron density in around *k* and *k'*, while freeing the electron density at peak *h*. These results also seem to be supported by FT-IR, which show evidence of Au-S bonding in the regime of 650 to 900 cm^{-1} (**Figure 68**).[154-157]

The charge state of Au within the GSSG-Au complex was also revealed to be exclusively Au(0) by XPS, as analysis of the Au 4f spectrum shows two distinct peaks at 83.8 eV and 87.5 eV (**Figure 69a**).[158,159] Additional XPS analysis of the S 2p peak regime showed a single peak at 162.4 eV of Au(0) bound to S (**Figure 69b**).[160] These results also support FT-IR and NMR that the binding location of Au within the complex is directly to the sulfur within GSSG. Further analysis of the purified GSSG-Au sample was done using ESI to confirm the mass found and is outlined in Chapter 7.

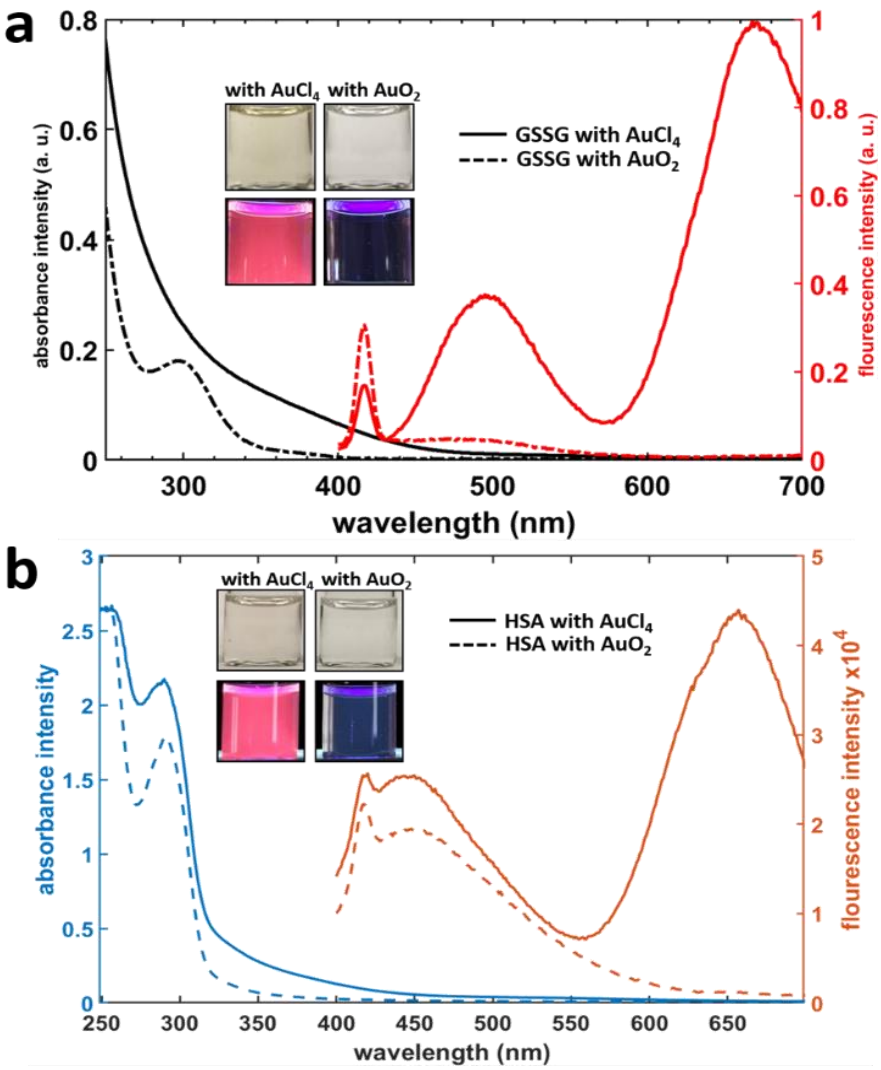

Figure 71. Reaction of HSA and GSSG starting with $AuCl_4$ or AuO_2. In each case allowing the reaction to start with $AuCl_4$ results in the expected red luminescent complex, while starting with AuO_2 inhibits red luminescence formation. (a) Solid line shows the absorbance and fluorescence of GSSG+$AuCl_4$ while the dotted line shows GSSG+AuO_2. The inset shows the visible and UV excited images of both samples. (b) Solid line shows the absorbance and fluorescence of HSA+$AuCl_4$ while the dotted line shows HSA+AuO_2. The inset shows the visible and UV excited images of both samples.

ESI of GSSG and GSSG-Au can be an effective tool to measure the exact mass the GSSG-Au complex and subsequently the number Au atoms.[161] ESI of GSSG-Au purified from gel electrophoresis shows a primary peak at 164.3 m/z, with a significantly less prominent peak at 145.3 m/z (**Figure 70**). The primary peak at 164.3 m/z could be

attributed to a GSSG-Au complex comprised of 2 with an additional combination of Cl or OH atoms, assuming a highly negative charge of -7.

First to determine whether Cl or OH is present, a reaction starting with AuOH instead of $AuCl_4$ was performed with both HSA and GSSG (**Figure 71**). While $AuCl_4$ is known to convert to AuOH over time in highly alkaline conditions, reactions that started with AuOH resulted in no luminescence.[162] This indicates that $AuCl_4$ is a required part of the luminescent complex, and thus Cl is required to be in the complex. To compensate for the remaining mass, 4 negatively charged Cl ions could be considered. Justification for the large negative charge observed could be attributed to -4 from the four present Cl ions and an additional -4 from GSSG itself since it will be deprotonated in alkaline solution and negatively charged. Thus, a total negative charge of -8 could be contained within the compound.

Since the pH of GSSG-Au after gel extraction is approximately 9.5, an equilibrium will result as one of the amine side groups (pK_a = 9.7) of GSSG may or may not be in a deprotonated state, resulting in two possible observable charges of GSSG (-3 or -4) and finally bringing the total charge of the system to either -7 or -8. This would justify the two observed peaks from the ESI spectra, and ultimately just the highly negative charge observed.

Assuming the -7 charge state of the complex, the peak of 164.3 m/z results in a mass of approximately 1150.1. This correlates best to a complex of GSSG plus two Au atoms and plus 4 Cl atoms. The secondary peak at 145.3 m/z corresponds to just a -8 charged GSSG+Au_2Cl_4. The results of ESI also support the findings from gel electrophoresis and EDX, which is discussed further in Chapter 7. The above results

indicate that the red luminescent GSSG-Au complex is a small Au-thiolate compound, with two Au atoms bound directly to the disulfide bond in GSSG.

Thus, the exact binding site of Au within HSA that is responsible for the formation of the red luminescent complex has been identified. Using molecular cloning techniques of HSA, this site has been identified to be the cysteine disulfide: Cys278-Cys289. It was found that the red luminescence observed in the smaller GSSG-Au was identical to that of HSA-Au and could then be used as an accurate analog to elucidate structural and mechanistic information about the HSA-Au complex. Comparing GSSG-Au and GSH-Au in highly alkaline conditions revealed that a disulfide bond is required for red luminescence to occur.

Analysis of purified GSSG-Au shows that luminescence is not due to a nanocluster, but generally follows a two-step nucleating mechanism where luminescent complexes eventually form nanoparticles. Further analysis of GSSG-Au revealed that only 2 neutral Au atoms are bound directly to the disulfide of GSSG and thus the fully uncovered red luminescent complex is GSSG+2Au^0, correlating to the same complex which is within red luminescent HSA-Au. Elucidation of the binding site, mechanism, and structure of HSA-Au and GSSG-Au has finally uncovered that these complexes are small thiol-bound Au compounds comprised of only two Au atoms. These findings reveal the structure and mechanism of formation of these luminescent Au-thiolate complexes and could lead to the understanding of other luminescent protein-Au complexes.

CHAPTER 7: RESOLVING THE MECHANISM OF NANOPARTICLE FORMATION IN RED LUMINESCENCT HSA-GOLD AND GSSG-GOLD COMPLEXES

The human serum albumin[23,163,164] (HSA) – gold (Au) complex has attracted considerable attention since the initial report by Xie et al.[12] due to the unique optical properties of the complex as well as its ease of synthesis.[71,165] Numerous applications for this complex have already been shown in fields of sensing,[35-37,41,70] imaging,[36,42,43,70] and nanomedicine.[18,19,42,44,45] The formation of this complex begins by mixing protein -such as serum albumin and Au at a pH equal or greater than 10, and after a short incubation time the red luminescent complex is formed.[13] It has been suggested by others that the origin of the red luminescence in these complexes is due to the nucleation of many Au(0) atoms into the center of the protein, resulting in a neutral, luminescent Au_{25} nanocluster.[22,47] While the existence of nanoparticles has been clearly observed many times, it has not been addressed what the formation mechanism of these nanoparticles nor confirmed that the nanoparticles themselves are red luminescent.[165] Furthermore, none have noted the discrepancy in the size of these 'red luminescent nanoparticles' which have been observed to be around 3 nm or larger compared to the expected size of an actual Au_{25} nanocluster.[12,49,165] Even though these 3 nm diameter nanoparticles have been reported as the source of red luminescence.[166-170]

Assuming 25 Au atoms will form a spherical shape and have an atomic radius of 135 pm,[171] then the largest sphere that can made by these gold atoms will have a diameter of no greater than 1.0 nm.[172] This result is consistent with the actual findings of the crystal structure of a Au_{25} nanocluster which was found to be 0.982 nm, measured across the entire

Au core.[47,173] This is significantly smaller than that of the reported red luminescent protein-Au complexes and raises an important question as to what these nanoparticles are if not the source of red luminescence and what their role in the reaction is.

In Chapter 3 the reaction kinetics of the bovine serum albumin (BSA)-Au complex was discussed and showed that a new Langmuir-type multi-site adsorption model for the formation of the BSA-Au complex was a better fit to the data.[1] This was in comparison to the traditional LaMer-type model of a single-site nanocluster nucleation.[94] The results were consistent with the adsorption model in which Au binds specifically to multiple sites, as well as nonspecifically to the proteins surface. It was also found in red luminescent BSA-Au and HSA-Au complexes that the binding domain responsible for the red luminescent complex is contained within the first 313 of the 584 total amino acids in the proteins.[66] Where this smaller subdomain of BSA may not even be able to support the formation of a nanocluster inside.

The formation of nanoparticles within samples of red luminescent protein-Au (HSA) and small-molecule-Au (oxidized glutathione – GSSG) is elucidated. Through separation of nanoparticles within the solution and the application of a two-step formation mechanism, nanoparticles were found to not be the source of red luminescence but a secondary product of the red luminescent complex itself.

7.1 Experimental Methodology and Instrumentation

The HSA-Au complexes, as well as the GSSG-Au complexes, were prepared following a similar protocol.[174] To synthesize the red luminescent complex, and the final nanoparticle of HSA-Au, 25 mg (0.375 mM) HSA was dissolved into 1 mL of HPLC grade water. Immediately after, 1 mL of 3.75 mM $HauCl_4$ aqueous solution was added. After 30

seconds, 1 M NaOH was added to the solution to bring the sample to a pH of 12.5. The sample was finally left to react in a water bath at 40^{o}C and 750 rpm for 2 hours. For time-course based reactions, the HSA-Au solution was left at a range of temperatures between 20-50^{o}C for up to 48 hours. GSSG-Au complexes were synthesized in a similar fashion wherein 0.613 mg (1 mM) GSSG was dissolved into 1 mL of HPLC grade water. Immediately after, 1 mL of 2 mM $HauCl_4$ aqueous solution was added. After 30 seconds, 1 M NaOH was added to the solution to bring the pH above 12.5. The sample was left to react in a water bath at 60^{o}C and 750 rpm for 4 hours. For time-course based reactions, the GSSG-Au solution was left at a range of temperatures between 40-70^{o}C for up to 48 hours. For ratio-metric based reactions, a range of $HauCl_4$ concentrations between 1 – 10 mM were used, followed by the standard protocol.

A large gel is hand cast without SDS to separate the extremely small molecular-weight GSSG-Au and maintain red luminescence,.[68] A 30% acrylamide resolving gel is made by adding 30 mL of 40% acrylamide (containing 5% crosslinker), with 10 mL of 1.5 M Tris-HCL (pH 8.8). Next, 400 µL of 10% APS and 16 µL of TEMED are added to polymerize the resolving gel. The stacking gel is made in the same way, but the concentration of acrylamide is reduced to produce a 5% acrylamide stacking gel and 1.0 M Tris-HCL (pH 6.8) is used. The running buffer is prepared right before use where 28.2 grams of glyceride powder is mixed with 33.4 mL of 1.5 M Tris-HCL (pH 8.8). A final volume of 2 L is then achieved by adding deionized water.

After synthesis of the GSSG-Au complex as described above, GSSG-Au was purified using a 1 kDa molecular weight cutoff (MWCO) filter. 20 mL of GSSG-Au at 1 mM are washed at 4000 rpm at 20^{o}C until the final concentration is ~15 mM. The purified

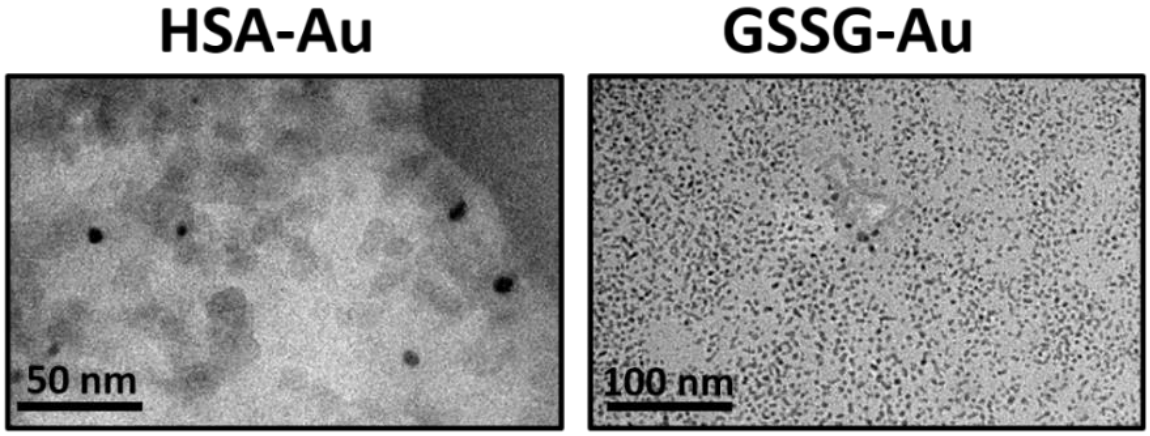

Figure 72. The synthesis for the formation of red luminescent HSA-Au and GSSG-Au both lead to the formation of nanoparticles after the reaction has proceeded for two hours. In this reaction nanoparticles are present as well as the solution being red luminescent. The size of nanoparticles for HSA-Au and GSSG-Au is around 3 nm.

and concentrated GSSG-Au is mixed with 100% glycerol solution at a volume ratio of GSSG-Au : glycerol = 1 : 1, to be used for gel electrophoresis. 150 uL of the glycerol-containing GSSG-Au is loaded into a hand-cast gel, as described above. The gel is then run at 200 V on ice for 18 hours. After the gel run has completed, the gel is placed into an Azure Biosystems gel imager where the luminescent bands are observed, using 350 nm excitation and 650 nm emission.

The separation of the GSSG-Au complex into a precipitate and supernatant is as detailed below. After the synthesis of the GSSG-Au complex the 1 mL of the light-yellow-colored, red luminescent solution is mixed with 12 mg of NaCl followed immediately by 2 mL of MeOH, added at once. After the addition of MEOH the solution transforms from clear to faintly cloudy. Next, the solution is centrifuged at 10,000 rpm for 20 minutes at 20^{o}C. The resultant sample is a small, black-colored pellet in the bottom of the vial with a clear supernatant.

Fluorescence spectroscopy (line scan) and excitation-scanned spectroscopy (excitation-emission mapping) were performed with a HORIBA FluoroMax-4 fluorescence spectrophotometer. For excitation-emission mapping, samples were excited with 5 nm intervals in wavelength between 300-500 nm and their emissions were recorded in 2 nm increments in wavelength between 300-700 nm. Different slit widths were used for line scans (slit width: 5 nm resolution; integration time: 0.1 s) and for excitation- S3 emission mapping (slit width: 1 nm resolution; integration time 0.1 s). This resulted in different measured intensities (photon counts per second, or CPS). Either a single line scan or excitation-emission mapping was performed to obtain any set of measurements. Ultraviolet-visible (UV-Vis) spectra were collected using a Shimadzu UV1800 spectrophotometer with 0.5 nm increments in wavelength.

7.2 Observance of Nanoparticles in Red Luminescence Complexes

In the standard synthesis of red luminescent HSA-Au complexes, as well as the synthesis of red luminescent small molecules, such as GSSG-Au, both lead to the formation of nanoparticles after some time,[1,13] and can be seen via TEM imaging (**Figure 72**). Since the initial discovery of these red luminescent complexes in bovine serum albumin (BSA)-Au, the predominant theory for red luminescence has relied on the idea that the nanoparticles formed are the source of red luminescence.[12]

Furthermore, the nanoparticles assumed to be responsible for red luminescence contain only 25 Au atoms. This luminescence is due to the expected optical properties of small Au-based (<50 atoms) nanoclusters, based on the spherical Jellium model.[48,175,176] Yet the size of the nanoparticles observed in these red luminescent solutions under TEM are on the order of 3 nm in diameter, or larger. This indicates that these nanoparticles would

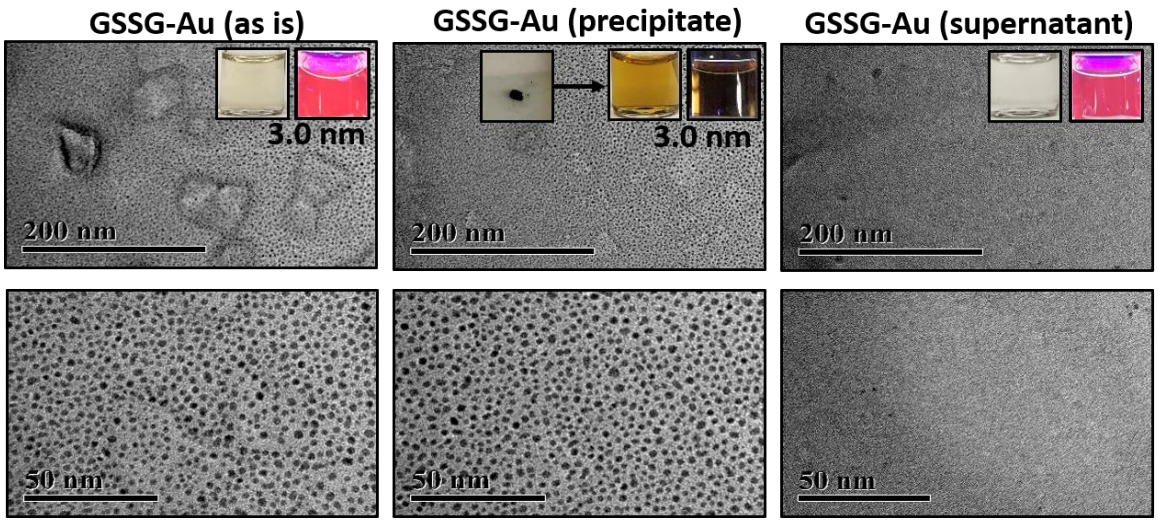

Figure 73. Washing shows two distinct compounds are present in solution, post-synthesis. (Left panels) The as-synthesized GSSG-Au is red luminescent and contains many nanoparticles are the reaction reaches peak intensity. (Middle panels) After washing, a precipitate is observed to come out of solution which can be seen to contain many nanoparticles but lacks luminescence. The ambient color of the sample also has darkened in intensity, indicating the yellow color may come from nanoparticles. (Right panels) The remaining supernatant is nearly entirely free of nanoparticles, yet still maintains its luminescent properties, indicating that luminescence must be coming from a smaller, non-nanoparticle source.

have thousands of Au atoms per nanoparticle, not 25. This overlooked discrepancy raises the question as to where the source of red luminescence in these complexes originates from and what role nanoparticles have in the overall process.

7.3 Separation of Nanoparticles from Red Luminescent Solutions

To begin understanding nanoparticle formation, the first logical step would be to separate the nanoparticles in solution and observe their luminescence outside of solution. Initial separation of the as-synthesized GSSG-Au sample following an ultra-centrifugal and salt-based separation[177] method revealed two distinct compounds within the GSSG-Au solution – a clear supernatant, and a black-colored pellet (**Figure 73**).

The clear supernatant appeared to contain no nanoparticles and was visibly red luminescent when illuminated with ultraviolet light. The black-colored precipitate

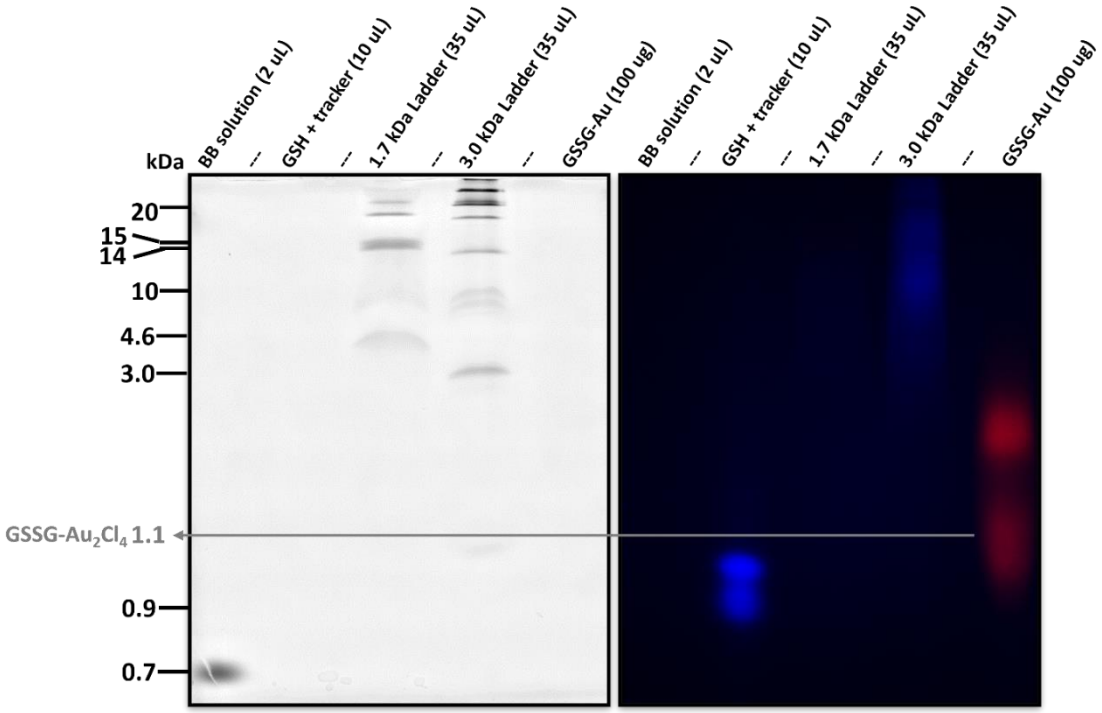

Figure 74. Raw visible and UV image of gel containing purified GSSG-Au. Using both the tagged-GSH and low molecular weight ladders the approximate mass of the luminescent GSSG-Au can be estimated. The nine lanes from left to right are as follows: (1) bromophenol blue; (2) [blank]; (3) tagged-GSH; (4) [blank]; (5) 4.6 kDa-containing protein ladder; (6) [blank]; (7) 3.0 kDa-containing protein ladder ; (8) [blank]; (9) purified GSSG-Au.

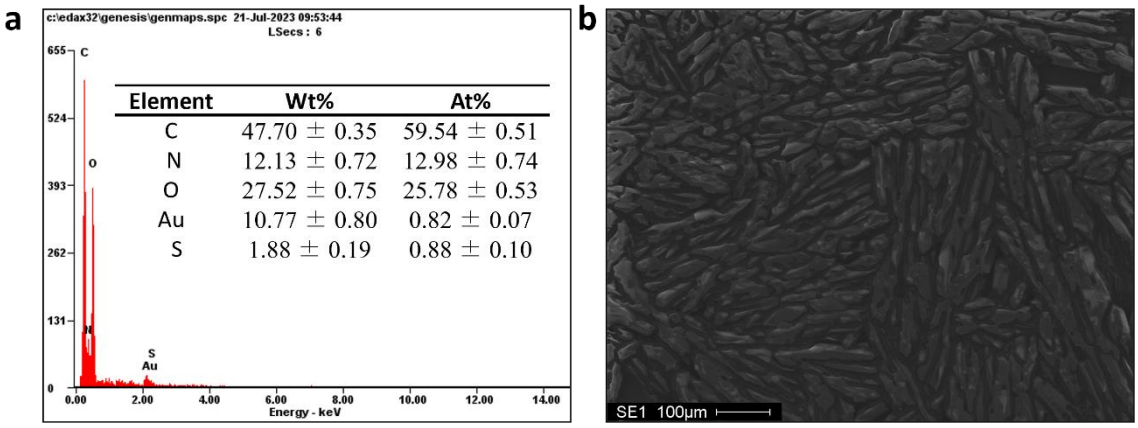

Figure 75. EDX of gel purified and dried GSSG-Au shows a ratio of Au : S equal to 0.82 : 0.88 or approximately 1 to 1, indicating that there are two Au atoms per GSSG molecule. (**a**) EDX result of GSSG-Au with an inset table showing the relative distribution of atoms in the complex. (**b**) SEM image of the dried GSSG-Au complex.

appeared to contain all the nanoparticles with no observable luminescence. When redissolving the pellet back into water, the sample was a dark yellow color and was still

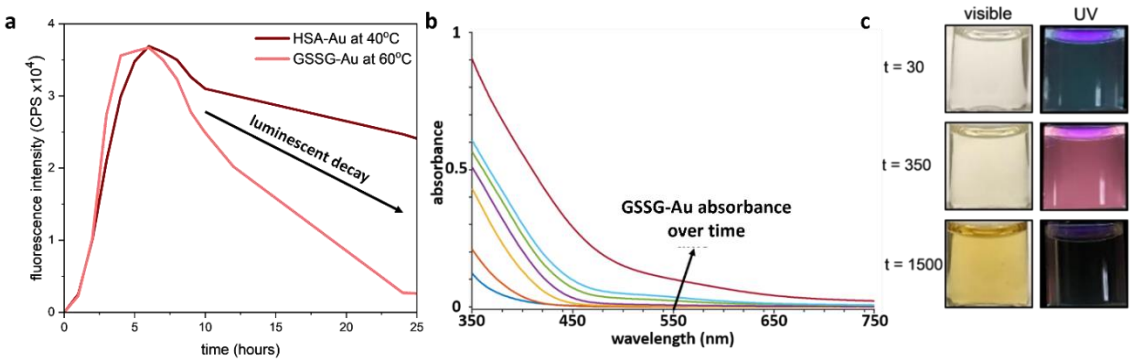

Figure 76. Time-course fluorescence and absorbance spectroscopy of HSA-Au and GSSG-Au. (a) Fluorescence spectra of HSA-Au and GSSG-Au over the course of 25 hours. After 5 hours peak luminescence intensity is observed and then immediately begins to decay. (b) Absorbance spectra of GSSG-Au show that at the same time, the general visible absorbance is slowly increasing. (c) Images of GSSG-Au solution at different times (in minutes) both under visible and under ultraviolet light. Under visible light the sample continues to darken while under ultraviolet light the sample reaches peak luminescence and then this luminescence decays.

non-luminescent when illuminated under ultraviolet light. This would indicate that the nanoparticles are not the source of luminescence, yet still appear to be a part of the overall reaction process. Thus, red luminescence in these solutions must be due to a distinct structure that is too small to be observed under TEM. In fact, using gel electrophoresis to differentiate GSSG-Au between the red luminescent complex and the nanoparticle red luminescence only occurs around the range of 1-2 kDa, suggesting that red luminescence within GSSG-Au is due only a couple Au atoms (**Figure 74**). These results are further supported by energy-dispersive X-ray spectroscopy (EDX). Where a sample of the gel-purified GSSG-Au (as shown in **Figure 74**) eluted from the gel and dried. The subsequent EDX result showed a ratio of sulfur to Au of 0.82 : 0.88, or around a ratio of 1 : 1 (**Figure 75**). This would indicate that there are two Au atoms per GSSG molecule and the complex has a mass around ~ 1.0 kDa, agreeing with the gel electrophoresis results of a ~1.1 kDa complex. Understanding of red luminescent complex formation, importantly relies on

understanding when the formation of nanoparticles occurs, and their overall role in the reaction.

When synthesizing the red luminescent complex solution at a constant temperature, it is expected that red luminescence would increase over time as the reaction proceeds and then stabilizes. Especially as all initial reactants are exhausted to form the red luminescent complex. This result is not the case, as once the reaction reaches a peak in red luminescence it begins to immediately decay (**Figure 76a**). Regardless of the starting temperature of the reaction in both HSA-Au and GSSG-Au, all samples will almost immediately undergo a loss in luminescence over time. This is also proportional to the temperature of the reaction (**Figure 77**). The loss in luminescence may be due to the formation of the non-luminescent nanoparticles.[178] Since the formation of nanoparticles leads to the formation of the dark yellow solution, the emergence of nanoparticles can be quantified using absorbance spectroscopy rather than fluorescence spectroscopy as with the red luminesce complex (**Figure 76**).

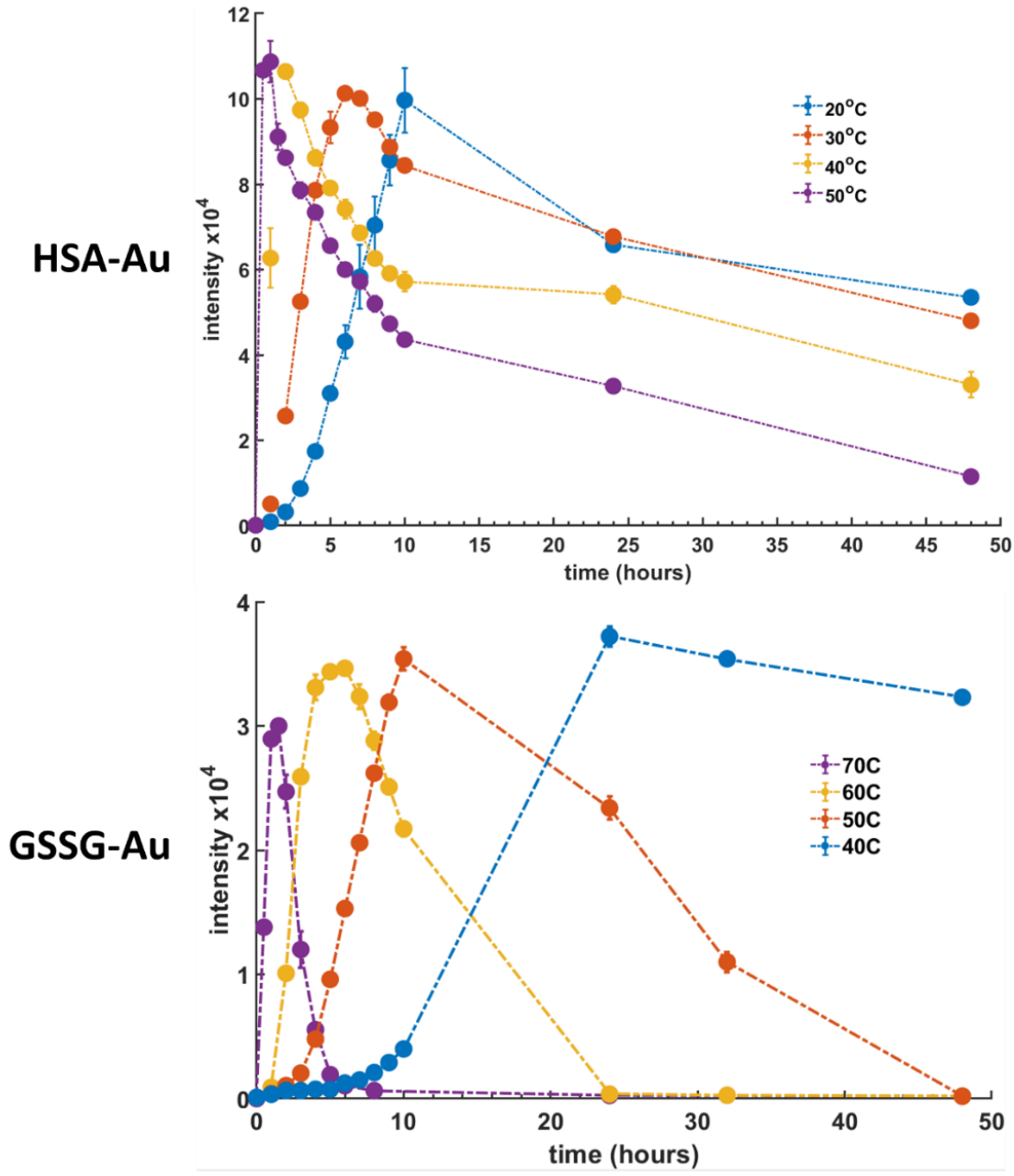

Figure 77. Temperature time-course fluorescence spectra of HSA-Au and GSSG-Au at various temperatures over the course of 48 hours. In every reaction, after red luminescence (measured at emission = 650 nm) peaks there is an immediate decay of the luminescence.

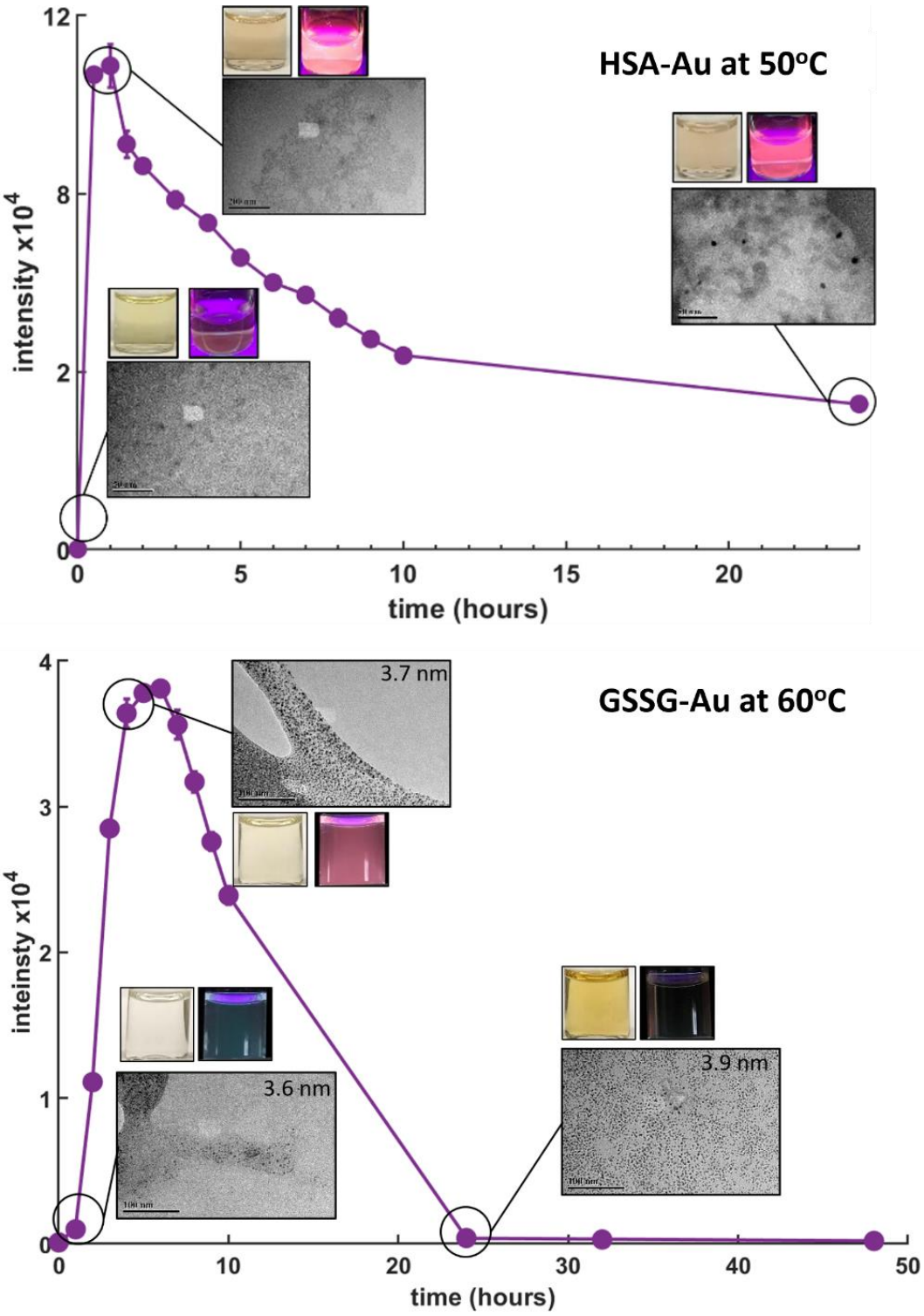

Figure 78. TEM time-course of HSA-Au and GSSG-Au both show the presence of nanoparticles as early as 30 minutes before red luminescence is even observed in the samples. As time progresses TEM continues to show the presence of nanoparticles while red luminescence peaks and then ultimately decays away.

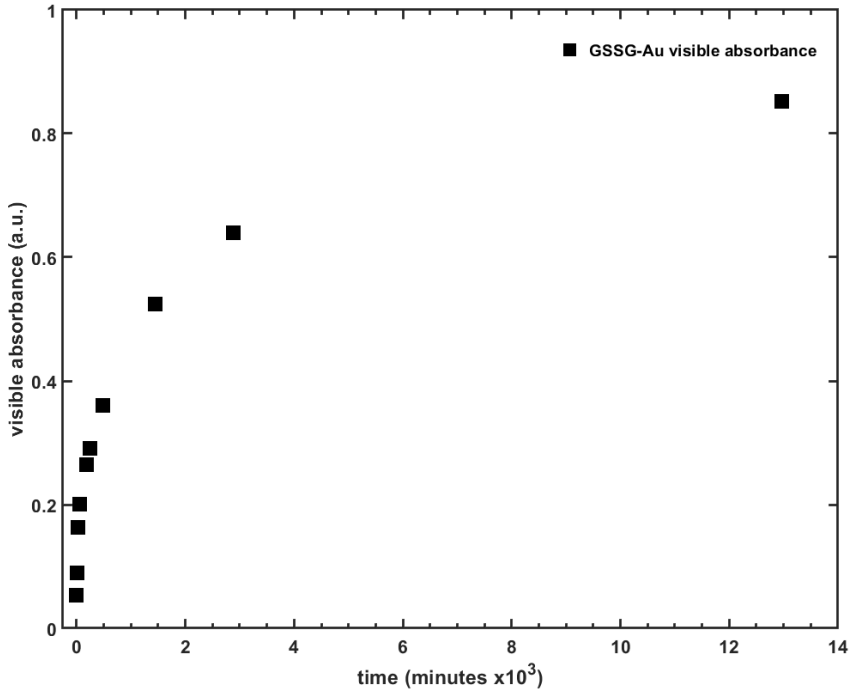

Figure 79. Using GSSG-Au the visible absorbance (averaging the absorbance between 350-800nm) over time can be tracked. This increase in visible absorbance can be related to the formation of nanoparticles.

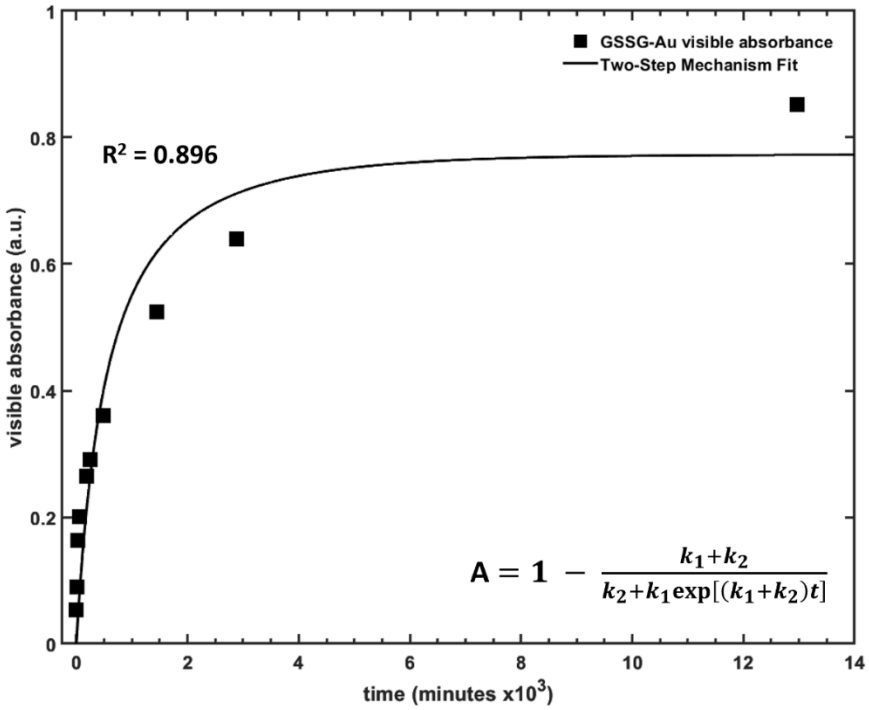

Figure 80. Fitting of the GSSG-Au absorbance data using the Finke-Watsky two-step model alone fits the data well in the short time regime but fails to encompass the entire time duration. Indicating that an additional correction term may be needed to fully predict the absorbance of the sample over time.

7.4 Using a Two-Step Mechanism to Describe Nanoparticle Formation

To understand the role of nanoparticles it is important to determine when nanoparticle formation begins alongside the formation of red luminescence. Additional time-course measurements of HSA-Au and GSSG-Au using TEM seems to show that nanoparticle formation occurs almost immediately upon the start of the reaction (**Figure 78**). This suggests that red luminescent complex formation as well as non-luminescent nanoparticle formation occurs simultaneously from the start of the reaction. Analyzing the temperature time-course data further in **Figure 76** also suggests that red luminescent complex formation may occur first followed by nanoparticle formation. Based on this, the time-course measurements appear to reveal two distinct phases kinetics, which could be attributed to two broad formation steps – one containing the formation of the very small red luminescent complex and the other containing the formation of the large non-red luminescent nanoparticles.

A multi-step process could be assumed to be the driving force for nanoparticle formation; assuming the formation of these nanoparticles comes about as a natural biproduct of the aggregation of the small red luminescent complexes. If the formation of nanoparticles is due to the aggregating of the luminescent complexes, then the overall reaction mechanism could be fit using a generalized, two-step mechanism.[179,180]

A commonly used and general two-step nucleation model for nanoparticle formation is the Finke-Watzky[181,182] (FW) nucleation model. This model begins with initial reactants which first form a single complex. In the next step, these complexes come together continuously and nucleate to form a larger aggregate, such as a nanoparticle.[181,182] In the first step of this reaction GSSG and Au first form the luminescent GSSG-Au

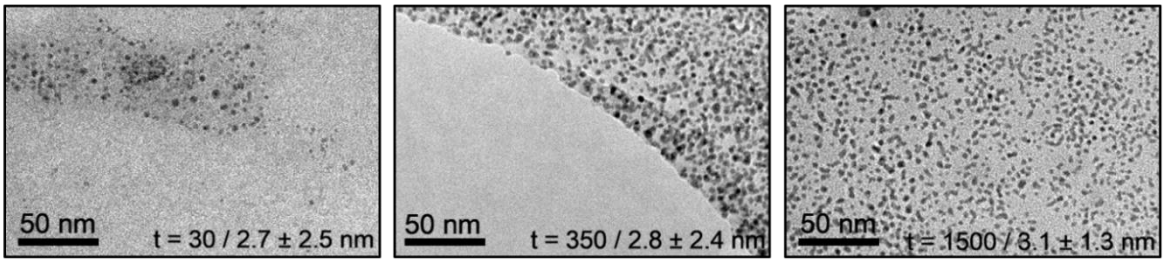

Figure 81. TEM time-course of GSSG-Au reacted at 60°C. After just 30 minutes with no red luminescence visible in solution there is still the formation of nanoparticles. At 350 minutes (5 hours), or peak luminescence intensity even more nanoparticles can be seen. Finally at 1500 minutes (25 hours) the sample is no longer visibly luminescent but contains the most amount of nanoparticles. As the reaction continues to progress TEM data shows that the size of the nanoparticles slowly increases, as well as the size distribution of nanoparticles decreases, indicating that Ostwald ripening has occurred.

complex. In the next step, multiple GSSG-Au complexes appear to aggregate over time, forming larger non-luminescent nanoparticles. Therefore, nucleation of nanoparticles could be fit by tracking the change in absorption over time, as an increase in absorption in the visible regime is equivalent to an increase in the number of nanoparticles (**Figure 79**). The stated two-step model that tracks those changes in absorption over time is given as follows:

$$[A]_t = 1 - \frac{k_1+k_2}{k_2+k_1\, exp[(k_1+k_2)t]} \quad (1)$$

where $[A]_t$ is the concentration of nanoparticles, k_1 (s^{-1}) is the rate of complex formation, k_2 (s^{-1}) is the rate of nanoparticle nucleation, and t (s) is time. Fitting of the absorption measurements with the two-step FW mechanism reveals an ideal fit in the short time regime of the total absorbance[181-184], but fails to encompass all time points, especially at later times (**Figure 80**). This makes it apparent that the addition of a secondary term in the equation is required to fit the absorptivity observed in the far time regime.

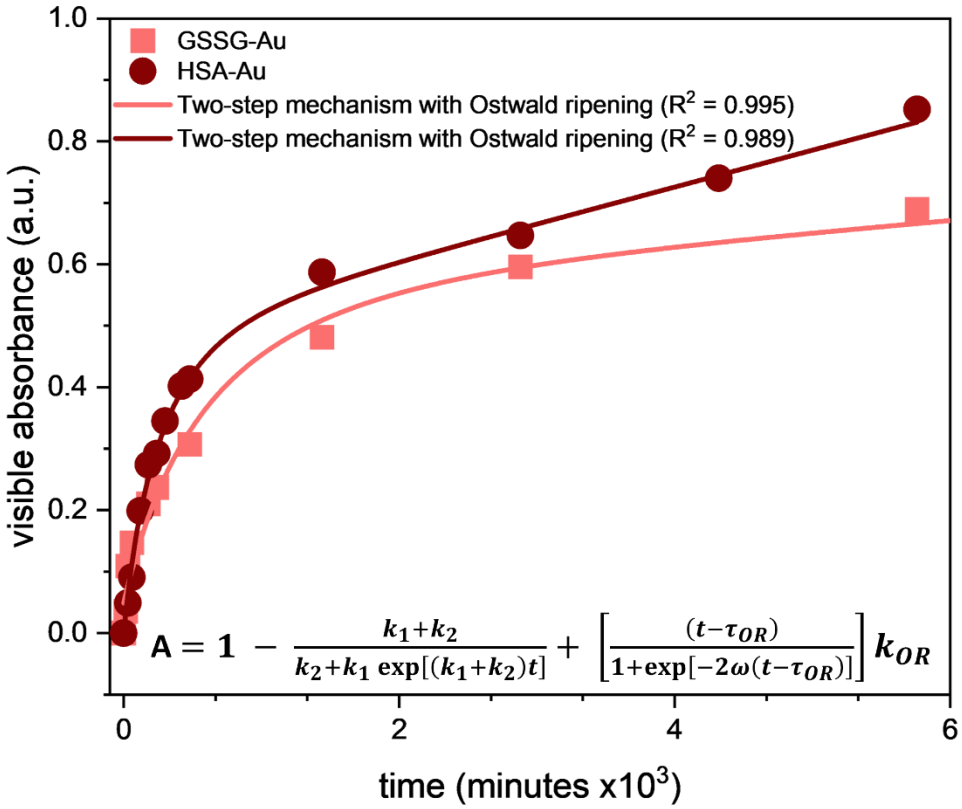

Figure 82. Averaged visible absorbance of HSA-Au and GSSG-Au over time fit with a Finke-Watsky two-step mechanism and corrected with an additional Ostwald ripening term. The use of the two-step model along with the addition of the Ostwald ripening term fits the data for both HSA-Au and GSSG-Au across all time points.

7.5 Ostwald Ripening Correction Factor to Fit Absorbance Data

Justification for this secondary term could be seen in the size and size narrowing of nanoparticles in TEM (**Figure 81**). An increase in size and size narrowing is a feature most found in nanoparticle synthesis reactions that undergo Ostwald ripening.[185-187] Ostwald ripening is a process that occurs after the initial formation of nanoparticles. In the first step of nanoparticle formation seeding occurs followed by the formation of small, less monodispersed nanoparticles. Finally, the size of nanoparticles increases as well as the monodispersity as smaller nanoparticles are absorbed by larger ones. Thus, the addition of a secondary modifying term to compensate for this Ostwald-ripening is required. Since

Ostwald ripening happens later in the reaction, this term will help to correct the absorption equation that can be used to fit the data at later time points.

$$[A]_t = 1 - \frac{k_1+k_2}{k_2+k_1\, exp[(k_1+k_2)t]} + \left[\frac{(t-\tau_{OR})}{1+exp\ [-2\omega(t-\tau_{OR})]}\right] k_{OR} \qquad (2)$$

Where τ_{OR} (s) is the activation time of Ostwald ripening, k_{OR} (s^{-1}) is the rate parameter for Ostwald ripening, and ω (s) is an arbitrary time-width to activate Ostwald ripening. The model almost ideally fits the observed absorptivity measurements across both short and long time ranges after the addition of this secondary correction term into the general two-step mechanism (**Figure 82**).[188] Applying the same procedure of tracking nanoparticle formation through absorbance spectra of HSA-Au yields the exact result where all time points are fit ideally.

Based on the absorption data, red luminescent complex formation appears to occur following a general two-step process, starting from reactants to a complex and finally to nanoparticles. This also appears to explain why others have reported alternative nanoparticle models to account for the red luminescent complex, since at peak luminescent intensity the small red luminescent complex and non-luminescent nanoparticle exist simultaneously.[165] While the two-step model generalizes the overall reaction that occurs from initial reactants to final products, the overall trend shows that nanoparticles are not the source of red luminescence and are in-fact the byproduct of multiple red luminescent complexes aggregating into larger structures.

7.6 Summarizing the Formation Mechanism of Nanoparticles in Protein-Au Complexes

We investigated the appearance of nanoparticles in these red luminescent complexes to determine their role in luminescence formation. Both HSA-Au and GSSG-Au appeared to form nanoparticles when left to react for a long period of time and were also red luminescent by the end of the process. Through separation of the sample via centrifugation it was determined that the nanoparticles in solution and the red luminescence in solution are not from the same source.

We were able to determine through large gel electrophoresis that the red luminescent complex must be around 1 kDa, not only significantly smaller than a 3 nm nanoparticle, but also smaller than a Au_{25} nanocluster. The formation of nanoparticles also appeared to influence the formation of red luminescence as time-course fluorescent line scans showed a decrease in red luminescence over time, regardless of the temperature of the reaction.

The longer the reaction proceeded the darker the sample appeared and this change in visible color over time can be directly quantified using absorbance spectroscopy. The total visible absorbance over time can be directed related to the formation of nanoparticles. Fitting of this absorbance data revealed that a two-step model was required to fit the change in absorbance over time. A further correction term to factor in the Ostwald ripening of nanoparticles resulted in an almost ideal fit of the data, suggesting that nanoparticle formation occurs after the formation of the red luminescent complex.

In summary, a new mechanism of nanoparticle formation has been proposed. The formation of nanoparticles occurs following a two-step mechanism wherein red luminescent HSA-Au and GSSG-Au complexes are converted into nanoparticles. These

results further support the evidence that the red luminescent complex is not a nanoparticle or nanocluster and that the existence of any nanoparticles in these samples is a result of secondary processes that occur after the formation of the red luminescent complex.

CHAPTER 8: DISCUSSION

Initial investigations into the red luminescent BSA-Au complex revealed that red luminescence was directly correlated to the pH of the surrounding solution.[13] Transformation of BSA from its natural conformational state to an extended, 'A-form' allowed for red luminescence to occur. Furthermore, cysteine residues, whether in their single cysteine thiol configuration or their Cys-Cys disulfide bond configuration, also appeared to play a role in luminescence formation.

In the single-site nucleating Au cluster theory, tyrosine and other aromatic residues are required to act as reducing agents to reduce Au^{+3} to Au^{0}.[12] This is likely not the primary mechanism for reduction, as red luminescence within BSA-Au can occur at pH values below 10, which is far below the reduction pH of tyrosine (pH ~11.5). While this mechanism for reduction is likely not the primary driver for the presence of Au^{0}, it could still be possible that tyrosine and other resides act to reduce Au.[189] Further reduction of the BSA-Au complex with $NaBH_4$ shows that not all Au is reduced within the protein or on the protein surface. If tyrosine and other residues were to be the source of Au reduction, the Au atoms would already need to be near the nucleation site and within the protein during the reduction process. From experimental evidence of the reaction kinetics of BSA-Au, Au appears to prefer random and non-specific binding throughout the protein, rather than single-site nucleation.

The importance of cystine residues as the nucleating site of the red luminescent complex agrees with our findings, as removal of all thiols lead to the red luminescence complex being unable to form.[1,13] As BSA is a large, 584 residue protein, with 35

individual cysteine residues, this leaves 35 potential binding locations for Au, and it is possible that more than one cysteine could be responsible for red luminescence when considering the existence of internal energy transfer pathways.[22,23] Excitation-emission spectra of the BSA-Au complex reveal these potential energy pathways. This could be the result of ligand field, ligand-to-metal charge transfer, or metal-to-ligand charge transfer.

Further investigations into the kinetics of the red luminescent BSA-Au complex, via gel electrophoresis, showed that a significant degree of nonspecific Au binding was occurring on the BSA surface. This was apparent by the smearing of gel bands and the existence of higher proportions of dimers, trimers, and N-mers of BSA.[1] The addition of Ni and Cu ions also appeared to produce the same results. Thus, non-specific, Langmuir-type, multiple-site binding model appears to be more likely over the alternative single-site nucleating model. While it was shown above that, theoretically, multiple-site adsorption appears to be more favorable in the context of the BSA-Au complex at temperatures at and above 298 K, it is still possible that single-site nucleation could be the mechanism for luminescent formation at lower temperatures. If this were the case, the rate of fluorescence increase should be strongly dependent on the concentration of Au. This dependence is not observed in the kinetic experiments performed on BSA-Au discussed in previous chapters.[75] Expanding these experiments in other proteins that are also red luminescent under similar conditions further supports the hypothesis that luminescence is not due to the single-site clustering of many Au.

Detailed kinetic experiments into red luminescent ovalbumin-Au, trypsin-Au, and insulin-Au showed identical kinetic results to those found in BSA-Au described in Chapter 3 and Chapter 4. When comparing the red luminescent properties of these four proteins, all

four showed the same charge transfer characteristics. These charge transfer characteristics from excitation-emission spectra indicate that red luminescence appears to be the result of ligand-to-metal or metal-to-ligand charge transfer.[190,191]

When comparing luminescence intensities of all protein-Au complexes, each complex appears to be similar in maximal intensity, yet the ratios at which this peak occurs are slightly different. In each case, the Langmuir-type, multiple-site adsorption model described in Chapter 3 and used for BSA-Au was still applicable. This model was able to accurately fit the increasing luminescence intensity curves for all proteins. The Langmuir-type multiple-site adsorption model does not explicitly prove that multiple-site adsorption is the mechanism of complex formation. In fact, it should be noted that this model only covers the range of luminescence where there is an increase in luminescence intensity. After a larger ratio of protein to Au is used, luminescence is gradually lost and the model no longer predicts high-concentration protein-Au complexes. The loss in luminescence is readily explained, and likely due to the formation of large non-emissive nanoparticles that form from the smaller luminescent complexes.[192]

These four proteins do indeed form the exact same complex yet there are a few slight differences, specifically when looking more in depth at the insulin-Au complex. The in-gel luminescence reveals that insulin-Au may require an insulin dimer to be red luminescent, while the others are luminescent in their monomer form. Insulin also undergoes a large conformational change at high pH, but no information is currently present describing the changes that occurred. Overall, the kinetics of luminophore formation are similar enough to include insulin-Au in the comparative analysis of all the proteins.

A study of each protein's structural characteristics was performed to find any commonalities between these proteins, after comparing their luminescent properties. Comparison of their three-dimensional crystal structures along with other red luminescent protein-Au complexes found in literature described potential common binding motifs centered around cystine. The determination of this common motif could be used to find other proteins that share these red luminescent properties. It is particularly important to note the limitations of this common motif study, as structural analysis was carried out on proteins under their native pH values and may not correlate directly to the high pH (≥10) values of the protein-Au complexes. Ideally, identification of a common motif would require the protein crystal structure of each protein in highly alkaline conditions. These results provide guidance to what is the likely motif that is responsible for red luminescence to occur. But the only way to determine if this common motif is accurate is to identify the single binding site responsible for red luminescence.

The binding domain of Au within protein was found first before determining the exact binding site. As described in Chapter 3 and Chapter 5, not only are cysteine residues important for the formation of red luminescence but an in-tact disulfide bond I also required for the formation of the red luminescent complex.[66,68] In the case of BSA and HSA, this means there are 17 possible binding locations for the red luminescent complex. Testing every binding site would ultimately be time consuming without first understanding the general region of the luminophore. Thus, creating two molecularly cloned domains is optimal, as it eliminates half of the potential binding sites. If both of the molecularly cloned domains were red luminescent, then this would indicate that multiple binding sites are in the protein or red luminescence is dependent on the entire structure. If neither cloned

domain is red luminescent then there would also be a dependence on the entire protein structure. Since it was found that only one domain was red luminescent, it can be assumed that luminescence is likely localized to only one or a few disulfide clusters in a small subdomain of the protein.

The synthesis of these molecularly cloned samples also required the addition of GST,[193] which itself shows red luminescent properties when interacting with Au on its own. This appears to conflict with evidence as GST does not contain any disulfide bonds, but disulfide bonds have been determined to be required for luminescence. Thus, the red luminescence of GST-Au may be a result of glutathione, which could be left behind in the protein and may not be due to a binding site specific to the protein itself. As the primary role of GST is to act to uptake excess glutathione in solution.[194,195] Most importantly, the addition of this GST tag was found to not influence the resulting luminescence of the HSA-Au interaction and displayed only minimal red luminescence. The peak luminescence intensity observed from GST alone was more than an order of magnitude below that of the control HSA-Au. This would indicate that the red luminescence observed in the molecularly cloned fragments are not due to GST in solution but are a result of the desired cloned HSA fragments. GST is also present in further single-site cloned experiments, but again appears to display minimal luminescence compared to the other cloned HSA fragments.

While it is of high importance to determine the exact binding location of Au within HSA, this does not reveal the overall structure, or the actual number of Au atoms bound around cystine. To fully elucidate the mechanism of formation, mechanism of luminescence, and number of Au atoms required for red luminescence, a smaller sized

protein with these luminescent properties is required. Unfortunately, the smallest known red luminescing protein-Au complex is insulin-Au at 6 kDa in size. Thus, techniques involving NMR, mass spectrometry, FT-IR, or XPS are difficult given the large protein size. Since there is a significant interference from the large number of additional amino acids within the protein that do not play a role in complex formation. Due to this interference, a small molecule found to display all the similar red luminescent properties and kinetics was required for more in-depth analysis into the mechanism and structure. This small molecule was found to be oxidized glutathione, which is only a 0.6 kDa compound, an order of magnitude smaller than insulin, and contains 6 total amino acids. By studying GSSG and GSSG-Au, techniques that may have been unavailable, can now be used to determine the structure and number of Au atoms more accurately.

GSSG allowed for the determination of the number of Au bound to the disulfide, mechanism of complex formation, and further information on the mechanism of luminescence. While GSSG-Au allowed for a greater understanding of the red luminescent protein-Au complexes, the overall Au bonds made with GSSG have not been determined and the exact mechanism of luminescence is only confirmed through further experiments such as fluorescence excitation-emission spectra, TCSPC, and TAS. It should be noted that to fully understand the luminescent complex within protein-Au systems, the crystal structure of these protein-Au's would need to be resolved.

Currently, the crystal structure of GSSG-Au alone has yet to be resolved. The mechanism of complex formation appears to follow a general model of a two-step mechanism, but that does not explicitly indicate that only two steps are involved.[181,182] More than likely there are numerous sub-steps that can be categorized together in each

primary step of the reaction including reactants, complex, and nanoparticle. Revealing the structure and mechanism of formation within GSSG-Au is a large step in understanding the current red luminescent protein-Au complexes that have already been discovered. Resolving of the overall complex could also aid in finding other unknown red luminescent proteins by more precisely revealing the common motif that allows for currently known proteins to be red luminescent.

CHAPTER 9: CONCLUSIONS

Overall, these observations provide strong evidence that the red luminescence observed in protein-Au systems is likely due to a small Au-bound-thiol complex, alternative to single-site nucleation models suggested by numerous others. Initially, red luminescence in BSA-Au was proposed to be due to the nucleation of a Au_{25} nanocluster bound to a single site within the protein.[12] Gold was assumed to be reduced from Au^{3+} to Au^{0} via reduction by surrounding amino acid residues. The mechanism of the red luminescence was based solely on the Jellium model of gold nanoclusters, which states that Au nanoclusters of small size (<50 atoms in size) are fluorescent in the visible regime (where more atoms in the nanocluster correspond to further red-shifted emissions).[196,197]

In the findings described above, BSA-Au appeared to be red luminescent due to a small Au-bound-thiolate and not luminescent via a small Au_{25} nanocluster. This is based on the evidence that BSA-Au luminescence is correlated to a pH-induced conformational change in the protein and occurs at pH values too low for amino acid reduction to take place.[13] Furthermore, red luminescence appeared to be the result of a transition of internal luminescence within BSA from blue to red. Continued studies into BSA-Au, HSA-Au, other protein-Au complexes, as well as GSSG-Au further confirms these initial findings that luminescence is not due to a single nanocluster.

Detailed studies into the kinetics of red luminescent BSA-Au revealed that a Langmuir-type, multiple-site adsorption model for the formation of the BSA−Au complex more accurately described the luminescent complex. This is compared to the LaMer-type model of a single-site nucleating nanocluster.[1] The kinetics of the red fluorophore

formation in the BSA−Au complex was measured under different reaction conditions, including pH, temperature, and BSA-to-Au ratio. The results were consistent with the Langmuir-type adsorption model, in which Au binds specifically to (i) the fluorophore-forming Cys−Cys disulfide bond site, (ii) the free thiol of Cys34, (iii) the Asp fragment of BSA, and (iv) nonspecifically to many surface sites via van der Waals interaction.

Examination of other red luminescent protein-Au complexes detailed in literature, including ovalbumin-Au, trypsin-Au, and insulin-Au, revealed the same fluorescence excitation emission spectra, which showed a potential cascaded energy transfer mechanism.[66] On top of this, the kinetics of all the other luminescent protein-Au complexes were identical and could be fit using the same multiple-site adsorption model. All these proteins are vastly different in size, shape, and functionality, yet they all produced the same luminescent complex. Further structural analysis of these proteins revealed that it was more than primary protein structures, but tertiary protein structures that were important for red luminescence formation. The structural analysis revealed that at least one unobstructed aromatic residue was found in each of the red luminescent proteins and was absent in the non-luminescent proteins. These proteins necessitated the presence of cysteine for the red luminescence and the kinetics could be all consistently described.

Determining the exact cystine that was necessary in the formation of the red luminescent complex protein required molecular cloning of HSA, performed along with limited tryptic digestion. HSA was molecularly cloned into two fragments and it was found that only one fragment containing amino acids 1-313 was necessary for the complex to form. Further tryptic digestion of BSA revealed only amino acids 117-313 may be necessary for complex formation. This fragment also only contained 9 of the 17 total Cys-

Cys disulfides, allowing for an optimal narrowing of the binding site(s) of Au. More refined molecular cloning of the GST-[HSA_{1-313}] fragment targeting single cysteine amino acid sites allowed for the identification of the single site responsible for red luminescence. The site of red luminescence was identified to be the cysteine disulfide of Cys278-Cys289 and was determined using molecular cloning techniques of HSA.

To gain a deeper understanding about the red luminescent complex, GSSG-Au was synthesized instead of protein-Au as it is significantly smaller than any protein-Au complex and is also similarly red luminescent. Analysis of GSSG-Au revealed luminescence did not result from nanocluster formation and followed a general two-step mechanism which produces both red luminescent complexes and non-luminescent nanoparticles. NMR, FT-IR, and XPS analysis also revealed that neutral Au is bound directly to the intact disulfide of GSSG. Mass spectroscopy, gel electrophoresis, and EDX all indicated that only two Au atoms are bound, revealing the final complex to be $GSSG+2Au^0$. Additional TCSPC data of purified GSSG-Au supports the fluorescent excitation-emission spectra that a LMCT/MLCT mechanism is responsible for red luminescence, though the dynamics of this mechanism are still being resolved.

These studies reveal the complex within red luminescent protein-Au systems are not nanoclusters, but are small, Au-bound disulfide complexes. These findings allow for a more transparent use of this complex in its proposed nanoscale applications, such as sensing, imaging, and detecting or as a new generation of fluorescent tags with a large stokes shift. Elucidation of the structure and mechanism of the luminophore as well as a common binding motif may lead to the discovery of other luminescent protein-Au

complexes and making this unique complex a more versatile and widely used organic fluorophore.

REFERENCES

1 Dixon, J. M. & Egusa, S. Kinetics of Fluorophore Formation in Bovine Serum Albumin-Gold Complexes. *Journal of Physical Chemistry C* **123**, 10094-10100 (2019). https://doi.org:10.1021/acs.jpcc.9b00413

2 Digiacomo, L., Pozzi, D., Palchetti, S., Zingoni, A. & Caracciolo, G. Impact of the protein corona on nanomaterial immune response and targeting ability. *Wiley Interdisciplinary Reviews-Nanomedicine and Nanobiotechnology* **12** (2020). https://doi.org:10.1002/wnan.1615

3 Yu, X. *et al.* Assembly of Protein Cages for Drug Delivery. *Pharmaceutics* **14** (2022). https://doi.org:10.3390/pharmaceutics14122609

4 Estrada, L. P. H. & Champion, J. A. Protein nanoparticles for therapeutic protein delivery. *Biomaterials Science* **3**, 787-799 (2015). https://doi.org:10.1039/c5bm00052a

5 Tsien, R. Y. The green fluorescent protein. *Annual Review of Biochemistry* **67**, 509-544 (1998). https://doi.org:10.1146/annurev.biochem.67.1.509

6 Chalfie, M., Tu, Y., Euskirchen, G., Ward, W. W. & Prasher, D. C. GREEN FLUORESCENT PROTEIN AS A MARKER FOR GENE-EXPRESSION. *Science* **263**, 802-805 (1994). https://doi.org:10.1126/science.8303295

7 Chudakov, D. M., Matz, M. V., Lukyanov, S. & Lukyanov, K. A. Fluorescent Proteins and Their Applications in Imaging Living Cells and Tissues. *Physiological Reviews* **90**, 1103-1163 (2010). https://doi.org:10.1152/physrev.00038.2009

8 Lambert, T. J. FPbase: a community-editable fluorescent protein database. *Nature Methods* **16**, 277-278 (2019). https://doi.org:10.1038/s41592-019-0352-8

9 Hudson, D. E., Hudson, D. O., Wininger, J. M. & Richardson, B. D. Penetration of Laser Light at 808 and 980nm in Bovine Tissue Samples. *Photomedicine and Laser Surgery* **31**, 163-168 (2013). https://doi.org:10.1089/pho.2012.3284

10 Santos, E. M. *et al.* Design of Large Stokes Shift Fluorescent Proteins Based on Excited State Proton Transfer of an Engineered Photobase. *Journal of the American Chemical Society* **143**, 15091-15102 (2021). https://doi.org:10.1021/jacs.1c05039

1 Dixon, J. M. & Egusa, S. Kinetics of Fluorophore Formation in Bovine Serum Albumin-Gold Complexes. *Journal of Physical Chemistry C* **123**, 10094-10100 (2019). https://doi.org:10.1021/acs.jpcc.9b00413

2 Alberts, B. *et al. Essential cell biology: An introduction to the molecular biology of the cell*. (1998).

3 Murray, C. B., Kagan, C. R. & Bawendi, M. G. Synthesis and characterization of monodisperse nanocrystals and close-packed nanocrystal assemblies. *Annual Review of Materials Science* **30**, 545-610 (2000). https://doi.org:10.1146/annurev.matsci.30.1.545

4 Witus, L. S. & Francis, M. B. Using Synthetically Modified Proteins to Make New Materials. *Accounts of Chemical Research* **44**, 774-783 (2011). https://doi.org:10.1021/ar2001292

5 Brodin, J. D. *et al.* Metal-directed, chemically tunable assembly of one-, two- and three-dimensional crystalline protein arrays. *Nature Chemistry* **4**, 375-382 (2012). https://doi.org:10.1038/nchem.1290

6 Matthaei, J. F. *et al.* Designing Two-Dimensional Protein Arrays through Fusion of Multimers and Interface Mutations. *Nano Letters* **15**, 5235-5239 (2015). https://doi.org:10.1021/acs.nanolett.5b01499

7 Gekle, M. Renal tubule albumin transport. *Annual Review of Physiology* **67**, 573-594 (2005). https://doi.org:10.1146/annurev.physiol.67.031103.154845

8 Moriya, M. *et al.* Copper is taken up efficiently from albumin and alpha(2)-macroglobulin by cultured human cells by more than one mechanism. *American Journal of Physiology-Cell Physiology* **295**, C708-C721 (2008). https://doi.org:10.1152/ajpcell.00029.2008

9 Glennon, J. D. & Sarkar, B. NICKEL(II) TRANSPORT IN HUMAN-BLOOD SERUM - STUDIES OF NICKEL(II) BINDING TO HUMAN-ALBUMIN AND TO NATIVE-SEQUENCE PEPTIDE, AND TERNARY-COMPLEX FORMATION WITH L-HISTIDINE. *Biochemical Journal* **203**, 15-23 (1982). https://doi.org:10.1042/bj2030015

10 Hurrell, R. F., Lynch, S. R., Trinidad, T. P., Dassenko, S. A. & Cook, J. D. IRON-ABSORPTION IN HUMANS - BOVINE SERUM-ALBUMIN COMPARED WITH BEEF MUSCLE AND EGG-WHITE. *American Journal of Clinical Nutrition* **47**, 102-107 (1988). https://doi.org:10.1093/ajcn/47.1.102

11 Bal, W., Sokolowska, M., Kurowska, E. & Faller, P. Binding of transition metal ions to albumin: Sites, affinities and rates. *Biochimica Et Biophysica Acta-General Subjects* **1830**, 5444-5455 (2013). https://doi.org:10.1016/j.bbagen.2013.06.018

12 Xie, J. P., Zheng, Y. G. & Ying, J. Y. Protein-Directed Synthesis of Highly Fluorescent Gold Nanoclusters. *Journal of the American Chemical Society* **131**, 888-+ (2009). https://doi.org:10.1021/ja806804u

13 Dixon, J. M. & Egusa, S. Conformational Change-Induced Fluorescence of Bovine Serum Albumin-Gold Complexes. *Journal of the American Chemical Society* **140**, 2265-2271 (2018). https://doi.org:10.1021/jacs.7b11712

14 Zhong, K., Hao, C., Liu, H., Yang, H. & Sun, R. Synthesis of dual-emissive ratiometric probe of BSA-Au NCs and BSA-Cu NCs and their sensitive and selective detection of copper and mercury ions. *Journal of Photochemistry and Photobiology a-Chemistry* **408** (2021). https://doi.org:10.1016/j.jphotochem.2020.113100

15 Ding, S.-N. & Guo, Y.-X. One-pot synthesis of dual-emitting BSA-Pt-Au bimetallic nanoclusters for fluorescence ratiometric detection of mercury ions and cysteine. *Analytical Methods* **7**, 5787-5793 (2015). https://doi.org:10.1039/c5ay01112d

16 Zu, L., Liu, L., Qin, Y., Liu, H. & Yang, H. Multifunctional BSA-Au nanostars for photoacoustic imaging and X-ray computed tomography. *Nanomedicine-Nanotechnology Biology and Medicine* **12**, 1805-1813 (2016). https://doi.org:10.1016/j.nano.2016.05.003

17 Zhao, W. *et al.* A biomimetic Au@BSA-DTA nanocomposites-based contrast agent for computed tomography imaging. *Materials Science & Engineering C-Materials for Biological Applications* **78**, 565-570 (2017). https://doi.org:10.1016/j.msec.2017.04.127

18 Huang, X. H., Jain, P. K., El-Sayed, I. H. & El-Sayed, M. A. Gold nanoparticles: interesting optical properties and recent applications in cancer diagnostic and therapy. *Nanomedicine* **2**, 681-693 (2007). https://doi.org:10.2217/17435889.2.5.681

19 Doane, T. L. & Burda, C. The unique role of nanoparticles in nanomedicine: imaging, drug delivery and therapy. *Chemical Society Reviews* **41**, 2885-2911 (2012). https://doi.org:10.1039/c2cs15260f

20 Egusa, S., Ebrahem, Q., Mahfouz, R. Z. & Saunthararajah, Y. Ligand exchange on gold nanoparticles for drug delivery and enhanced therapeutic index evaluated in acute myeloid leukemia models. *Experimental Biology and Medicine* **239**, 853-861 (2014). https://doi.org:10.1177/1535370214536648

21 Khullar, P. *et al.* Bovine Serum Albumin Bioconjugated Gold Nanoparticles: Synthesis, Hemolysis, and Cytotoxicity toward Cancer Cell Lines. *Journal of Physical Chemistry C* **116**, 8834-8843 (2012). https://doi.org:10.1021/jp300585d

22 Chevrier, D. M. *et al.* Structure and formation of highly luminescent protein-stabilized gold clusters. *Chemical Science* **9**, 2782-2790 (2018). https://doi.org:10.1039/c7sc05086k

23 Russell, B. A., Jachimska, B., Kralka, I., Mulheran, P. A. & Chen, Y. Human serum albumin encapsulated gold nanoclusters: effects of cluster synthesis on natural protein characteristics. *Journal of Materials Chemistry B* **4**, 6876-6882 (2016). https://doi.org:10.1039/c6tb01827k

24 Russell, B. A., Kubiak-Ossowska, K., Mulheran, P. A., Birch, D. J. S. & Chen, Y. Locating the nucleation sites for protein encapsulated gold nanoclusters: a molecular dynamics and fluorescence study. *Physical Chemistry Chemical Physics* **17**, 21935-21941 (2015). https://doi.org:10.1039/c5cp02380g

25 de Chermont, Q. l. M. *et al.* Nanoprobes with near-infrared persistent luminescence for in vivo imaging. *Proceedings of the National Academy of Sciences of the United States of America* **104**, 9266-9271 (2007). https://doi.org:10.1073/pnas.0702427104

26 Wei, H. *et al.* Lysozyme-stabilized gold fluorescent cluster: Synthesis and application as Hg2+ sensor. *Analyst* **135**, 1406-1410 (2010). https://doi.org:10.1039/c0an00046a

27 Kawasaki, H., Hamaguchi, K., Osaka, I. & Arakawa, R. ph-Dependent Synthesis of Pepsin-Mediated Gold Nanoclusters with Blue Green and Red Fluorescent Emission. *Advanced Functional Materials* **21**, 3508-3515 (2011). https://doi.org:10.1002/adfm.201100886

28 Kawasaki, H., Yoshimura, K., Hamaguchi, K. & Arakawa, R. Trypsin-Stabilized Fluorescent Gold Nanocluster for Sensitive and Selective Hg2+ Detection. *Analytical Sciences* **27**, 591-596 (2011). https://doi.org:10.2116/analsci.27.591

29 Liu, C.-L. *et al.* Insulin-Directed Synthesis of Fluorescent Gold Nanoclusters: Preservation of Insulin Bioactivity and Versatility in Cell Imaging. *Angewandte Chemie-International Edition* **50**, 7056-7060 (2011). https://doi.org:10.1002/anie.201100299

30 Wen, F. *et al.* Horseradish Peroxidase Functionalized Fluorescent Gold Nanoclusters for Hydrogen Peroxide Sensing. *Analytical Chemistry* **83**, 1193-1196 (2011). https://doi.org:10.1021/ac1031447

31 Jr., T. P. Serum Albumin. *Advances in Protein Chemistry* **37**, 161-245 (1985).

32 Jr., T. P. *All About Albumin*. (Academic Press, 1996).

33 Majorek, K. A. *et al.* Structural and immunologic characterization of bovine, horse, and rabbit serum albumins. *Molecular Immunology* **52**, 174-182 (2012). https://doi.org:10.1016/j.molimm.2012.05.011

34 Cui, M. L., Zhao, Y. & Song, Q. J. Synthesis, optical properties and applications of ultra-small luminescent gold nanoclusters. *Trac-Trends in Analytical Chemistry* **57**, 73-82 (2014). https://doi.org:10.1016/j.trac.2014.02.005

35 Saha, K., Agasti, S. S., Kim, C., Li, X. N. & Rotello, V. M. Gold Nanoparticles in Chemical and Biological Sensing. *Chemical Reviews* **112**, 2739-2779 (2012). https://doi.org:10.1021/cr2001178

36 Zhang, Y. C. *et al.* New Gold Nanostructures for Sensor Applications: A Review. *Materials* **7**, 5169-5201 (2014). https://doi.org:10.3390/ma7075169

37 Chen, L. Y., Wang, C. W., Yuan, Z. Q. & Chang, H. T. Fluorescent Gold Nanoclusters: Recent Advances in Sensing and Imaging. *Analytical Chemistry* **87**, 216-229 (2015). https://doi.org:10.1021/ac503636j

38 Aswathy, B. & Sony, G. Cu2+ modulated BSA-Au nanoclusters: A versatile fluorescence turn-on sensor for dopamine. *Microchemical Journal* **116**, 151-156 (2014). https://doi.org:10.1016/j.microc.2014.04.016

39 Akshath, U. S., Bhatt, P. & Singh, S. A. Differential Interaction of Metal Ions with Gold Nanoclusters and Application in Detection of Cobalt and Cadmium. *Journal of Fluorescence* **30**, 537-545 (2020). https://doi.org:10.1007/s10895-020-02509-y

40 Guan, R. *et al.* Selective determination of Ag(+)in the presence of Cd2+, Hg(2+)and Cu(2+)based on their different interactions with gold nanoclusters. *Rsc Advances* **10**, 33299-33306 (2020). https://doi.org:10.1039/d0ra05787h

41 Cai, W., Gao, T., Hong, H. & Sun, J. Applications of gold nanoparticles in cancer nanotechnology. *Nanotechnology, science and applications* **1**, 17-32 (2008). https://doi.org:10.2147/nsa.S3788

42 Nune, S. K. *et al.* Nanoparticles for biomedical imaging. *Expert Opinion on Drug Delivery* **6**, 1175-1194 (2009). https://doi.org:10.1517/17425240903229031

43 Dorsey, J. F. *et al.* Gold nanoparticles in radiation research: potential applications for imaging and radiosensitization. *Translational Cancer Research* **2**, 280-291 (2013). https://doi.org:10.3978/j.issn.2218-676X.2013.08.09

44 Daniel, M. C. & Astruc, D. Gold nanoparticles: Assembly, supramolecular chemistry, quantum-size-related properties, and applications toward biology, catalysis, and nanotechnology. *Chemical Reviews* **104**, 293-346 (2004). https://doi.org:10.1021/cr030698+

45 Ferrari, M. Cancer nanotechnology: Opportunities and challenges. *Nature Reviews Cancer* **5**, 161-171 (2005). https://doi.org:10.1038/nrc1566

46 Arvizo, R., Bhattacharya, R. & Mukherjee, P. Gold nanoparticles: opportunities and challenges in nanomedicine. *Expert Opinion on Drug Delivery* **7**, 753-763 (2010). https://doi.org:10.1517/17425241003777010

47 Kang, X., Chong, H. B. & Zhu, M. Z. Au-25(SR)(18): the captain of the great nanocluster ship. *Nanoscale* **10**, 10758-10834 (2018). https://doi.org:10.1039/c8nr02973c

48 Zheng, J., Nicovich, P. R. & Dickson, R. M. Highly fluorescent noble-metal quantum dots. *Annual Review of Physical Chemistry* **58**, 409-431 (2007). https://doi.org:10.1146/annurev.physchem.58.032806.104546

49 Le Guevel, X. *et al.* Formation of Fluorescent Metal (Au, Ag) Nanoclusters Capped in Bovine Serum Albumin Followed by Fluorescence and Spectroscopy. *Journal of Physical Chemistry C* **115**, 10955-10963 (2011). https://doi.org:10.1021/jp111820b

50 Tong, J.-Q. *et al.* Probing the adverse temperature dependence in the static fluorescence quenching of BSA induced by a novel anticancer hydrazone. *Photochemical & Photobiological Sciences* **11**, 1868-1879 (2012). https://doi.org:10.1039/c2pp25162k

51 Lakatos, B., Szentmihalyi, K., Vinkler, P., Balla, J. & Balla, G. The role of essential metal ions in the human organism and their oral supplementation to the human body in deficiency states. *Orvosi Hetilap* **145**, 1315-1319 (2004).

52 Klotz, I. M. & Curme, H. G. THE THERMODYNAMICS OF METALLO-PROTEIN COMBINATIONS - COPPER WITH BOVINE SERUM ALBUMIN. *Journal of the American Chemical Society* **70**, 939-943 (1948). https://doi.org:10.1021/ja01183a015

53 Fiess, H. A. & Klotz, I. M. THE THERMODYNAMICS OF METALLO PROTEIN COMBINATIONS - COMPARISON OF COPPER COMPLEXES WITH NATURAL

PROTEINS. *Journal of the American Chemical Society* **74**, 887-891 (1952). https://doi.org:10.1021/ja01124a008

54 Liu, Y., Xia, H. & Rong, D. in *2nd International Conference on Chemical Engineering and Advanced Materials (CEAM 2012).* 1831-1834 (2012).

55 Saito, M. *et al.* Molecular Mechanisms of Nickel Allergy. *International Journal of Molecular Sciences* **17** (2016). https://doi.org:10.3390/ijms17020202

56 Patel, S. U., Sadler, P. J., Tucker, A. & Viles, J. H. Direct detection of albumin in human blood plasma by proton NMR spectroscopy. Complexation of nickel2+. *Journal of the American Chemical Society* **115**, 9285-9286 (1993). https://doi.org:10.1021/ja00073a053

57 Carter, E. L., Flugga, N., Boer, J. L., Mulrooney, S. B. & Hausinger, R. P. Interplay of metal ions and urease. *Metallomics* **1**, 207-221 (2009). https://doi.org:10.1039/b903311d

58 Mothes, E. & Faller, P. Evidence that the principal Co-II-binding site in human serum albumin is not at the N-terminus: Implication on the albumin cobalt binding test for detecting myocardial ischemia. *Biochemistry* **46**, 2267-2274 (2007). https://doi.org:10.1021/bi061783p

59 Sokolowska, M., Wszelaka-Rylik, M., Poznanski, J. & Bal, W. Spectroscopic and thermodynamic determination of three distinct binding sites for Co(II) ions in human serum albumin. *Journal of Inorganic Biochemistry* **103**, 1005-1013 (2009). https://doi.org:10.1016/j.jinorgbio.2009.04.011

60 Stewart, A. J., Blindauer, C. A., Berezenko, S., Sleep, D. & Sadler, P. J. Interdomain zinc site on human albumin. *Proceedings of the National Academy of Sciences of the United States of America* **100**, 3701-3706 (2003). https://doi.org:10.1073/pnas.0436576100

61 Bal, W., Christodoulou, J., Sadler, P. J. & Tucker, A. Multi-metal binding site of serum albumin. *Journal of Inorganic Biochemistry* **70**, 33-39 (1998). https://doi.org:10.1016/s0162-0134(98)00010-5

62 Sheftel, A. D., Mason, A. B. & Ponka, P. The long history of iron in the Universe and in health and disease. *Biochimica Et Biophysica Acta-General Subjects* **1820**, 161-187 (2012). https://doi.org:10.1016/j.bbagen.2011.08.002

63 McKie, A. T. *et al.* A novel duodenal iron-regulated transporter, IREG1, implicated in the basolateral transfer of iron to the circulation. *Molecular Cell* **5**, 299-309 (2000). https://doi.org:10.1016/s1097-2765(00)80425-6

64 Silva, A. M. N. & Hider, R. C. Influence of non-enzymatic post-translation modifications on the ability of human serum albumin to bind iron Implications for non-transferrin-bound iron speciation. *Biochimica Et Biophysica Acta-Proteins and Proteomics* **1794**, 1449-1458 (2009). https://doi.org:10.1016/j.bbapap.2009.06.003

65 Shi, H., Ou, M. Y., Cao, J. P. & Chen, G. F. Synthesis of ovalbumin-stabilized highly fluorescent gold nanoclusters and their application as an Hg2+ sensor. *Rsc Advances* **5**, 86740-86745 (2015). https://doi.org:10.1039/c5ra15559b

66 Dixon, J. M., Tomida, J. & Egusa, S. Identifying the Red-Luminophore-Forming Domain in Serum Albumin-Gold Complexes. *Journal of Physical Chemistry Letters* **11**, 3345-3349 (2020). https://doi.org:10.1021/acs.jpclett.0c00805

67 Toseland, C. P. Fluorescent labeling and modification of proteins. *Journal of chemical biology* **6**, 85-95 (2013). https://doi.org:10.1007/s12154-013-0094-5

68 Dixon, J. M. & Egusa, S. Limited Proteolysis and Gel Electrophoresis in the Presence of Metal Cations: Au(III)-binding Luminescent Domain in Serum Albumins. *Journal of visualized experiments : JoVE* (2021). https://doi.org:10.3791/61905

69 Saha, K., Agasti, S. S., Kim, C., Li, X. & Rotello, V. M. Gold Nanoparticles in Chemical and Biological Sensing. *Chemical Reviews* **112**, 2739-2779 (2012). https://doi.org:10.1021/cr2001178

70 Zhang, Y. *et al.* New Gold Nanostructures for Sensor Applications: A Review. *Materials* **7**, 5169-5201 (2014). https://doi.org:10.3390/ma7075169

71 Qu, X. *et al.* Fluorescent Gold Nanoclusters: Synthesis and Recent Biological Application. *Journal of Nanomaterials* **2015** (2015). https://doi.org:10.1155/2015/784097

72 Sadler, P. J. & Tucker, A. PH-INDUCED STRUCTURAL TRANSITIONS OF BOVINE SERUM-ALBUMIN - HISTIDINE PKA VALUES AND UNFOLDING OF THE N-TERMINUS DURING THE N TO F TRANSITION. *European Journal of Biochemistry* **212**, 811-817 (1993). https://doi.org:10.1111/j.1432-1033.1993.tb17722.x

73 Zhang, Y. & Wilcox, D. E. Thermodynamic and spectroscopic study of Cu(II) and Ni(II) binding to bovine serum albumin. *Journal of Biological Inorganic Chemistry* **7**, 327-337 (2002). https://doi.org:10.1007/s00775-001-0302-6

74 Narasinga Rao, M. S. A Study of the Interaction of Nickel(II) with Bovine Serum Albumin. *Journal of the American Chemical Society* **84**, 1788-1790 (1962). https://doi.org:10.1021/ja00869a003

75 Lamer, V. K. & Dinegar, R. H. THEORY, PRODUCTION AND MECHANISM OF FORMATION OF MONODISPERSED HYDROSOLS. *Journal of the American Chemical Society* **72**, 4847-4854 (1950). https://doi.org:10.1021/ja01167a001

76 Lamer, V. K. NUCLEATION IN PHASE TRANSITIONS. *Industrial and Engineering Chemistry* **44**, 1270-1277 (1952).

77 Sugimoto, T., Shiba, F., Sekiguchi, T. & Itoh, H. Spontaneous nucleation of monodisperse silver halide particles from homogeneous gelatin solution I: silver chloride. *Colloids and Surfaces a-Physicochemical and Engineering Aspects* **164**, 183-203 (2000). https://doi.org:10.1016/s0927-7757(99)00366-0

78 Hendricks, M. P., Campos, M. P., Cleveland, G. T., Jen-La Plante, I. & Owen, J. S. A tunable library of substituted thiourea precursors to metal sulfide nanocrystals. *Science* **348**, 1226-1230 (2015). https://doi.org:10.1126/science.aaa2951

79 Samia, A. C. S., Cody, J., Fahrni, C. J. & Burda, C. The effect of ligand constraints on the metal-to-ligand charge-tranfer relaxation dynamics of copper(I)-phenanthroline complexes: A comparative study by femtosecond time-resolved spectroscopy. *Journal of Physical Chemistry B* **108**, 563-569 (2004). https://doi.org:10.1021/jp036857a

80 Wittekindt, C., Schwarz, M., Friedrich, T. & Koslowski, T. Aromatic Amino Acids as Stepping Stones in Charge Transfer in Respiratory Complex I: An Unusual Mechanism Deduced from Atomistic Theory and Bioinformatics. *Journal of the American Chemical Society* **131**, 8134-8140 (2009). https://doi.org:10.1021/ja900352t

81 Crouse, H. F. *et al.* Quenching of tryptophan fluorescence in various proteins by a series of small nickel complexes. *Dalton Transactions* **41**, 2720-2731 (2012). https://doi.org:10.1039/c2dt12169g

82 Dulkeith, E. *et al.* Fluorescence quenching of dye molecules near gold nanoparticles: Radiative and nonradiative effects. *Physical Review Letters* **89** (2002). https://doi.org:10.1103/PhysRevLett.89.203002

83 Adamson, A. W. & Gast, A. P. *Physical Chemistry of Surfaces, 6th ed.*, (Wiley-Interscience, 1997).

84 Hill, T. L. *An introduction to statistical thermodynamics*. (Addison-Wesley Pub. Co., 1960).

85 Kusaka, I. *Statistical Mechanics for Engineers*. (Springer, 2015).

86 Brunauer, S., Emmett, P. H. & Teller, E. Adsorption of gases in multimolecular layers. *Journal of the American Chemical Society* **60**, 309-319 (1938). https://doi.org:10.1021/ja01269a023

87 Brewer, S. H., Glomm, W. R., Johnson, M. C., Knag, M. K. & Franzen, S. Probing BSA binding to citrate-coated gold nanoparticles and surfaces. *Langmuir* **21**, 9303-9307 (2005). https://doi.org:10.1021/la050588t

88 Ulman, A. Formation and structure of self-assembled monolayers. *Chemical Reviews* **96**, 1533-1554 (1996). https://doi.org:10.1021/cr9502357

89 Cottrell, T. L. *The strengths of chemical bonds*. (Butterworths scientific publications, 1958).

90 Lakowicz, J. R. *Principles of Fluorescence Spectroscopy, 3rd ed.*, (Springer, 1999).

91 Christodoulou, J., Sadler, P. J. & Tucker, A. A NEW STRUCTURAL TRANSITION OF SERUM-ALBUMIN DEPENDENT ON THE STATE OF CYS34 - DETECTION BY H-1-NMR SPECTROSCOPY. *European Journal of Biochemistry* **225**, 363-368 (1994). https://doi.org:10.1111/j.1432-1033.1994.00363.x

92 Thiele, E. W. Relation between catalytic activity and size of particle. *Industrial and Engineering Chemistry* **31**, 916-920 (1939). https://doi.org:10.1021/ie50355a027

93 Moraillon, A., Gouget-Laemmel, A. C., Ozanam, F. & Chazalviel, J. N. Amidation of monolayers on silicon in physiological buffers: A quantitative IR study. *Journal of Physical Chemistry C* **112**, 7158-7167 (2008). https://doi.org:10.1021/jp7119922

94 Whitehead, C. B., Ozkar, S. & Finke, R. G. LaMer's 1950 model of particle formation: a review and critical analysis of its classical nucleation and fluctuation theory basis, of competing models and mechanisms for phase-changes and particle formation, and then of its application to silver halide, semiconductor, metal, and metal-oxide nanoparticles. *Materials Advances* **2**, 186-235 (2021). https://doi.org:10.1039/d0ma00439a

95 Oxtoby, D. W. Nucleation of first-order phase transitions. *Accounts of Chemical Research* **31**, 91-97 (1998). https://doi.org:10.1021/ar9702278

96 Oxtoby, D. W. & Kashchiev, D. A GENERAL RELATION BETWEEN THE NUCLEATION WORK AND THE SIZE OF THE NUCLEUS IN MULTICOMPONENT NUCLEATION. *Journal of Chemical Physics* **100**, 7665-7671 (1994). https://doi.org:10.1063/1.466859

97 Viisanen, Y., Strey, R. & Reiss, H. HOMOGENEOUS NUCLEATION RATES FOR WATER. *Journal of Chemical Physics* **99**, 4680-4692 (1993). https://doi.org:10.1063/1.466066

98 Ford, I. J. Nucleation theorems, the statistical mechanics of molecular clusters, and a revision of classical nucleation theory. *Physical Review E* **56**, 5615-5629 (1997). https://doi.org:10.1103/PhysRevE.56.5615

99 Laaksonen, A., Talanquer, V. & Oxtoby, D. W. Nucleation: Measurements, Theory, and Atmospheric Applications. *Annual Review of Physical Chemistry* **46**, 489-524 (1995). https://doi.org:10.1146/annurev.pc.46.100195.002421

100 Cha, S.-H., Kim, J.-U., Kim, K.-H. & Lee, J.-C. Preparation and photoluminescent properties of gold(I)-alkanethiolate complexes having highly ordered supramolecular structures. *Chemistry of Materials* **19**, 6297-6303 (2007). https://doi.org:10.1021/cm7024944

101 Mansour, M. A., Connick, W. B., Lachicotte, R. J., Gysling, H. J. & Eisenberg, R. Linear chain Au(I) dimer compounds as environmental sensors: A luminescent switch for the detection of volatile organic compounds. *Journal of the American Chemical Society* **120**, 1329-1330 (1998). https://doi.org:10.1021/ja973216i

102 Lanci, C. J. *et al.* Computational design of a protein crystal. *Proceedings of the National Academy of Sciences of the United States of America* **109**, 7304-7309 (2012). https://doi.org:10.1073/pnas.1112595109

103 Sinclair, J. C., Davies, K. M., Venien-Bryan, C. & Noble, M. E. M. Generation of protein lattices by fusing proteins with matching rotational symmetry. *Nature Nanotechnology* **6**, 558-562 (2011). https://doi.org:10.1038/nnano.2011.122

104 Amaral, M. *et al.* Protein conformational flexibility modulates kinetics and thermodynamics of drug binding. *Nature Communications* **8** (2017). https://doi.org:10.1038/s41467-017-02258-w

105 Yu, E., Gaucher, S. P. & Hadi, M. Z. Probing Conformational Changes in Ape1 during the Progression of Base Excision Repair. *Biochemistry* **49**, 3786-3796 (2010). https://doi.org:10.1021/bi901828t

106 Xavier, P. L., Chaudhari, K., Verma, P. K., Pal, S. K. & Pradeep, T. Luminescent quantum clusters of gold in transferrin family protein, lactoferrin exhibiting FRET. *Nanoscale* **2**, 2769-2776 (2010). https://doi.org:10.1039/c0nr00377h

107 Chen, Y. *et al.* Papain-directed synthesis of luminescent gold nanoclusters and the sensitive detection of Cu2+. *Journal of Colloid and Interface Science* **396**, 63-68 (2013). https://doi.org:10.1016/j.jcis.2013.01.031

108 Tanford, C. & Roxby, R. INTERPRETATION OF PROTEIN TITRATION CURVES - APPLICATION TO LYSOZYME. *Biochemistry* **11**, 2192-& (1972). https://doi.org:10.1021/bi00761a029

109 Smith, M. B. & Back, J. F. STUDIES ON OVALBUMIN .2. FORMATION AND PROPERTIES OF S-OVALBUMIN A MORE STABLE FORM OF OVALBUMIN. *Australian Journal of Biological Sciences* **18**, 365-& (1965). https://doi.org:10.1071/bi9650365

110 Bechet, J. J. & Dalbis, A. BINDING OF COMPETITIVE INHIBITORS TO DIFFERENT PH-DEPENDENT FORMS OF TRYPSIN. *Biochimica Et Biophysica Acta* **178**, 561-& (1969). https://doi.org:10.1016/0005-2744(69)90225-3

111 Kim, Y. *et al.* PH DEPENDENT CONFORMATIONAL-CHANGES IN THE T-STATES AND R-STATES OF INSULIN IN SOLUTION - CIRCULAR DICHROIC STUDIES IN THE PH RANGE OF 6 TO 12. *Faseb Journal* **6**, A465-A465 (1992).

112 Kim, Y. & Shields, J. E. PH DEPENDENT CONFORMATIONAL-CHANGES IN THE T-STATES AND R-STATES OF INSULIN IN SOLUTION - CIRCULAR DICHROIC STUDIES IN THE PH RANGE OF 6 TO 10. *Biochemical and Biophysical Research Communications* **186**, 1115-1120 (1992). https://doi.org:10.1016/0006-291x(92)90862-f

113 Goux, W. J. & Venkatasubramanian, P. N. METAL-ION BINDING-PROPERTIES OF HEN OVALBUMIN AND S-OVALBUMIN - CHARACTERIZATION OF THE METAL-ION BINDING-SITE BY P-31 NMR AND WATER PROTON RELAXATION RATE ENHANCEMENTS. *Biochemistry* **25**, 84-94 (1986). https://doi.org:10.1021/bi00349a013

114 Chambers, J. L., Christoph, G. G., Krieger, M., Kay, L. & Stroud, R. M. SILVER ION INHIBITION OF SERINE PROTEASES - CRYSTALLOGRAPHIC STUDY OF SILVER-TRYPSIN. *Biochemical and Biophysical Research Communications* **59**, 70-74 (1974). https://doi.org:10.1016/s0006-291x(74)80175-0

115 Coffman, F. D. & Dunn, M. F. INSULIN METAL-ION INTERACTIONS - THE BINDING OF DIVALENT-CATIONS TO INSULIN HEXAMERS AND TETRAMERS AND THE ASSEMBLY OF INSULIN HEXAMERS. *Biochemistry* **27**, 6179-6187 (1988). https://doi.org:10.1021/bi00416a053

116 Permyakov, E. A. *Luminescent Spectroscopy of Proteins*. (CRC Press, 1992).

117 Dokmanic, I., Sikic, M. & Tomic, S. Metals in proteins: correlation between the metal-ion type, coordination number and the amino-acid residues involved in the coordination. *Acta Crystallographica Section D-Biological Crystallography* **64**, 257-263 (2008). https://doi.org:10.1107/s090744490706595x

118 Pakiari, A. H. & Jamshidi, Z. Nature and Strength of M-S Bonds (M = Au, Ag, and Cu) in Binary Alloy Gold Clusters. *Journal of Physical Chemistry A* **114**, 9212-9221 (2010). https://doi.org:10.1021/jp100423b

119 Forward, J. M., Fackler, J. P. & Assefa, Z. Photophysical and photochemical properties of Gold(I) complexes. *Optoelectronic Properties of Inorganic Compounds*, 195-229 (1999).

120 Chen, S.-C. *et al.* A Series of Polynuclear Complexes of d10 Metals With Interesting Luminescent Properties. *Figshare* (2010). https://doi.org:http://dx.doi.org/10.1021/cg901031x.s002

121 Palermo, G. A., Tarannum, M. & Egusa, S. Luminescence Onset and Mechanism of the Formation of Gold(I)- Thiolate Complexes as the Precursors to Nanoparticles. *Journal of Physical Chemistry C* **124**, 11248-11255 (2020). https://doi.org:10.1021/acs.jpcc.0c02725

122 Lavenn, C. *et al.* Shedding light on an ultra-bright photoluminescent lamellar gold thiolate coordination polymer Au(p-SPhCO2Me) (n). *Chemical Communications* **52**, 9063-9066 (2016). https://doi.org:10.1039/c5cc10448c

123 Negishi, Y., Nobusada, K. & Tsukuda, T. Glutathione-protected gold clusters revisited: Bridging the gap between gold(I)-thiolate complexes and thiolate-protected gold nanocrystals. *Journal of the American Chemical Society* **127**, 5261-5270 (2005). https://doi.org:10.1021/ja042218h

124 Luo, Z. *et al.* From Aggregation-Induced Emission of Au(I)-Thiolate Complexes to Ultrabright Au(0)@Au(I)-Thiolate Core-Shell Nanoclusters. *Journal of the American Chemical Society* **134**, 16662-16670 (2012). https://doi.org:10.1021/ja306199p

125 Henzler-Wildman, K. & Kern, D. Dynamic personalities of proteins. *Nature* **450**, 964-972 (2007). https://doi.org:10.1038/nature06522

126 He, X. M. & Carter, D. C. ATOMIC-STRUCTURE AND CHEMISTRY OF HUMAN SERUM-ALBUMIN. *Nature* **358**, 209-215 (1992). https://doi.org:10.1038/358209a0

127 Steinhardt, J., Krijn, J. & Leidy, J. G. DIFFERENCES BETWEEN BOVINE AND HUMAN SERUM ALBUMINS - BINDING ISOTHERMS, OPTICAL ROTATORY

DISPERSION, VISCOSITY, HYDROGEN ION TITRATION, AND FLUORESCENCE EFFECTS. *Biochemistry* **10**, 4005-+ (1971). https://doi.org:10.1021/bi00798a001

128 Tomida, J. *et al.* REV7 is essential for DNA damage tolerance via two REV3L binding sites in mammalian DNA polymerase zeta. *Nucleic Acids Research* **43**, 1000-1011 (2015). https://doi.org:10.1093/nar/gku1385

129 Sato, K., Toda, K., Ishiai, M., Takata, M. & Kurumizaka, H. DNA robustly stimulates FANCD2 monoubiquitylation in the complex with FANCI. *Nucleic Acids Research* **40**, 4553-4561 (2012). https://doi.org:10.1093/nar/gks053

130 Takata, K.-i., Shimizu, T., Iwai, S. & Wood, R. D. Human DNA polymerase N (POLN) is a low fidelity enzyme capable of error-free bypass of 5S-thymine glycol. *Journal of Biological Chemistry* **281**, 23445-23455 (2006). https://doi.org:10.1074/jbc.M604317200

131 Work, T. S. *Laboratory Techniques in Biochemistry and Molecular Biology*. Vol. 9 (North-Holland Publishing Company, 1981).

132 Heaney-Kieras, J. & King, T. P. LIMITED PEPSIN DIGESTION OF HUMAN PLASMA ALBUMIN. *Journal of Biological Chemistry* **252**, 4326-4329 (1977).

133 King, T. P. & Spencer, M. STRUCTURAL STUDIES AND ORGANIC LIGAND-BINDING PROPERTIES OF BOVINE PLASMA ALBUMIN. *Journal of Biological Chemistry* **245**, 6134-+ (1970).

134 Reed, R. G., Feldhoff, R. C., Clute, O. L. & Peters, T. FRAGMENTS OF BOVINE SERUM-ALBUMIN PRODUCED BY LIMITED PROTEOLYSIS - CONFORMATION AND LIGAND-BINDING. *Biochemistry* **14**, 4578-4583 (1975). https://doi.org:10.1021/bi00692a004

135 Peters, T. & Feldhoff, R. C. FRAGMENTS OF BOVINE SERUM-ALBUMIN PRODUCED BY LIMITED PROTEOLYSIS - ISOLATION AND CHARACTERIZATION OF TRYPTIC FRAGMENTS. *Biochemistry* **14**, 3384-3391 (1975). https://doi.org:10.1021/bi00686a015

136 Kazanov, M. D. *et al.* Structural Determinants of Limited Proteolysis. *Figshare* (2011). https://doi.org:http://dx.doi.org/10.1021/pr200271w.s004

137 Ortiz, M. L., Calero, M., Patron, C. F., Castellanos, L. & Mendez, E. IMIDAZOLE-SDS-ZN REVERSE STAINING OF PROTEINS IN GELS CONTAINING OR NOT SDS AND MICROSEQUENCE OF INDIVIDUAL UNMODIFIED ELECTROBLOTTED

PROTEINS. *Febs Letters* **296**, 300-304 (1992). https://doi.org:10.1016/0014-5793(92)80309-5

138 Lee, C., Levin, A. & Branton, D. COPPER STAINING - A 5-MINUTE PROTEIN STAIN FOR SODIUM DODECYL-SULFATE POLYACRYLAMIDE GELS. *Analytical Biochemistry* **166**, 308-312 (1987). https://doi.org:10.1016/0003-2697(87)90579-3

139 Sudlow, G., Birkett, D. J. & Wade, D. N. CHARACTERIZATION OF 2 SPECIFIC DRUG BINDING-SITES ON HUMAN-SERUM ALBUMIN. *Molecular Pharmacology* **11**, 824-832 (1975).

140 Ghuman, J. *et al.* Structural basis of the drug-binding specificity of human serum albumin. *Journal of Molecular Biology* **353**, 38-52 (2005). https://doi.org:10.1016/j.jmb.2005.07.075

141 Komatsu, T. *et al.* O-2 and CO binding properties of artificial hemoproteins formed by complexing iron protoporphyrin IX with human serum albumin mutants. *Journal of the American Chemical Society* **127**, 15933-15942 (2005). https://doi.org:10.1021/ja054819u

142 Coolbaugh, M. J., Tang, M. J. S. & Wood, D. W. High-throughput purification of recombinant proteins using self-cleaving intein tags. *Analytical Biochemistry* **516**, 65-74 (2017). https://doi.org:10.1016/j.ab.2016.10.016

143 Lu, S. C. Glutathione synthesis. *Biochimica Et Biophysica Acta-General Subjects* **1830**, 3143-3153 (2013). https://doi.org:10.1016/j.bbagen.2012.09.008

144 Srinivasan, U., Mieyal, P. A. & Mieyal, J. J. pH profiles indicative of rate-limiting nucleophilic displacement in thioltransferase catalysis. *Biochemistry* **36**, 3199-3206 (1997). https://doi.org:10.1021/bi962017t

145 Shaked, Z., Szajewski, R. P. & Whitesides, G. M. RATES OF THIOL-DISULFIDE INTERCHANGE REACTIONS INVOLVING PROTEINS AND KINETIC MEASUREMENTS OF THIOL PKA VALUES. *Biochemistry* **19**, 4156-4166 (1980). https://doi.org:10.1021/bi00559a004

146 Houk, J., Singh, R. & Whitesides, G. M. MEASUREMENT OF THIOL DISULFIDE INTERCHANGE REACTIONS AND THIOL PKA VALUES. *Methods in Enzymology* **143**, 129-140 (1987).

147 Trivedi, M. V., Laurence, J. S. & Siahaan, T. J. The Role of Thiols and Disulfides on Protein Stability. *Current Protein & Peptide Science* **10**, 614-625 (2009). https://doi.org:10.2174/138920309789630534

148 Arunachalam, V., Tummanapelli, A. K. & Vasudevan, S. The multiple dissociation constants of glutathione disulfide: interpreting experimental pH-titration curves with ab initio MD simulations. *Physical Chemistry Chemical Physics* **21**, 9212-9217 (2019). https://doi.org:10.1039/c9cp00761j

149 Tummanapelli, A. K. & Vasudevan, S. Ab Initio MD Simulations of the Bronsted Acidity of Glutathione in Aqueous Solutions: Predicting pK(a) Shifts of the Cysteine Residue. *Journal of Physical Chemistry B* **119**, 15353-15358 (2015). https://doi.org:10.1021/acs.jpcb.5b10093

150 Guo, C. & Yarger, J. L. Characterizing gold nanoparticles by NMR spectroscopy. *Magnetic Resonance in Chemistry* **56**, 1074-1082 (2018). https://doi.org:10.1002/mrc.4753

151 Giustarini, D., Dalle-Donne, I., Milzani, A., Fanti, P. & Rossi, R. Analysis of GSH and GSSG after derivatization with N-ethylmaleimide. *Nature Protocols* **8**, 1660-1669 (2013). https://doi.org:10.1038/nprot.2013.095

152 Novotny, J. *et al.* Linking the Character of the Metal-Ligand Bond to the Ligand NMR Shielding in Transition-Metal Complexes: NMR Contributions from Spin-Orbit Coupling. *Journal of Chemical Theory and Computation* **13**, 3586-3601 (2017). https://doi.org:10.1021/acs.jctc.7b00444

153 Vicha, J. *et al.* Relativistic Heavy-Neighbor-Atom Effects on NMR Shifts: Concepts and Trends Across the Periodic Table. *Chemical Reviews* **120**, 7065-7103 (2020). https://doi.org:10.1021/acs.chemrev.9b00785

154 Thamri, A. *et al.* MHDA-Functionalized Multiwall Carbon Nanotubes for detecting non-aromatic VOCs. *Scientific Reports* **6** (2016). https://doi.org:10.1038/srep35130

155 Svorcik, V. *et al.* "Soft and rigid" dithiols and Au nanoparticles grafting on plasma-treated polyethyleneterephthalate. *Nanoscale Research Letters* **6** (2011). https://doi.org:10.1186/1556-276x-6-607

156 Bohli, N., Belkilani, M., Casanova-Chafer, J., Llobet, E. & Abdelghani, A. Multiwalled carbon nanotube based aromatic volatile organic compound sensor: sensitivity enhancement through 1-hexadecanethiol functionalisation. *Beilstein Journal of Nanotechnology* **10**, 2364-2373 (2019). https://doi.org:10.3762/bjnano.10.227

157 Aldewachi, H., Woodroofe, N. & Gardiner, P. Study of the Stability of Functionalized Gold Nanoparticles for the Colorimetric Detection of Dipeptidyl Peptidase IV. *Applied Sciences-Basel* **8** (2018). https://doi.org:10.3390/app8122589

158 Moulder, J. F., Stickle, W. F., Sobol, P. E. & Bomben, K. D. *Handbook of X-Ray Photoelectron Spectroscopy*. Vol. 1 182-183 (Perkin-Elmer Corporation, 1992).

159 Xue, Y., Li, X., Li, H. & Zhang, W. Quantifying thiol-gold interactions towards the efficient strength control. *Nature Communications* **5** (2014). https://doi.org:10.1038/ncomms5348

160 Castner, D. G., Hinds, K. & Grainger, D. W. X-ray photoelectron spectroscopy sulfur 2p study of organic thiol and disulfide binding interactions with gold surfaces. *Langmuir* **12**, 5083-5086 (1996). https://doi.org:10.1021/la960465w

161 Mao, F. *et al.* Real-time monitoring of electroreduction and labelling of disulfide-bonded peptides and proteins by mass spectrometry. *Analyst* **144**, 6898-6904 (2019). https://doi.org:10.1039/c9an01420a

162 Paclawski, K., Zajac, D. A., Borowiec, M., Kapusta, C. & Fitzner, K. EXAFS Studies on the Reaction or Gold (III) Chloride Complex Ions with Sodium Hydroxide and Glucose. *Journal of Physical Chemistry A* **114**, 11943-11947 (2010). https://doi.org:10.1021/jp102836f

163 Rajamanikandan, R. & Ilanchelian, M. Red emitting human serum albumin templated copper nanoclusters as effective candidates for highly specific biosensing of bilirubin. *Mater. Sci. Eng. C-Mater. Biol. Appl.* **98**, 1064-1072 (2019). https://doi.org:10.1016/j.msec.2019.01.048

164 Desai, M. L., Basu, H., Saha, S., Singhal, R. K. & Kailasa, S. K. Fluorescence enhancement of bovine serum albumin gold nanoclusters from La³⁺ ion: Detection of four divalent metal ions (Hg²⁺, Cu²⁺, Pb²⁺ and Cd²⁺). *Journal of Molecular Liquids* **336** (2021). https://doi.org:10.1016/j.molliq.2021.116239

165 Chen, L. *et al.* Advances in bovine serum albumin-protected gold nanoclusters: from understanding the formation mechanisms to biological applications. *Materials Today Chemistry* **29** (2023). https://doi.org:10.1016/j.mtchem.2023.101460

166 Geng, T. *et al.* Bovine Serum Albumin-Encapsulated Ultrasmall Gold Nanoclusters for Photodynamic Therapy of Tumors. *Acs Applied Nano Materials* **4**, 13818-13825 (2021). https://doi.org:10.1021/acsanm.1c03209

167 Govindaraju, S., Ankireddy, S. R., Viswanath, B., Kim, J. & Yun, K. Fluorescent Gold Nanoclusters for Selective Detection of Dopamine in Cerebrospinal fluid. *Scientific Reports* **7** (2017). https://doi.org:10.1038/srep40298

168 Niu, Y. *et al.* Fluorescence switch of gold nanoclusters stabilized with bovine serum albumin for efficient and sensitive detection of cysteine and copper ion in mice with Alzheimer 's disease. *Talanta* **223** (2021). https://doi.org:10.1016/j.talanta.2020.121745

169 Wang, T. & Xiao, D. Rapid synthesis of fluorescent bovine serum albumin-gold nanoclusters complex for glutathione determination. *Microchimica Acta* **188** (2021). https://doi.org:10.1007/s00604-021-04844-8

170 Yan, L. *et al.* Microwave-assisted synthesis of BSA-stabilized and HSA-protected gold nanoclusters with red emission. *Journal of Materials Chemistry* **22**, 1000-1005 (2012). https://doi.org:10.1039/c1jm13457d

171 Slater, J. C. ATOMIC RADII IN CRYSTALS. *Journal of Chemical Physics* **41**, 3199-& (1964). https://doi.org:10.1063/1.1725697

172 Wu, Y. G., Fan, Z. G. & Lu, Y. Z. Bulk and interior packing densities of random close packing of hard spheres. *Journal of Materials Science* **38**, 2019-2025 (2003). https://doi.org:10.1023/a:1023597707363

173 Heaven, M. W., Dass, A., White, P. S., Holt, K. M. & Murray, R. W. (Figshare, 2008).

174 Dixon, J. M. & Egusa, S. Luminophore Formation in Various Conformations of Bovine Serum Albumin by Binding of Gold(III). *Jove-Journal of Visualized Experiments* (2018). https://doi.org:10.3791/58141

175 Xu, W. W., Zhu, B., Zeng, X. C. & Gao, Y. A grand unified model for liganded gold clusters. *Nature Communications* **7** (2016). https://doi.org:10.1038/ncomms13574

176 Zheng, J., Zhang, C. W. & Dickson, R. M. Highly fluorescent, water-soluble, size-tunable gold quantum dots. *Physical Review Letters* **93** (2004). https://doi.org:10.1103/PhysRevLett.93.077402

177 Blaskovicova, J., Vyskocil, V., Augustin, M. & Purdesova, A. Ethanol and NaCl-Induced Gold Nanoparticle Aggregation Toxicity toward DNA Investigated with a DNA/GCE Biosensor. *Sensors* **23** (2023). https://doi.org:10.3390/s23073425

178 Bastus, N. G., Comenge, J. & Puntes, V. Kinetically Controlled Seeded Growth Synthesis of Citrate-Stabilized Gold Nanoparticles of up to 200 nm: Size Focusing versus Ostwald Ripening. *Langmuir* **27**, 11098-11105 (2011). https://doi.org:10.1021/la201938u

179 Thanh, N. T. K., Maclean, N. & Mahiddine, S. Mechanisms of Nucleation and Growth of Nanoparticles in Solution. *Chemical Reviews* **114**, 7610-7630 (2014). https://doi.org:10.1021/cr400544s

180 Perala, S. R. K. & Kumar, S. On the Two-Step Mechanism for Synthesis of Transition-Metal Nanoparticles. *Langmuir* **30**, 12703-12711 (2014). https://doi.org:10.1021/la503199m

181 Watzky, M. A. & Finke, R. G. Gold Nanoparticle Formation Kinetics and Mechanism: A Critical Analysis of the "Redox Crystallization" Mechanism. *Acs Omega* **3**, 1555-1563 (2018). https://doi.org:10.1021/acsomega.7b01772

182 Watzky, M. A. & Finke, R. G. Transition metal nanocluster formation kinetic and mechanistic studies. A new mechanism when hydrogen is the reductant: Slow, continuous nucleation and fast autocatalytic surface growth. *Journal of the American Chemical Society* **119**, 10382-10400 (1997). https://doi.org:10.1021/ja9705102

183 Sanchez, J. F. M., Sanchez, M. D., Falcone, R. D. & Ritacco, H. A. Production of Pd nanoparticles in microemulsions. Effect of reaction rates on the particle size. *Physical Chemistry Chemical Physics* **24**, 1692-1701 (2022). https://doi.org:10.1039/d1cp05049d

184 Patakfalvi, R., Viranyi, Z. & Dekany, I. Kinetics of silver nanoparticle growth in aqueous polymer solutions. *Colloid and Polymer Science* **283**, 299-305 (2004). https://doi.org:10.1007/s00396-004-1138-8

185 Gommes, C. J. Ostwald ripening of confined nanoparticles: chemomechanical coupling in nanopores. *Nanoscale* **11**, 7386-7393 (2019). https://doi.org:10.1039/c9nr01349k

186 Zhang, Z. *et al.* Redox reaction induced Ostwald ripening for size- and shape-focusing of palladium nanocrystals. *Chemical Science* **6**, 5197-5203 (2015). https://doi.org:10.1039/c5sc01787d

187 Voorhees, P. W. THE THEORY OF OSTWALD RIPENING. *Journal of Statistical Physics* **38**, 231-252 (1985). https://doi.org:10.1007/bf01017860

188 Harada, M. & Kamigaito, Y. Nucleation and Aggregative Growth Process of Platinum Nanoparticles Studied by in Situ Quick XAFS Spectroscopy. *Langmuir* **28**, 2415-2428 (2012). https://doi.org:10.1021/la204031j

189 Daima, H. K. *et al.* Synergistic influence of polyoxometalate surface corona towards enhancing the antibacterial performance of tyrosine-capped Ag nanoparticles. *Nanoscale* **6**, 758-765 (2014). https://doi.org:10.1039/c3nr03806h

190 Phillips, S. M. & Smith, G. D. Further Evidence for Charge Transfer Complexes in Brown Carbon Aerosols from Excitation-Emission Matrix Fluorescence Spectroscopy. *Journal of Physical Chemistry A* **119**, 4545-4551 (2015). https://doi.org:10.1021/jp510709e

191 Thiagarajan, V., Selvaraju, C., Malar, E. J. P. & Ramamurthy, P. A novel fluorophore with dual fluorescence: Local excited state and photoinduced electron-transfer-promoted charge-transfer state. *Chemphyschem* **5**, 1200-1209 (2004). https://doi.org:10.1002/cphc.200400064

192 Zheng, J., Zhou, C., Yu, M. & Liu, J. Different sized luminescent gold nanoparticles. *Nanoscale* **4**, 4073-4083 (2012). https://doi.org:10.1039/c2nr31192e

193 Frangioni, J. V. & Neel, B. G. SOLUBILIZATION AND PURIFICATION OF ENZYMATICALLY ACTIVE GLUTATHIONE-S-TRANSFERASE (PGEX) FUSION PROTEINS. *Analytical Biochemistry* **210**, 179-187 (1993). https://doi.org:10.1006/abio.1993.1170

194 Hayes, J. D. & Pulford, D. J. The glutathione S-Transferase supergene family: Regulation of GST and the contribution of the isoenzymes to cancer chemoprotection and drug resistance. *Critical Reviews in Biochemistry and Molecular Biology* **30**, 445-600 (1995). https://doi.org:10.3109/10409239509083491

195 Armstrong, R. N. Structure, catalytic mechanism, and evolution of the glutathione transferases. *Chemical Research in Toxicology* **10**, 2-18 (1997). https://doi.org:10.1021/tx960072x

196 Mingos, D. M. P. THEORETICAL ANALYSES AND ELECTRON COUNTING RULES FOR HIGH NUCLEARITY CLUSTERS. *Journal of the Chemical Society-Chemical Communications*, 1352-1354 (1985). https://doi.org:10.1039/c39850001352

197 Wales, D. J. & Mingos, D. M. P. SPLITTING OF CLUSTER ORBITALS. *Inorganic Chemistry* **28**, 2748-2754 (1989). https://doi.org:10.1021/ic00313a012